



NTNU – Trondheim
Norwegian University of
Science and Technology

One-Pot Conversion of Cellulose to Ethylene Glycol and Propylene Glycol over Nickel Zinc Oxide Catalysts with CNT Support

Ingvild Skeie Liland

Chemical Engineering and Biotechnology

Submission date: July 2013

Supervisor: De Chen, IKP

Co-supervisor: Tao Zhang, Dalian Institute of Chemical Physics
Aiqin Wang, Dalian Institute of Chemical Physics

Norwegian University of Science and Technology
Department of Chemical Engineering

Abstract

Ni-Zn oxide catalysts with CNT support were prepared by the pechini method, and evaluated for the conversion of cellulose to polyols. The catalysts were characterized by XRD, SEM/TEM, N₂ adsorption, temperature programmed oxidation, CO₂ desorption and H₂ Chemisorption. The experiments were conducted at DICP (Dalian Institute of Chemical Physics, China) and the study is based on the previous work done by the author at NTNU (Norwegian University of Science and Technology) the fall of 2012, in which four 20Ni-ZnO/CNT catalysts with ZnO-loading 26-46% were prepared. The four catalysts were brought to DICP and tested for the conversion of cellulose (reaction time, activity and selectivity). The Ni-ZnO/CNT catalysts completely converted cellulose under hydrothermal conditions, and the highest EG (32,8%) and 1,2-PG (15,2%) yields were obtained over the 20Ni-26ZnO/CNT catalyst. In order to investigate the function of the different components in the CNT supported nickel zinc oxide catalyst, 26ZnO/CNT, 20Ni/CNT and 20Ni/26ZnO catalysts were prepared and tested for the conversion of cellulose. Nickel promoted hydrogenation and a synergistic effect between the Ni and ZnO components were observed. Activated carbon was considered as an alternative to CNT support, and therefore two batches of 20Ni-26ZnO/AC catalysts were prepared. One batch was prepared by the pechini method, and the other batch was prepared by incipient wetness impregnation. SEM and TEM characterization indicated that incipient wetness impregnation resulted in better nickel dispersion than the pechini method for the preparation of activated carbon supported Ni-ZnO catalysts. The CNT supported 20Ni-26ZnO catalyst was superior to the AC supported catalysts, therefore further investigations were done to reveal the mechanism for cellulose conversion via the 20Ni-26ZnO/CNT catalyst. Sorbitol and mannitol feedstocks could be converted to EG and 1,2-PG over the 20Ni-26ZnO/CNT catalyst. Yield as a function of time was studied and the results indicate that the main pathway for the conversion of cellulose over the 20Ni-26ZnO/CNT catalyst happens via hexitols (sorbitol and mannitol). Next, Ni-26ZnO/CNT catalysts with nickel loading 5-30% were prepared and tested for cellulose conversion in order to investigate the effect of nickel loading. The EG yield increased as the nickel loading increased. The highest EG yield, 34,6%, and 1,2-PG yield, 17,8%, was obtained over the 30Ni-26ZnO/CNT catalyst, thus a combined EG and 1,2-PG yield of 52,3% was achieved. Finally, 30Ni-26ZnO/CNT catalysts were prepared with different reduction temperature to study basicity as a function of reduction temperature. A correlation between basic sites, reduction temperature and product yield was found, and a reaction mechanism was suggested. The reusability of some of the catalysts was briefly tested, and discussions related to the results are presented in order to provide ideas for future studies.

Preface

First of all, I would like to thank my supervisor at NTNU, Professor De Chen for giving me the opportunity to continue our work from the specialization topic at DICP, Dalian Institute of Chemical Physics. He has been available for guidance over email, and additionally visited DICP during the spring semester, which gave me a unique opportunity to discuss my progress with him. Additionally I would like to thank Post. Doc. Jun Zhu (who worked with me on the specialization topic) for his advice throughout this study. He has been available on email, and given me feedback on my work at DICP.

I would also like to thank Professor Tao Zhang for the invitation to join his research group at DICP. It has been an incredible experience to be a part of the world's leading research environment on biomass conversion. The time I spent at DICP has given me knowledge and memories that I value highly, and I am forever grateful to the staff and students for their warm welcome and guidance throughout my stay in Dalian. I would especially like to express my sincere gratitude to my supervisor at DICP Professor Aiqin Wang, who gave me continuous feedback on my results and advise during the progress. She showed excitement about my findings, and was a motivating source during my entire stay at DICP. I thank her for being available for guidance at all times, and additionally for teaching me about the Chinese culture.

Last, but not least, I would like to give a big thank you to master student Cecilie Bjørgen, who shared the experience at DICP with me. I think it has been a pleasure working with you.

I declare that this is an independent work according to the exam regulations of the Norwegian University of Science and Technology (NTNU).

Place and Date:

Bergen, Norway. 08.07.2013

Signature:



(Ingvild Skeie Liland)

Table of Contents

1. Introduction	14
2. Background and Theoretical Concepts.....	16
2.1 Conversion of lignocellulosic biomass	16
2.1.1 Lignocellulosic biomass to fuels and high-value chemicals.....	16
2.1.2 State of the art - One-pot conversion of biomass.....	17
2.2 Carbon Nanofibers	21
2.2.1 History	21
2.2.2 Growth of carbon nanofibers.....	22
2.2.3 Carbon nanofibers as catalyst support material.....	24
2.3 Oxide coating.....	26
2.3.1 Introduction	26
2.3.2 Incipient wetness impregnation	26
2.3.3 The electroless plating method	26
2.3.4 The Sol-gel method.....	27
2.3.5 The Pechini method	28
3. Catalyst Preparation and Characterization	30
3.1 An overview of the catalyst preparation.....	30
3.2 Pretreatment of the carbon supports.....	32
3.2.1 CNT	32
3.2.2 AC	32
3.3 Preparation of the Ni-ZnO/CNT catalysts.....	32
3.3.1 Impregnation of Zn-precursor	32
3.3.2 Calcination	32
3.3.3 Impregnation of Ni-precursor.....	33
3.3.4 – Reduction.....	33
3.4 Preparation of the AC-supported catalysts	34
3.5 Preparation of the different components in the 20Ni-26ZnO/CNT catalyst: 20Ni/CNT, 26ZnO/CNT and 20Ni/26ZnO.....	34
3.6 Catalyst characterization.....	35
3.6.1 Temperature programmed desorption (TPD).....	35

CO ₂ -TPD.....	35
NH ₃ -TPD.....	35
3.6.2 N ₂ -adsorption measurements.....	35
3.6.3 X-Ray Diffraction (XRD).....	36
3.6.4 TGA.....	36
3.6.5 SEM and TEM.....	36
3.6.6 H ₂ -Chemisorption.....	36
3.6.7 Temperature programmed reduction (H ₂ -TPR).....	36
3.6.8 ICP analysis.....	37
3.7 Activity measurement – Conversion of cellulose.....	37
4. Results and Discussion.....	38
4.1 Outline.....	38
4.2 Optimal reaction time for the Ni-ZnO/CNT catalysts.....	38
4.3 The effect of higher reaction temperature.....	39
4.4 Cellulose conversion over 20Ni-ZnO/CNT catalysts with different ZnO-loading.....	41
4.5 Investigations of each component in the 20Ni-26,1ZnO/CNT catalyst: 20Ni/CNT, 26ZnO/CNT and 20Ni/26ZnO catalysts.....	42
4.5.1 Cellulose conversion.....	42
4.5.2 BET measurements.....	44
4.5.3 XRD.....	45
4.6 The mechanism for cellulose conversion over the 20Ni-26ZnO/CNT catalyst.....	47
4.6.1 Sorbitol and Mannitol as feedstock.....	47
4.6.2 Yield vs. time.....	48
4.7 AC as support as an alternative to CNT – 20Ni-26ZnO/AC catalysts.....	52
4.7.1 SEM/TEM Characterization.....	52
4.7.2 – Conversion of cellulose.....	55
4.7.3 BET measurements.....	56
4.7.4 XRD characterization.....	57
4.7.5 TGA.....	59
20Ni-26ZnO/AC (incipient).....	60
20Ni-26ZnO/CNT (pechini).....	61
4.8 Ni-26ZnO/CNT catalysts with Ni-loading 5-30%.....	62
4.8.1 Cellulose conversion.....	62

4.8.2 BET measurements	64
4.8.3 XRD analysis.....	65
4.8.4 TGA	66
5Ni-26ZnO/CNT.....	66
10Ni-26ZnO/CNT	67
15Ni-26ZnO/CNT	67
25Ni-26ZnO/CNT	68
30Ni-26ZnO/CNT-red 400.....	69
4.9 Basicity, reduction temperature and product selectivity for 30Ni-26ZnO/CNT catalysts.....	71
4.9.1 CO ₂ -TPD	71
4.9.2 NH ₃ -TPD.....	74
4.9.3 Sorbitol conversion	75
4.9.4 Further development of the reaction mechanism.....	77
4.9.5 BET measurements	79
4.9.6 XRD	80
4.9.7 TGA	81
30Ni-26ZnO/CNT-red 300.....	81
30Ni-26ZnO/CNT -red350	82
30Ni-26ZnO/CNT-red 400.....	82
30Ni-26ZnO/CNT - red450.....	83
4.10 Reusability and ICP	85
4.10.1 Reusability.....	85
4.10.2 Leaching of nickel and zinc - ICP	87
4.11 Hydrogen Chemisorption	89
5. Future studies and perspectives.....	91
6. Conclusion	93
References.....	94

Appendices

A Impregnation of Zn precursor and calculation of ZnO-loading	97
B Impregnation of Ni precursor and calculation of Ni-loading	100
C Nickel and zinc oxide loading in the Ni/ZnO catalysts	102
D HPLC plots	103
E GC results	123
E. 1 GC plots	123
E.2 Calculation of gas products	133
F Calculation of conversion of cellulose	137
G – The conversion of cellulose over 20Ni-26,1ZnO/CNT - Yield vs. time	138
H - SEM/TEM pictures of the Ni-ZnO/AC catalysts	142
I Calculation of the theoretical loading of the catalysts for TGA analysis	148
J TGA of the CNT support	151
K – CO ₂ -TPD for the 30Ni-26ZnO/CNT catalysts	154
L - ICP analysis	156
L.1 Nickel leaching - Conversion from ppm to %	156
L.2 Zinc leaching – Conversion from ppm to %	157
M – Risk Assessment	157

List of Tables

Table 1 - An overview of the catalysts prepared and tested herein: Catalyst name, Preparation method and Reduction temperature is given for each catalyst.....	31
Table 2 – Reduction conditions for the reduction of the 30Ni-26ZnO/CNT catalysts.....	33
Table 3 – The Product distribution for the conversion of cellulose over Ni-ZnO/CNT catalysts as a function of reaction time ^a	39
Table 4 – Product distribution for the conversion of cellulose over Ni-ZnO/CNT catalysts with different ZnO-loading ^a	41
Table 5 – Product distribution for the conversion of cellulose ^a over 20Ni-26ZnO/CNT and 20Ni/CNT catalysts.....	43
Table 6 – Product distribution for the conversion of cellulose over the Ni/ZnO catalysts ^a	44
Table 7 – The results from the BET measurements for the 20Ni/CNT, 26ZnO/CNT and 20Ni/26ZnO catalysts	44
Table 8 – Product distribution for the conversion of mannitol and sorbitol over 20Ni-26ZnO/CNT and Ni-WO ₃ /CNT catalysts ^a	48
Table 9 – Product distribution from the conversion of cellulose over 20Ni-26ZnO catalysts with AC and CNT support ^a	55
Table 10 – The results from the BET measurements of the 20Ni-26ZnO/AC and 20Ni/AC catalysts	56
Table 11 – Total loading for the 20Ni-26ZnO/AC catalysts according to TGA analysis and theoretical calculations.....	61
Table 12 - Product distribution for the conversion of cellulose over Ni-26,1ZnO/CNT catalyst with different Ni-loading ^a	63
Table 13 – The results from the BET measurements of the Ni-26ZnO/CNT catalysts with nickel loading 5-30%	64
Table 14 - Total loading for the Ni-26ZnO/CNT catalysts with Ni-loading 5-30% according to TGA analysis and theoretical calculations	70
Table 15 – Peak information from the CO ₂ -TPD of the 30Ni-26ZnO/CNT catalysts with different reduction temperature	73
Table 16 – Peak information Peak from the NH ₃ -TPD of the 20Ni-26ZnO/CNT catalyst.....	75
Table 17 – Product distribution from the cellulose conversion over 30Ni-26ZnO/CNT catalysts prepared by different reduction temperatures.....	75
Table 18 – The results from the BET measurements of the 30Ni-26ZnO/CNT catalysts.....	79

Table 19 - Total loading for the 30Ni-26ZnO/CNT catalysts with different reduction temperature according to TGA analysis and theoretical calculations	84
Table 20 – Product distribution from the first and second run of cellulose conversion of Ni-ZnO/CNT catalysts	86
Table 21 – Leaching of zinc and nickel after cellulose conversion over a 20Ni-26ZnO/CNT catalyst according to the results from the ICP analysis	87
Table 22 – H ₂ -Chemisorption results (cubic crystallite size and metal dispersion) for the Ni-ZnO catalysts with carbon support	90
Table 23 – Chemicals used in the complex solution for the impregnation of zinc precursor on the 15Ni-26ZnO/CNT catalyst.....	97
Table 24 – The complex solution used for the impregnation of zinc-precursor on the pretreated CNTs.....	98
Table 25 – Chemicals used for the incipient wetness impregnation of zinc precursor on AC.....	99
Table 26 – Chemicals used for the impregnation of nickel for the 15Ni-26ZnO/CNT catalyst.....	100
Table 27 - Chemicals used for the nickel impregnation on the carbon supported catalysts.....	101
Table 28 – Chemicals used for the nickel impregnation on commercial zinc oxide support.....	102
Table 29 – Gas products from the conversion of cellulose over Ni-ZnO catalysts with carbon support and Ni catalysts with carbon support.....	135
Table 30 – Gas products for the conversion of cellulose over Ni-ZnO/CNT catalysts	136
Table 31 – Product distribution as a function of time for the cellulose conversion over a 20Ni-26ZnO/CNT catalyst	138
Table 32 – Amounts of chemicals used for the impregnation of nickel in the 15Ni-26ZnO/CNT catalyst	148
Table 33 – The theoretical NiO loading in the Ni-ZnO/CNT catalysts	149
Table 34 – The total theoretical loading for the Ni-ZnO catalysts with carbon support that were tested with TGA.....	150

List of Figures

Figure 1 - The structure of lignocellulosic biomass with cellulose, hemicelluloses and lignin represented, adapted from ref. [3].....	15
Figure 2 - Illustration of the reaction mechanism for cellulose conversion to EG over the combined H_2WO_4 and Ru/C catalyst. Red: The overall reaction. Black: The three consecutive reactions. Blue: The temperature-controlled phase behaviour of tungsten acid. Adapted from ref. [16]	18
Figure 3 - Reusability of W_xC/MC , 2% Ni- W_2C/AC , and 1,2% Ru/AC + H_2WO_4 catalysts, adapted from ref. [8].....	19
Figure 4 - a: Electron micrograph revealing individual single-shell nanotubes. The tube labelled 1 has a diameter equal to 0,75 nm, and tube 2 is 1,37 nm in diameter. The picture is adapted from ref [29] b: TEM image of a section of a single-walled nanotube, adapted from ref. [30]	22
Figure 5 - Illustration of the metal-catalyzed growth of a carbon nanofiber from gaseous hydrocarbons.....	23
Figure 6 - Structures of different categories of CNFs: a) platelet CNFs, b) ribbon or tube CNFs, and c) fishbone CNFs, adapted from ref. [33]	24
Figure 7 - The principles for rational catalyst design by using CNFs as a platform, adapted from ref. [32].....	25
Figure 8 - The main steps in the sol gel process, adapted from ref. [46]	27
Figure 9 - The general scheme of the polymerization process in the Pechini method, adapted from ref. [50].....	29
Figure 10 - Bright field STEM (a,c) and secondary electrons (b,d) at 50 nm of a $26ZnO/CNT$ catalyst prepared by the pechini method and subsequent incipient wetness impregnation.	29
Figure 11 - Overview of the preparation steps for the Ni-ZnO/CNT catalyst.....	30
Figure 12 - The Product distribution for the conversion of cellulose over the 20Ni- $26ZnO/CNT$ catalysts as a function of reaction temperature.....	40
Figure 13 - The HPLC plot from the cellulose conversion over the $26ZnO/CNT$ catalyst.....	42
Figure 14 - The XRD patterns for Ni/ZnO catalyst A and B.....	45
Figure 15 - The XRD pattern for the $26ZnO/CNT$ catalyst.....	46
Figure 16 - Sorbitol and mannitol yields during the conversion of cellulose over a 20Ni- $26,1ZnO/CNT$ catalyst. Reaction conditions: 60 bar (RT), 245 °C, rx. time: 2,5 h and stirring rate 800 rpm. 0,8015 g cellulose,0,2427 g 20Ni- $26,1ZnO/CNT$ catalyst and 80 ml deionized water was mixed in an 300 mL autoclave reactor.	49

Figure 17 – EG, 1,2-PG and hexitol yields during the conversion of cellulose over a 20Ni-26ZnO/CNT catalyst.....	50
Figure 18 – Suggested mechanism	50
Figure 19 – Product distribution as a function of time for the conversion of cellulose over a 20Ni-ZnO/CNT catalyst.	51
Figure 20 – TEM (a,c) and SEM (b,d) pictures at 100 nm of the 20Ni-26,1ZnO/AC (pechini) catalyst.	53
Figure 21 - SEM (a,c) and TEM pictures (b,d) at 100 nm of 20Ni-26,1ZnO/AC (incipient) catalyst.....	54
Figure 22 - Bright field STEM (a) and secondary electrons (b) at 50 nm for the 26ZnO/CNT catalyst.....	54
Figure 23 – XRD patterns for the 20Ni-26ZnO catalysts with CNT and AC support	57
Figure 24 – XRD patterns for the 20Ni/AC and 20Ni/CNT catalysts	58
Figure 25 – DTG and TG cor. (from TGA analysis) as a function of temperature for the 20Ni-26ZnO/AC (incipient) catalyst.....	60
Figure 26 - DTG and TG cor. (from TGA analysis) as a function of temperature for the 20Ni-26ZnO/AC (pechini) catalyst.....	61
Figure 27 – The EG yield as a function of Ni-loading as a result of cellulose conversion over various Ni-26,1ZnO/CNT catalysts.	64
Figure 28 – XRD patterns for the Ni-26ZnO/CNT catalysts with nickel loading 5-30%...	65
Figure 29 – DTG and TG cor. (from TGA) as a function of temperature for the 5Ni-26ZnO/CNT catalyst.....	66
Figure 30 - DTG and TG cor. (from TGA) as a function of temperature for the 10Ni-26ZnO/CNT catalyst.....	67
Figure 31 - DTG (from TGA) as a function of temperature for the 15Ni-26ZnO/CNT catalyst.....	67
Figure 32 – TG cor. (from TGA) as a function of temperature for the 15Ni-26ZnO/CNT catalyst.....	68
Figure 33 – DTG and TG cor. (from TGA) as a function of temperature for the 25Ni-26ZnO/CNT catalyst.....	68
Figure 34 - DTG and TG cor. (from TGA) as a function of temperature for the 30Ni-26ZnO/CNT-red400 catalyst.....	69
Figure 35 – CO ₂ -TPD: TCD signal as a function of temperature for the 20Ni-26ZnO/CNT catalyst.....	72
Figure 36 – CO ₂ -TPD: TCD signal as a function of temperature for 30Ni-26ZnO/CNT catalysts with different reduction temperature	72

Figure 37 – NH ₃ -TPD: TCD signal as a function of temperature for the 20Ni-26ZnO/CNT catalyst	74
Figure 38 – Correlation between the glycol yield (after cellulose conversion), basic sites and reduction temperature for the 30Ni-26ZnO/CNT catalysts	76
Figure 39 - Correlation between the ethylene glycol yield (after cellulose conversion), basic sites and reduction temperature for the 30Ni-26ZnO/CNT catalysts.....	76
Figure 40 – Suggested mechanism for the conversion of cellulose over Ni-ZnO/CNT catalysts.....	78
Figure 41 – XRD patterns for the 30Ni-26ZnO/CNT catalysts prepared with different reduction temperature	80
Figure 42 – DTG and TG cor. (from TGA) as a function of temperature for the 30Ni-26ZnO/CNT-red300 catalyst.....	81
Figure 43 - DTG and TG cor. (from TGA) as a function of temperature for the 30Ni-26ZnO/CNT-red350 catalyst.....	82
Figure 44 – DTG as a function of temperature for the 30Ni-26ZnO/CNT-red400 catalyst.....	82
Figure 45 - TG cor. (from TGA) as a function of temperature for the 30Ni-26ZnO/CNT-red400 catalyst.....	83
Figure 46 - DTG and TG cor. (from TGA) as a function of temperature for the 30Ni-26ZnO/CNT-red450 catalyst.....	83
Figure 47 – Plots of the product distribution as a function of time for the cellulose conversion over a 20Ni-26ZnO/CNT catalyst.....	138
Figure 48 - Plots of the EG, 1,2-PG and Sor yields as a function of time for the cellulose conversion over a 20Ni-26ZnO/CNT catalyst.....	139
Figure 49 - Plots of the Man, Gly and Ery yields as a function of time for the cellulose conversion over a 20Ni-26ZnO/CNT catalyst.....	140
Figure 50 - Plots of the HA yield and the sum of yields as a function of time for the cellulose conversion over a 20Ni-26ZnO/CNT catalyst.....	141
Figure 51 – SEM and TEM pictures of the 20Ni-26ZnO/AC (incipient) catalyst.....	142
Figure 52 - SEM and TEM pictures of the 20Ni-26ZnO/AC (incipient) catalyst	143
Figure 53 - SEM and TEM pictures of the 20Ni-26ZnO/AC (pechini) catalyst	144
Figure 54 - SEM and TEM pictures of the 20Ni-26ZnO/AC (pechini) catalyst	145
Figure 55 - SEM and TEM pictures of the 20Ni-26ZnO/AC (pechini) catalyst	146
Figure 56 - SEM and TEM pictures of the 20Ni-26ZnO/AC (pechini) catalyst	147
Figure 57 – DTG and TG cor. (from TGA) as a function of temperature for the CNT #1N support.....	151

Figure 58 - DTG and TG cor. (from TGA) as a function of temperature for the CNT #2N support.....	152
Figure 59 - DTG and TG cor. (from TGA) as a function of temperature for the CNT #1D support.....	153
Figure 60 - CO ₂ -TPD: TCD signal as a function of temperature for the 30Ni-26ZnO/CNT-red300 catalyst.....	154
Figure 61 - CO ₂ -TPD: TCD signal as a function of temperature for the 30Ni-26ZnO/CNT-red350 catalyst.....	154
Figure 62 - CO ₂ -TPD: TCD signal as a function of temperature for the 30Ni-26ZnO/CNT-red400 catalyst.....	155
Figure 63 - CO ₂ -TPD: TCD signal as a function of temperature for the 30Ni-26ZnO/CNT-red450 catalyst.....	155

List of symbols and abbreviations

Symbol	Units	Explanation
EG		Ethylene Glycol
1,2-PG		1,2-Propylene Glycol
1,2-But		1,2-Butanediol
Man		Mannitol
Sor		Sorbitol
Ery		Erythritol
HA		Acetol
λ	nm	X-Ray wavelength
Θ	°	Bragg diffraction angle
D	%	Dispersion
M	g/mol	Molecular weight
m	g	Mass
n	mol	Number of mol
#		Number
P	atm/ bar/mm Hg	Pressure
T	°C/K	Temperature
V	cm ³ /mL	Volume
X	%	Conversion
V_p	cm ³ /g	Pore Volume
W	Kg*m ² /s ³	Power
M		Metal
R		Alkyl group
M(OR)_x		Metal alkoxides with x being the valence state of M
ROH		Alcohol

1. Introduction

At the present time scientists all over the world are faced with challenges related to the growing energy demand as a result of the increasing population. Predictions presented in the IE02011 (International Energy Outlook 2011) by the U.S. EIA (Energy Information Administration) expect that the energy consumption worldwide will increase from 505 quadrillion Btu in 2008 to 770 quadrillion Btu in 2035, thus an increase of 53% is predicted [1]. This major increase is mainly due to the economic growth and expanding populations in the developing countries in the world, with China and India as the two nations growing fastest. According to the IE02011 their combined energy consumption will more than double, and account for 31% of the total world energy consumption in 2035. With this in mind, there is a widespread concern about the depletion of fossil fuels, the environmental consequences of increasing concentrations of CO₂ and other greenhouse gases in the atmosphere, and the production of the required amount of energy to cover the world's increasing energy demand [2]. As a result, research related to alternative fuels has gained attention from governments in many countries in the world during the last decade. The IE02011 predicts that renewable fuels will be the fastest-growing source of world energy from 2008 to 2035, with an average increase of 2,8 % per year [1]. In addition to the fuel industry, the replacement of petroleum derived chemicals, such as EG and 1,2-PG, with products derived from renewable biomass is highly desirable in order to reduce the environmental impacts from production and/or disposal. An integrated biomass refinery with the production of fuels and chemicals would therefore be an interesting option from an economic and environmentally friendly perspective [3]. Up to date, the biomass-derived fuels successfully implemented in the transportation sector are biodiesel and starch-derived ethanol, however these fuel types compete with food industry in terms of resources and area. In a world where hunger and malnutrition are the number one risk to the health worldwide [4], a production of fuels that threatens food industry is hard to justify. Thus a renewable feedstock which is non-competitive with food industry is necessary. Non-edible lignocellulosic biomass (such as forestry wastes) could be the solution as this renewable and abundant supply of biomass consumes CO₂ during growth, and can guarantee a stable production of liquid transportation fuels if the methods and infrastructure can be sufficiently advanced in the future. The composition of lignocellulose is dependent on the biomass feedstock, and consists of cellulose, hemicellulose and lignin, as illustrated in Figure 1 [3]. Cellulose and hemicellulose represent the carbohydrate fraction of lignocellulose, and occupies 40-50% and 25-35% of the biomass feedstock respectively, while lignin is the minor component with its 15-20% [5]. Lignin, with its amorphous 3D-polymer structure (based on the three main units illustrated in Figure 1), is the most complex fraction in lignocellulose, which makes it more difficult to process than the two other fractions. As a result lignin has typically been treated as a waste stream, however the potential for production of important aromatics from the upgrading of lignin has recently become of interest [3]. Hemicellulose and cellulose on the other hand are easier to process than lignin, and especially the amorphous polymer hemicellulose is

relatively easy to crack. Cellulose is slightly more difficult due to hydrogen bonds between the chains [5]. Since cellulose is the most abundant biomass on earth [6] it is being considered as one of the most promising feedstocks for the sustainable production of chemicals and fuels. Therefore many studies, including this master thesis, start with cellulose as feedstock for the evaluation of catalysts for biomass conversion. As the catalyst development proceeds, the cellulose feedstock should be replaced with lignocellulosic material in order to create an environment suitable for industrial use.

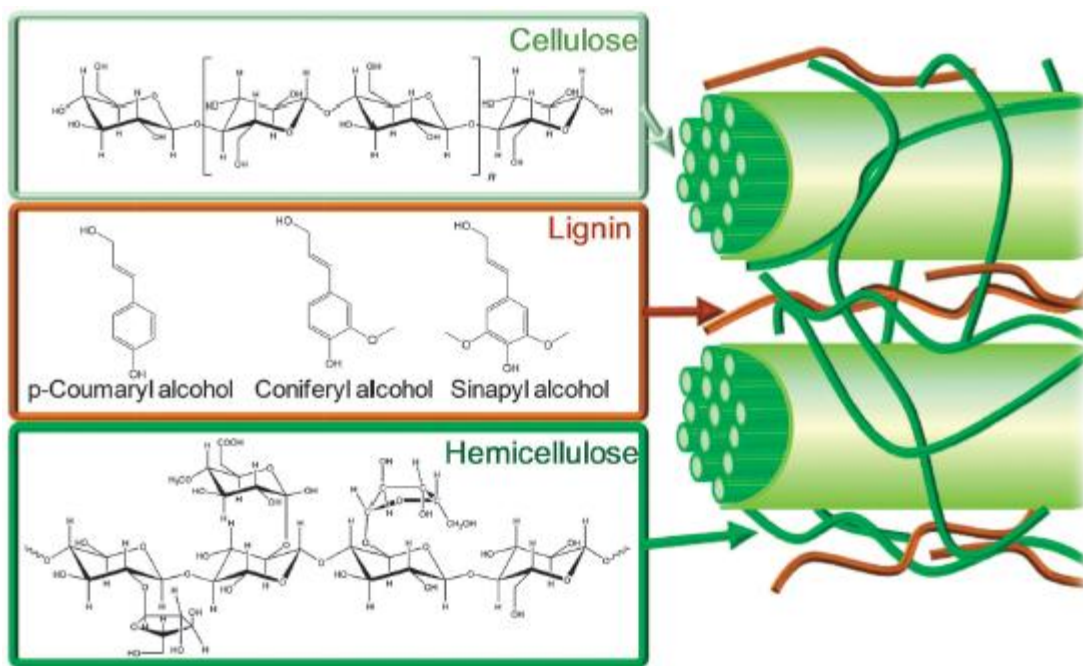


Figure 1 - The structure of lignocellulosic biomass with cellulose, hemicelluloses and lignin represented, adapted from ref. [3]

2. Background and Theoretical Concepts.

2.1 Conversion of lignocellulosic biomass

2.1.1 Lignocellulosic biomass to fuels and high-value chemicals

As a result of the increasing interest in a sustainable production of liquid fuels, a variety of processes have been studied in the literature. Detailed reviews related to the thermal and aqueous phase pathways for the conversion of biomass to liquid hydrocarbon fuel have been published by Professor James A. Dumesic's group [3, 7]. In general, the main advantage with the thermal routes, pyrolysis and gasification, is the ability to utilize all three components of the lignocellulose (even the complex lignin component). The downside is that these processes require high temperature which leads to poor control of the chemical structure in the product mixture. Thus a broad molecular weight distribution is obtained in the product mixture, and the selectivity is low. Additional steps are therefore necessary to remove impurities from the mixture prior to the upgrading process to the high molecular weight alkanes in liquid fuels [7]. The catalytic aqueous phase pathways on the other hand, can be processed under milder reaction conditions, which allows high selectivity and therefore high-purity organic streams can be produced. The main advantage with the catalytic aqueous phase routes is the selectivity towards the desired product(s), while a significant drawback is the lack of ability to convert the entire lignocellulosic feedstock. Unlike the thermal routes, the catalytic aqueous phase routes are at the present time only able to convert the sugar fraction, cellulose and hemicellulose, in the lignocellulose. Therefore expensive pretreatment steps to hydrolyze solid lignocellulose to aqueous sugars and separate the lignin fraction are necessary [7]. Another promising approach for the sustainable production of fuels (and high-value chemicals) from lignocellulosic biomass is the one-pot catalytic transformation to polyols. A state-of-the-art description of this process is given in the following section. In this pathway, the selectivity towards a certain polyol is the key aspect, and the catalyst choice should therefore be chosen carefully. The product could either be used as a chemical itself or be upgraded to liquid fuels. There is a significant difference in the atom economy related to the transformation of cellulose to fuels and the transformation of cellulose into important oxygenates, such as EG and 1,2-PG. The latter preserves the oxygen-containing functional groups in cellulose, and is therefore highly atom-economic [8]. Ethylene Glycol (EG) and Propylene Glycol (1,2-PG) are important renewable chemicals because of their extensive application in the plastic industry, food industry and in the pharmaceutical industry. At the present time, fossil-based resources are utilized for the production of EG, which dominates the market compared to other polyols [8]. As oppose to the production of oxygenates, the catalytic conversion of cellulose to fuels require oxygen removal (e.g. C-O hydrogenolysis, dehydration, hydrogenation) in order to satisfy the low O/C ratio in fuels. High molecular weight alkanes are required for transportation fuels, therefore the mixture derived from the one-pot conversion of biomass has to undergo C-C coupling reactions

(such as oligomerization, aldolcondensation and ketonization) in addition to the removal of excess oxygen [9]. The one-pot conversion of biomass to polyols and the subsequent upgrading process to fuels are both based on complex catalytic systems and are therefore being studied in two individual master thesis at NTNU the spring of 2013. Herein, the focus will be on the first step, the one-pot conversion of cellulose.

2.1.2 State of the art - One-pot conversion of biomass

The catalytic one-pot conversion of cellulose into sugar alcohols was first demonstrated by Fukuoka et al. [10], and since then this route has become one of the most promising routes for the sustainable production of polyols and liquid fuels. In 2008, Ji N. et al. [11] developed a catalytic system based on a nickel-promoted tungsten carbide catalyst for the production of EG from cellulose. Under hydrothermal conditions, at temperatures above 503 K, hydrolytic hydrogenolysis of cellulose was carried out in the presence of the Ni-W₂C/AC catalyst, and EG was formed as the main product. Further studies were done to improve the understanding of this nickel-promoted tungsten carbide catalyst, and in 2012, Changzhi Li et al. achieved an advance in the catalytic conversion of raw woody biomass to polyols [12]. The previously developed Ni-W₂C/AC catalyst converted cellulose and hemicelluloses to EG and other diols with a total yield as high as 75,6 %. Additionally, the lignin component was converted to monophenols with a yield of 46,5 %. Degradation mechanisms from cellulose, hemicellulose and lignin were suggested, and the formation of EG and 1,2-PG involve hydrolysis, retro-aldol condensation, dehydration and hydrogenation reactions. Two noteworthy trends related to the catalytic activity and the choice of lignocellulosic feedstock were reported in this study. The 1,2-PG yield increased with the hemicellulose content, and a high amount of lignin present in the feedstock lead to low degradation and thus low activity, which supports previous findings for corn stalk conversion [13]. Even though the selectivity towards diols obtained over the Ni-W₂C/AC catalyst is excellent, the stability remains a challenge because W₂C is a subject to oxidation under hydrothermal reaction conditions [11, 14]. Further studies of the nickel-promoted tungsten catalyst were done in order to improve the stability of the catalyst. For instance, the traditional activated carbon support was replaced with mesoporous carbon, which improved the resistance to deactivation and increased the selectivity towards EG to 72,9% [14]. The EG yield over the mesoporous carbon-supported WC_x catalyst decreased by 15 % over four repeated runs, while more than 50% was lost over the active carbon-supported WC_x catalyst. This improvement can partially be ascribed to the 3D interconnected mesoporous structure, which allows a high tungsten carbide dispersion and facilitates transportation [8]. In another study, Ming-Yuan Zheng et al. [15] investigated the synergistic effect between nickel and tungsten, and as a result a series of highly active M(8,9,10)-W bimetallic catalysts were developed for the conversion of EG from cellulose. While tungsten affected the degradation of cellulose, the hydrogenation reactions of unsaturated intermediates were

controlled by the transition metals. Thus the selectivity towards EG can be tuned by the weight ratio of M(8,9,10) to W. The highest EG yield, 76%, was achieved over a SBA-15 supported Ni-W bimetallic catalyst. However, the collapse of the mesoporous structure of SBA-15 support makes it impossible to reuse the catalyst [8]. A stable catalyst for the one-pot conversion of cellulose is necessary if the process is going to be scaled up for industrial use. Therefore it was a great achievement when Zhijun Tai et al. in 2012 [16] reported their development of a temperature-controlled phase-transfer catalyst system based on a combination of tungsten acid (H_2WO_4) and an activated carbon supported Ru catalyst (Ru/AC), as illustrated in Figure 2. The catalyst dissolves in hot water and under hydrothermal reaction conditions it promotes the hydrolysis and C-C cleavage reactions of cellulose, which leads to the formation of glycoaldehyde which is subsequently hydrogenated to EG over the Ru/AC catalyst. An EG yield up to 54,4 % was reported. The fascinating and unique advantage with this newly developed catalyst system is the superior stability, which allows more than 30 runs before a remarkable decrease in the EG yield is observed [8]. The excellent reusability of this catalytic system makes it attractive for commercial use, and as illustrated in Figure 3, the combined tungsten acid and Ru/C catalyst is superior to the previous mentioned W_xC/AC and $2Ni-W_2C/AC$ catalysts. The combination of outstanding reusability and cheap, commercially available tungsten acid [16] gives reason to believe that industrial production of EG in the future could be based on the one-pot conversion of biomass over a combined tungsten acid and Ru/AC catalyst.

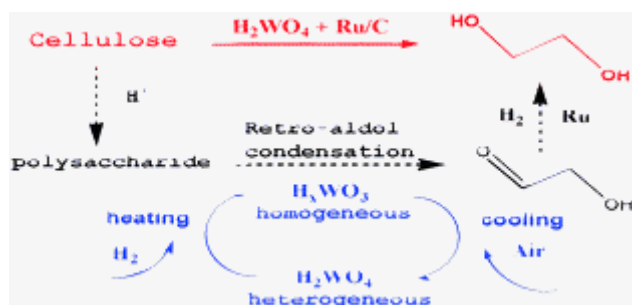


Figure 2 - Illustration of the reaction mechanism for cellulose conversion to EG over the combined H_2WO_4 and Ru/C catalyst. Red: The overall reaction. Black: The three consecutive reactions. Blue: The temperature-controlled phase behaviour of tungsten acid. Adapted from ref. [16]

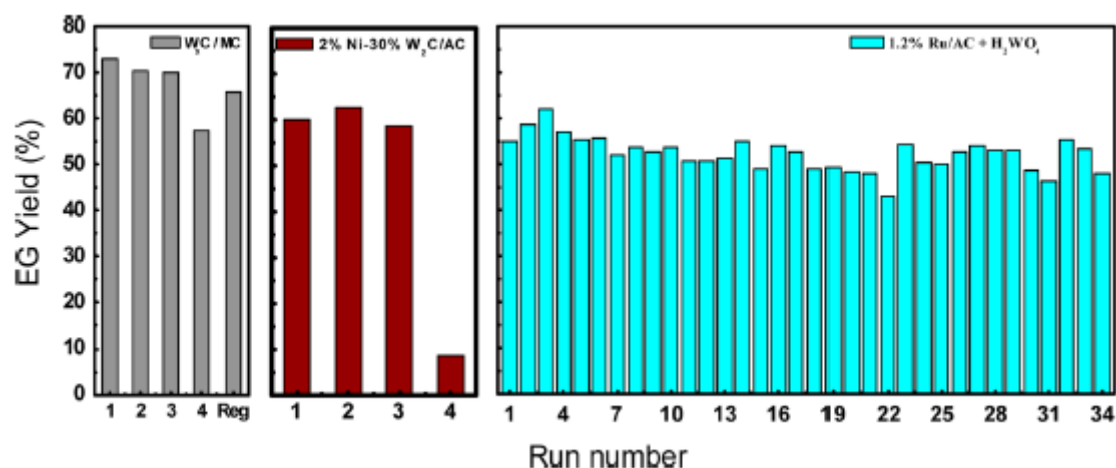


Figure 3 - Reusability of W₅C/MC, 2% Ni-W₂C/AC, and 1,2% Ru/AC + H₂WO₄ catalysts, adapted from ref. [8]

The tungsten based catalysts described above have been developed by scientists in Prof. Tao Zhang's group at DICP, and is, to the best of my knowledge, the most efficient catalysts for the one-pot conversion of cellulose to EG. However, as the interest in this process has increased during the last decade, other groups have also reported interesting findings related to EG production and especially the focus on 1,2-PG production from cellulose is relatively new. For instance, the selective conversion of cellulose to ethylene glycol, propylene glycol or sorbitol was reported by Yue Liu et al. in 2012 [17]. A catalytic system based on Ru/C in the presence of WO₃ was used for cellulose conversion under hydrothermal conditions, and the selectivity towards 1,2-PG is especially noteworthy with a yield as high as 30,7 %. According to the authors, the surface basicity of the AC support accelerated the isomerization reaction of glucose to fructose, while the WO₃ promoted both the hydrolysis of cellulose and C-C bond cleavage. It is easy to see similarities between this WO₃ and Ru/C system and the previous mentioned H₂WO₄ and Ru/AC system, which showed remarkable reusability results. The WO₃ and Ru/C system was only tested for 5 runs, therefore further studies related to reusability is necessary, however the similarities to the H₂WO₄ and Ru/AC system gives reason to expect good reusability results. Another study written by Zihui Xiao et al. [2] describes the conversion of cellulose to propylene glycol and ethylene glycol over a highly efficient CuCr catalyst. The highest 1,2-PG and EG yields achieved were 42,6 % and 31,6 % respectively when a co-catalyst, Ca(OH)₂, was added in addition to the CuCr catalyst. The cellulose conversion was carried out over the CuCr catalyst without the formation of coke-like precipitates, which makes it an interesting option for industrial scale-up. The findings related to the CuCr catalyst was published in 2013, therefore this new catalytic system for cellulose conversion is under further development. However, it is highly interesting for the future production of polyols. The last catalytic system for the one-pot conversion of cellulose that will be presented herein was recently developed by Xicheng Wang et al. [18], and reveals that a 20% Ni/ZnO catalyst can be used for the conversion of cellulose to 1,2-alkanediols with a glycol yield

up to 70,4%. Especially noteworthy is the high yield of 1,2-Propane Diol (1,2-PG), which was reported to be as high as 34,4 %. According to the NH₃-TPD and CO₂-TPD analysis, the Ni/ZnO catalyst possesses both acidic and basic sites. The authors suggested that the basic sites contribute to the activity and selectivity of the catalyst, while the acidic sites may not play a critical role under the reaction conditions used in the study. In the bifunctional ZnO-supported Ni catalyst, nickel promotes hydrogenation while ZnO is active for dehydration. The dehydration step is critical for the formation of intermediates from cellulose, and determines the overall conversion of cellulose. The conversion of cellulose at different reaction times showed that 2 h was enough to gain excellent performance over 20% Ni/ZnO. Correspondingly to the nickel supported tungsten catalyst, the drawback of the 20% Ni/ZnO catalyst is the relatively poor hydrothermal stability. The total glycol yield decreased from 70,4% to 62,0% in the second run, and further dropped to 45,6% in the third run. However, the product distribution did not change significantly. Xicheng Wang et al continued to develop the Ni/ZnO catalyst and investigated if the combination of Ni and Cu would promote the production of diols from cellulose. In a recent publication [19] this group reports that Ni-Cu/ZnO catalysts efficiently converts high-crystalline cellulose into polyols, primarily 1,2-alkanediols (up to 72,5 % selectivity with the main products 32,9 % 1,2-PD and 22,8 % EG). It is also confirmed that Cu/ZnO is an effective catalyst for the hydrogenolysis of glycerol to 1,2-PD as earlier reported in the literature [20]. A thorough stability study has not been reported for the ZnO-supported Ni-Cu catalyst yet, but at least the following three recycling tests gave similar conversion with a slight reduction in the 1,2-alkanediol selectivity, which is promising for further work.

A catalyst study based on the Ni/ZnO catalyst was done by the author of this report at NTNU (Norwegian University of Science and Technology) the fall of 2012, in which Ni-Zn oxide catalysts supported on carbon nanotubes were prepared for the conversion of cellulose to light oxides. The purpose of this project was to develop a preparation method suitable for the coating of ZnO on CNT-support and to carry out catalyst characterization of the Ni-ZnO/CNT catalysts. By using the Pechini method followed by incipient wetness impregnation a uniform ZnO-layer was coated onto the CNT support, and four catalysts with different ZnO-loading were prepared (26%, 28%, 40% and 46%). The Ni-loading was kept constant at 20wt% for all catalysts. The characterization results from S(T)EM and XRD measurements indicated that the ZnO-coating of the catalyst with 26% ZnO-loading had a uniform layer, while the catalysts with higher loading had a more uneven impregnation of ZnO. Herein the catalytic performance of these four Ni-ZnO/CNT catalysts was tested, and based on the results further studies were done in order to improve the Ni-ZnO/CNT catalyst for the one-pot conversion of cellulose.

2.2 Carbon Nanofibers

2.2.1 History

Carbon nanofibers (also known as carbon filaments) have been mentioned in the literature for more than a century, and the attitude towards these fibers has drastically changed from negative to positive. In 1889, a method for the growth of carbon filaments was reported by Hughes & Chambers [21], in which an iron catalyst and carbon containing gases were used. However, the appreciation and industrial importance of these fibers did not occur until years later. The development of the Transmission Electron Microscope made it possible to analyze the structure of the carbon filaments, and in 1952, Radushkevich & Lukyanovich reported the first TEM evidence of hollow nano-sized carbon fibers with diameter 50 nm, as mentioned in [22]. Until the 1980s, the growth of carbon nanofibers was considered harmful to catalysts and reactors. The problem was that carbon nanofibers unintentionally were grown during important reactions involving a metal catalyst and carbon-containing gases, such as Fischer-Tropsch or steam-methane reforming, which lead to catalyst deactivation and severe damage to the reactor walls [23]. Due to these difficulties a lot of research was done to be able to understand the formation of carbon nanofibers. Even though the purpose of these studies was to suppress the formation of carbon nanofibers, the results have proven to be very useful in the field of nanotechnology. In 1985, the third form of ordered carbon, buckminsterfullerene C₆₀, was discovered by Kroto et al. [24]. The discovery of buckminsterfullerene C₆₀, commonly known as fullerenes, was an unexpected finding during laser spectroscopy experiments, and involved laser vaporisation of carbon which resulted in a stable cluster of 60 carbon atoms. Before this revolutionary discovery, ordered carbon was only known in the structure of diamond, which consists of neighbouring carbon atoms with strong covalent bonding, and graphite, which is made up of layers of hexagonal arrays of carbon. C₆₀ on the other hand, is shaped like a soccer ball, and consists of carbon atoms bonded in hexagonal and pentagonal configurations [25]. Fullerene chemistry has since its discovery in 1985 become a research field of great interest, and in 1996, Robert F. Curl, Jr., Richard E. Smalley, and Sir Harold W. Kroto were honoured with the Nobel Prize in chemistry for “their discovery of fullerenes” [26]. In addition to graphite, diamond and C₆₀, carbon nanofibers is another form of carbon which finally captured the attention of researchers worldwide in the 1990`s. The famous publication by Iijima in 1991 [27], in which MWNTs (multi-walled nanotubes) were formed on the negative electrode during an arc-discharge evaporation method for the preparation of fullerenes, triggered an enormous focus on carbon nanofibers and nanotubes [23]. A year later, in 1992, Ebbesen and Ajayan reported large-scale synthesis of graphitic nanotubes using a version of the common arc-discharge technique for fullerene synthesis [28]. Then, in 1993, SWNTs (single-wall nanotubes) were reported by both Iijima and Ichihashi [29] and Bethune et al. [30]. The latter research team observed that covaporizing carbon and cobalt in an arc generator resulted in single-walled carbon nanotubes with diameters approximately 1,2

nm. Iijima and Ichihashi on the other hand, used two vertical electrodes filled with a small piece of iron in an arc-discharge chamber, and a gas mixture of argon (40 torr) and methane (10 torr) filled the evaporation chamber. The single-walled carbon nanotubes were grown in the gas phase and the diameters were about 1 nm. Pictures from both publications are presented in Figure 4a (Iijima and Ichihashi) and Figure 4b (Bethune et al).

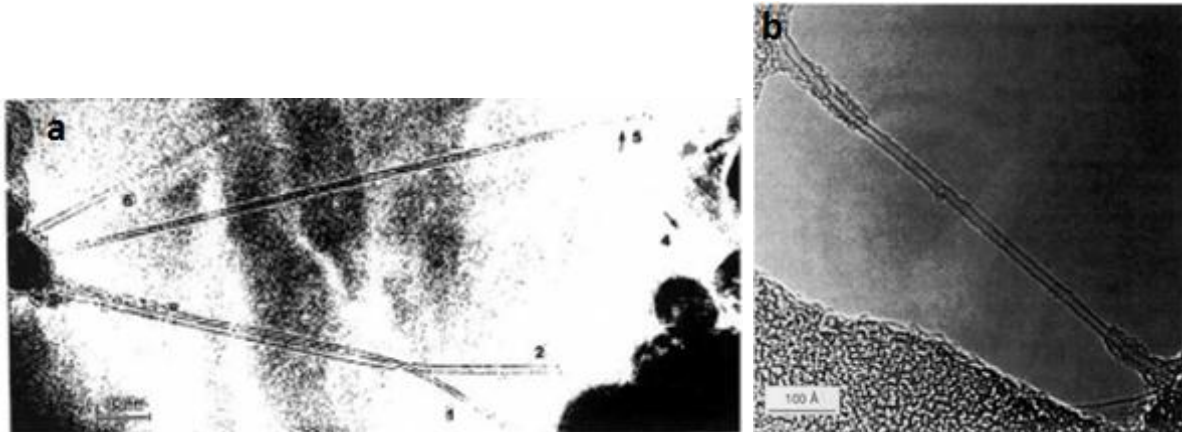


Figure 4 - a: Electron micrograph revealing individual single-shell nanotubes. The tube labelled 1 has a diameter equal to 0,75 nm, and tube 2 is 1,37 nm in diameter. The picture is adapted from ref [29] b: TEM image of a section of a single-walled nanotube, adapted from ref. [30]

The growing interest and knowledge related to carbon nanofibers have already resulted in numerous solutions for the improvement of technology in a variety of fields, including material science, nanotechnology, electronics, architecture and optics [31]. The catalytic conversion from biomass to fuels and other chemicals is no exception, in which carbon supports such as CNF and CNT have gained attention due to their unique properties facilitating metal dispersion and mass transfer[32]. These properties are further discussed in section 2.2.3, and are two of many advantages related to CNTs and CNFs support for catalysts used in liquid phase biomass conversion.

2.2.2 Growth of carbon nanofibers

The general mechanism for the growth of carbon nanofibers is given in Figure 5, and involves the catalytic decomposition of carbon-containing gases (such as methane, carbon monoxide, synthesis gas (H_2/CO), ethyne, and ethene) on small metal surfaces. The hydrocarbon from the gas decomposes on the metal surface under the formation of carbon with concomitant desorption of hydrogen. Next, the carbon diffuses from the metal surface to the interface on the other side, where it precipitates as graphite. The growth continues at the interface of the initial nucleation of graphite, and finally a carbon nanofiber is formed [23].

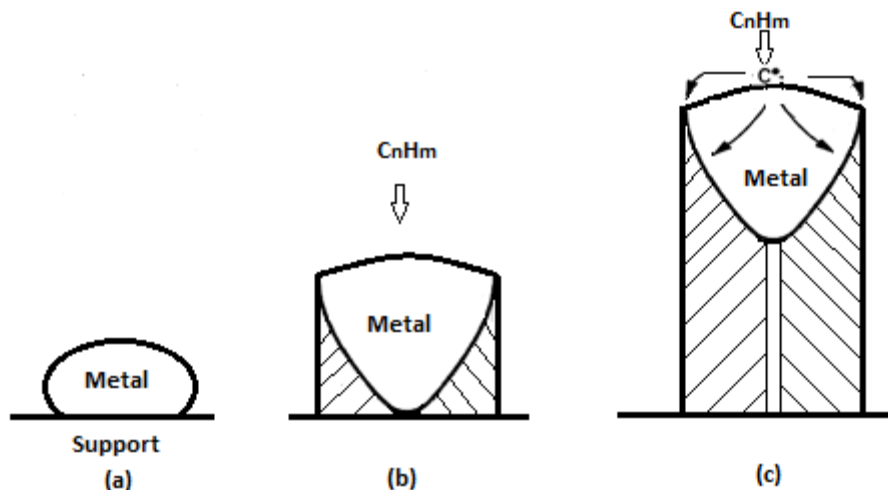


Figure 5 - Illustration of the metal-catalyzed growth of a carbon nanofiber from gaseous hydrocarbons.

Carbon nanofibers consist of stacked and curved graphene layers, and can be divided into three categories according to the angle between the graphene layer and the fiber axis: platelet-type ($\alpha=90$), ribbon- or tubular-type ($\alpha=0$), and fishbone-type ($0<\alpha<90$) [32, 33], as illustrated in Figure 6. The structure of platelet carbon nanofibers is made up by graphene layers perpendicular to the fiber axis, while the tubular carbon nanofibers (carbon nanotubes) and the ribbon carbon nanofibers both consist of graphene layers that are parallel to the fiber axis. The difference between the latter two fibers is that the tubular-type is made up by cylindric graphene layers (single or multiple carbon nanotubes, SWNT and MWNT) and the ribbon-type consists of straight, unrolled graphene layers with non-cylindrical cross-sections. In the fishbone-type fibers, the graphene layers are inclined with respect to the fiber axis, and these fibers can have either a hollow core or a solid core [34]. The surface structure and surface chemistry of the carbon nanofibers can be controlled to a certain degree by the growth conditions and catalyst choice [35]. The growth of parallel carbon nanofibers (ribbon or tube) typically involves an iron catalyst, while the growth of fishbone-type fibers mainly has been reported with nickel catalysts. In general, metal catalysts based on iron, cobalt and nickel are the most common catalysts for the growth of graphitic carbon nanofibers [23].

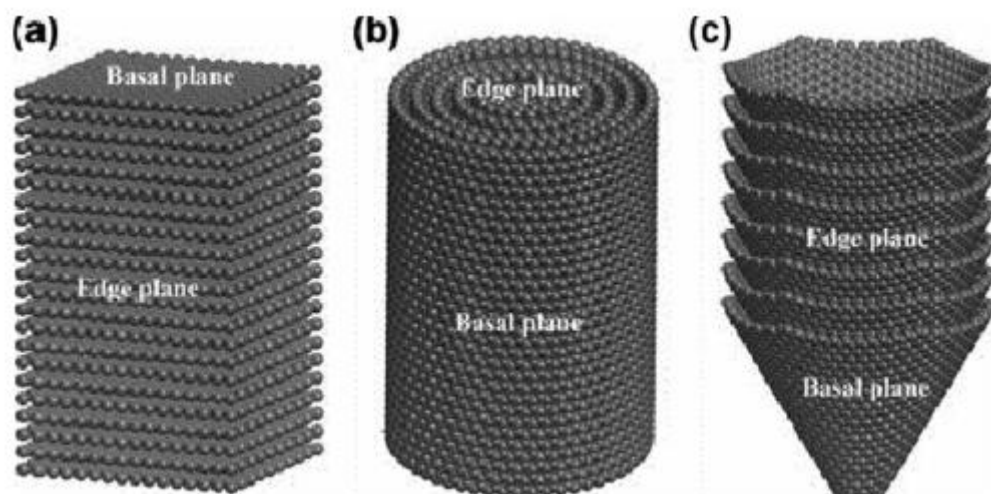


Figure 6 - Structures of different categories of CNFs: a) platelet CNFs, b) ribbon or tube CNFs, and c) fishbone CNFs, adapted from ref. [33]

2.2.3 Carbon nanofibers as catalyst support material

In liquid-phase catalysis, carbon is often used as support material for heterogeneous catalysts, and especially activated carbon has been used widely in this field. However, there are some challenges related to activated carbon support, such as reproducibility, microporosity and filtration time. Carbon nanofibers on the other hand, are reproducible on a large scale and additionally better filterable than activated carbon [23]. Due to these advantages carbon nanofibers is an interesting alternative to activated carbon support. In this section, the use of carbon nanofibers as catalyst support is briefly discussed. First of all, the ability to tailor the surface structure and properties of CNFs makes it a potential support material for a broad selection of catalytic systems. As mentioned in section 2.2.2, carbon nanofibers can be synthesized to structures containing a large number of edges, which can function as anchoring sites for catalyst precursors. The edge structure also impacts the proton affinity of the carbon nanofibers in the following order: platelet>fishbone>tube. Additionally, carbon nanofibers typically have tunable surface functional groups that will affect the proton affinity [32]. Second, carbon nanofibers are mesoporous and provide large surface area [23], which makes them suitable as support material for reactions where mass-transfer limitations can be a challenge, such as in 3-phase systems. The conversion of cellulose is typically carried out by using high pressures of hydrogen in an autoclave, which has been preloaded with water, cellulose, and a solid catalyst. The mass-transfer in this slurry-system could therefore benefit from the use of mesoporous carbon nanofibers as oppose to traditional activated carbon support. Additionally, the filtration step to retrieve catalyst will be faster with CNF support as mentioned above. A third advantage related to CNFs support is the possibility of interactions between metal atoms and the carbon nanofiber surface, thus the catalyst will also possess electrical properties. By manipulating these metal-

support interactions, it is possible to tailor the redox potential for metal catalysts. In addition, the interactions between the metal and support will influence the dispersion and stability of the catalyst [32]. The ability to tailor these structural and electronic properties of carbon nanofibers make them suitable for rational catalyst design, as recently suggested by Jun Zhu et al [32]. In their publication, a schematic representation of CNFs as platform for catalyst design was proposed, as illustrated in Figure 7. Basically, you start out with the primary structure (such as platelet-, fishbone- or tubular CNFs), and then move on to secondary properties such as electronic properties, proton affinity, surface area and porosity. Finally you evaluate the possible applications for the catalyst based on the primary and secondary properties. With this in mind, it is clear that carbon nanofibers is an interesting support material for many catalytic systems.

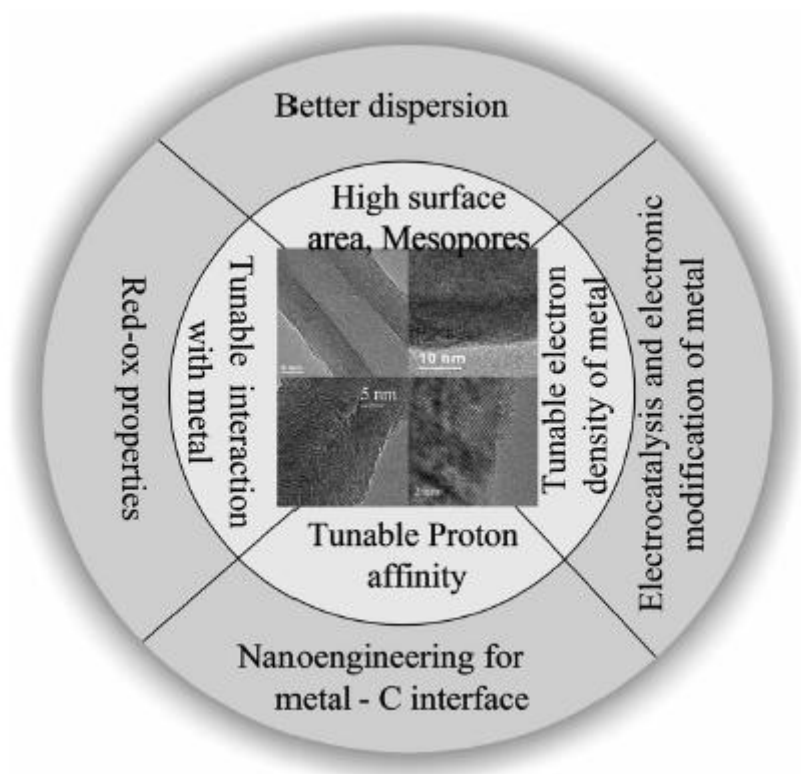


Figure 7 - The principles for rational catalyst design by using CNFs as a platform, adapted from ref. [32]

2.3 Oxide coating

2.3.1 Introduction

Lignocellulosic biomass can be converted to a variety of products, thus the choice of catalyst and reaction conditions will determine the selectivity of the process. Catalyst performance, such as selectivity, activity and stability, is highly dependent on the catalyst synthesis, therefore the preparation method should be chosen carefully. A variety of synthesis methods [36], such as electrostatic adsorption, impregnation, deposition-precipitation, sol-gel, co-precipitation, chemical vapour deposition, etc. can be used for catalyst preparation. Among which, impregnation is the most common method used for the preparation of supported metal catalysts [37]. For the preparation of Ni-ZnO/CNT catalysts, incipient wetness impregnation, electroless plating, sol-gel and the Pechini method might be suitable preparation methods, and each of these synthesis routes are presented in the following sections.

2.3.2 Incipient wetness impregnation

Incipient wetness impregnation is a simple and commonly used preparation method for the synthesis of metal oxides [37]. First, the pore volume of the support is empirically determined by typically measuring the amount of water necessary to wet the powder (support). Water (or another relevant liquid) is slowly added and thus occupies more and more of the pore volume, and finally the pores are completely filled up and the surface starts to look wet. Second, a solution (typically aqueous) with the active precursor(s) is prepared in a volume corresponding to the previous determined pore volume of the support. The solution is subsequently impregnated onto the support. It is important that the solution and the support is mixed very well in order to get an even impregnation [38]. The final steps transform this precursor into its active phase and typically involve drying, calcination and/or reduction [37].

2.3.3 The electroless plating method

The electroless plating method is often used for catalyst preparation because it has the ability to deposit many metals on a variety of substrates [39]. Originally, the term electroless plating was used by Brenner and Riddell for the process of plating metallic substrates with nickel or cobalt alloys without the use of an external source of electric current [40]. However, these days the term is being used for any process that continuously deposits metal from an aqueous medium. A typical electroless nickel plating process involves a source of nickel ions, a reducing agent, suitable complexing agents, stabilizers/inhibitors and energy (heat). The process is characterized by the selective reduction of nickel ions at the surface of a catalytic substrate, which is immersed into an aqueous solution of metal ions. The continuous deposition on the substrate is catalyzed by the substrate itself, which is why this process is referred to as

autocatalytic [40]. In 1997, Qunqing et al. reported the formation of one dimensional nanoscale composite based on the Ni-coating of CNT by the electroless plating method, which is now considered an effective and common method for the formation of nanotube/metal systems and especially Ni/CNT catalysts [41-44]. Considering that electroless nickel plating is the most important catalytic plating process used in industry today [40], and that many reports describe the successful preparation of Ni/CNT catalysts by electroless plating, this method might be suitable for the preparation of Ni-ZnO/CNT catalysts.

2.3.4 The Sol-gel method

Another preparation method that could be suitable for the preparation of Ni-ZnO/CNT catalysts is the Sol-gel method. This method is often used to prepare metal oxides, and involves a hydrolysis reaction and a polymerization reaction of metal precursors in liquid phase. In principle, the sol-gel process involves the formation of a gel due to attractive forces between particles in a sol. The liquid in the wet gel is removed by either evaporative drying or supercritical drying (in pressure and temperature beyond the critical point) which results in a dry material referred to as the xerogel or aerogel respectively [45]. An illustration of the sol gel process is given in Figure 8.

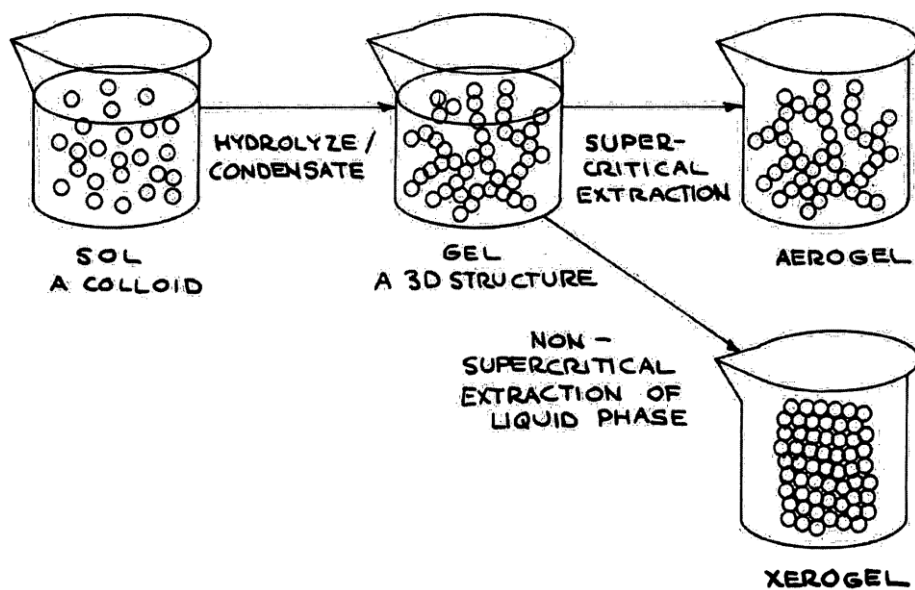


Figure 8 - The main steps in the sol gel process, adapted from ref. [46]

The sol-gel process for the preparation of metal oxides typically involves metal alkoxides ($M(OR)_x$) as the starting material(s), because they are soluble in alcohol and easily hydrolyzed to the corresponding hydroxide. The hydrolysis reaction follows the reaction presented below:



where M is the metal, R is an alkyl group (such as $-CH_3$, $-C_2H_5$, $-C_3H_7$ or $-C_4H_9$), ROH is an alcohol and x is the valence state of M. The hydrolysis reaction could either be completed, which means that all the -OR will be replaced by -OH (Eq. 2), or stop as the metal remains partially hydrolyzed, $M(OR)_{x-n}(OH)_n$.



One of the main advantages of the sol-gel process is that the initial solution contains both the metal(s) precursor and the support precursor(s). This gives it an advantage compared to the common commercial preparation methods for supported metal catalysts, which usually process the preparation of the support and the distribution of the active metal precursor on the support as two separate steps [45]. In addition to the convenience of lowering the amount of production steps, the possibility of introducing the metal(s) during the formation of the support leads to advantages such as superior homogeneity, high dispersion and improved thermal stability [47]. Because all the components can be added to the solution during the sol-gel step, this method is especially suitable for the preparation of bimetallic catalysts with single or mixed oxides as supporting material, as well as carbon support [45].

2.3.5 The Pechini method

Another possibility one should consider when the objective is to obtain a successful oxide coating is the Pechini method, which is a modified Sol-gel process involving the formation of a 3D polymer resin of a metal complex with subsequent calcination at elevated temperature to obtain the oxides [37]. The origin of the Pechini method is dated back to the Pechini patent in 1967 [48], when it was first used for the production of thin film capacitors. This technique is based on the in situ polymerization of monomers in a solution combined with a suitable metal precursor. First, an aqueous solution of suitable oxides or salts is mixed with an alpha-hydroxy-carboxylic acid, typically CA (citric acid). Second, chelation, or the formation of complex ring-shaped compounds around the metal cations, takes place in the solution. Third, a polyalcohol, such as EG or PEG is added which establishes linkages between the chelates by a polyesterification reaction, and as a result gelation of the reaction mixture occurs. After drying, the gel is finally heated to initiate pyrolysis of the organic species, and ultimately a mixed oxide is obtained [49]. Thus the key step in the Pechini method is the in situ polymerization between CA (citric acid) and EG (ethylene glycol), which leads to the formation of a metal citrate complex. The general steps in polymerization process in the Pechini method is illustrated in Figure 9.

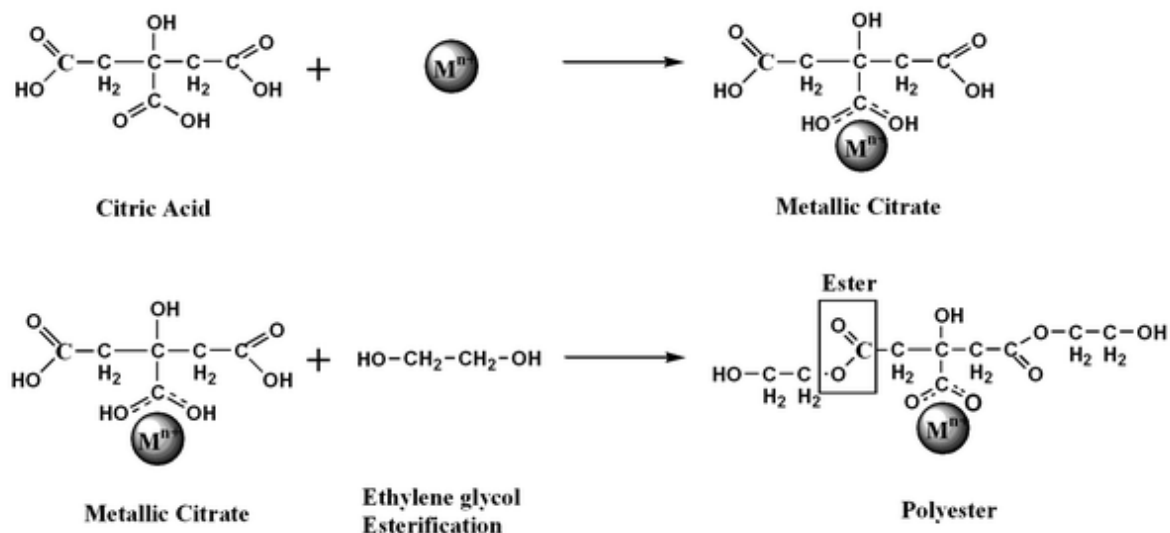


Figure 9 - The general scheme of the polymerization process in the Pechini method, adapted from ref. [50]

Based on the previous work done by the author at NTNU [51], the pechini method combined with subsequent incipient wetness impregnation can be used to obtain an even oxide coating of ZnO on carbon nanotubes, as demonstrated by the S(T)EM pictures in Figure 10.

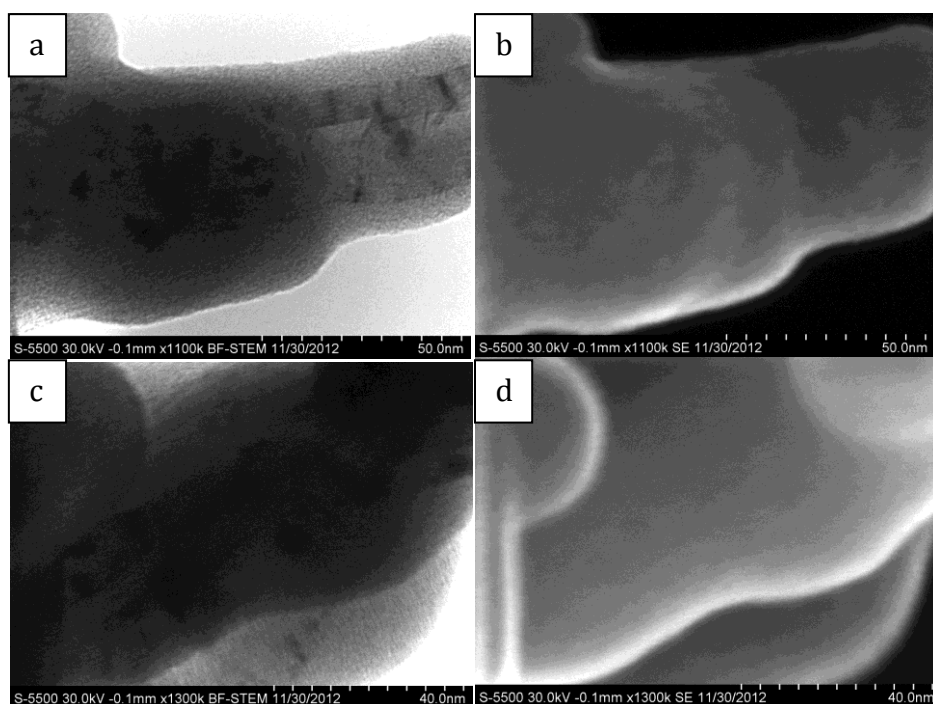


Figure 10 - Bright field STEM (a,c) and secondary electrons (b,d) at 50 nm of a 26ZnO/CNT catalyst prepared by the pechini method and subsequent incipient wetness impregnation.

3. Catalyst Preparation and Characterization

3.1 An overview of the catalyst preparation

In this master thesis, Ni-ZnO catalysts with carbon support have been investigated for the conversion of cellulose. The different steps in the catalyst preparation method are summarized in Figure 11.

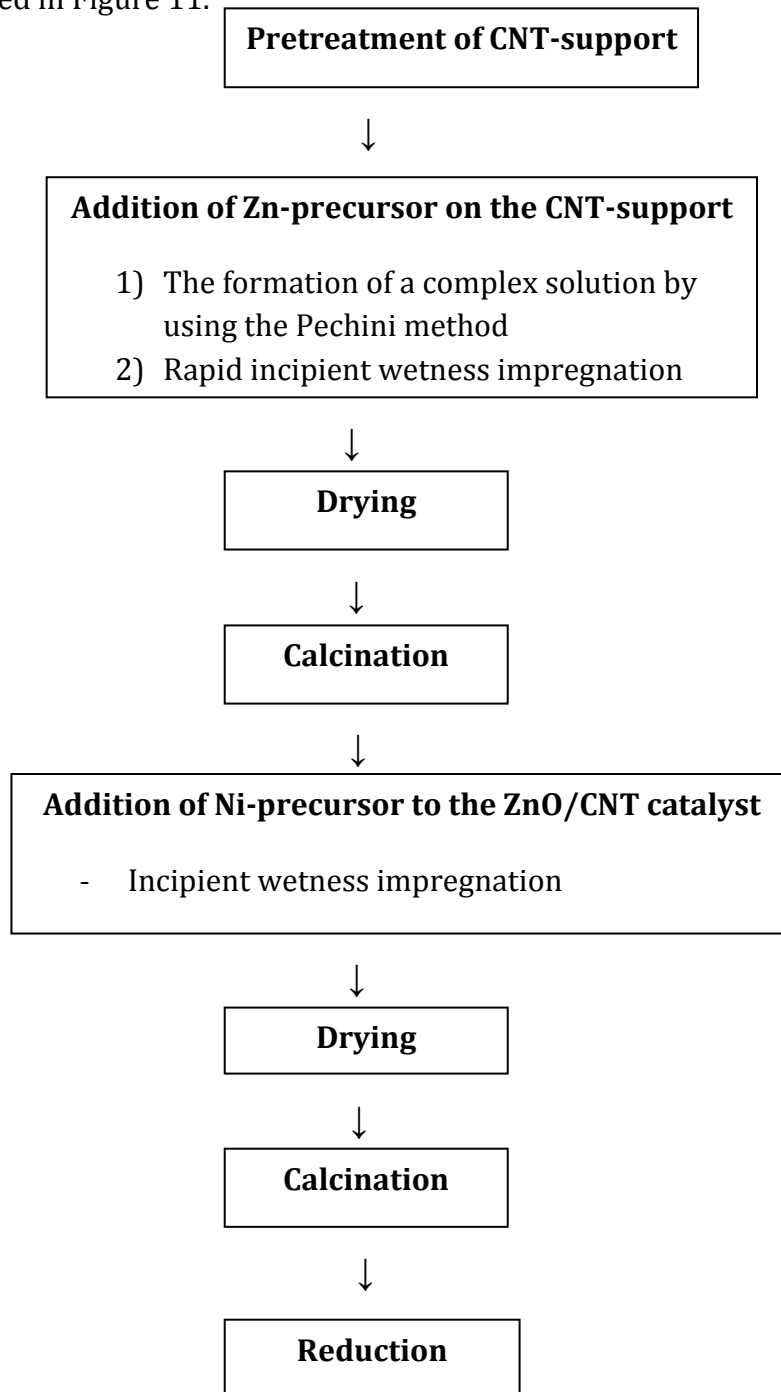


Figure 11 – Overview of the preparation steps for the Ni-ZnO/CNT catalyst

As illustrated in Figure 11 the main steps in the preparation of Ni-ZnO/CNT catalysts involve the pretreatment of the support, impregnation of Zn- and Ni-precursor onto the support, calcination and reduction. The details related to each of these steps are presented in the following sections. In order to give the reader a quick overview of the catalysts prepared and tested in this study, a summary is given in Table 1. The four first catalysts (#1-4) were prepared by the author at NTNU the fall of 2012 as part of her specialization project [51], and brought to DICP for activity tests. Catalyst number 5-8 was prepared to investigate the different components in catalyst number 1 (20Ni-26ZnO/CNT). Catalyst number 9-11 was prepared to compare activated carbon support with CNT-support. Catalyst number 12-16 was prepared to study the effect of Ni-loading, and finally catalyst number 16-19 was prepared to investigate the effect of different reduction temperature.

Table 1 - An overview of the catalysts prepared and tested herein: Catalyst name, Preparation method and Reduction temperature is given for each catalyst

#	Catalyst name	Preparation method	Reduction temp. [°C]
1	20Ni-26ZnO/CNT	Pechini method + Incipient wetness	400
2	20Ni-28ZnO/CNT	Pechini method + Incipient wetness	400
3	20Ni-40ZnO/CNT	Pechini method + Incipient wetness	400
4	20Ni-46ZnO/CNT	Pechini method + incipient wetness	400
5	20Ni/CNT	Incipient wetness	400
6	26ZnO/CNT	Pechini method + Incipient wetness	400
7	Ni/ZnO A	Incipient wetness	400
8	Ni/ZnO B	Incipient wetness	400
9	20Ni-26ZnO/AC (pechini)	Pechini method + Incipient wetness	400
10	20Ni-26ZnO/AC (incipient)	Incipient wetness	400
11	20Ni/AC	Incipient wetness	400
12	5Ni-26ZnO/CNT	Pechini method + Incipient wetness	400
13	10Ni-26ZnO/CNT	Pechini method + Incipient wetness	400
14	15Ni-26ZnO/CNT	Pechini method + Incipient wetness	400
15	25Ni-26ZnO/CNT	Pechini method + Incipient wetness	400
16	30Ni-26ZnO/CNT-red300	Pechini method + Incipient wetness	300
17	30Ni-26ZnO/CNT-red350	Pechini method + Incipient wetness	350
18	30Ni-26ZnO/CNT-red400	Pechini method + Incipient wetness	400
19	30Ni-26ZnO/CNT-red450	Pechini method + Incipient wetness	350

3.2 Pretreatment of the carbon supports

3.2.1 CNT

The commercial CNTs (Chengdu Organic Chemicals Co. Ltd) were pretreated with nitric acid (65%) in order to remove remaining growth catalyst and other impurities from production. The pretreatment was carried out according to the procedure used in the previous work related to the Ni-ZnO/CNT catalyst [51]. Approximately 10 g of CNTs were treated with 250 mL nitric acid at 100 °C for 1 hour, and the acid treatment was repeated 3 times. The CNTs were subsequently filtrated and washed with deionized water, and finally dried at 110°C overnight. In total 3 batches of CNT were pretreated, of which two batches were prepared at NTNU and one batch was prepared at DICP. The CNTs are correspondingly referred to as CNT #1N, CNT #2N and CNT #1D.

3.2.2 AC

The activated carbon support (Norit Company, the Netherlands) was pretreated with nitric acid (65%) at 80°C in order to remove impurities from production. Approximately 25 g of AC was mixed with 125 mL of deionized water, and 125 mL nitric acid (65%) was subsequently added to the solution. The acid treatment was carried out for 24 h at 80°C, according to the procedure used in [52]. After the treatment, the AC was dried at 110 °C overnight.

3.3 Preparation of the Ni-ZnO/CNT catalysts

3.3.1 Impregnation of Zn-precursor

The Zn-precursor was introduced to the pretreated CNT support by the Pechini method followed by rapid incipient wetness impregnation. The complex metal solution was prepared by mixing zinc nitrate hexahydrate, citric acid (CA), polyethylene glycol (PEG), and deionized water by ultrasonic treatment. The solution was immediately impregnated on the CNTs by incipient wetness impregnation, and dried at 110 °C overnight. The amounts of chemicals used for each catalyst and the calculations of loading can be found in Appendix A.

3.3.2 Calcination

In order to burn of the precursors from the complex solution and obtain ZnO/CNT catalysts, the impregnated CNTs were calcined for 10 min in 10% O₂ in N₂ flow at 400°C. The heating rate used was 5 K/min, and both heating and cooling were done in N₂ flow.

3.3.3 Impregnation of Ni-precursor

Nickel(II)nitrate hexahydrate was impregnated on the calcined ZnO/CNT catalysts by incipient wetness, and the catalysts were dried at 110°C overnight. Different amounts of nickel was loaded the catalysts, and subsequent calcination (at similar conditions to those described in section 3.3.2) was carried out to burn of the unwanted compounds in the Ni-precursor. The details related to the incipient wetness impregnation of Ni on the ZnO/CNT catalysts are given in Appendix B

3.3.4 Reduction

In general, the catalysts were reduced in pure Hydrogen flow for 5 hours at 400°C (flow rate: 63 mL/min, heating rate: 2K/min), with subsequent passivation in 1%O₂/N₂ flow for 2 hours. Additionally, four 30Ni-26ZnO/CNT catalysts were prepared to study the effect of reduction temperature. The detailed information related to the reduction of these four catalysts is given in Table 2.

Table 2 - Reduction conditions for the reduction of the 30Ni-26ZnO/CNT catalysts

Catalyst name	Heating rate [K/min]	Reduction temperature [°C]	Reduction time [h]	Flow rate [mL/min]
30Ni-26ZnO/CNT-red300	2	300	5	63
30Ni-26ZnO/CNT-red350	2	350	5	63
30Ni-26ZnO/CNT-red400	2	400	5	63
30Ni-26ZnO/CNT-red450	2	450	5	63

3.4 Preparation of the AC-supported catalysts

Three catalysts with activated carbon support were prepared in order to compare AC with CNT as support material for the Ni-ZnO catalysts. One 20Ni-26ZnO/AC catalyst was prepared by the pechini method with subsequent incipient wetness impregnation (referred to as 20Ni-26ZnO/AC (pechini), while another 20Ni-26ZnO/AC catalyst was prepared by incipient wetness impregnation (referred to as 20Ni-26ZnO/AC (incipient)). Additionally, a 20Ni/AC catalyst was prepared by incipient wetness impregnation. The calcination and reduction steps were identical to the procedure described in section 3.3.2 and section 3.3.4. The detailed amount of chemicals and the calculation of the ZnO- and Ni-loading for the activated carbon supported Ni-ZnO catalysts can be found in Appendix A and Appendix B.

3.5 Preparation of the different components in the 20Ni-26ZnO/CNT catalyst: 20Ni/CNT, 26ZnO/CNT and 20Ni/26ZnO.

In order to get a better understanding of the components in the 20Ni-26ZnO/CNT catalyst, 20Ni/CNT, 26ZnO/CNT and 20Ni/26ZnO catalysts were prepared. The 26ZnO/CNT catalyst was prepared according to section 3.3.1, and the chemicals used are given in Appendix A, as well as the calculation of ZnO-loading.

Additionally, a 20Ni/CNT catalyst and two batches of 20Ni/26ZnO catalyst were prepared by incipient wetness impregnation. The details can be found in Appendix B and Appendix C respectively.

3.6 Catalyst characterization

3.6.1 Temperature programmed desorption (TPD)

CO₂-TPD

CO₂-TPD was carried out to investigate the basic properties of the 30Ni-26ZnO/CNT catalysts. A MICROMERITICS AutoChem II 2920 automated Catalyst Characterisation System with a U-shaped quartz reactor was used, and helium was used as purge gas (PG). The samples (0,1 g) were heated to 300 °C (10K/min) in He flow (20mL/min), and kept at 300 °C for 1 hour. After the samples had cooled down to 80 °C, they were exposed to CO₂ (30 mL/min, PG: He30) by manually injecting CO₂ with a syringe. Injections were done until the peaks of adsorbed CO₂ recorded on the instrument were stabile. The samples were then purged with PG:30 for 4 hours. Finally, the samples were heated to 900 °C (10K/min) with PG: 30.

NH₃-TPD

NH₃-TPD measurements were done on the same instrument as for CO₂-TPD in order to test the acidic properties of the 20Ni-26ZnO/CNT catalyst. Helium was used as purge gas. The samples were heated to 200 °C (10K/min) in He flow (20mL/min), and kept at 200 °C for 30 minutes. After the samples had cooled down to 100 °C, they were exposed to NH₃ (30 mL/min, PG: He30) by manually injecting NH₃ with a syringe. Injections were done until the peaks of adsorbed NH₃ recorded on the instrument were stabile. The samples were then purged with PG:30 for 4 hours. Finally, the samples were heated to 900 °C (10K/min) with PG: 30.

3.6.2 N₂-adsorption measurements

The physical properties of the catalysts and support materials were investigated by N₂-adsorption measurements in a Micromeritics ASAP 2010 apparatus at -196 °C. Prior to the measurements, the samples were vacuumed and degassed. First, the empty tubes were vacuumed in fast mode until the qm Hg reached 005/006. The samples were then vacuumed in slow mode until the qm Hg were less than 500, and subsequently vacuumed in fast mode until the qm Hg reached 005/006. Next, the samples were degassed at 110 °C for 1 hour. The temperature was then increased to 300 °C, and the samples were degassed until the qm Hg reached 005/006. After the samples had cooled down to room temperature the analysis was conducted. The Brunauer-Emmett-Teller (BET) method was used to calculate the specific surface area, S_{BET} , and the pore size distribution was obtained from the N₂-adsorption branches of the isotherms using the Barrett-Joyner-Halenda (BJH) method.

3.6.3 X-Ray Diffraction (XRD)

XRD measurements were carried out with a PANalytical X'Pert-Pro powder X-ray diffractometer, using Cu K α monochromatized radiation ($\lambda=0,1541$ nm) at a scan speed of 5° min⁻¹. Diffractograms were obtained in the 2 θ range of 10-80° with a step size of 0.033° and a counting time of 19.7 s.

3.6.4 TGA

TG-DSC information was recorded by a Setaram Setsys 16/18 thermoanalyzer (Setaram, France). The samples were heated from room temperature to 1200 °C with a constant heating rate of 10K/min in air flow.

3.6.5 SEM and TEM

Transmission electron microscopy (TEM) was carried out with a Tecnai G2 Spirit (FEI) microscope at 120kV, while high-resolution transmission electron microscopy (HRSEM) was conducted with a Hitachi S5500. Prior to the analysis, a small amount of powder sample was dispersed in ethanol and a drop of the dispersion was placed on a Cu grid.

3.6.6 H₂-Chemisorption

Hydrogen Chemisorption was carried out in a Micromeritics AutoChem II 2920 automated Catalyst Characterisation System with a pulse chemisorptions mode. Prior to the measurement, the catalyst sample (100 mg) was reduced in pure hydrogen. A similar reduction procedure to the reduction described in section 3.3.4 was used with flow rate 20 cm³/min. After reduction at 400°C, the sample was purged in Ar flow for 1 h, and subsequently cooled down to 40°C. The gas flow was then switched to 10%H₂/Ar and the hydrogen chemisorption experiment was started. H₂ loop gas was used for each pulse, and several pulses were introduced until saturation. The amount of H₂ was recorded with a thermal conductivity detector (TCD), and the analysis was carried out in a temperature range of 50 – 900 °C.

3.6.7 Temperature programmed reduction (H₂-TPR)

Temperature programmed reduction (H₂-TPR) was carried out on the same instrument as for chemisorption. Prior to the measurements, the sample was pre-treated in Ar flow at 200°C (heating rate 10°C/min) for 30 minutes, and subsequently cooled down to room temperature. The gas was then switched from Ar to 10%H₂/Ar, and the sample was heated to 900°C with heating rate 10°C/min. The consumption of H₂ was measured with TCD.

3.6.8 ICP analysis

Inductively coupled plasma (ICP) analysis was carried out on an IRIS Intrepid II XSP instrument (Thermo Electron Corporation), and microwave treatment was done on MARS 240/50 (CEM Corporation) with power 800 W. The temperature was first increased from 20°C to 120°C with heating rate 10K/min, and kept at 120°C for 2 min. The temperature was then further increased to 200°C (80K/min) and kept at 200°C for 20 min.

3.7 Activity measurement – Conversion of cellulose

The catalytic conversion of cellulose was carried out in a stainless-steel autoclave (Parr Instrument Company, 75 ml). The reactor was loaded with cellulose (0,25 g), catalyst (0.075 g), and water (25 mL), and purged with hydrogen gas 6 times. Then, 60 bar H₂ gas was introduced to the reactor at room temperature, and the stirring rate was set to 800 rpm. The reaction temperature was set to 245 °C (or 255°C in a few cases), the cooling water turned on and the heating system started. The fastest heating rate possible for the reaction system was used, which means that approximately 40 minutes heating was necessary to go from room temperature to 245°C. The reaction time used was 2,5 hours unless stated otherwise. After the reactor had cooled down to room temperature again, samples were taken (liquid and gas) and filtration was done to retrieve the catalyst. Reactions with sorbitol and mannitol as feedstock were also conducted according to the reaction conditions described above. For these reactions the ratios between feed, catalyst and water were identical to those used for cellulose conversion. The liquid-phase products were analyzed by external standard method with HPLC system (Agilent 1200, Shodex Sugar SC1011 column, differential refractive index detector (RID), water as mobile phase, flow rate: 0.6 ml min⁻¹, Inj Vol: 5.0 µl, RID opt T: 35 oC, Oven T:45 oC). The HPLC plots are given in Appendix D. The gas analysis was done in a gas chromatograph (Agilent 6890N, TDX-1 column, TCD detector). First, the temperature of the column was kept at 110°C for 2min. Then, the temperature was increased to 250 oC at a heating rate of 8 K/min and kept at 250 oC for 10min. Helium gas was used as carrier gas. The plots for the gas analysis and a table summarizing the results are given in Appendix E. The conversion was calculated according to Appendix F, based on weight calculations.

4. Results and Discussion

4.1 Outline

Chapter 4 is presented according to the chronological development during this master thesis, and a brief outline is given in this section. 1) The four Ni-ZnO/CNT catalysts from NTNU were tested for the conversion of cellulose (reaction time, reaction temperature, activity and selectivity). 2) The catalyst with the highest EG-yield was studied further and the different components of the catalyst (ZnO/CNT, Ni/CNT and Ni/ZnO) were investigated for the conversion of cellulose. 3) Activated carbon was tested as an alternative to carbon nanofibers as catalyst support. 4) Yield as a function of time was studied to reveal the mechanism for cellulose conversion via the Ni-ZnO/CNT catalyst. Additionally, sorbitol and mannitol feedstocks were used to confirm the mechanism. 5) The effect of different nickel loading was investigated. 6) Correlations between reduction temperature and basicity were studied. 7) The reusability of the Ni-ZnO/CNT catalysts was briefly tested.

4.2 Optimal reaction time for the Ni-ZnO/CNT catalysts

The 20Ni-26ZnO/CNT and 20Ni-40ZnO/CNT catalysts were tested for the catalytic conversion of cellulose in order to find the optimal reaction time for the selectivity towards EG and PG products. The reaction time was varied from 2 to 3 hours, and the product distribution is presented in Table 4. The results indicate that 2,5 hours is the ideal reaction time for these Ni-ZnO/CNT catalysts. For the 20Ni-40ZnO/CNT catalyst, the EG yield and PG yield increased from 27,8% and 12,8% to 31,0% and 13,8% respectively as the reaction time was changed from 2 hours to 2,5 hours. Similarly the EG yield and PG yield increased from 31,2% and 13,3% to 32,8% and 15,2% when the 20Ni-26ZnO/CNT catalyst was used. When the reaction time was further increased to 3 hours the EG and PG yields were constant for the 20Ni-40ZnO/CNT catalyst and only slightly changed for the 20Ni-26ZnO/CNT catalyst, therefore it seems like 2,5 hours is enough time to produce as much EG and PG as possible over the Ni-ZnO/CNT catalysts.

Table 3 - The Product distribution for the conversion of cellulose over Ni-ZnO/CNT catalysts as a function of reaction time^a

Catalyst	Conv.	EG	1,2-PG	1,2-But	Sor	Man	Gly	Ery	HA	Rx. time	Sum
20Ni-26ZnO/CNT	100	31,2	13,3	2,1	1,3	2,0	11,5	2,3	7,9	2	71,5
20Ni-26ZnO/CNT	100	32,8	15,2	2,9	1,1	1,5	14,4	1,6	8,7	2,5	78,2
20Ni-26ZnO/CNT	100	31,4	15,9	2,8	0,7	3,1	13,0	1,1	9,3	3	77,3
20Ni-40ZnO/CNT	100	27,8	12,8	2,4	1,2	1,9	15,6	2,7	7,8	2	72,2
20Ni-40ZnO/CNT	100	31,0	13,8	2,6	0,6	1,1	12,7	1,7	7,9	2,5	71,4
20Ni-40ZnO/CNT	100	31,0	13,9	2,8	0,7	3,1	11,6	1,4	8,2	3	72,7

a: The catalytic conversion of cellulose was carried out in a stainless-steel autoclave (75 mL). Cellulose (0,25g), catalyst (0,075 g), and deionized water (25 mL) were charged into the autoclave and stirred at a rate of 800 rpm. The pressure was 60 bar (RT) and the reaction temperature 245 °C.

4.3 The effect of higher reaction temperature

The temperature was increased from 245 °C to 255 °C in order to investigate the effect of higher temperature on the EG and 1,2-PG yields. The 20Ni-26ZnO/CNT catalyst was used for the conversion of cellulose, and the results are presented in Figure 12. The trend observed supports the previous findings of Likun Zhou et al. [53], and indicates that the PG yield increases with higher temperature, while the EG yield decreases. In their publication, Likun Zhou and co-workers studied the reaction temperature and how it affected the main product distribution in the conversion of Jerusalem artichoke tuber (JAT) (a fructose-based form of Biomass). The yields of EG and 1,2-PG were lower than 13% in the temperature interval 150-200°C, however, upon increasing the temperature above 200 °C the 1,2-PG yield increased sharply and reached its highest yield at 255°C. As illustrated in Figure 12, the highest 1,2-PG yield was also achieved at 255 °C when the 20Ni-26ZnO/CNT catalyst was used for the conversion for cellulose. As the reaction temperature was increased from 245 °C to 255 °C the 1,2-PG yield increased from 13,3 % to 15,8 % with reaction time 2 hours, while the EG yield decreased from 31,2 % to 27,9 %. Similarly the EG yield decreased from 32,8 % to 25,8 % when the reaction time used was 2,5 hours, and additionally a small increase in the PG yield was observed. This is an interesting observation since the two main polyols produced from the 20Ni-

26ZnO/CNT catalyst are EG, and 1,2-PG. Clearly a small change in temperature, 10 °C, will have a significantly negative effect on the EG yield, which is the main product with a selectivity over 30% when reaction temperature 245 °C is used. Based on the influence of the reaction temperature and reaction time (section 4.2) observed herein, the optimum reaction conditions for the selective production of EG from cellulose over an 20Ni-26ZnO/CNT catalyst is 2,5 hours at 245 °C (with an initial pressure of 60 bar hydrogen). These conditions were consequently used in the following experiments in this master thesis.

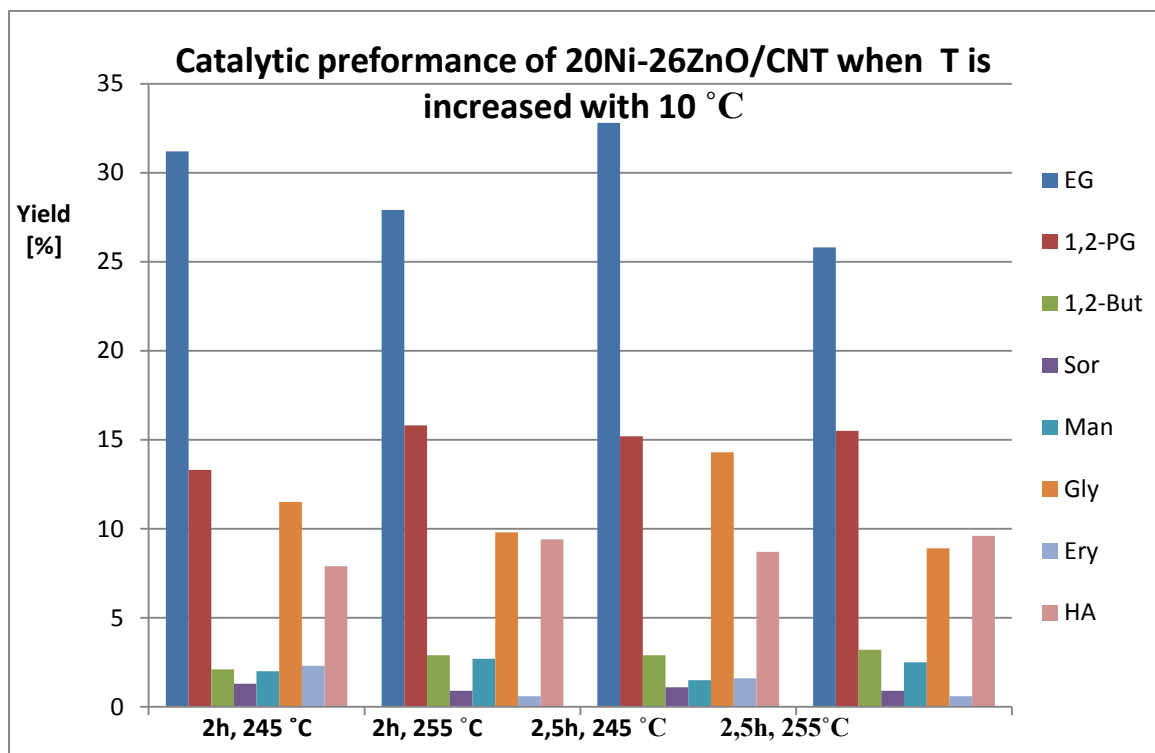


Figure 12 - The Product distribution for the conversion of cellulose over the 20Ni-26ZnO/CNT catalysts as a function of reaction temperature.

The catalytic conversion of cellulose was carried out in a stainless-steel autoclave (75 mL). Cellulose (0,25g), catalyst (0,075 g), and deionized water (25 mL) were charged into the autoclave and stirred at a rate of 800 rpm. The pressure was 60 bar (RT), the reaction temperature 245/255 °C, and the reaction time 2/2,5 h

4.4 Cellulose conversion over 20Ni-ZnO/CNT catalysts with different ZnO-loading

The catalytic performance of the four Ni-ZnO/CNT catalysts with different ZnO-loading (26%, 28%, 40%, 46%) was tested for the conversion of cellulose, according to the chosen reaction conditions in section 4.3. The product distribution from each reaction is given in Table 5, and the results indicate that the product distribution is quite stable and do not change significantly as the ZnO-loading is varied from 26 % to 46 %. The yields of the main products, EG and 1,2-PG, are approximately 31-32 % and 14-15 % respectively for all catalysts. The 20Ni-26ZnO/CNT catalyst provided the highest EG yield (32,8 %) and PG yield (15,2 %), and was therefore chosen for further studies in the following sections.

Table 4 - Product distribution for the conversion of cellulose over Ni-ZnO/CNT catalysts with different ZnO-loading^a

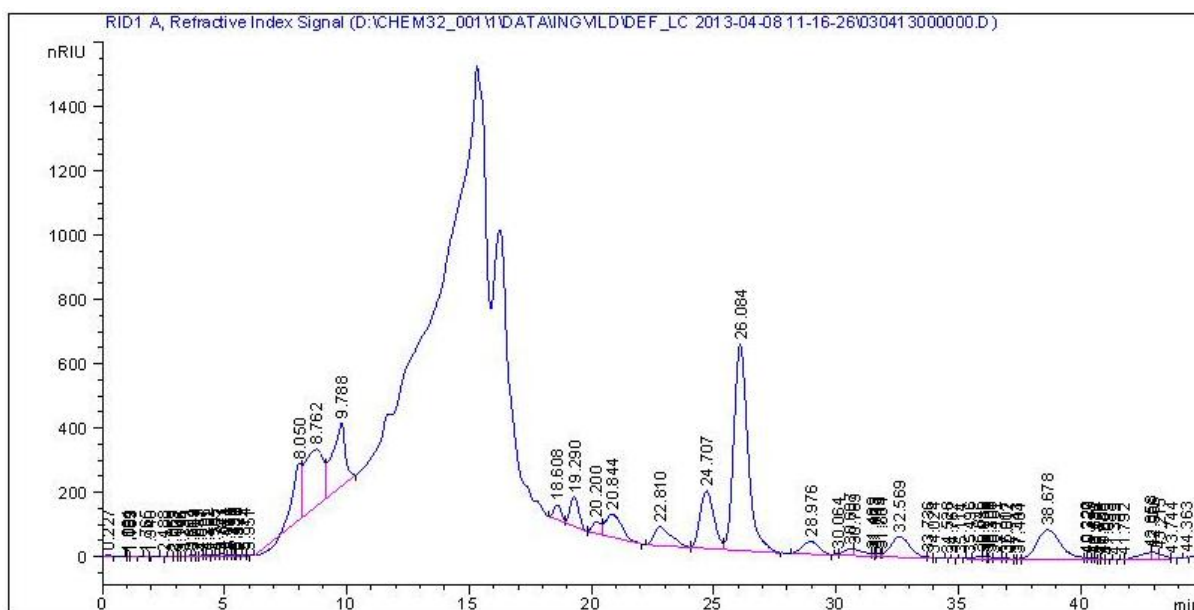
#	Catalyst	Conv.	EG	1,2-PD	1,2-BUT	Sor	Man	Gly	Ery	HA	Sum
1	20Ni-26ZnO /CNT	100	32,8	15,2	2,9	1,1	1,5	14,4	1,6	8,7	78,2
2	20Ni-28ZnO/CNT	100	32,1	13,8	2,7	0,6	0,7	11,3	1,5	7,8	70,6
3	20Ni-40ZnO/CNT	100	31,0	13,8	2,6	0,6	1,1	12,7	1,7	7,9	71,4
4	20Ni-46ZnO/CNT	100	31,3	14,0	2,8	0,6	0,9	12,4	1,7	8,1	71,8

a: The catalytic conversion of cellulose was carried out in a stainless-steel autoclave (75 mL). Cellulose (0,25g), catalyst (0,075 g), and water (25 mL) were charged into the autoclave and stirred at a rate of 800 rpm. The pressure was 60 bar (RT), the reaction temperature 245 °C and the reaction time 2,5 h.

4.5 Investigations of each component in the 20Ni-26,1ZnO/CNT catalyst: 20Ni/CNT, 26ZnO/CNT and 20Ni/26ZnO catalysts

4.5.1 Cellulose conversion

In order to get a better understanding of the 20Ni-26ZnO/CNT catalyst, the different components, 20Ni/CNT, 26ZnO/CNT and 20Ni/ZnO were prepared as described in section 3.4, and the catalytic performance of each component was tested for the conversion of cellulose. The 26ZnO/CNT catalyst (0,075 g), cellulose (0,25g) and 25 mL deionized water were loaded in a 75 mL autoclave, and the following conditions were used: initial hydrogen pressure of 60 bar, temperature 245 °C, reaction time 2,5 h and stirring rate 800 rpm. The results from the HPLC analysis, given in Figure 13, show that there is one broad peak, in which it is not possible to distinguish each product, and additionally one peak for acetol, which corresponds to an HA yield of 7,94. Since the 26,1ZnO/CNT catalyst does not contain any nickel it was expected that there would be no hydrogenation products in the product distribution, as confirmed by this test.



Next, the function of the 20Ni/CNT catalyst was tested for the conversion of cellulose, and the product distribution is compared with the results from the cellulose conversion over the 20Ni-26ZnO/CNT catalyst and given in Table 5. As oppose to the results when the 26ZnO/CNT catalyst was used (Figure 13), the 20Ni/CNT catalyst demonstrated hydrogenation properties and the product distribution was similar to when the 20Ni-26ZnO/CNT catalyst was used for the conversion of cellulose. However the yields were different. For instance, the EG yield, 1,2-PG yield and Gly yield were much lower (23,9 %, 7,4 % and 9,4 % respectively) when the 20Ni/CNT catalyst was used than when the ZnO-component was present in the 20Ni-26,1ZnO/CNT catalyst (32,8 % EG, 15,2 % 1,2-PG and 14,4 % Gly), which clearly demonstrates that there is a synergistic effect between the Ni and ZnO components. It is also noteworthy that the sorbitol and mannitol yields were as high as 9,5 % and 7,6 % (respectively) when the 20Ni/CNT catalyst was used, and as low as 1,1 % and 1,5 % when the 20Ni-26ZnO/CNT catalyst was used. This will be further discussed in section 4.6.

Table 5 - Product distribution for the conversion of cellulose^a over 20Ni-26ZnO/CNT and 20Ni/CNT catalysts

Catalyst	Conv.	EG	1,2-PG	1,2-BUT	Sor	Man	Gly	Ery	HA	Sum
20Ni/CNT	100	23,9	7,4	2,1	9,5	7,6	9,4	2,7	9,9	72,6
20Ni-26,1ZnO/CNT	100	32,8	15,2	2,9	1,1	1,5	14,4	1,6	8,7	78,2

a: The catalytic conversion of cellulose was carried out in a stainless-steel autoclave (75 mL). Cellulose (0,25g), catalyst (0,075 g), and water (25 mL) were charged into the autoclave and stirred at a rate of 800 rpm. The pressure was 60 bar (RT), the reaction temperature 245 °C and the reaction time 2,5 h.

Two batches of 20Ni/26ZnO catalysts were prepared by incipient wetness impregnation as described in section 3.5, and tested for the conversion of cellulose. The product distribution is given in Table 6. Also in this case, the sorbitol and mannitol yields are higher than for the cellulose conversion over the 20Ni-26ZnO/CNT catalyst. The yields of the other products are in general lower in comparison to the product distribution obtained over the 20Ni-26ZnO/CNT catalyst. There is one noteworthy difference in the product distribution for the two Ni/ZnO catalysts, the EG yield for Ni/ZnO A was as high as 28,9 %, while the EG yield for the Ni/ZnO B catalyst only was 23,9 %. These catalysts have been prepared by incipient wetness impregnation and identical amounts of ZnO-support, deionized water and Ni-precursor have been used. The significant difference in the EG yield implies that incipient wetness impregnation might not be an ideal preparation method for Ni/ZnO catalysts, and the performance of the final catalyst could

vary. Other preparation methods such as coprecipitation [18] have been reported with better catalyst performance for 20Ni/ZnO catalysts.

Table 6 – Product distribution for the conversion of cellulose over the Ni/ZnO catalysts^a

#	Catalyst	EG	1,2-PD	1,2-BUT	So r	Man	Gly	Ery	HA	Sum	Conv [%]
1	Ni/ZnO A	28,9	13,1	2,8	6,7	3,2	10,3	1,6	6,8	73,5	100
2	Ni/ZnO B	23,9	12,6	2,5	6,0	2,8	10,8	1,5	6,5	66,6	100
3	20Ni-26ZnO/CNT	32,8	15,2	2,9	1,1	1,5	14,4	1,6	8,7	78,2	100

a: The catalytic conversion of cellulose was carried out in a stainless-steel autoclave (75 mL). Cellulose (0,25g), catalyst (0,075 g), and water (25 mL) were charged into the autoclave and stirred at a rate of 800 rpm. The pressure was 60 bar (RT), the reaction temperature 245 °C and the reaction time 2,5 h.

4.5.2 BET measurements

The Brunauer-Emmet-Teller (BET) method was used to calculate the surface area of the 20Ni/CNT, 26ZnO/CNT and 20Ni/26ZnO catalysts, and the pore volume and pore size distributions were obtained from N₂-adsorption using the Barrett-Joyner-Halenda (BJH) method. The results are presented in Table 7, and clearly demonstrate the effect of CNT on the BET surface area. The CNT supported catalysts, 20Ni/CNT and 26ZnO/CNT, have BET surface areas of respectively 106,7 m²/g and 91,0 m²/g, while the ZnO-supported catalysts, Ni/ZnO A and Ni/ZnO B, have BET Surface areas as low as 10,6 0 m²/g and 10,4 0 m²/g respectively (The surface area of the ZnO-support was 52 m²/g). These low surface areas suggest that the Ni-dispersion on the Ni/ZnO catalysts is much poorer than the Ni-dispersion on the 20Ni/CNT, which could lead to lower glycol yields.

Table 7 – The results from the BET measurements for the 20Ni/CNT, 26ZnO/CNT and 20Ni/26ZnO catalysts

Catalyst	BET Surface Area [m ² /g]	Pore Volume [cm ³ /g]	Pore Size [Å]	t-Plot micropore volume [cm ³ /g]
20Ni/CNT	106,7	0,40	11,6	0,001
26ZnO/CNT	91,0	0,27	9,4	0,000
Ni/ZnO A	10,6	0,03	10,7	0,000
Ni/ZnO B	10,4	0,03	12,2	0,000

4.5.3 XRD

X-ray diffraction analysis was carried out to identify the components in the 20Ni/CNT, 26ZnO/CNT and 20Ni/26ZnO. Figure 14 illustrates the XRD patterns for Ni/ZnO catalyst A and B, and the peaks are identified as nickel, zinc oxide and nickel oxide. The nickel oxide peaks imply that the nickel in the catalysts is not fully reduced to metallic nickel. In general, the diffraction patterns of 20Ni/26ZnO A and 20Ni/26ZnO B are very similar, and it is not possible to distinguish an explanation for the different EG yields based on these results. The sharp peaks observed for both catalysts imply that the particle size is big.

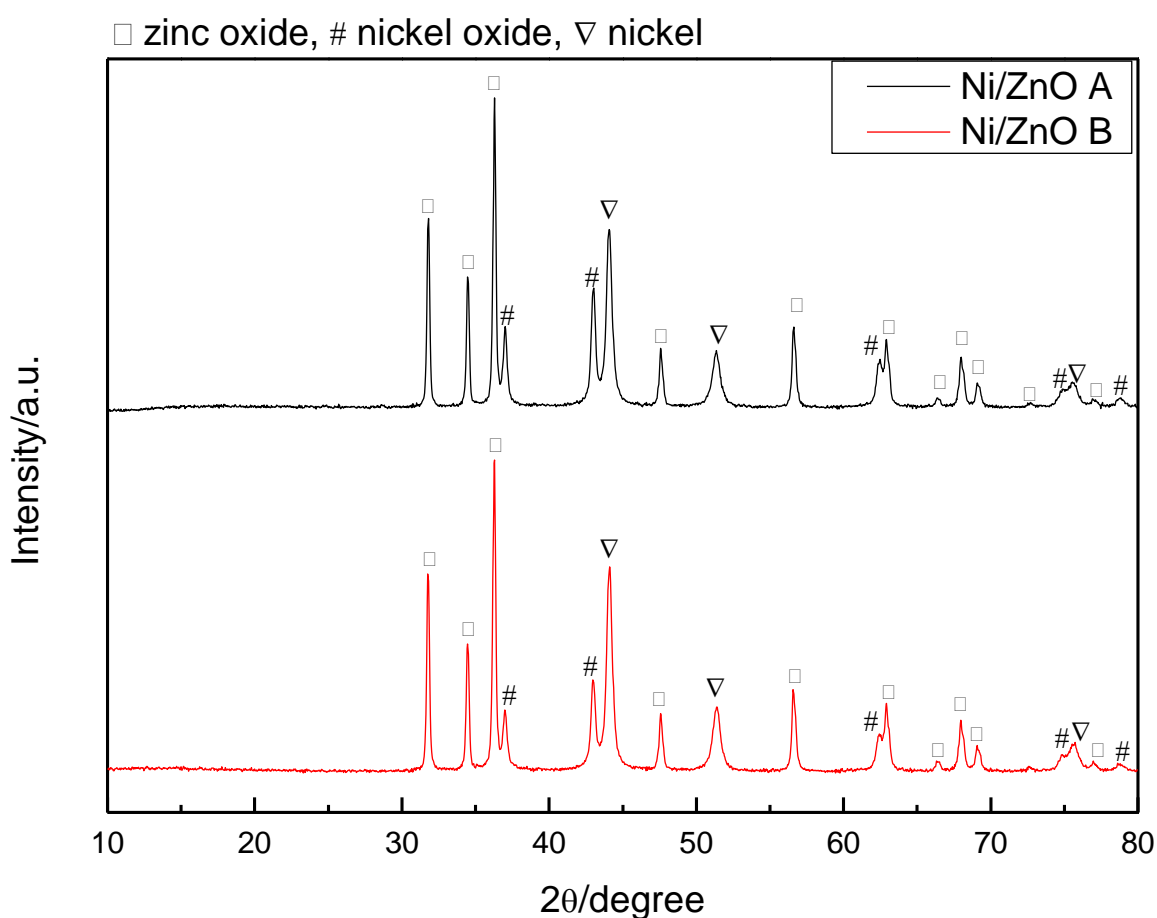


Figure 14 - The XRD patterns for Ni/ZnO catalyst A and B

Figure 15 illustrates the diffraction pattern for the 26ZnO/CNT catalyst. The first peak is recognized as carbon, and is followed by three large peaks for ZnO. As the 2θ /degree increases further, small peaks of nickel, nickel oxide and zinc oxide can be found. The XRD results for the Ni/CNT catalyst is presented together with the XRD results for the Ni/AC catalyst in section 4.7.4.

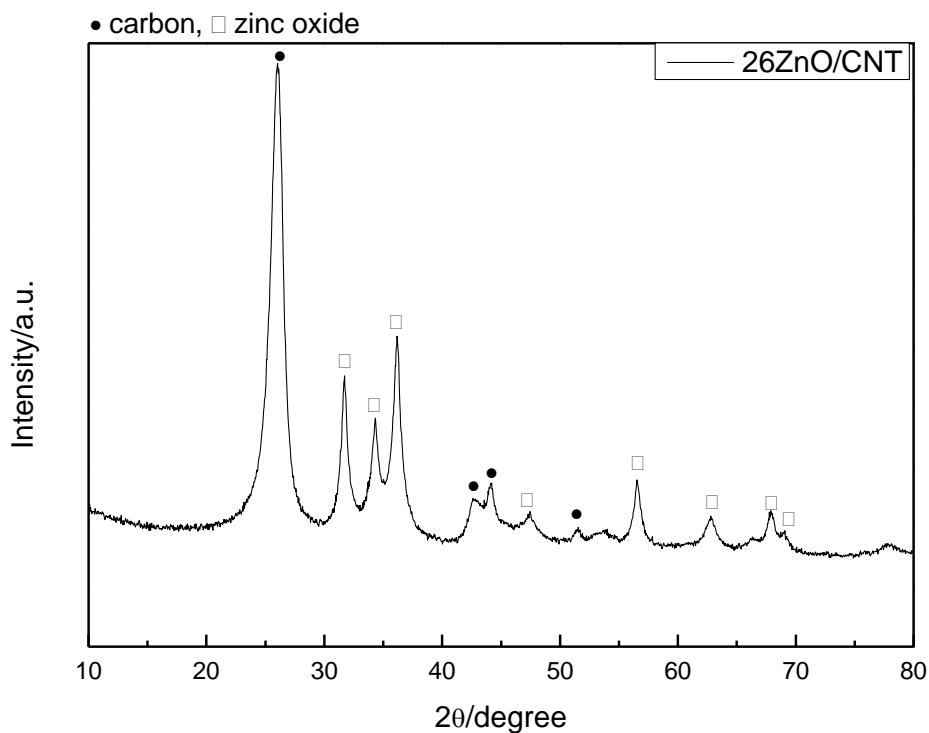


Figure 15 - The XRD pattern for the 26ZnO/CNT catalyst

4.6 The mechanism for cellulose conversion over the 20Ni-26ZnO/CNT catalyst

4.6.1 Sorbitol and Mannitol as feedstock

In the previous two sections, differences in the sorbitol and mannitol yields were reported for the conversion of cellulose over 20Ni/CNT, 20Ni/26ZnO and 20Ni-26ZnO/CNT catalysts. The latter produced sorbitol and mannitol in a very low amount compared to the 20Ni/CNT and 20Ni/26ZnO catalysts. To investigate these differences further the 20Ni-26ZnO/CNT catalyst was tested for the conversion of sorbitol and mannitol. Additionally a 2Ni-20WO₃/CNT catalyst, prepared by master student Cecilie Bjørgen according to [54], was used to demonstrate the different reaction pathways in the Ni-WO₃ system and the Ni-ZnO system. The product distribution is given in Table 8. The 20Ni-26ZnO/CNT catalyst have the ability to completely convert sorbitol and mannitol to EG and 1,2-PG, while the Ni-WO₃/CNT catalyst is not active for the conversion of sorbitol. In the reactions with sorbitol as feedstock, the 20Ni-26ZnO/CNT catalyst produced EG and 1,2-PG with yields 26,6% and 21,3% respectively, and the remaining sorbitol yield was as low as 0,5%. The Ni-WO₃/CNT catalyst on the other hand, only produced minor amounts of EG and 1,2-PG, 3,3 % and 2,0 % respectively, and the yield of the feedstock, sorbitol, was as high as 44,1 %. Clearly these catalytic systems follow different reaction pathways for the conversion of cellulose, and the results in Table 5 strongly indicate that sorbitol and mannitol are intermediates when cellulose is transformed to EG and 1,2-PG over the 20Ni-26ZnO/CNT catalyst. The mechanism for the tungsten-based catalyst on the other hand, has been studied previously [8], and involves three reactions in which cellulose is first hydrolyzed into cellooligosaccharides and glucose, then the sugar intermediates undergo C-C cleavage by retro-aldol reactions yielding glycolaldehyde which is subsequently hydrogenated into EG. The tungsten-based catalysts produce higher sorbitol and mannitol yields [55] than the CNT supported Ni-ZnO catalysts.

Table 8 - Product distribution for the conversion of mannitol and sorbitol over 20Ni-26ZnO/CNT and Ni-WO₃/CNT catalysts^a

#	Feedstock	Catalyst	EG	1,2-PG	1,2-BUT	Sor	Man	Gly	Ery	HA	Sum
1	Mannitol	20Ni-26,1ZnO/CNT	23,2	20,8	7,6	0,6	2,1	9,6	ND	ND	63,8
2	Sorbitol	20Ni-26,1ZnO/CNT	26,6	21,3	7,6	0,5	2,5	15,9	0,6	ND	75,0
3	Sorbitol	Ni-WO ₃ /CNT	3,3	2,0	ND	44,1	0,9	ND	1,7	ND	52,2

a: The catalytic conversion of sorbitol/mannitol was carried out in a stainless-steel autoclave (75 mL). Feedstock (0,25g), catalyst (0,075 g), and water (25 mL) were charged into the autoclave and stirred at a rate of 800 rpm. The pressure was 60 bar (RT), the reaction temperature 245 °C and the reaction time 2,5 h.

4.6.2 Yield vs. time

In order to reveal the mechanism for the cellulose conversion over the Ni-ZnO/CNT catalyst, an experiment to investigate yield as a function of time was carried out. According to the results discussed in the previous section, a likely pathway involves cellulose conversion into hexitols, sorbitol and mannitol, which subsequently undergo hydrogenolysis to form EG and 1,2-PG. To investigate this theory further 8 samples were taken during the conversion of cellulose over the 20Ni-26ZnO/CNT catalyst. As expected, a maxima for sorbitol and mannitol was found, and the yields of the two hexitols subsequently decreased to 0,7 % and 0,6 % respectively. This trend is illustrated in Figure 16.

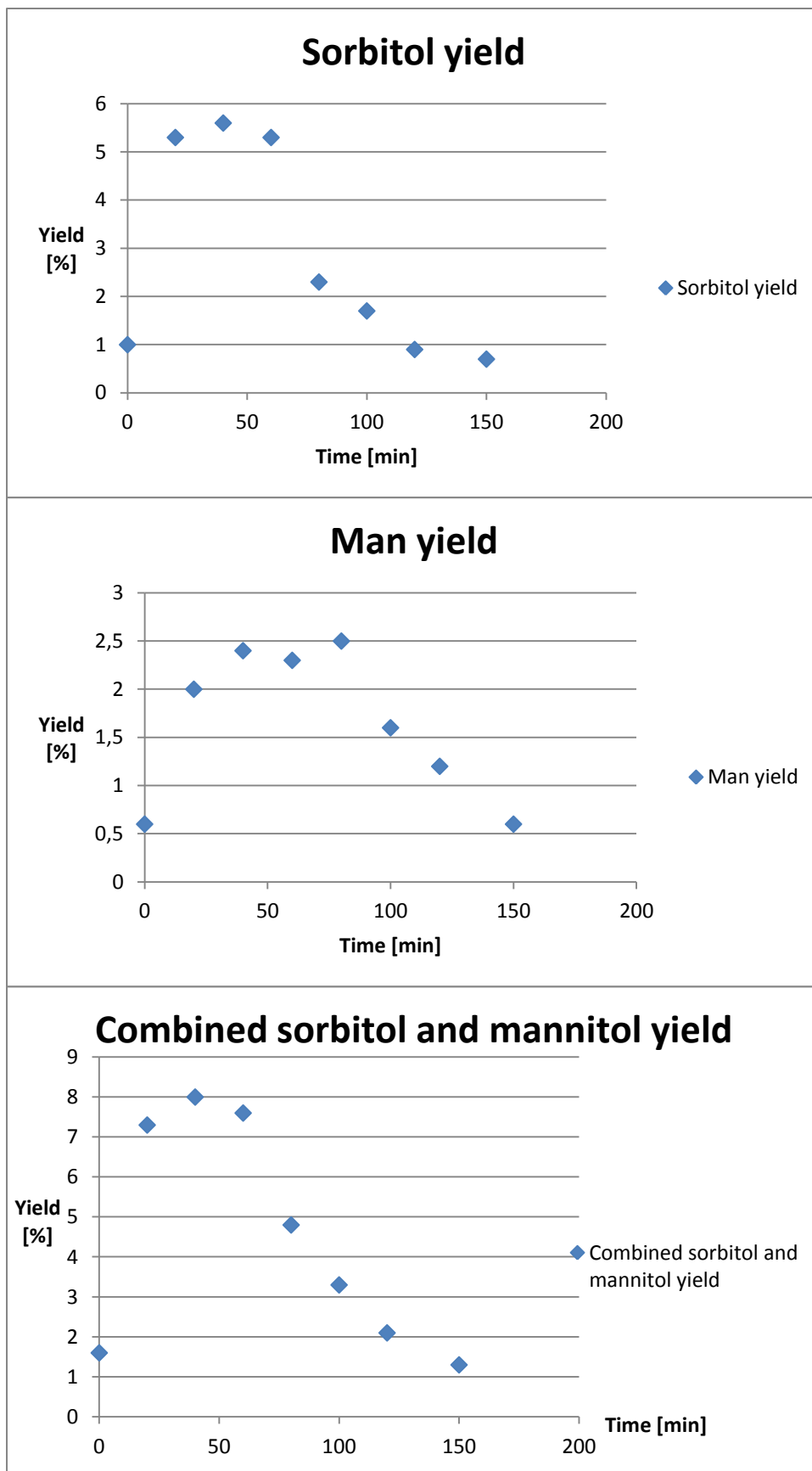


Figure 16 - Sorbitol and mannitol yields during the conversion of cellulose over a 20Ni-26,1ZnO/CNT catalyst. Reaction conditions: 60 bar (RT), 245 °C, rx. time: 2,5 h and stirring rate 800 rpm. 0,8015 g cellulose,0,2427 g 20Ni-26,1ZnO/CNT catalyst and 80 ml deionized water was mixed in an 300 mL autoclave reactor.

The yields for EG and 1,2-PG are compared with the hexitol (sorbitol and mannitol) yield in Figure 17, and clearly demonstrates how the hexitol yield decreases as the EG and 1,2-PG yields increases. Thus the suspicion of a reaction mechanism that occurs via hexitols is confirmed. With this in mind, it is likely that the main pathway in the cellulose conversion over the 20Ni-26ZnO/CNT catalyst happens from cellulose via sorbitol (mainly) and mannitol to EG and 1,2-PG. In addition, there is probably another minor route that also converts cellulose to EG and 1,2-PG. The suggested overall mechanism for the cellulose conversion over the Ni-ZnO/CNT catalyst is illustrated in Figure 18. The indirect pathway via hexitols is referred to as Path 1, while the direct pathway from cellulose to EG and 1,2-PG is labelled as Path 2.

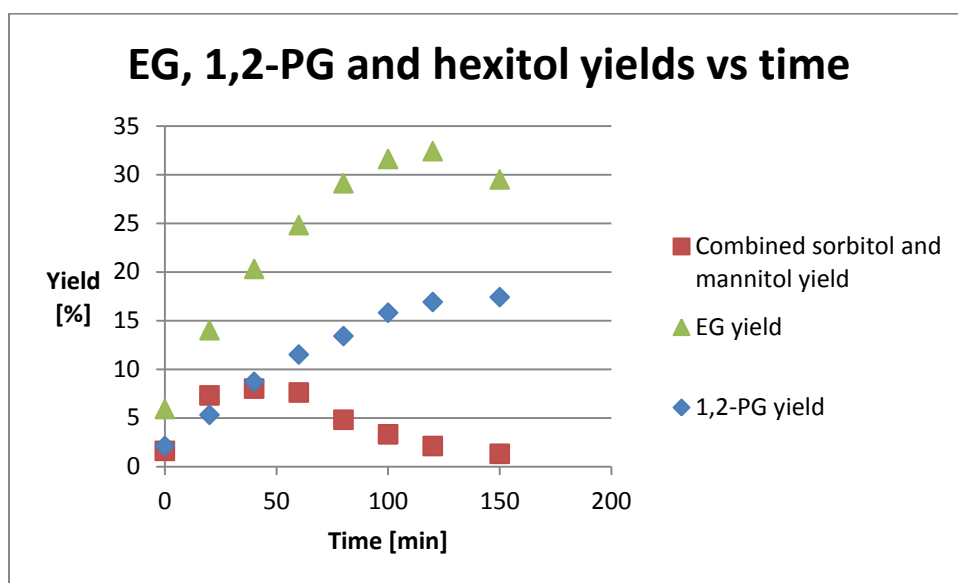


Figure 17 - EG, 1,2-PG and hexitol yields during the conversion of cellulose over a 20Ni-26ZnO/CNT catalyst.

Reaction conditions: 60 bar (RT), 245 °C, rx. time: 2,5 h and stirring rate 800 rpm. 0,8015 g cellulose, 0,2427 g 20Ni-26,1ZnO/CNT catalyst and 80 ml deionized water was mixed in an 300 mL autoclave reactor.

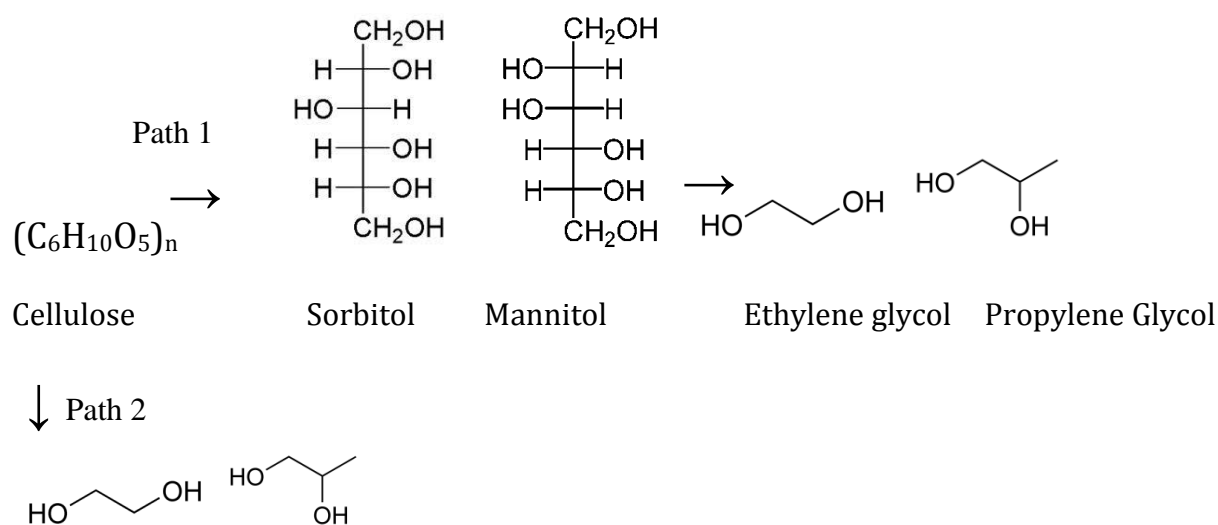


Figure 18 - Suggested mechanism

The product distribution from the experiment discussed above is given in Figure 19, and plots of each product, as well as a table summarizing all yields can be found in Appendix G. In the last measurement the EG yield drops a little bit from the previous measurement. This is probably because the experiment had to be carried out in a 300 mL reactor (to be able to get enough liquid samples from one reaction), and in this reactor it is not possible to heat the mixture as fast as in the 75 mL reactor, which has been used for all of the other experiments. The 300 mL reactor used 1 hour to heat the mixture from room temperature to 245 °C, while the 75 mL reactor (which was used to determine the optimal reaction time) used less than 40 minutes. Therefore the last measurement that was done in the 300 mL reactor (after 2,5 hours) showed a similar trend to the measurement done after 3 hours in the 75 mL reactor, in which the EG yield had dropped from 32,8% to 31,4 % as discussed in section 4.2.

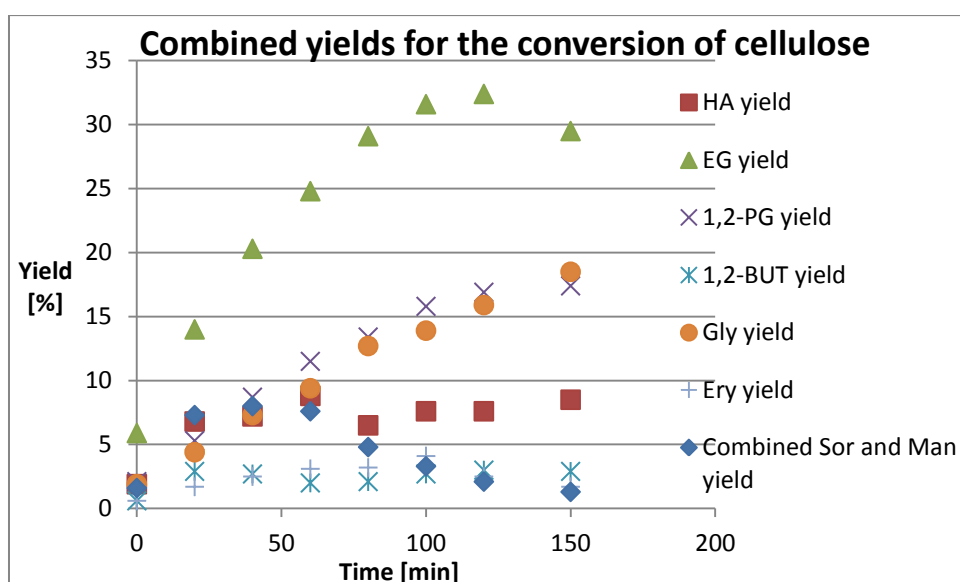


Figure 19 – Product distribution as a function of time for the conversion of cellulose over a 20Ni-ZnO/CNT catalyst.

Reaction conditions: 60 bar (RT), 245 °C, rx. time: 2,5 h and stirring rate 800 rpm. 0,8015 g cellulose, 0,2427 g 20Ni-26,1ZnO/CNT catalyst and 80 ml deionized water was mixed in an 300 mL autoclave reactor.

4.7 AC as support as an alternative to CNT – 20Ni-26ZnO/AC catalysts

Two batches of 20Ni-26,1ZnO/AC catalysts were prepared as given in section 3.4, one with the pechini method and one with incipient wetness impregnation, in order to compare AC support and CNT support for the Ni/ZnO catalysts.

4.7.1 SEM/TEM Characterization

SEM/TEM characterization was done of the Ni-ZnO/AC catalysts in order to compare the two catalysts prepared by different preparation methods. The pictures of the 20Ni-26,1ZnO/AC catalyst prepared by the pechini method are given in Figure 20, and the pictures of the 20Ni-26,1ZnO/AC catalyst prepared by incipient wetness impregnation are shown in Figure 21 (additionally, several pictures can be found on Appendix H). According to these pictures it seems like incipient wetness impregnation results in a Ni-ZnO/AC catalyst with better Ni-dispersion than the Ni-ZnO/AC catalyst prepared by the pechini method. The smallest Ni-particles in the 20Ni-26,1ZnO/AC (incipient) catalyst (Figure 21) are approximately 5 nm and many of these are only visible in the SE pictures as they are imbedded in the pores. The Ni particles in the 20Ni-26,1ZnO/AC (pechini) catalyst are in general larger than those in the 20Ni-26,1ZnO/AC (incipient) catalyst and aggregation of Ni-particles are more frequently observed in the pictures of the 20Ni-26,1ZnO/AC (pechini) catalyst. Thus these results indicate that incipient wetness impregnation might be a better option for the preparation of Ni-ZnO/AC catalysts. The pechini method involves the formation of a large complex, which might have difficulties with accessing the pores in microporous carbon materials (such as AC). Carbon nanofibers on the other hand, are mesoporous and therefore suitable for the use of the pechini method. As mentioned in section 2.3.6, the author has previously proven that the pechini method can be used to obtain an even oxide coating of ZnO on carbon nanotubes as illustrated in Figure 22. Similar pictures are not possible to find from the SEM/TEM characterization of the Ni-ZnO/AC catalysts because the contrast between ZnO and AC is not strong enough to separate these compounds. The indications that make it likely to believe that incipient wetness impregnation is a better suited preparation method than the pechini method for the Ni-ZnO/AC catalysts is therefore based on the finer Ni-particles found on the Ni-ZnO/AC (incipient) catalyst, and that the microporous AC could make it difficult for the pechini complex to enter the pores.

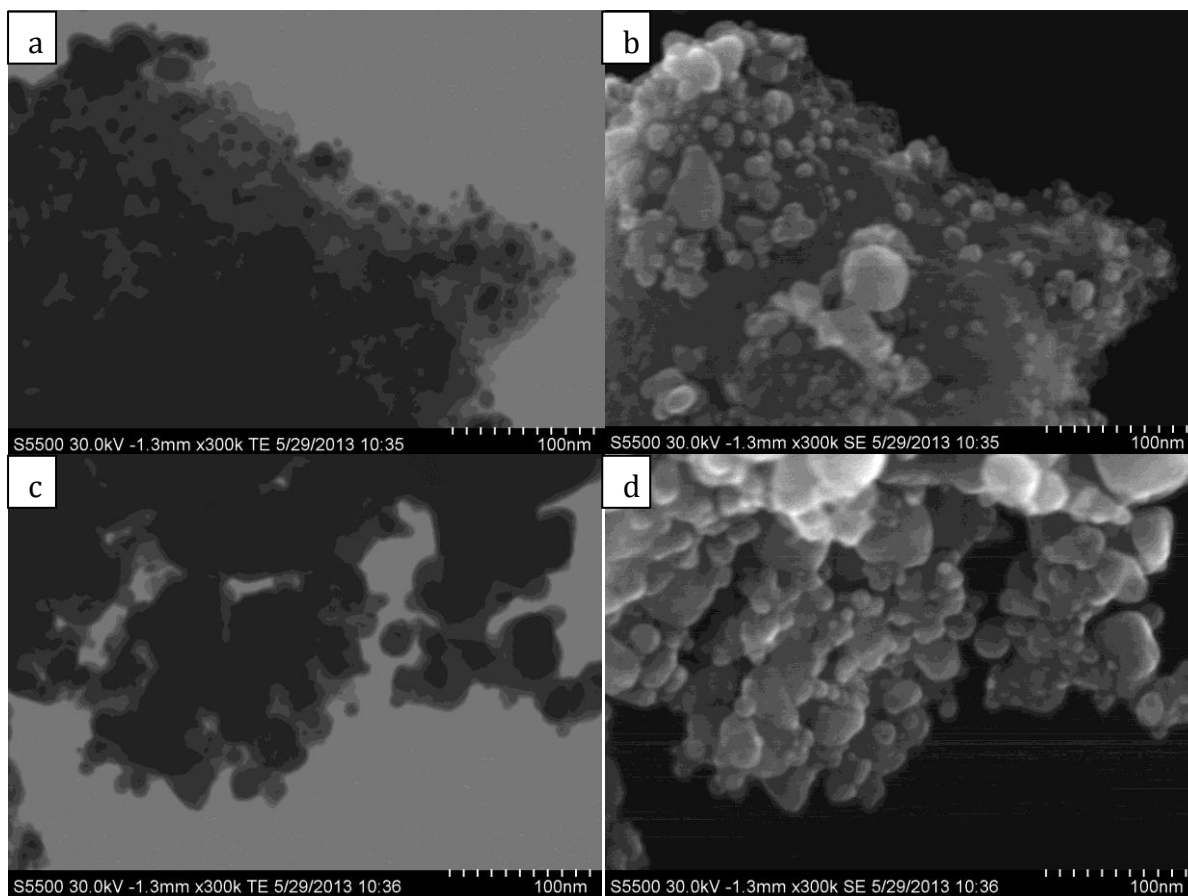


Figure 20 - TEM (a,c) and SEM (b,d) pictures at 100 nm of the 20Ni-26,1ZnO/AC (pechini) catalyst.

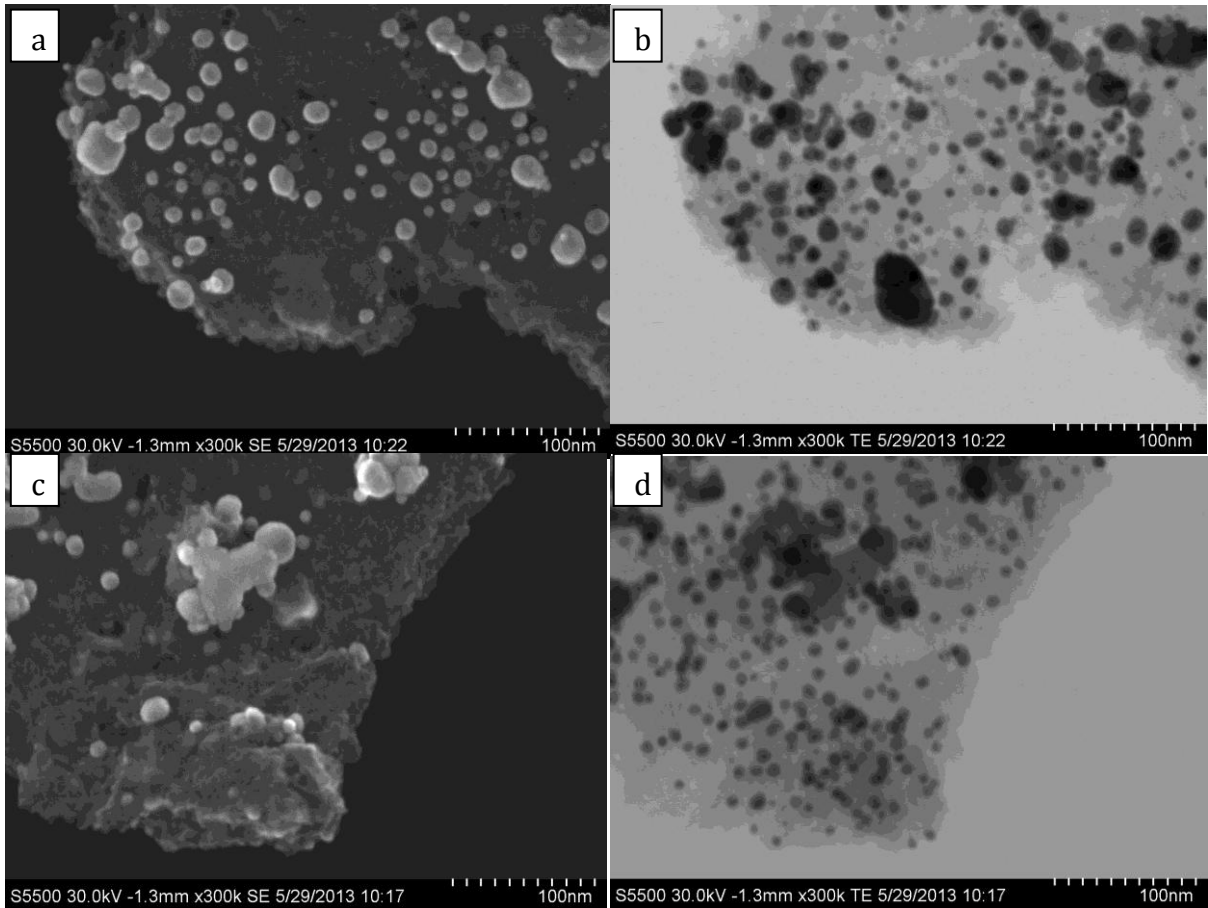


Figure 21 - SEM (a,c) and TEM pictures (b,d) at 100 nm of 20Ni-26,1ZnO/AC (incipient) catalyst

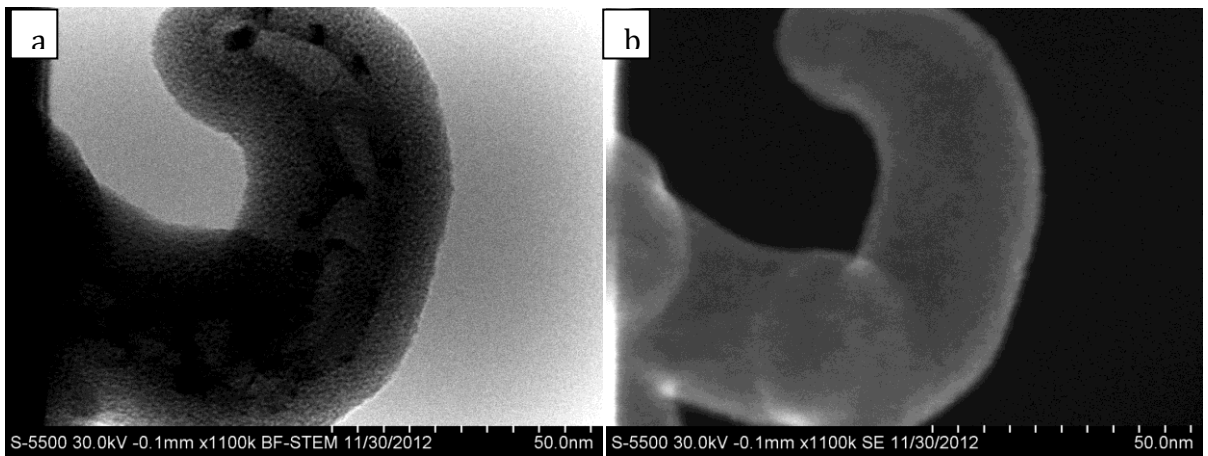


Figure 22 - Bright field STEM (a) and secondary electrons (b) at 50 nm for the 26ZnO/CNT catalyst

4.7.2 Conversion of cellulose

The product distribution for the conversion of cellulose over the 20Ni-26ZnO/AC catalysts and the 20Ni-26ZnO/CNT catalyst are compared and given in table 9. The CNT-supported catalyst provided the highest EG and 1,2-PG yields (32,8 % and 15,2 % respectively) however, the Ni-ZnO/AC catalysts were both able to transform cellulose to EG and 1,2-PG with high yields. The 20Ni-26,1ZnO/AC catalyst prepared by incipient wetness impregnation produced 30,7 % EG and 14,0 % 1,2-PG, while the 20Ni-26,1ZnO/AC catalyst prepared by the pechini method produced 28,9 % EG and 14,9 % 1,2-PG. Since the 20Ni-26ZnO/CNT catalyst provided the best result for the production of EG and 1,2-PG, the CNT-support was preferred over the AC support for the nickel zinc oxide catalysts prepared in this study. The following catalysts were therefore prepared with CNT-support.

Table 9 - Product distribution from the conversion of cellulose over 20Ni-26ZnO catalysts with AC and CNT support^a

#	Catalyst	EG	1,2-PG	1,2-BUT	Sor	Man	Gly	Ery	HA	Sum	Conv
1	20Ni-26,1ZnO/AC (incipient)	30,7	14,0	2,0	0,9	1,9	12,6	2,0	7,6	71,7	100
2	20Ni-26,1ZnO/AC (pechini)	28,9	14,9	2,6	1,1	1,7	15,1	2,1	8,3	74,7	100
3	20Ni-26,1ZnO/CNT	32,8	15,2	2,9	1,1	1,5	14,4	1,6	8,7	78,2	100

a: The catalytic conversion of cellulose was carried out in a stainless-steel autoclave (75 mL). Cellulose (0,25g), catalyst (0,075 g), and water (25 mL) were charged into the autoclave and stirred at a rate of 800 rpm. The pressure was 60 bar (RT), the reaction temperature 245 °C and the reaction time 2,5 h.

4.7.3 BET measurements

BET measurements were done to determine the surface area of the AC supported catalysts, as given in Table 10. The BET surface area of the commercial AC support was 709 m²/g, and after the metal(s) were introduced to the support the surface area decreased. The 20Ni-26ZnO/AC catalyst prepared by the pechini method had a BET surface area of 336,1 m²/g, while the 20Ni-26ZnO/CNT catalyst prepared by incipient wetness had a BET surface area of 458,8 m²/g. It is likely that this significant difference in BET surface area is related to the different preparation methods. The formation of a large complex takes place in the pechini method, and as previously mentioned in section 4.7.1 it might be difficult for this complex to enter the microporous structure of the AC-support, thus this will have a negative effect on the BET surface area. Incipient wetness impregnation on the other hand, only requires the metal precursors to dissolve in water, and the microporous structure might therefore be more accessible when this preparation method is used. The BET results of the 20Ni-26ZnO/AC catalysts supports the SEM and TEM results which indicate that the Ni-dispersion in 20Ni-26ZnO/CNT (incipient) catalyst might be better than the Ni-dispersion in the similar catalyst prepared by the pechini method. The 20Ni/AC catalyst was also prepared by incipient wetness impregnation, and as given in table 10 the BET surface area was as high as 686,4 m²/g. Thus only a small decrease in surface area was noted compared to the commercial AC support (709 m²/g). The 20Ni/AC catalyst only contains one metal, Ni, thus the preparation is even more straightforward than for the 20Ni-26ZnO/CNT (incipient) catalyst, which was impregnated twice to introduce both Zn and Ni.

Table 10 - The results from the BET measurements of the 20Ni-26ZnO/AC and 20Ni/AC catalysts

Catalyst	BET Surface Area [m ² /g]	Pore Volume [cm ³ /g]	Pore Size [Å]	t-Plot micropore volume [cm ³ /g]
20Ni-26ZnO/AC (pechini)	336,1	0,18	4,4	0,067
20Ni-26ZnO/AC (incipient)	458,8	0,20	3,4	0,064
20Ni/AC	686,4	0,33	3,8	0,142

4.7.4 XRD characterization

The XRD patterns for the 20Ni-26ZnO catalysts with AC and CNT support are presented in Figure 23. The first peak is assigned carbon, and the following three peaks are identified as zinc oxide. A big peak for nickel zinc is then found, which additionally has a shoulder peak of nickel. Some smaller peaks for nickel zinc, nickel and zinc oxide are located as the 2θ /degree increases towards 80. These XRD results confirm the formation of Ni-Zn compound in all three catalysts. The XRD patterns for the AC-supported catalysts are very similar, thus the different preparation methods do not result in obvious differences detectable with XRD analysis. XRD analysis was also conducted for the 20Ni/AC catalyst, and the result is compared with the XRD pattern of the 20Ni/CNT catalyst in Figure 24. Similar to the 20Ni-26ZnO/AC catalysts, a peak for carbon was first located, and then three nickel peaks were detected.

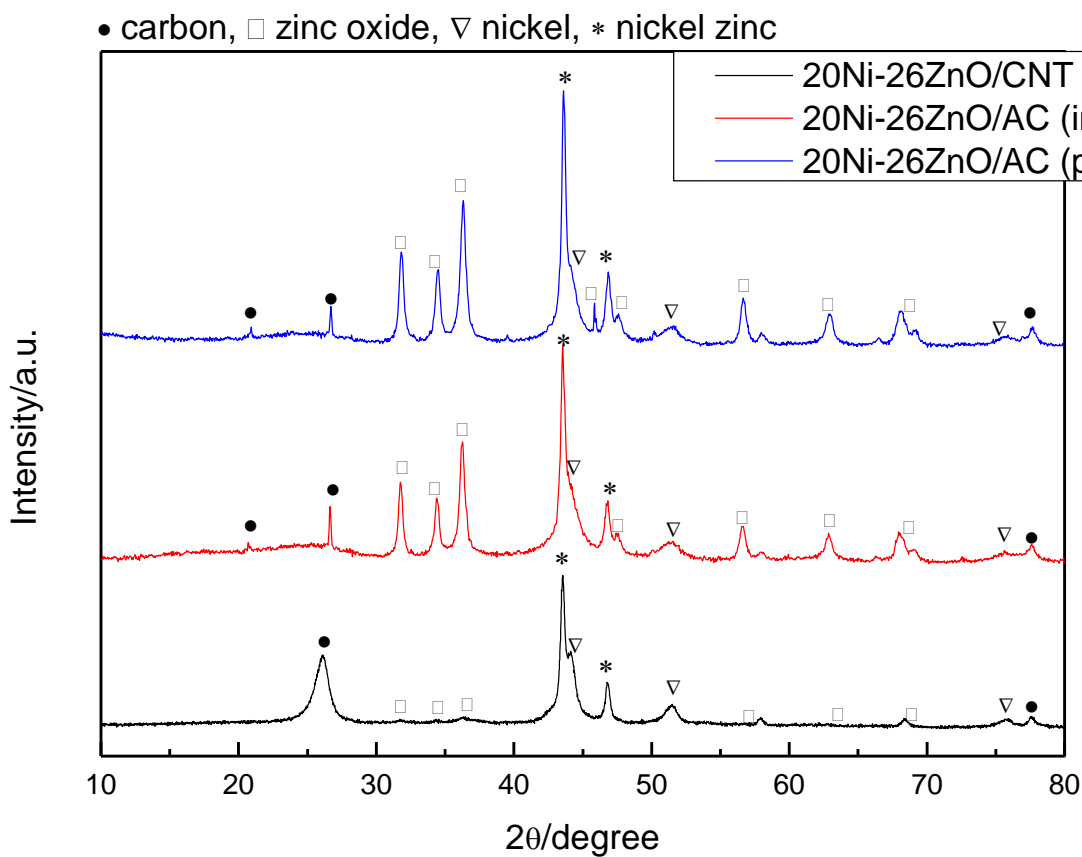


Figure 23 – XRD patterns for the 20Ni-26ZnO catalysts with CNT and AC support

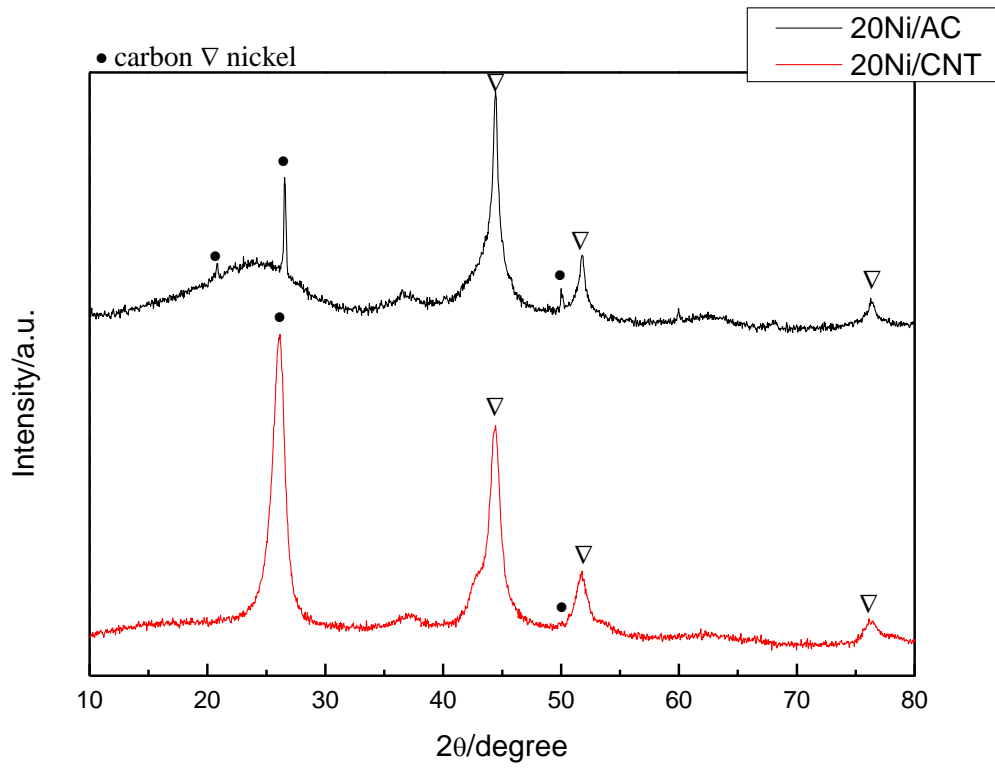


Figure 24 - XRD patterns for the 20Ni/AC and 20Ni/CNT catalysts

4.7.5 TGA

TG analysis was carried out for the 20Ni-26ZnO/AC supported catalysts in order to determine the overall metal loading. Figure 25 illustrates DTG and TG as a function of temperature for the 20Ni-26ZnO/AC (incipient) catalyst. The plots reveal that the Ni catalysts are oxidized in air as there is a small increase in the DTG and TG plots before the mass decreases. Carbon oxidation of the catalysts starts at approximately 350°C, and reaches its maximum close to 450°C. The total metal loading was determined from the TGA results by subtracting the overall mass loss (%) from 100%, and the results are compared with the theoretical total loading (calculated according to Appendix I) in Table 11. For the 20Ni-26ZnO/AC (incipient) catalyst, the total loading obtained from the TGA results was 56,6%, while the theoretical calculated loading was 50,4%. Thus the theoretical value was lower than the value calculated based on the TGA characterization. A similar trend was obtained for the 20Ni-26ZnO/AC (pechini) catalyst, Figure 26, which had a theoretical overall loading of 50,1 % and a loading calculated from the TGA results as high as 66,6%. There is not a straightforward explanation to why the theoretical loading is higher than the loading according to TGA characterization, but a possibility is that methanation occurs and significantly affects the loading of the catalysts. If methanation ($C + H_2 \rightarrow CH_4$) is significant, carbon will be lost and thus the metal loading will increase. Another possibility is that impurities from production affect the loading in the catalyst sample tested for TGA. The impurities left in the activated carbon support are not identical in the entire batch from production. Therefore certain areas of the support might be very pure, while others could be seriously affected by metal leftovers and other impurities from production.

20Ni-26ZnO/AC (incipient)

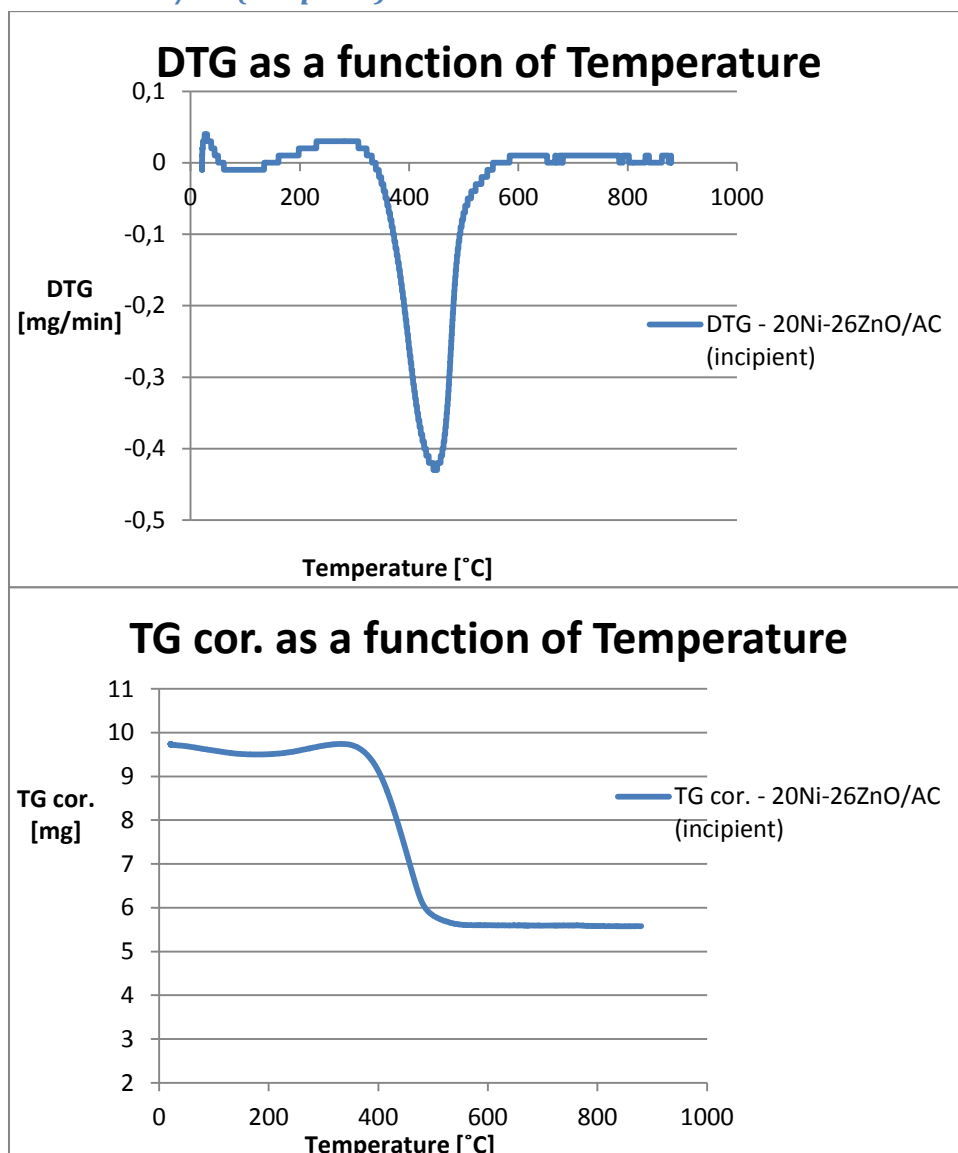


Figure 25 - DTG and TG cor. (from TGA analysis) as a function of temperature for the 20Ni-26ZnO/AC (incipient) catalyst

20Ni-26ZnO/CNT (pechini)

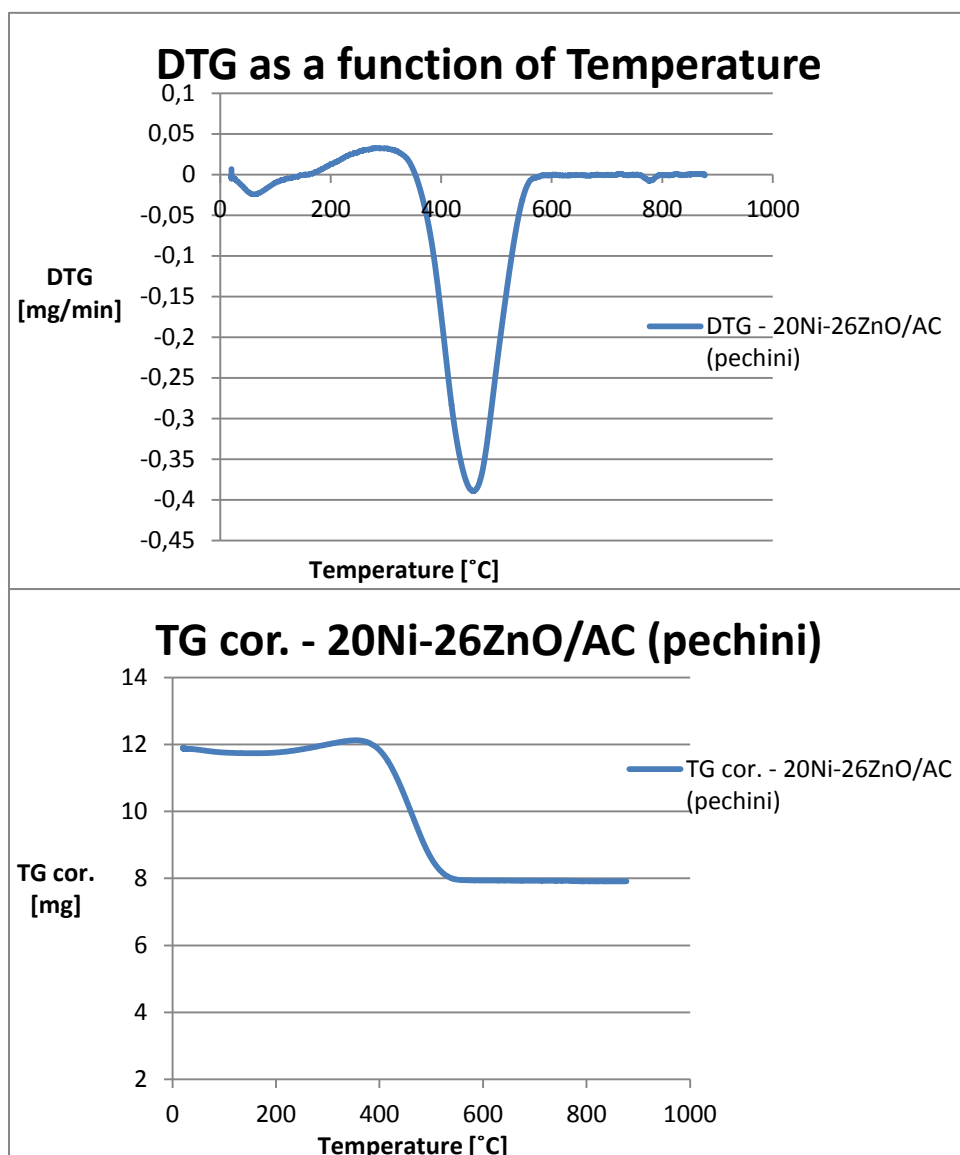


Figure 26 - DTG and TG cor. (from TGA analysis) as a function of temperature for the 20Ni-26ZnO/AC (pechini) catalyst

Table 11 - Total loading for the 20Ni-26ZnO/AC catalysts according to TGA analysis and theoretical calculations

Catalyst	Mass loss [%]	Total loading according to TGA [%]	Total theoretical loading [%]
20Ni-26ZnO/AC (incipient)	-43,4	56,6	50,4
20Ni-26ZnO/AC (pechini)	-33,4	66,6	50,1

4.8 Ni-26ZnO/CNT catalysts with Ni-loading 5-30%

4.8.1 Cellulose conversion

To investigate the effect of Ni-loading in the Ni-26ZnO/CNT catalyst, different catalysts with Ni-loading in the range 5-30 % were prepared (according to section 3.3) and compared for the conversion of cellulose. The product distribution is given in Table 12, and these results reveal that the main products EG and 1,2-PG increases with higher Ni-loading. The catalyst with the lowest Ni-loading, 5Ni-26,1ZnO/CNT, converted cellulose to 23,8 % EG and 14,4 % 1,2-PG, while the 30Ni-26,1ZnO/CNT catalyst produced EG and 1,2-PG yields equal to 34,6% and 17,8 % respectively. Thus the combined yield for EG and 1,2-PG was as high as 52,4 %. The 30Ni-26,1ZnO/CNT catalyst therefore offers an interesting alternative to the 20Ni/ZnO catalyst developed by Xicheng Wang et al. [18] (section 2.1.2), and the catalyst choice should be done according to the desired selectivity for cellulose conversion. If the 20Ni/ZnO catalyst prepared according to Xicheng Wang et al. is used the main products will be 1,2-PG (34,4%) and EG (19,1%), while if the 30Ni-26ZnO/CNT catalyst developed herein is used the selectivity will shift from 1,2-PG to EG and yields of 34,6 % and 17,8 % respectively can be achieved. All the Ni-26ZnO/CNT catalysts with different Ni-loading were active for the conversion of cellulose. From the results in Table 12 it is clear that higher Ni-loading increases the selectivity towards the main products EG and 1,2-PG, and especially the EG yield is affected by the change in Ni-loading, which follows a linear trend as illustrated in Figure 27.

Table 12 - Product distribution for the conversion of cellulose over Ni-26,1ZnO/CNT catalyst with different Ni-loading^a

#	Catalyst	EG	1,2-PD	1,2-BUT	Sor	Man	Gly	Ery	HA	Sum	Conv [%]
1	5Ni-26,1ZnO/CNT	23,8	14,4	2,9	6,7	4,0	10,6	1,9	7,3	71,5	100
	10Ni-26,1ZnO/CNT	28,1	14,4	2,3	1,2	1,8	13,0	2,1	8,2	71,0	100
2	15Ni-26,1ZnO/CNT	27,8	14,1	2,6	0,5	2,7	14,2	1,0	7,6	70,6	99,7
3	20Ni-26,1ZnO/CNT	32,8	15,2	2,9	1,1	1,5	14,4	1,6	8,7	78,2	100
4	25Ni-26,1ZnO/CNT	30,2	14,9	3,4	0,8	ND	11,9	1,3	9,1	71,5	100
5	30Ni-26,1ZnO/CNT	34,6	17,8	3,0	0,7	ND	9,1	1,5	9,4	75,9	100

a: The catalytic conversion of cellulose was carried out in a stainless-steel autoclave (75 mL). Cellulose (0,25g), catalyst (0,075 g), and water (25 mL) were charged into the autoclave and stirred at a rate of 800 rpm. The pressure was 60 bar (RT), the reaction temperature 245 °C and the reaction time 2,5 h.

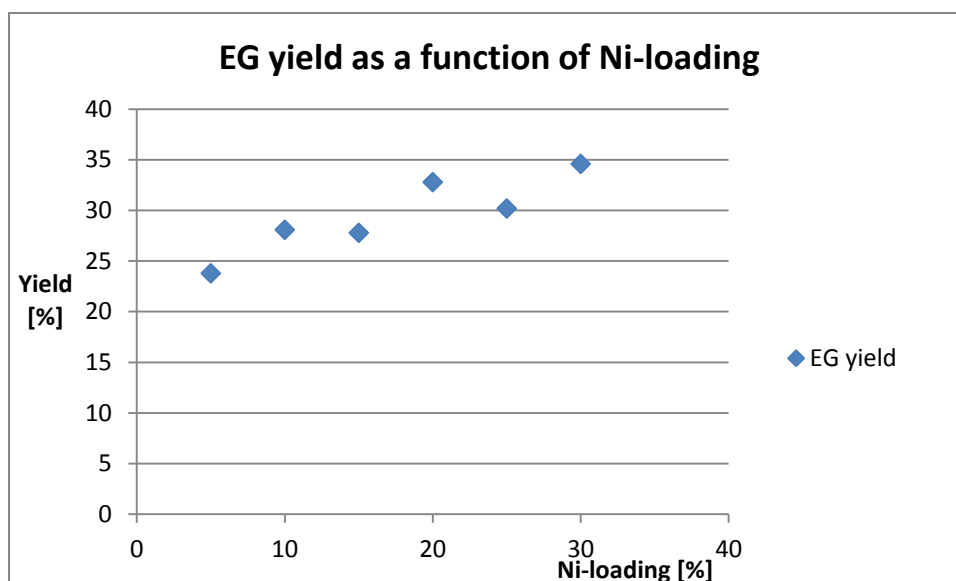


Figure 27 – The EG yield as a function of Ni-loading as a result of cellulose conversion over various Ni-26,1ZnO/CNT catalysts.

a: The catalytic conversion of cellulose was carried out in a stainless-steel autoclave (75 mL). Cellulose (0,25g), catalyst (0,075 g), and water (25 mL) were charged into the autoclave and stirred at a rate of 800 rpm. The pressure was 60 bar (RT), the reaction temperature 245 °C and the reaction time 2,5 h.

4.8.2 BET measurements

BET measurements were carried out for the Ni-26ZnO/CNT catalyst prepared with different nickel loading at DICP, and the results are given in Table 13. A trend in which the BET surface area decreases as the nickel loading increases was observed. The catalyst with the lowest nickel loading, 5%, had a BET surface area of 112,2 m²/g, while the catalyst with the highest nickel loading, 30%, had a BET surface area of 83,7 m²/g. As more nickel is impregnated on the 26ZnO/CNT catalysts, the surface area decreases and this might lead to poorer Ni-dispersion.

Table 13 – The results from the BET measurements of the Ni-26ZnO/CNT catalysts with nickel loading 5-30%

Catalyst	BET Surface Area [m ² /g]	Pore Volume [cm ³ /g]	Pore Size [Å]	t-Plot micropore volume [cm ³ /g]
5Ni-26ZnO/CNT	112,2	0,45	12,2	0,000
10Ni-26ZnO/CNT	102,1	0,48	14,7	0,002
15Ni-26ZnO/CNT	95,6	0,43	14,0	0,002
25Ni-26ZnO/CNT	88,7	0,41	14,2	0,002
30Ni-26ZnO/CNT-red400	83,7	0,36	13,8	0,000

4.8.3 XRD analysis

XRD analysis was carried out for the Ni-26ZnO/CNT catalysts in order to identify the components and compare the patterns for the catalysts with different nickel loading. Similarly to the previous XRD patterns, the first four peaks in Figure 28 are assigned to carbon and zinc oxide. The fourth (nickel zinc) and fifth peak (nickel) clearly demonstrates the different nickel loading in these six catalysts. Starting at the black plot, which represent the 5Ni-26ZnO/CNT catalyst, two relatively small peaks are observed and recognized as nickel zinc and nickel. The nickel zinc peak is larger than the nickel peak, and when the nickel loading is increased these peaks grow larger and larger and the nickel peak becomes the dominant peak. The following two nickel peaks observed for all six catalysts also becomes bigger as the nickel loading is increased, thus the XRD results are in agreement with the impregnated amount of nickel precursor.

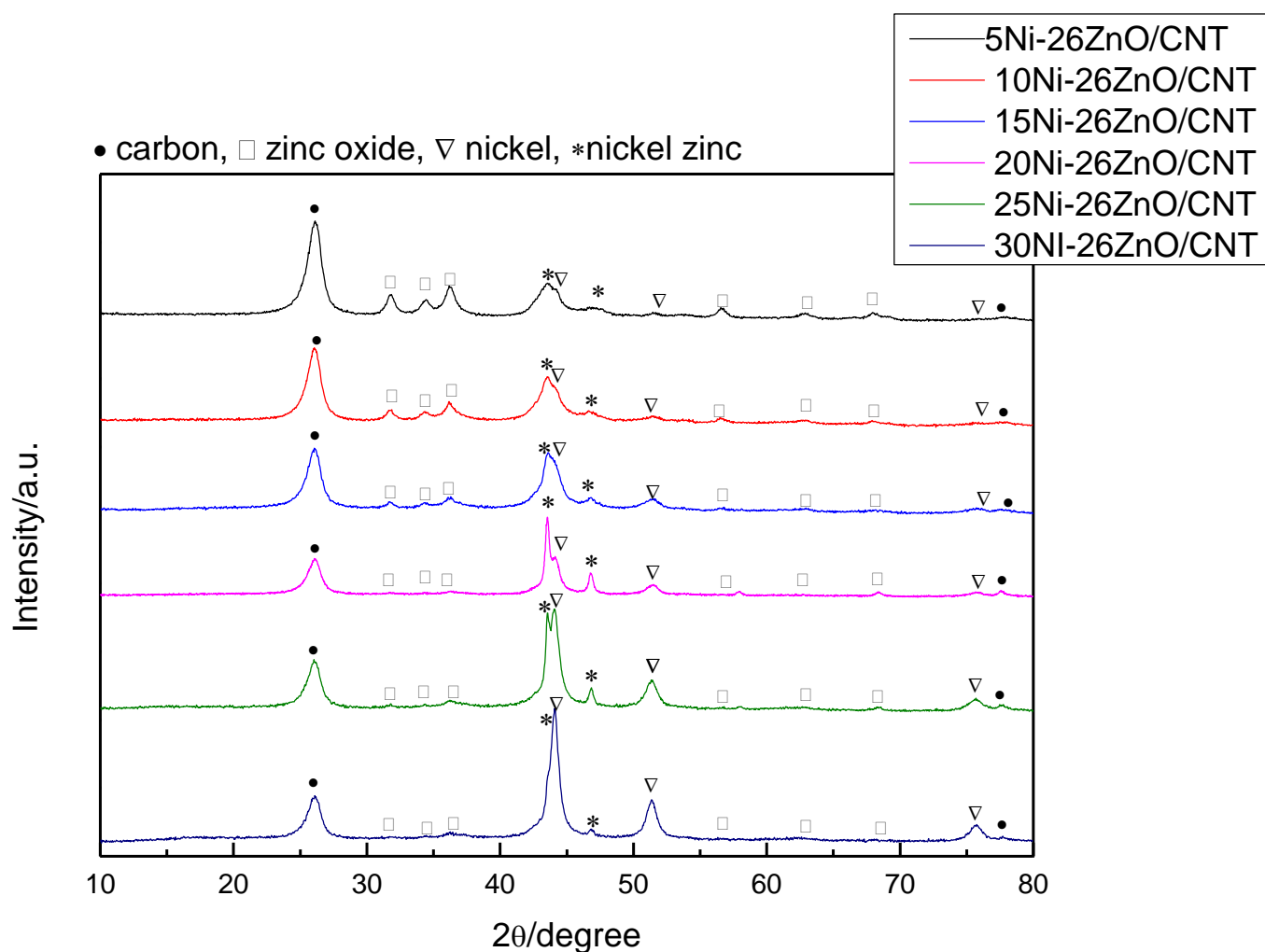


Figure 28 – XRD patterns for the Ni-26ZnO/CNT catalysts with nickel loading 5-30%

4.8.4 TGA

The loading of the Ni-26ZnO/CNT catalysts were investigated with TGA, and the DTG and TG plots are given as a function of temperature in Figure 29-34. According to these figures, there is a small increase in mass for all catalysts prior to the oxidation of carbon, which indicates that the catalyst samples are oxidized in air. In general, the mass drop occurs from 400°C to 600-650°C, and the carbon oxidation reaches its maximum in between 500°C and 600°C. It can be noted that the mass loss stabilizes earlier for the catalysts with high nickel loading than for the catalysts with nickel loading of 5% and 10%. For instance the mass loss for the 5Ni-26ZnO/CNT catalyst is stabilized at 650°C, while the mass loss for the 30Ni-26ZnO/CNT-red300 catalysts stabilizes right before the temperature reaches 600°C. This is because the 30Ni-26ZnO/CNT catalyst have more nickel mass than the 5Ni-26ZnO/CNT catalyst, thus the latter catalyst has more carbon mass and the carbon oxidation will therefore continue longer.

5Ni-26ZnO/CNT

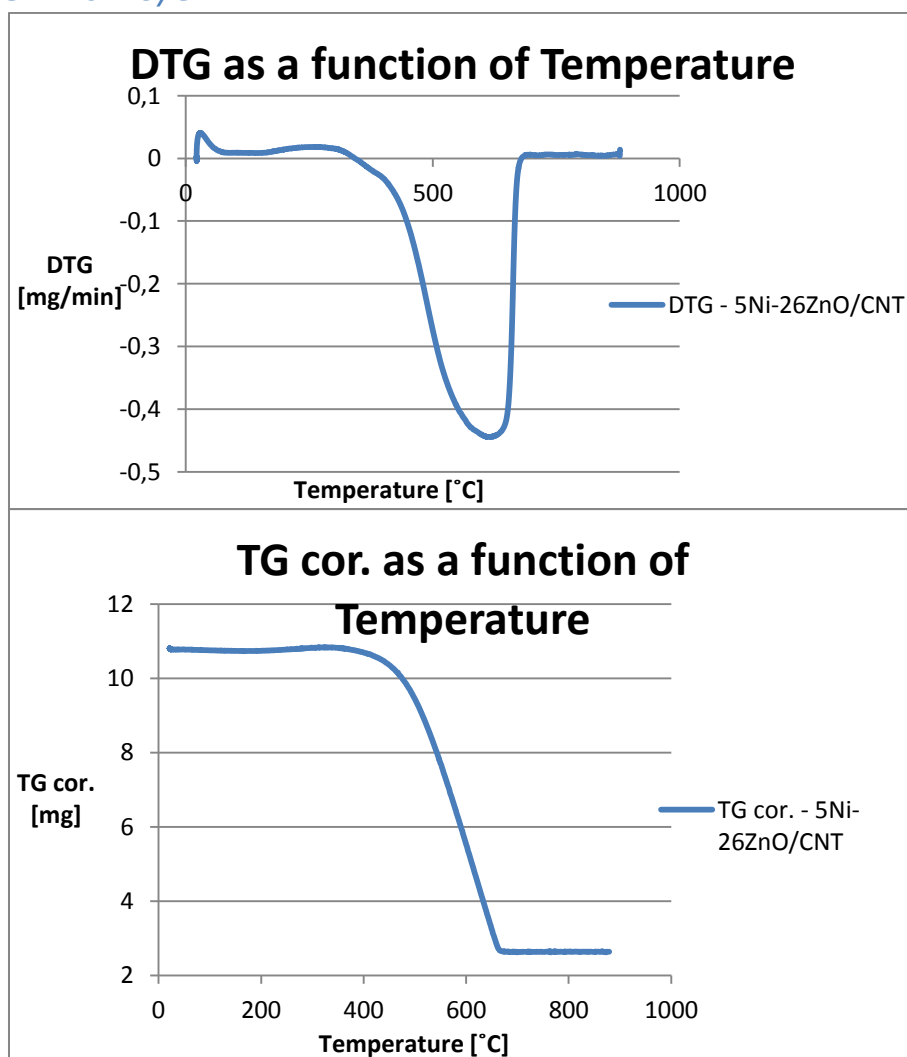


Figure 29 - DTG and TG cor. (from TGA) as a function of temperature for the 5Ni-26ZnO/CNT catalyst

10Ni-26ZnO/CNT

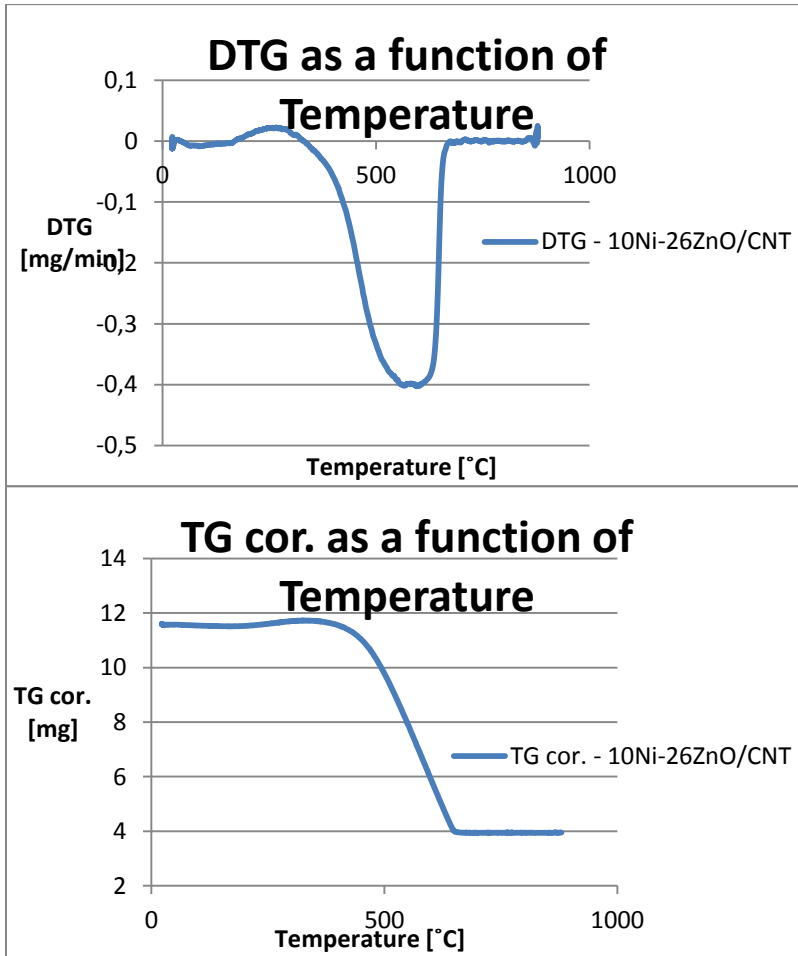


Figure 30 - DTG and TG cor. (from TGA) as a function of temperature for the 10Ni-26ZnO/CNT catalyst

15Ni-26ZnO/CNT

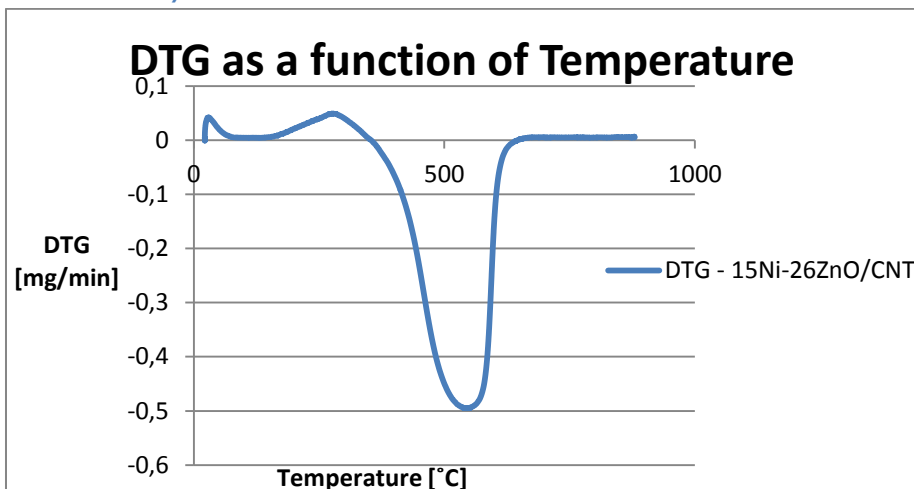


Figure 31 - DTG (from TGA) as a function of temperature for the 15Ni-26ZnO/CNT catalyst

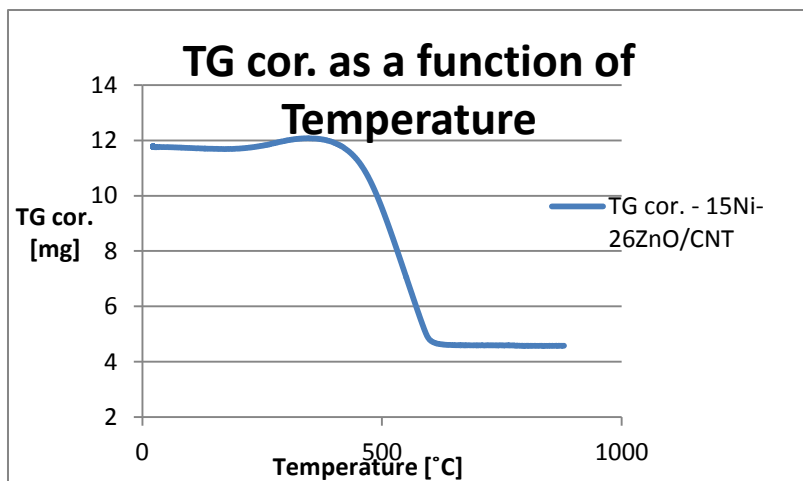


Figure 32 - TG cor. (from TGA) as a function of temperature for the 15Ni-26ZnO/CNT catalyst

25Ni-26ZnO/CNT

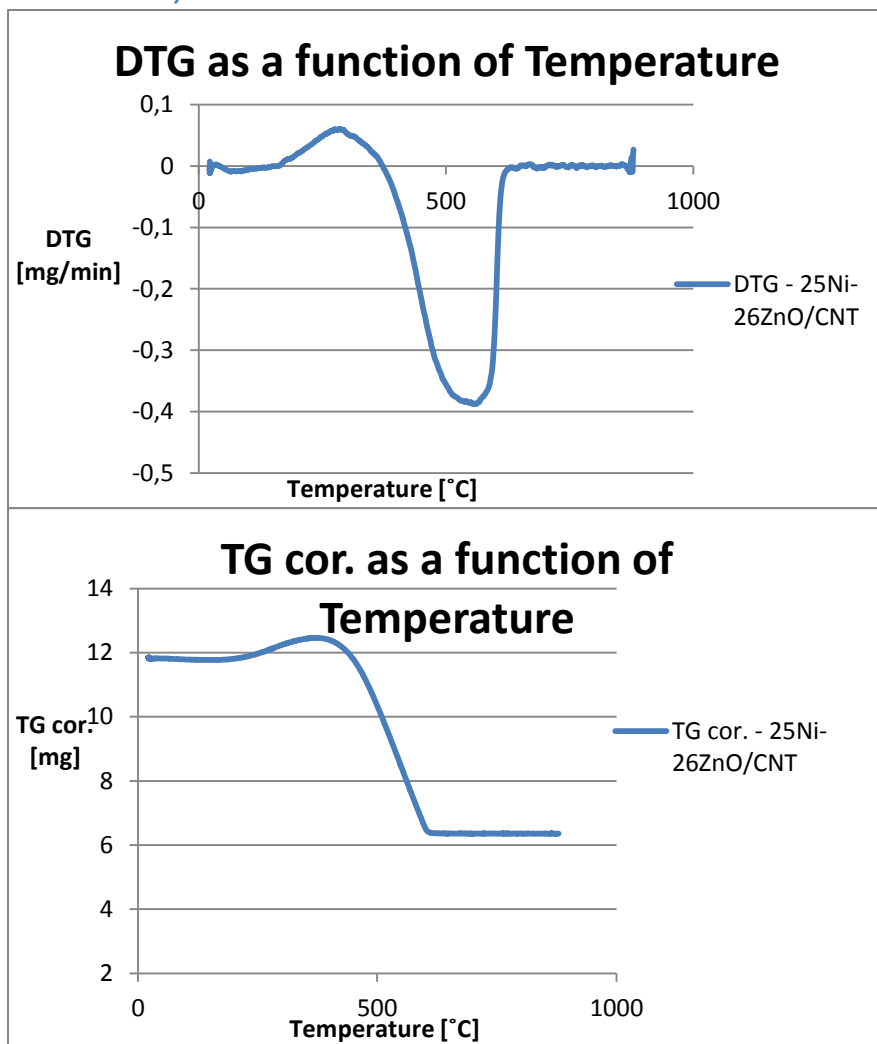


Figure 33 - DTG and TG cor. (from TGA) as a function of temperature for the 25Ni-26ZnO/CNT catalyst

30Ni-26ZnO/CNT-red 400

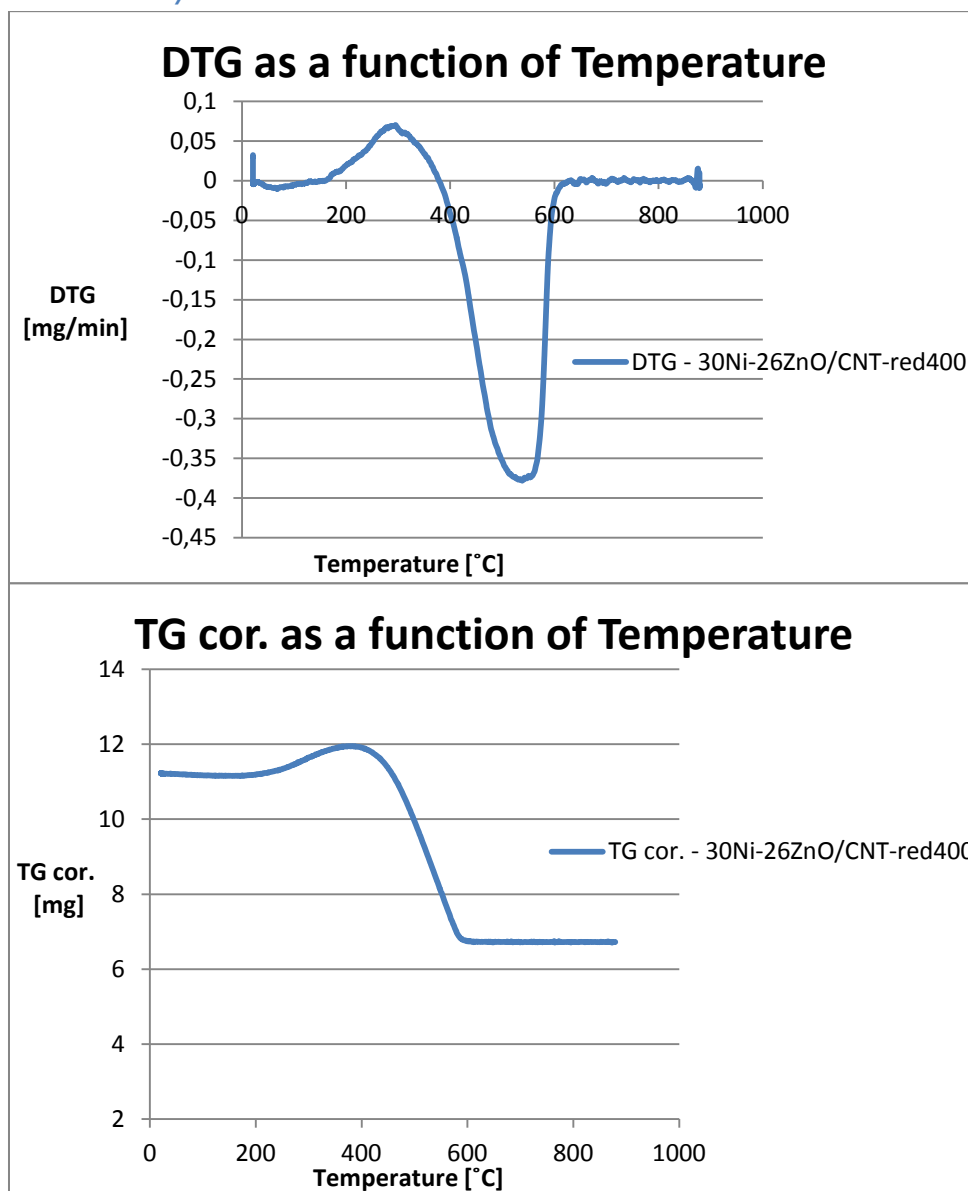


Figure 34 - DTG and TG cor. (from TGA) as a function of temperature for the 30Ni-26ZnO/CNT-red400 catalyst

The total loading of each catalyst was obtained by subtracting the mass loss (%) obtained by TGA from 100%. A comparison of the theoretical total loading, which was calculated according to Appendix I, and the loading obtained from the TGA is presented in Table 14. For all the catalysts, the theoretical value for the total loading is higher than the loading obtained from TGA. Additionally, the impurities in the CNT support affect the overall loading obtained from TGA, thus the difference becomes even bigger. The different batches of CNT support were tested with TGA, and the results reveal that they constitute 0-6% of the mass in the catalysts depending on which batch that was used. The plots for the TGA of the CNT support can be found in Appendix J. However it should be mentioned that the impurities in the CNT support probably not is evenly distributed. For instance there can be areas of the support that has no nickel leftovers from the catalyst used in production, while other areas can be severely affected. Therefore the 10 mg of CNT sample used in the analysis will not fully reflect the batch of support material, and therefore some samples show that the metal leftovers from production is negligible, while others report impurities up to 6%.

As mentioned in section 4.7.5 methanation might be related to the differences in the theoretical loading and the loading obtained from TGA for the AC supported catalysts. This does not seem likely for the CNT supported catalysts, because the theoretical value is higher than the value found from TGA. In this case, it seems like methanation is negligible, and the differences must be due to something else. It is difficult to explain exactly why the TGA loading is higher than the theoretical loading, but at least the trend is similar for all the catalysts and the TGA loading increases as the theoretical loading increases.

Table 14 - Total loading for the Ni-26ZnO/CNT catalysts with Ni-loading 5-30% according to TGA analysis and theoretical calculations

Catalyst	Mass loss [%]	Total loading according to TGA [%]	Total theoretical loading [%]
5Ni-26ZnO/CNT	-73	26,4	32,7
10Ni-26ZnO/CNT	-63,8	36,2	38,9
15Ni-26ZnO/CNT	-62,0	38,0	44,6
25Ni-26ZnO/CNT	-47,4	52,6	56,3
30Ni-26ZnO/CNT-red400	-40,5	59,5	61,2

4.9 Basicity, reduction temperature and product selectivity for 30Ni-26ZnO/CNT catalysts

4.9.1 CO₂-TPD

The basicity of the Ni-ZnO/CNT catalyst is important for the selectivity in the conversion of cellulose, and is determined by the formation of Ni-Zn-O compound, thus the reduction step. To investigate the basic properties as a function of reduction temperature, four 30Ni-26ZnO/CNT catalysts were prepared by using different reduction temperature (300°C, 350°C, 400°C and 450°C as described in section 3.3), and CO₂-TPD analysis were carried out for each catalyst. In order to decide which reduction temperatures to study, H₂-TPR results from the 20Ni-26ZnO/CNT catalyst were used, as illustrated in Figure 35. When the temperature approaches 600°C nickel is completely reduced, however at temperatures this high it is possible that carbon gasification will affect the CNT support. Therefore four temperatures from 300°C to 450°C was chosen for further studies. Figure 36 illustrates the combined plots for the 30Ni-26ZnO/CNT catalysts prepared with different reduction temperature, in which the TCD signal is plotted as a function of temperature. The separate plots for each catalyst can be found in Appendix K. From Figure 36 a correlation between the reduction temperature and the number of basic sites can be found, which indicates that low reduction temperature (300°C) leads to strong basicity and the number of basic sites decreases as the reduction temperature increases to 450°C. In general there are two peaks observed for the catalysts in Figure 36, one peak representing the number of weak basic sites (located at temperatures over 400 °C) and one peak representing the number of strong basic sites (located at temperatures over 500°C). The desorption data from the CO₂-Temperature Programmed Desorption is presented in Table 15. If the weak and strong basic sites are added for each catalyst the total number of basic sites are 70,95 cm³/g, 44,02 cm³/g, 26,87 cm³/g and 18,83 cm³/g for the 30Ni-ZnO/CNT catalysts reduced at 300°C, 350°C, 400°C and 450°C respectively. Thus the choice of reduction temperature will determine the basic properties of the 30Ni-26ZnO/CNT catalyst.

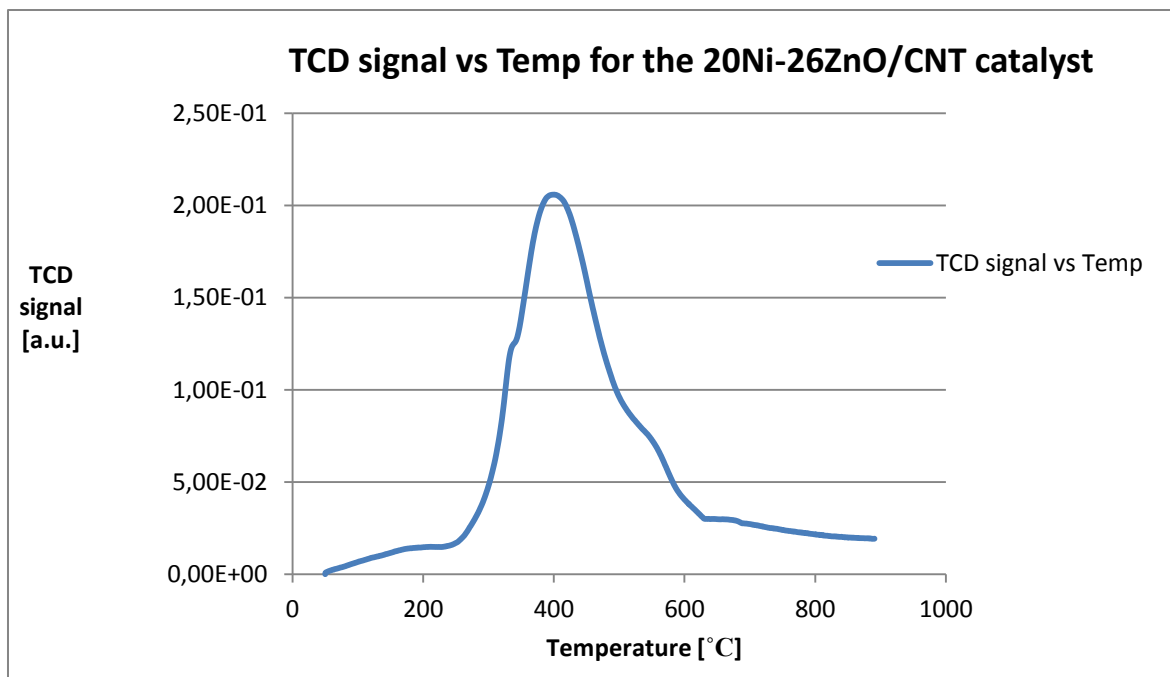


Figure 35 – CO₂-TPD: TCD signal as a function of temperature for the 20Ni-26ZnO/CNT catalyst

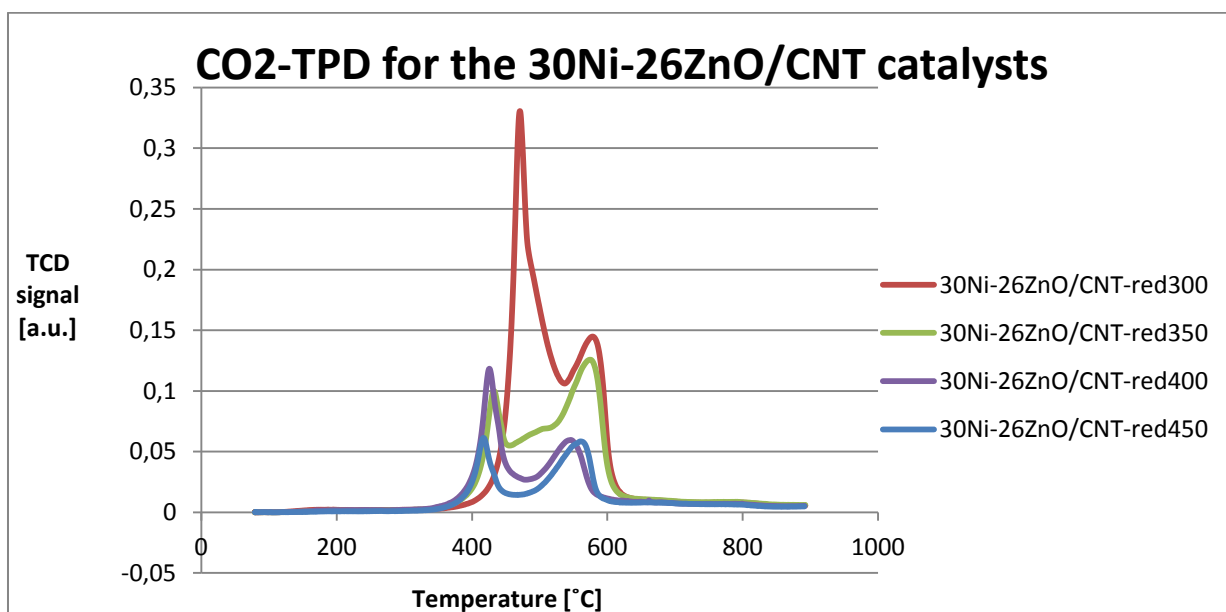


Figure 36 – CO₂-TPD: TCD signal as a function of temperature for 30Ni-26ZnO/CNT catalysts with different reduction temperature

Table 15 – Peak information from the CO₂-TPD of the 30Ni-26ZnO/CNT catalysts with different reduction temperature

Catalyst	Peak Number	Temperature at Maximum [°C]	Quantity [cm³/g]	Peak Hight
30Ni-26ZnO/CNT-red300	1	470,7	47,74	0,33
30Ni-26ZnO/CNT-red300	2	577,8	23,21	0,14
30Ni-26ZnO/CNT-red350	1	432,5	10,21	0,10
30Ni-26ZnO/CNT-red350	2	517,4	10,77	0,07
30Ni-26ZnO/CNT-red350	1+2		20,98	0,17
30Ni-26ZnO/CNT-red350	3	573,6	23,05	0,12
30Ni-26ZnO/CNT-red400	1	425,7	15,09	0,12
30Ni-26ZnO/CNT-red400	2	545,9	11,78	0,06
30Ni-26ZnO/CNT-red450	1	417,1	7,04	0,06
30Ni-26ZnO/CNT-red450	2	560,9	11,79	0,06

4.9.2 NH₃-TPD

In their study of the 20Ni/ZnO catalyst Xicheng Wang et al. [18] catalyst conducted NH₃-TPD and CO₂-TPD characterization, and reported that both acidic and basic sites were found on the catalyst surface. However, a correlation between acidity and catalytic activity was not found, which made the authors suggest that the acidic sites on the catalyst surface might not play a significant role for the cellulose conversion. The strong basic sites on the other hand, were reported as critical for the activity and selectivity of the Ni/ZnO catalyst. With this in mind, the basic sites as a function of reduction temperature were studied herein (section 4.9.1), and not much attention has been given to the acidity of the catalysts. However, one run with NH₃-TPD was done for the 20Ni-26ZnO/CNT catalyst in order to confirm that the acidic properties in the catalyst were weak. The TCD signal is given as a function of temperature in Figure 37. Two peaks were located at 391.5°C and 569.8°C with quantity (cm³/g STP) 3.85 and 22.63 respectively, thus acidic sites are present on the surface. However they are weak compared to the basic sites found for the 30Ni-26ZnO/CNT catalysts, which had a TCD signal 10 times higher than the TCD signal for the NH₃-TPD measurement of the 20Ni-26ZnO/CNT catalyst. It should be mentioned that the basic and acidic properties also will be affected by the metal loading (in addition to the reduction temperature), therefore the purpose of presenting the result for the NH₃-TPD measurement of the 20Ni-26ZnO/CNT catalyst is not to compare it with the 30Ni-26ZnO/CNT catalysts, but to demonstrate that the NH₃ adsorption is relatively small. The data related to the NH₃-TPD measurement can be found in Table 16.

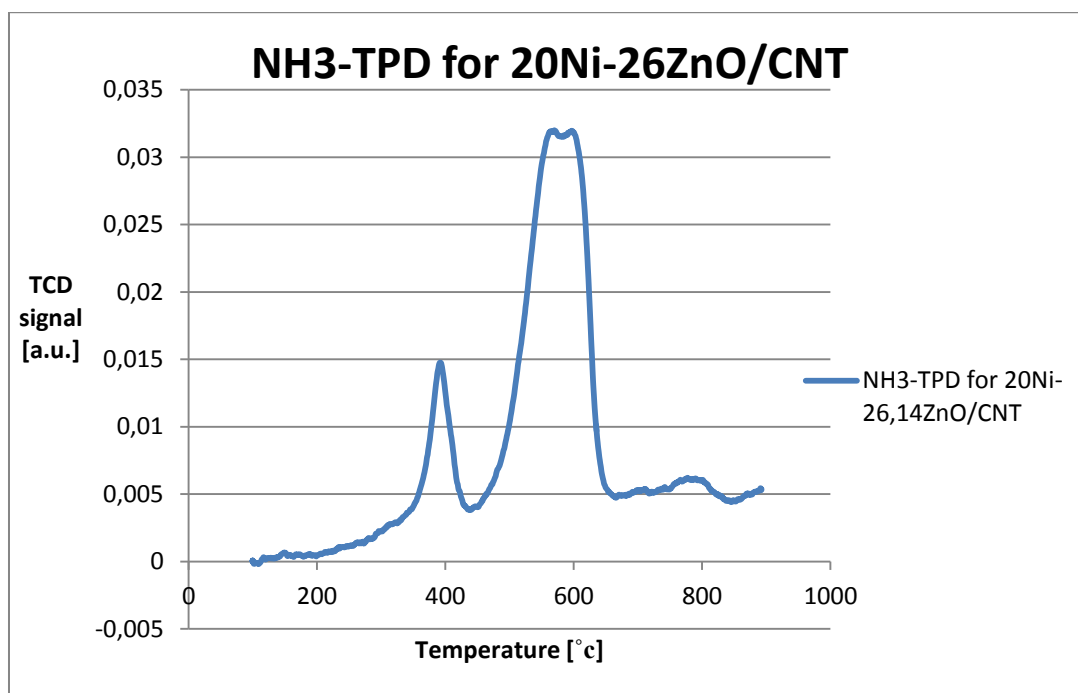


Figure 37 - NH₃-TPD: TCD signal as a function of temperature for the 20Ni-26ZnO/CNT catalyst

Table 16 – Peak information Peak from the NH₃-TPD of the 20Ni-26ZnO/CNT catalyst

Peak number	Temperature at maximum [°C]	Quantity [cm³/g STP]	Peak Height
1	391,5	3,85	0,01
2	569,8	22,63	0,03

4.9.3 Sorbitol conversion

In section 4.6.2 an overall pathway for the conversion of cellulose over a 20Ni-26ZnO/CNT catalyst was suggested, in which cellulose is converted to polyols via hexitols (mainly sorbitol). The catalytic performance of the 30Ni-26ZnO/CNT catalysts was therefore tested for the conversion of sorbitol, and the results are presented in Table 17. The reduction temperature varied from 300 °C to 450 °C, and the results revealed that both the EG yield and the Gly yield were affected by reduction temperature. The Gly yield decreased with higher reduction temperature, while the EG yield slightly increased as a function of reduction temperature. Thus it seems like there is a correlation between basic sites, reduction temperature and the selectivity towards EG and Gly. The strong correlation between basic sites, reduction temperature and Gly yield is illustrated in Figure 38, and indicates that glycerol production mainly takes place on basic sites. Additionally, a weak correlation between the basic sites, reduction temperature and the EG yield was observed, as illustrated in Figure 39. As the number of basic sites decreases, the EG yield increases. However this trend is not as clear as the correlation between Gly product and basic sites.

Table 17 – Product distribution from the cellulose conversion over 30Ni-26ZnO/CNT catalysts prepared by different reduction temperatures.

#	Red. T	Conv	EG	1,2-PD	1,2-BUT	Sor	Man	Gly	Ery	HA	Sum
1	300	100	22,6	20,1	0,8	0,5	1,1	19,1	1,5	9,9	75,6
	350	100	26,1	19,1	2,7	0,8	-	13,1	-	11,5	73,1
2	400	100	26,0	17,9	2,4	0,7	-	9,4	-	11,2	67,6
3	450	100	27,7	20,8	2,5	0,8	-	11,4	-	11,4	74,6

a: The catalytic conversion of cellulose was carried out in a stainless-steel autoclave (75 mL). Cellulose (0,25g), catalyst (0,075 g), and water (25 mL) were charged into the autoclave and stirred at a rate of 800 rpm. The pressure was 60 bar (RT), the reaction temperature 245 °C and the reaction time 2,5 h.

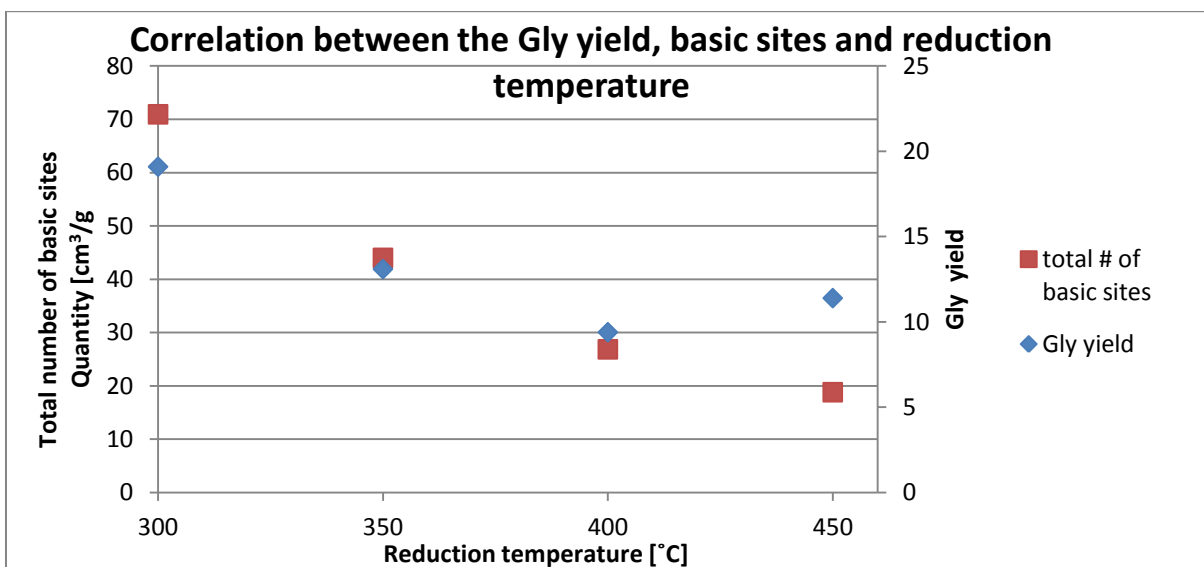


Figure 38 - Correlation between the glycol yield (after cellulose conversion), basic sites and reduction temperature for the 30Ni-26ZnO/CNT catalysts

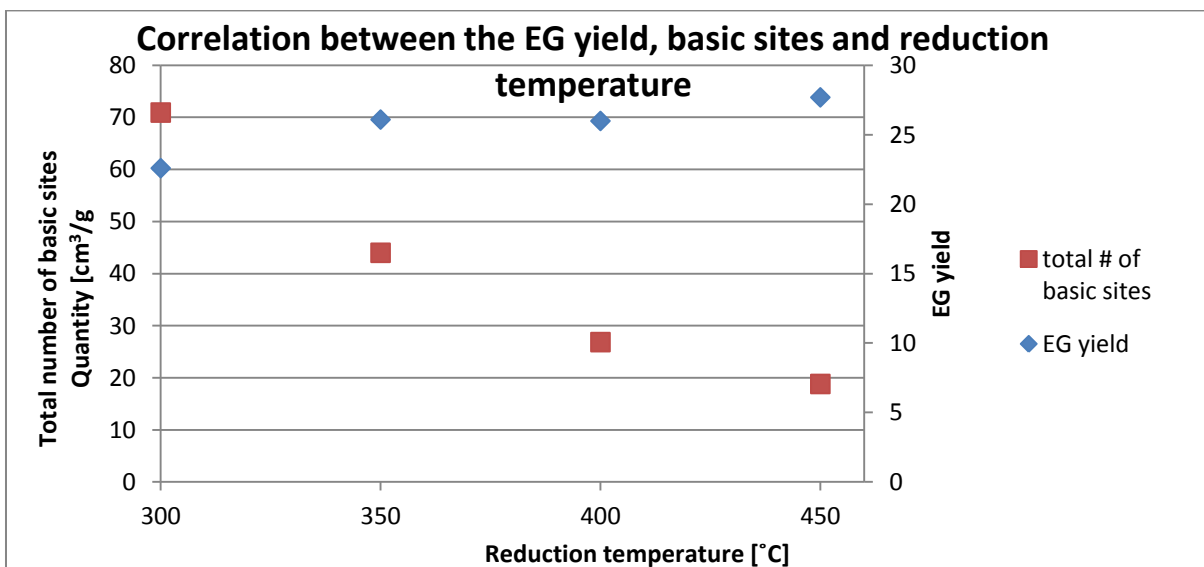
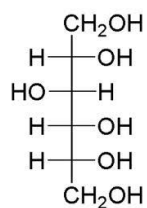


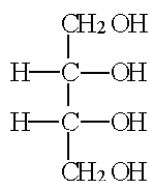
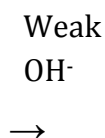
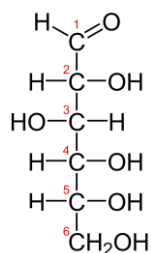
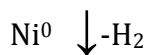
Figure 39 - Correlation between the ethylene glycol yield (after cellulose conversion), basic sites and reduction temperature for the 30Ni-26ZnO/CNT catalysts

4.9.4 Further development of the reaction mechanism

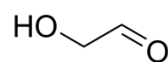
The correlation between basic sites and the yields of EG and Gly are interesting and add further information to the kinetics involved in the cellulose conversion over the Ni-ZnO/CNT catalysts. Based on the correlations discussed in the previous section and previous findings in literature related to glucose and fructose decomposition [56, 57] as well as the degradation kinetics of dihydroxyacetone and glyceraldehyde [58], a more detailed suggestion of the mechanism developed in section 4.6.2 is presented in Figure 40. Sorbitol undergoes dehydrogenation over metallic nickel and glucose is formed. Isomerization between glucose and fructose is established, and the next step is dependent on the basicity of the catalyst, which determines where the C-C cleavage takes place. If the basic sites are strong the isomerization towards fructose is dominant and the C-C cleavage tends to happen on the third carbon atom in fructose. As a result glycerol is formed in addition to 1,3-Dihydroxyacetone, which can react further to form 1,2-PG. However, if the basicity is not as strong, the isomerization towards glucose is usually dominant and the C-C cleavage might occur on the second carbon atom in glucose, which leads to the formation of Erythritol and Glycolaldehyde. Finally, EG is produced from glycolaldehyde over metallic nickel. The suggested mechanism can explain why more glycerol was produced for the catalyst with the strongest basicity, 30Ni-26ZnO/CNT-red300, and also why the decrease in basic sites led to a higher EG yield. According to this mechanism the key related to the change in Gly yield and EG yield is the dominant compound in the isomerisation reaction between glucose and fructose, which will be affected by the basicity. However, this is only a suggested mechanism based on the results achieved herein, and it can be used as basis for more detailed kinetic studies.



Sorbitol



+

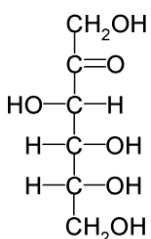


Glucose

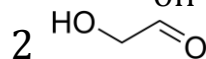
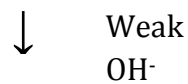
Erythritol

Glycolaldehyde

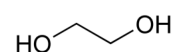
Isomerization



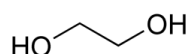
Fructose



Glycolaldehyde

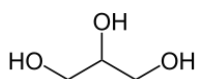


Ethylene Glycol

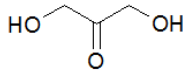


Ethylene Glycol

C-C
cleavage

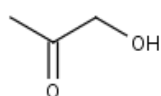


+

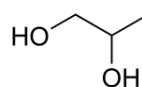


Glycerol

1,3-Dihydroxyacetone



Acetol



Propylene Glycol

Figure 40 - Suggested mechanism for the conversion of cellulose over Ni-ZnO/CNT catalysts

4.9.5 BET measurements

BET measurements were done in order to determine the BET surface area of the 30Ni-26ZnO/CNT catalysts, and the results are given in Table 18. The values for the BET surface area are similar for three of the catalysts and lies between 83 and 84 m²/g. The 30Ni-26ZnO/CNT catalyst reduced at 300°C on the other hand, has a BET surface area of 98,9 m²/g. This high surface area is not necessarily related to the reduction temperature as there is no trend as the reduction temperature increases to 450°C for the other three catalysts. Additionally, the BET measurements described in section 4.8.1 indicate that a BET surface area of 98,9 m²/g for a 30Ni-26ZnO/CNT catalyst is unlikely, and it is therefore possible that the high surface area obtained for the 30Ni-26ZnO/CNT-red300 catalyst is not accurate. Explanations could be related to differences in the CNT support, or some kind of measurement error.

Table 18 - The results from the BET measurements of the 30Ni-26ZnO/CNT catalysts

Catalyst	BET Surface Area [m ² /g]	Pore Volume [cm ³ /g]	Pore Size [Å]	t-Plot micropore volume [cm ³ /g]
30Ni-26ZnO/CNT-red300	98,9	0,42	13,5	0,001
30Ni-26ZnO/CNT-red350	84,3	0,40	16,3	0,006
30Ni-26ZnO/CNT-red400	83,7	0,36	13,8	0,000
30Ni-26ZnO/CNT-red450	84,4	0,35	13,2	0,001

4.9.6 XRD

XRD analysis was carried out for the 30Ni-26ZnO/CNT catalysts prepared with different reduction temperature, and the XRD patterns are presented in Figure 41. As the reduction temperature increases from 300°C to 450°C the peaks for nickel zinc and nickel increases. This is because higher reduction temperature corresponds to more complete reduction of nickel, and thus the nickel peaks will increase. The XRD patterns therefore confirm the expected change in peaks according to reduction temperature.

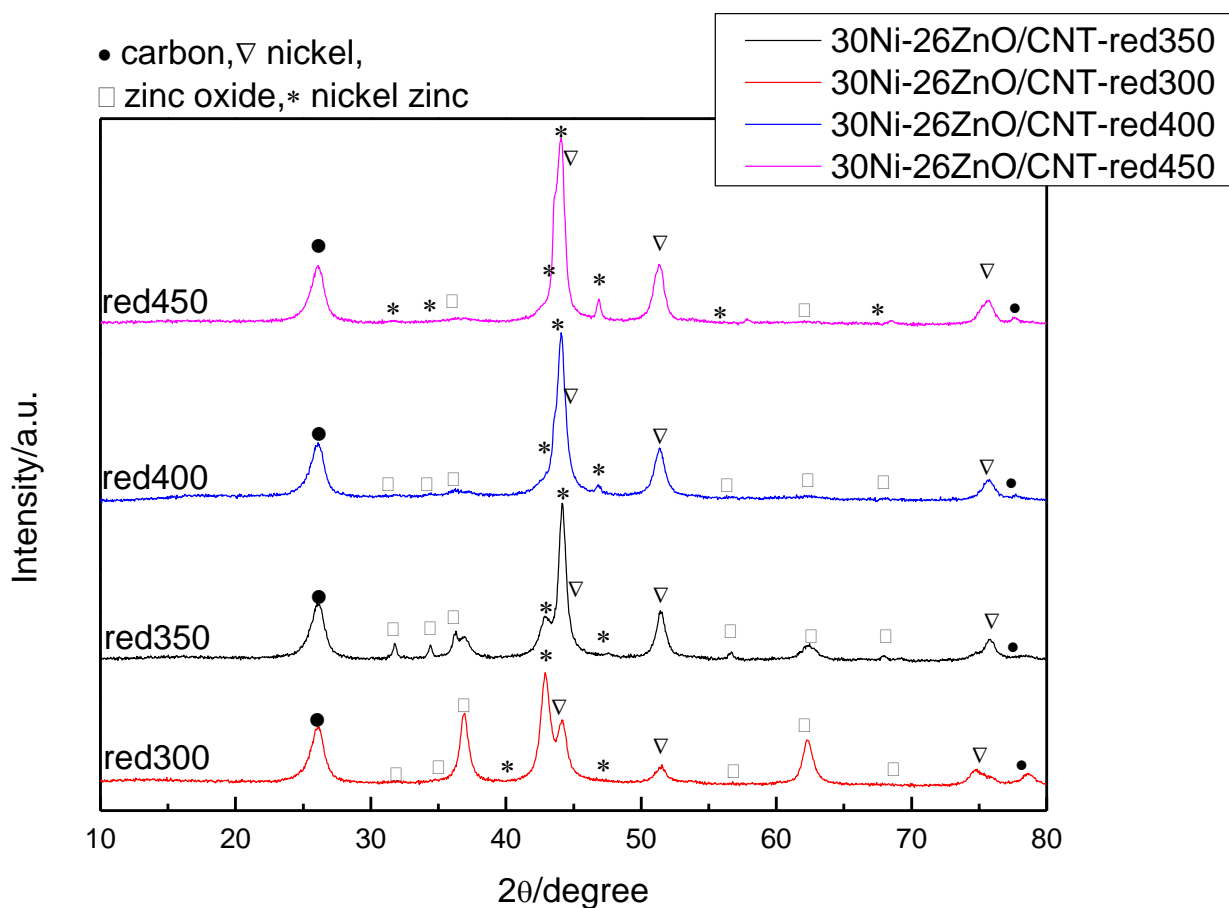


Figure 41 - XRD patterns for the 30Ni-26ZnO/CNT catalysts prepared with different reduction temperature

4.9.7 TGA

TGA was carried out to investigate the overall loading in the 30Ni-26ZnO/CNT catalysts. The plots for DTG and TG as a function of temperature are presented in Figure 42-46. As for the other catalysts tested with TGA, the small increase in mass implies that the samples are oxidized in air before carbon oxidation occurs. The carbon oxidation starts at approximately 400°C, reaches its maximum at 530-550°C, and stabilizes at 600°C for the 30Ni-26ZnO/CNT catalysts. The total loading for each catalyst has been calculated by subtracting the mass loss found from TGA from 100% and the results are presented in Table 19 where they are compared with the theoretical loading (calculated in Appendix I). Similarly to the 20Ni-26ZnO/CNT catalysts with different nickel loading, the theoretical loading is higher than the loading obtained from TGA and the discussion in section 4.8.3 therefore also concerns the 30Ni-26ZnO/CNT catalysts.

30Ni-26ZnO/CNT-red 300

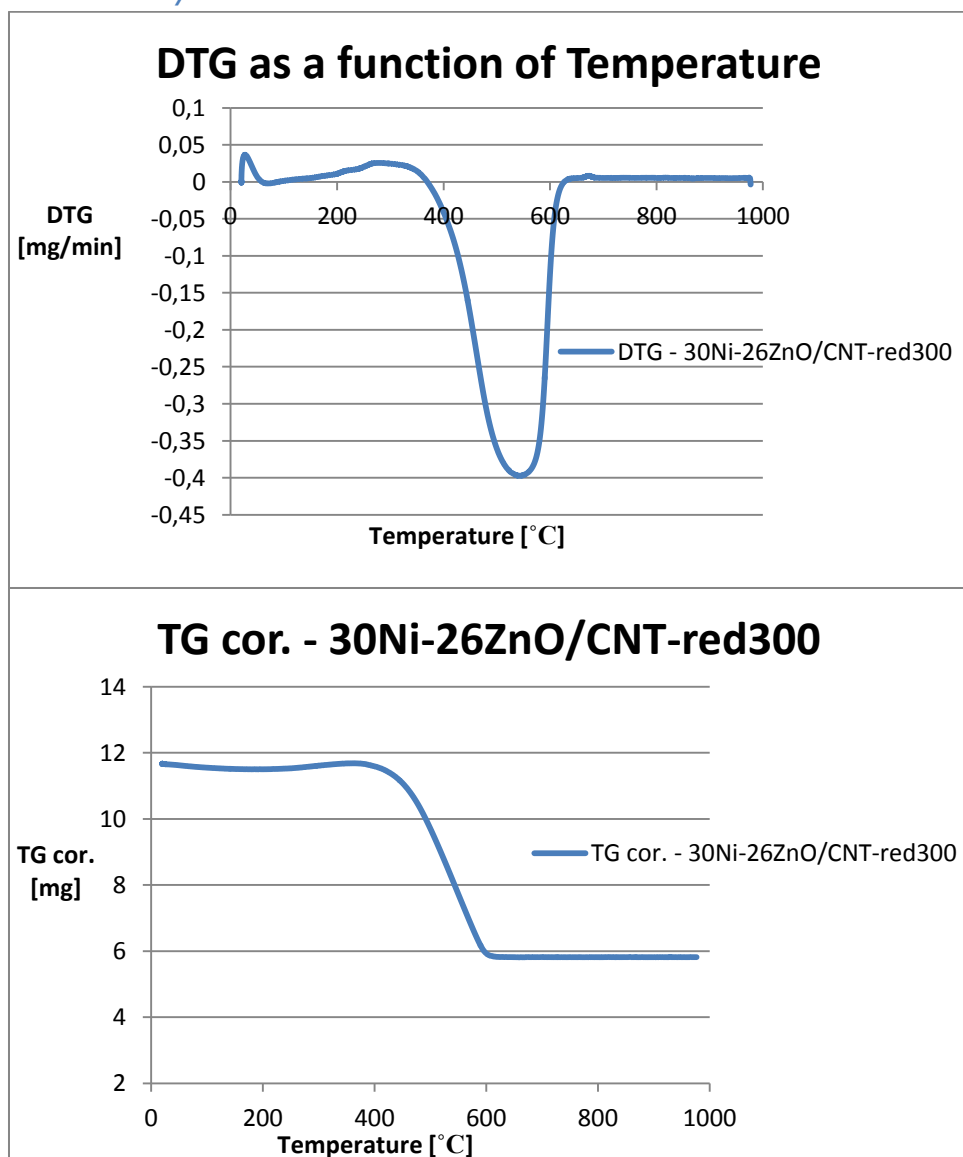


Figure 42 - DTG and TG cor. (from TGA) as a function of temperature for the 30Ni-26ZnO/CNT-red300 catalyst

30Ni-26ZnO/CNT-red350

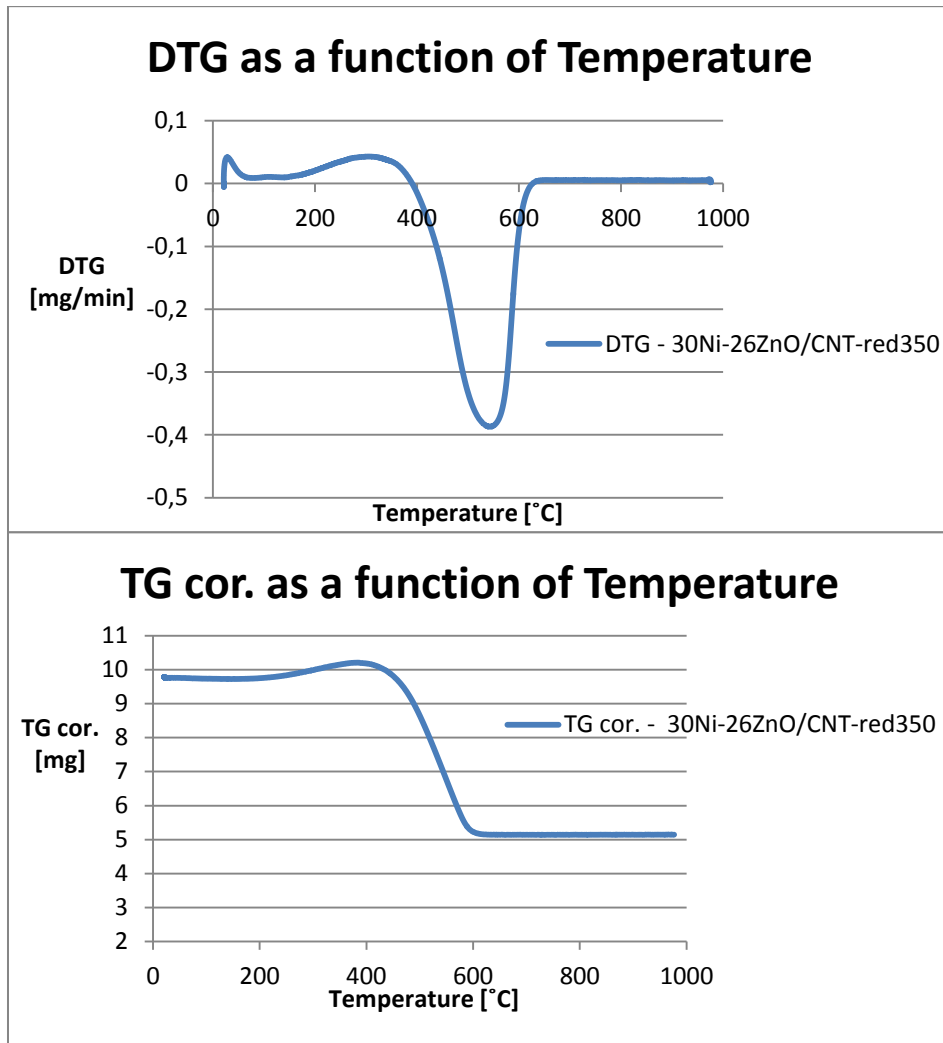


Figure 43 - DTG and TG cor. (from TGA) as a function of temperature for the 30Ni-26ZnO/CNT-red350 catalyst

30Ni-26ZnO/CNT-red 400

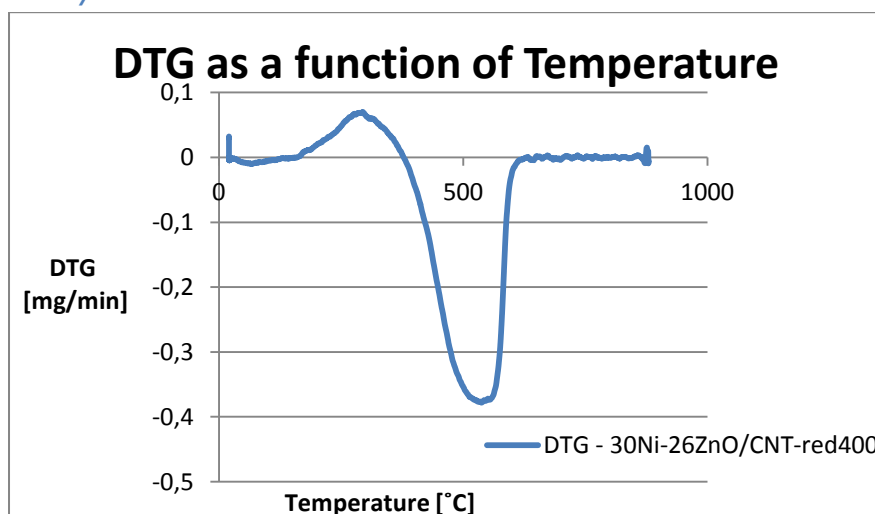


Figure 44 - DTG as a function of temperature for the 30Ni-26ZnO/CNT-red400 catalyst

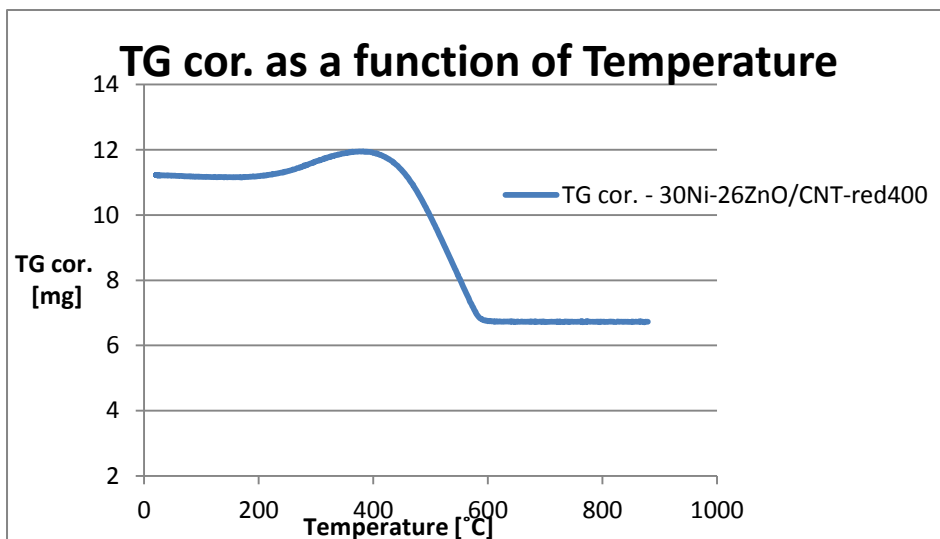


Figure 45 - TG cor. (from TGA) as a function of temperature for the 30Ni-26ZnO/CNT-red400 catalyst

30Ni-26ZnO/CNT - red450

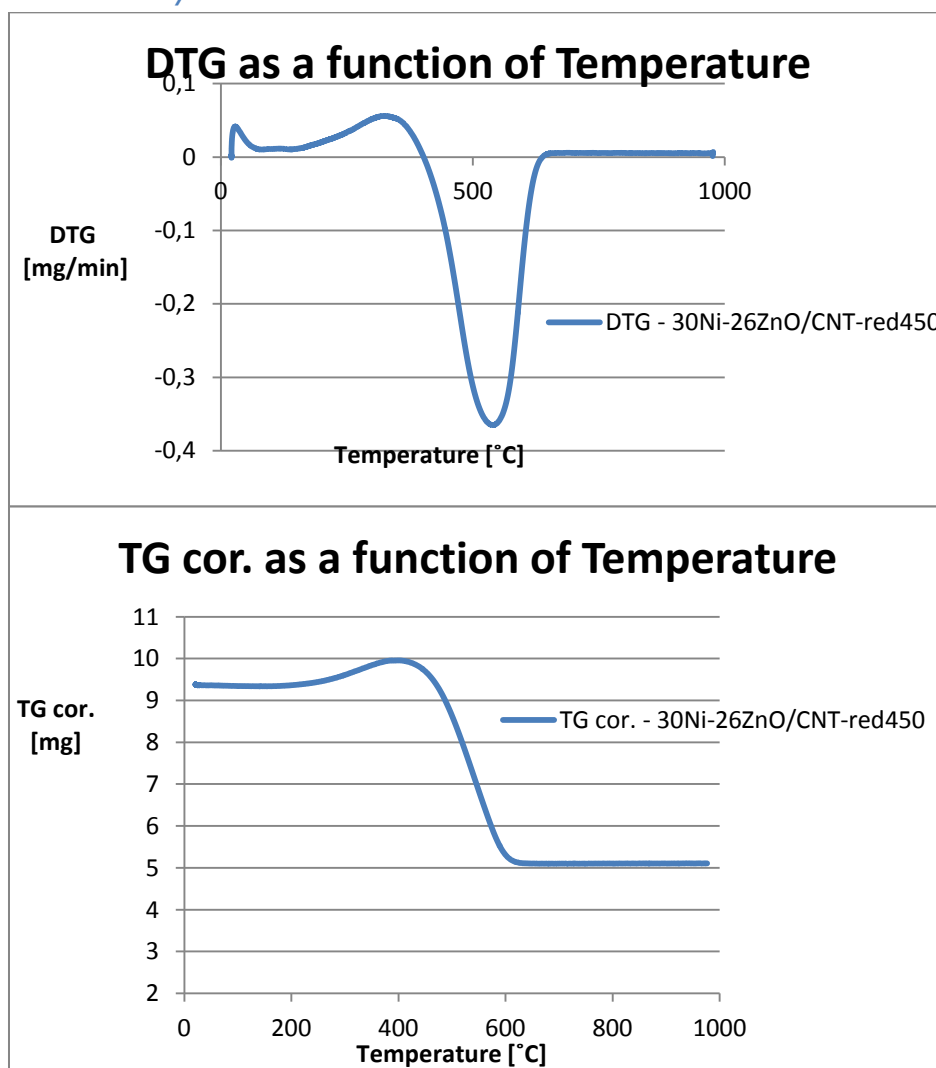


Figure 46 - DTG and TG cor. (from TGA) as a function of temperature for the 30Ni-26ZnO/CNT-red450 catalyst

Table 19 - Total loading for the 30Ni-26ZnO/CNT catalysts with different reduction temperature according to TGA analysis and theoretical calculations

Catalyst	Mass loss [%]	Total loading according to TGA [%]	Total theoretical loading [%]
30Ni-26ZnO/CNT-red300	-50,9	49,1	61,7
30Ni-26ZnO/CNT-red350	-48,8	51,2	61,5
30Ni-26ZnO/CNT-red400	-40,5	59,5	61,2
30Ni-26ZnO/CNT-red450	-45,5	54,5	61,6

4.10 Reusability and ICP

4.10.1 Reusability

In this master thesis, the focus has been on the understanding and improvement of the 20Ni-26ZnO/CNT catalyst prepared at NTNU the fall of 2012. However, studies related to the reusability of the Ni-ZnO/CNT catalysts have been started and the results might be useful in future studies. Three of the Ni-ZnO/CNT catalysts that were used for the conversion of cellulose, were retrieved and used for a second run of cellulose conversion. The product distribution from each reaction is given in Table 20, and there are especially three trends of interest. First of all, a significant drop in the EG yield was observed for all three catalysts. For instance, the EG yield produced by the 20Ni-28ZnO/CNT catalyst decreased from 32,1 % in the first run to 23,6 % in the second run. Second, an opposite trend was observed for the 1,2-PG yield which increased in the second run for all three catalysts. In the first reaction over the 20Ni-28,3ZnO/CNT catalyst, the 1,2-PG yield was 13,8 %, while in the second run the 1,2-PG yield had increased to 17,9 %. Third, a significant increase in the sorbitol and mannitol yields was observed for the Ni-ZnO/CNT catalysts with Ni-loading 20%. This is interesting because the conversion of cellulose to EG over the Ni-ZnO/CNT catalyst is expected to occur via the formation of sorbitol and mannitol. Therefore it seems like the catalyst does not have the ability to transform all the hexitols to EG via hydrogenolysis in the second run. In order to look for some explanation for the different trends observed in the second run, the leaching of Ni and Zn was tested, and the results are discussed in the following two sections.

Table 20 – Product distribution from the first and second run of cellulose conversion of Ni-ZnO/CNT catalysts

#	Catalyst	Run	EG	1,2-PD	1,2-BUT	Sor	Man	Gly	Ery	HA	Sum
1	20Ni-28,3ZnO /CNT	1	32,1	13,8	2,7	0,6	0,7	11,3	1,5	7,8	70,6
2	20Ni-28,3ZnO /CNT	2	23,6	17,9	3,9	5,3	3,0	12,2	2,1	8,6	76,5
3	20Ni-46,6 ZnO /CNT	1	31,3	14,0	2,8	0,6	0,9	12,4	1,7	8,1	71,8
4	20Ni-46,6 ZnO /CNT	2	24,9	17,1	4,0	4,1	2,3	13,5	2,3	11,3	79,5
5	5Ni-26,1ZnO /CNT	1	23,8	14,4	2,9	6,7	4,0	10,6	1,9	7,3	71,5
6	5Ni-26,1ZnO /CNT	2	12,5	16,6	2,1	4,3	-	1,5	0,4	4,8	42,2

4.10.2 Leaching of nickel and zinc - ICP

ICP analysis was done to investigate the leaching of Zinc and Nickel. The filtrate after the cellulose conversion over the 20Ni-26ZnO/CNT catalyst was used to prepare the sample, and the results are presented in Table 21. The calculations can be found in Appendix L. Based on the results from the ICP analysis, it is clear that the leaching of Zn, 2,97 %, is much more severe than the leaching of Ni, 0,15 %.

Table 21 - Leaching of zinc and nickel after cellulose conversion over a 20Ni-26ZnO/CNT catalyst according to the results from the ICP analysis

Compound	Detected amount in sample [ppm]	Leaching after reaction [%]
Ni	0,0179	0,15
Zn	0,465	2,97

The change in product distribution from the first run of cellulose conversion to the second run might be related to the leaching of zinc. If a significant amount of zinc is leached during the first reaction it is highly likely that the basic properties of the catalyst will change, and the product distribution in the following run will be affected. The ICP analysis revealed that almost 3 % of Zinc was leached during the first reaction. It is therefore possible that the decrease in the EG yield might be related to a change in basicity as a result of zinc leaching. Another possible explanation for the differences in the product distribution in the first and second reaction is Ni aggregation [59]. The ICP analysis revealed that a very small amount of Ni leaching, 0,15%, was detected after the first run of cellulose conversion. However, this does not necessarily mean that the leaching of nickel is neglectable. One possible scenario involves Ni aggregation. Nickel leaching can occur on the surface of the catalyst at hydrothermal conditions, and the leached metal ions in the hot water subsequently aggregate onto another nickel particle on the catalyst surface [59]. If this is the case, the total amount of leached nickel will not be detected during ICP analysis (because re-deposition of the leached metal ions occurs on the catalyst surface). The aggregation of nickel will lead to bigger Ni particles, and as a result the catalyst will be less active. The decrease in activity will affect the product distribution, and intermediates that are known to be unstable under hydrothermal conditions, such as glycolaldehyde, may undergo side reactions. The reaction mechanism proposed in section 4.9.4 illustrates that glycolaldehyde is an intermediate to EG, thus a less active catalyst (due to nickel aggregation) will allow this unstable compound to undergo side reactions (such as condensations reactions). Glucose and acetol on the other hand, are stable under hydrothermal conditions, and both these compounds are intermediates on the suggested pathway to the formation of 1,2-PG. Thus a loss in activity due to nickel aggregation could shift the selectivity towards the

more stable pathway towards 1,2-PG as oppose to EG. The third trend discussed in section 4.10.1 involves the significant increase in the hexitol yield (sorbitol and mannitol) from the first run of cellulose conversion to the second run. For instance, the sorbitol and mannitol yields produced over the 20Ni-28ZnO/CNT catalyst increased from 0,6 % and 0,7 % respectively (first run) to 5,5 % and 3,0 % (second run). Thus the hydrogenolysis activity dramatically changed in the catalyst. This change might be related to nickel aggregation as well, and one can speculate that if nickel aggregation occurs, the resulting loss in catalyst activity might primarily be related to the hydrogenolysis activity, which seems more sensitive to the changes from the first to the second run than the hydrogenation activity.

It should be emphasized that further studies are necessary to understand the complex kinetics related to the reusability of the Ni-ZnO/CNT catalyst. The suggested explanations related to the change in the EG yield, hexitol yield and 1,2-PG yield (in the reusability tests) are only meant as possible scenarios based on the findings herein, and more detailed studies are necessary to confirm or invalidate these ideas.

4.11 Hydrogen Chemisorption

It should be mentioned that an attempt to investigate the nickel dispersion in the catalysts was done by H₂-chemisorption characterization. However, the results given in Table 22 seem highly unlikely and are not in agreement with the SEM and TEM results. For instance, nickel particles with diameter as small as 5 nm were found in the SEM and TEM characterization of the 20Ni-26ZnO/AC (incipient) catalyst, but the cubic crystalline size obtained from the H₂ chemisorption indicates 334,1 nm and a metal dispersion of 0,25%, which is extremely low. Except for the 20Ni catalysts with AC and CNT support, the dispersion for the Ni-ZnO/CNT and Ni-ZnO/AC catalysts is so low that one should question the credibility of these values. Similar measurements problems have been encountered in the past when samples involving metal NPs supported on carbon or CNT have been tested in the instrument used for H₂ chemisorption. Even though the explanation to these difficulties remains unclear, it seems like it is difficult to measure the precise dispersion for metal NPs with CNT or AC support in the apparatus used for H₂ chemisorption. Hydrogen chemisorption has also been carried out at NTNU for the 20Ni-28ZnO/CNT catalyst as part of the lab work in the specialization project the fall of 2012, and the result obtained is indeed very different than the low value presented in Table 22. The metal dispersion from the analysis done at NTNU was 2,8% and the crystalline size 35,9 nm, which seem much more likely than 0,21% and 403,7 nm. Therefore the exact values in Table 22 should not be paid much attention to. However, it is possible to observe some form of logic from the results obtained for the Ni-26ZnO/CNT catalyst with nickel loading 5-30%. Even though the dispersion values seem too low, they decrease as the nickel loading increases from 5% to 30%, which is reasonable because high nickel loading could lead to poorer dispersion.

Table 22 - H₂-Chemisorption results (cubic crystallite size and metal dispersion) for the Ni-ZnO catalysts with carbon support

Catalyst	Metal dispersion [%]	Cubic Crystallite Size [nm]
20Ni-26ZnO /CNT	1.00	84.0
20Ni-28ZnO/CNT	0,21	403,7
20Ni-40ZnO/CNT	0,29	292,3
20Ni-46ZnO/CNT	0,16	538,8
5Ni-26ZnO/CNT	0.93	90.4
10Ni-26ZnO/CNT	0.58	144.3
15Ni-26ZnO/CNT	0.81	104.1
25Ni-26ZnO/CNT	0,53	158,2
30Ni-26ZnO/CNT	0,11	737,8
20Ni/CNT	4,56	18,5
20Ni/AC	3,25	26,0
20Ni-26ZnO /AC (incipient)	0.25	334.1
20Ni-26ZnO /AC (pechini)	0.22	82.6

5. Future studies and perspectives

Herein Ni-26ZnO/CNT catalysts with nickel loading from 5% to 30% were studied for the conversion of cellulose. The highest yields of the main products EG (34,6%) and 1,2-PG (34,6%) were obtained over the 30Ni-26ZnO/CNT catalyst, and a trend in which the EG yield increased as a function of nickel loading was reported. Therefore it would be interesting to increase the nickel loading further to figure out if an even higher nickel loading would improve the EG yield further, or if a maximum would be found when the nickel loading in the catalyst is 30%. Another consideration for future studies is to investigate the consequences of lowering the ZnO-loading from 26% to mass percentages down to 5%, while the nickel loading is kept constant at 30%. This should change the basic properties of the catalyst, and it is therefore likely that the selectivity will be affected too. A third modification that possibly could improve the Ni-ZnO/CNT catalysts would be to introduce Cu in order to promote a higher 1,2-PG yield on the expense of glycerol. As mentioned in section 2.1.2, Cu/ZnO catalysts have been reported as effective for the hydrogenolysis of glycerol to 1,2-PG. These findings show great potential for improvement of the Ni-ZnO/CNT catalysts because glycerol is produced as one of the main products after EG and 1,2-PG. If the glycerol product could be converted to 1,2-PG the combined yield for EG and 1,2-PG would exceed 52,4% and thus the catalytic performance in terms of selectivity would be improved. The reusability of the Ni-ZnO/CNT catalysts is definitely something one should look into in the future to fully understand the observations reported in this study, and to gain knowledge in order to make the catalyst stable for several runs and thus suitable for industrial use. The conversion of cellulose is carried out under hydrothermal conditions in a 3-phase system, thus transportation limitations can occur and the support material should therefore be chosen carefully. Herein, Ni-ZnO catalysts with activated carbon support was prepared and compared to the CNT supported Ni-ZnO catalysts. The results for the cellulose conversion operated at 245°C, 60 bar (RT) and with reaction time 2,5 hours revealed that the CNT supported catalyst provided the highest EG and 1,2-PG yield. The focus in this study was therefore kept at CNT supported Ni-ZnO catalysts. However, the Ni-ZnO catalysts with activated carbon support also converted cellulose to EG and 1,2-PG with high yields. If one would like to investigate the differences between these two support materials further, a similar experiment as the one described in section 4.6.2, in which yield was studied as a function of time, could be done for the Ni-ZnO/AC supported catalysts. This would provide information of the product distribution obtained over the AC supported catalysts at low conversion, and observations related to activity and diffusion limitations might be found. As a final remark, a few comments about the potential usage and future perspectives of the Ni-ZnO/CNT catalyst are given. First of all, the Ni-ZnO/CNT catalyst has recently been developed for the conversion of cellulose, therefore there are still many possibilities for improvement and optimization of the catalyst, as there are many areas that have not been explored yet. However, the ability to convert cellulose to EG and 1,2-PG with yields as high as 34,6% and 17,8% respectively is noteworthy and makes the Ni-ZnO/CNT catalyst an

interesting option to consider for biomass conversion. Advantages such as good diffusion environment and rapid filtration (to recover catalyst) are important for industrial production, and make the Ni-ZnO/CNT catalyst an interesting alternative to traditionally AC supported catalysts. In the future it might even be an option to grow the CNTs inside the reactor and in this scenario the catalyst would be fixed in a continuous reactor, which would make the cellulose production much more efficient than when powder catalysts are used and recovered after each batch. The products, EG and 1,2-PG, are valuable and could either be used as chemicals themselves, or upgraded to transportation fuels to provide an alternative to the fossil fuels industry.

6. Conclusion

Ni-ZnO/CNT catalysts were prepared by the pechini method, and tested for the conversion of cellulose. i) An optimal reaction time of 2,5 h was found, and the catalytic performance of 20Ni-ZnO/CNT catalysts with ZnO-loading 26-46% revealed that the highest EG and 1,2-PG yield (32,8% and 15,2% respectively) were obtained over the 20Ni-26ZnO/CNT catalyst. ii) 26ZnO/CNT, 20Ni/CNT and 20Ni/26ZnO catalysts were prepared and evaluated for the conversion of cellulose, which demonstrated that a synergistic effect between Ni and ZnO occur in the Ni-ZnO/CNT catalyst and that Ni promotes hydrogenation. iii) Two batches of activated carbon supported Ni-ZnO catalysts were prepared by the pechini method and incipient wetness impregnation. The SEM and TEM pictures indicated that the incipient wetness impregnation leads to better dispersion for these Ni-ZnO/AC catalysts. The conversion of cellulose was tested over the activated carbon supported Ni-ZnO catalysts, and the EG and 1,2-PG-yields obtained were not as high as for the CNT supported Ni-ZnO catalyst. iv) Sorbitol, mannitol and cellulose feedstock were tested over the 20Ni-26ZnO/CNT catalyst, which was able to convert all three feedstocks to EG and 1,2-PG. Yield as a function of time was studied, and the results suggested that the main pathway from cellulose to EG and 1,2-PG over the 20Ni-26ZnO/CNT catalyst happens via sorbitol and mannitol. v) Ni-26ZnO/CNT catalyst with nickel loading 5-30% were prepared and evaluated for the conversion of cellulose. A trend in which the EG yield increased as a function of nickel loading was observed, and the best results were therefore obtained over the 30Ni-26ZnO/CNT catalyst, which produced an EG yield of 34,6% and a 1,2-PG yield of 17,8%. Thus a combined EG yield and 1,2-PG yield of 52,3% was achieved. vi) 30Ni-26ZnO/CNT catalysts with different reduction temperature were prepared, and the CO₂-TPD characterization revealed that the number of basic sites decreased as the reduction temperature increased. A strong correlation between basic sites, reduction temperature and glycerol was found, in which the glycerol yield decreased with higher reduction temperature (thus less basic sites). This observation indicates that the glycerol production mainly takes place on basic sites. Additionally, a weak correlation between the EG yield, reduction temperature and basic sites were found, in which the EG yield slightly increased as the number of basic sites decreased. A reaction mechanism for the conversion of cellulose over Ni-ZnO/CNT catalysts was suggested. vii) Reusability studies have been started, and three trends were observed when the product distribution in first run of cellulose conversion was compared to second run. The EG yield decreased, the 1,2-PG yield increased, and the sorbitol and mannitol yields were significantly higher in the second run. Zinc leaching, and nickel aggregation have been discussed as possible explanations.

References

1. Administration), T.U.S.E.E.I., *International Energy Outlook 2011*. Report No. DOE/EIA-0484(2011) Available electronically at: [www.eia.gov/ieo/pdf/0484\(2011\).pdf](http://www.eia.gov/ieo/pdf/0484(2011).pdf), 2011.
2. Xiao, Z., et al., *Conversion of highly concentrated cellulose to 1,2-propanediol and ethylene glycol over highly efficient CuCr catalysts*. *Green Chemistry*, 2013. **15**(4): p. 891-895.
3. Alonso, D.M., S.G. Wettstein, and J.A. Dumesic, *Bimetallic catalysts for upgrading of biomass to fuels and chemicals*. *Chemical Society Reviews*, 2012. **41**(24): p. 8075-8098.
4. (WFP), W.F.P., *The world's largest humanitarian agency fighting hunger worldwide*. <http://www.wfp.org/hunger>.
5. Li, C., et al., *One-pot catalytic hydrocracking of raw woody biomass into chemicals over supported carbide catalysts: simultaneous conversion of cellulose, hemicellulose and lignin*. *Energy & Environmental Science*, 2012. **5**(4): p. 6383-6390.
6. George W. Huber, S.I., and A. Corma, *Synthesis of Transportation Fuels from Biomass: Chemistry, Catalysts, and Engineering*. *Chemical Reviews*, 2006. **106**(Available at: http://works.bepress.com/george_huber/32): p. 4044-4098.
7. Carlos Serrano-Ruiz, J. and J.A. Dumesic, *Catalytic routes for the conversion of biomass into liquid hydrocarbon transportation fuels*. *Energy & Environmental Science*, 2011. **4**(1): p. 83-99.
8. Zhang, A.W.a.T., *One-pot Conversion of Cellulose to Ethylene Glycol with Multifunctional Tungsten-Based Catalysts*. *Accounts of Chemical Research*, 2013.
9. Sad, M.E., M. Neurock, and E. Iglesia, *Formation of C-C and C-O Bonds and Oxygen Removal in Reactions of Alkanediols, Alkanols, and Alkanals on Copper Catalysts*. *Journal of the American Chemical Society*, 2011: p. 133(50): p. 20384-20398.
10. Fukuoka, A.a.P.L.D., *Catalytic conversion of cellulose into sugar alcohols*. *Angewandte Chemie-International Edition*, 2006: p. 45(31): p. 5161-5163.
11. Ji, N., et al., *Direct Catalytic Conversion of Cellulose into Ethylene Glycol Using Nickel-Promoted Tungsten Carbide Catalysts*. *Angewandte Chemie-International Edition*, 2008(47(44)): p. 8510-8513).
12. Li, C., et al., *One-pot catalytic hydrocracking of raw woody biomass into chemicals over supported carbide catalysts: simultaneous conversion of cellulose, hemicellulose and lignin*. *Energy & Environmental Science*, 2012: p. 5(4): p. 6383-6390.
13. Pang, J., et al., *Catalytic Hydrogenation of Corn Stalk to Ethylene Glycol and 1,2-Propylene Glycol*. *Industrial & Engineering Chemistry Research*, 2011: p. 50(11): p. 6601-6608.
14. Zhang, Y., A. Wang, and T. Zhang, *A new 3D mesoporous carbon replicated from commercial silica as a catalyst support for direct conversion of cellulose into ethylene glycol*. *Chemical Communications*, 2010: p. 46(6): p. 862-864.
15. Zheng, M.-Y., et al., *Transition Metal-Tungsten Bimetallic Catalysts for the Conversion of Cellulose into Ethylene Glycol*. *Chemsuschem*, 2010: p. 3(1): p. 63-66.
16. Tai, Z., et al., *Temperature-controlled phase-transfer catalysis for ethylene glycol production from cellulose*. *Chemical Communications*, 2012: p. 48(56): p. 7052-7054.
17. Liu, Y., C. Luo, and H. Liu, *Tungsten Trioxide Promoted Selective Conversion of Cellulose into Propylene Glycol and Ethylene Glycol on a Ruthenium Catalyst*. *Angewandte Chemie-International Edition*, 2012: p. 51(13): p. 3249-3253.
18. Wang, X., et al., *Efficient conversion of microcrystalline cellulose to 1,2-alkanediols over supported Ni catalysts*. *Green Chemistry*, 2012. **14**(3): p. 758-765.
19. Wang, X., et al., *Ni-Cu/ZnO-catalyzed Hydrogenolysis of Cellulose for the Production of 1,2-Alkanediols in Hot Compressed Water*. *Chemistry Letters*, 2012. **41**(5): p. 476-478.
20. ten Dam, J. and U. Hanefeld, *Renewable Chemicals: Dehydroxylation of Glycerol and Polyols*. *Chemsuschem*, 2011. **4**(8): p. 1017-1034.

21. Chambers, T.V.H.a.C.R., *Manufacture of Carbon Filaments*. US Patent No. 405, 480, 1889.
22. Monthieux, M. and V.L. Kuznetsov, *Who should be given the credit for the discovery of carbon nanotubes?* Carbon, 2006. **44**(9): p. 1621-1623.
23. Geus, K.P.J.a.J.W., *Carbon Nanofibers: Catalytic Synthesis and Applications*. Catal. Rev.-Sci. Eng., 2000. **42**: p. 481-510.
24. Kroto, H.W., et al., *C-60 - BUCKMINSTERFULLERENE*. Nature, 1985. **318**(6042): p. 162-163.
25. Subramoney, S., *Novel nanocarbons - Structure, properties, and potential applications*. Advanced Materials, 1998. **10**(15): p. 1157-+.
26. "The Nobel Prize in Chemistry, 1996", Nobelprice.org, May 2013.
http://www.nobelprize.org/nobel_prizes/chemistry/laureates/1996/#, 1996.
27. Iijima, S., *HELICAL MICROTUBULES OF GRAPHITIC CARBON*. Nature, 1991. **354**(6348): p. 56-58.
28. Ebbesen, T.W. and P.M. Ajayan, *LARGE-SCALE SYNTHESIS OF CARBON NANOTUBES*. Nature, 1992. **358**(6383): p. 220-222.
29. Iijima, S. and T. Ichihashi, *SINGLE-SHELL CARBON NANOTUBES OF 1-NM DIAMETER*. Nature, 1993. **363**(6430): p. 603-605.
30. Bethune, D.S., et al., *COBALT-CATALYZED GROWTH OF CARBON NANOTUBES WITH SINGLE-ATOMIC-LAYERWALLS*. Nature, 1993. **363**(6430): p. 605-607.
31. Mostofizadeh, A., et al., *Synthesis, Properties, and Applications of Low-Dimensional Carbon-Related Nanomaterials*. Journal of Nanomaterials, 2011.
32. Zhu, J., A. Holmen, and D. Chen, *Carbon Nanomaterials in Catalysis: Proton Affinity, Chemical and Electronic Properties, and their Catalytic Consequences*. Chemcatchem, 2013. **5**(2): p. 378-401.
33. Cheng, H.Y., et al., *Modeling of fishbone-type carbon nanofibers with cone-helix structures*. Carbon, 2012. **50**(12): p. 4359-4372.
34. Martin-Gullon, I., et al., *Differences between carbon nanofibers produced using Fe and Ni catalysts in a floating catalyst reactor*. Carbon, 2006. **44**(8): p. 1572-1580.
35. Yu, Z.X., et al., *Effect of support and reactant on the yield and structure of carbon growth by chemical vapor deposition*. Journal of Physical Chemistry B, 2005. **109**(13): p. 6096-6102.
36. De Jong, K.P., *Synthesis of Solid Catalysts*. Wiley-VCH, 2009. **Weinheim**.
37. Zhao, T.J., et al., *Synthesis of Supported Catalysts by Impregnation and Calcination of Low-Temperature Polymerizable Metal-Complexes*. Topics in Catalysis, 2011. **54**(16-18): p. 1163-1174.
38. Haber, J., J.H. Block, and B. Delmon, *MANUAL OF METHODS AND PROCEDURES FOR CATALYST CHARACTERIZATION*. Pure and Applied Chemistry, 1995. **67**(8-9): p. 1257-1306.
39. Caturla, F., et al., *Electroless plating of graphite with copper and nickel*. Journal of the Electrochemical Society, 1995. **142**(12): p. 4084-4090.
40. G. O. Mallory, J.B.H., *Electroless Plating: Fundamentals & Applications*. American Electroplaters and Surface Finishers Society, 1990. **Orlando, Florida**.
41. Li, Q.Q., et al., *Coating of carbon nanotube with nickel by electroless plating method*. Japanese Journal of Applied Physics Part 2-Letters, 1997. **36**(4B): p. L501-L503.
42. Liu, H.P., et al., *Influence of synthesis process on preparation and properties of Ni/CNT catalyst*. Diamond and Related Materials, 2006. **15**(1): p. 15-21.
43. Liu, H.P., et al., *Influence of acid treatments of carbon nanotube precursors on Ni/CNT in the synthesis of carbon nanotubes*. Journal of Molecular Catalysis a-Chemical, 2005. **230**(1-2): p. 17-22.
44. Zeng, Q., et al., *Coating of SWNTs with nickel by electroless plating method*, in *Prism 5: The Fifth Pacific Rim International Conference on Advanced Materials and Processing, Pts 1-5*, Z.Y. Zhong, et al., Editors. 2005. p. 1013-1018.
45. Benoît Heinrichs, S.L., Nathalie Job, and Jean-Paul Pirard, *Catalyst Preparation - Science and Engineering - Sol-Gel Synthesis of Supported Metals*. 2006: p. 163-208.
46. Alexander Gash, L.W.H., Randall L. Simpson, Thomas M. Tillotson, *Method for producing nanostructured metal-oxides*. Patent US6986818 B2, 2006.
<http://www.google.com/patents/US6986818>(Reference date: 19.05.13).

47. Lambert, C.K. and R.D. Gonzalez, *Sol-gel preparation and thermal stability of Pd/gamma-Al₂O₃ catalysts*. Journal of Materials Science, 1999. **34**(13): p. 3109-3116.
48. Pechini, M.P., *US Patent 3,330,97*.
<http://www.google.com/patents/about?id=D3sfAAAAEBAJ&dq=3,330,697>, 1967.
reference date: 19.05.13.
49. Kakihana, V.P.a.M., *Handbook of sol-gel science and technology. Sol-gel processing*. 2005. **1**: p. 77-97.
50. Lee, H., et al., *A novel approach to preparing nano-size Co₃O₄-coated Ni powder by the Pechini method for MCFC cathodes*. Journal of Materials Chemistry, 2003. **13**(10): p. 2626-2632.
51. Liland, I.S., *Direct catalysis of lignocellulosic material into polyols using a CNT-supported Ni-ZnO catalyst*. Specialization project in TKP4530, NTNU, 2012.
52. Ji, N., et al., *Catalytic conversion of cellulose into ethylene glycol over supported carbide catalysts*. Catalysis Today, 2009. **147**(2): p. 77-85.
53. Zhou, L., et al., *Selective Production of 1,2-Propylene Glycol from Jerusalem Artichoke Tuber using Ni-W₂C/AC Catalysts*. Chemsuschem, 2012. **5**(5): p. 932-938.
54. Bjørgen, C., *One-pot conversion of cellulose to ethylene glycol and propylene glycol over tungsten based catalysts on carbon support*. Master thesis, 2013. **NTNU (Norwegian University of Science and Technology)**.
55. Zhijun Tai, J.Z., Aiqin Wang, Mingyuan Zheng and Tao Zhang, *Temperature-controlled phase-transfer catalysis for ethylene glycol production from cellulose*. Chem. Commun, 2012. **48**: p. 7052-7054.
56. Bernard M. Kabyemela, T.A., Roberto M. Malaluan, and Kunio Arai, *Glucose and Fructose Decomposition in Subcritical and Supercritical Water: Detailed Reaction Pathway, Mechanisms, and Kinetics*. American Chemical Society, 1999. **Ind. Eng. Chem. Res.** **38**: p. 2888-2895.
57. Yu, Y. and H.W. Wu, *Kinetics and Mechanism of Glucose Decomposition in Hot-Compressed Water: Effect of Initial Glucose Concentration*. Industrial & Engineering Chemistry Research, 2011. **50**(18): p. 10500-10508.
58. Bernard M. Kabyemela, T.A., Roberto M. Malaluan, and Kunio Arai, *Degradation Kinetics of Dihydroxyacetone and Glyceraldehyde in Subcritical and Supercritical water*. American Chemical Society, 1997. **Ind. Eng. Chem. Res.** **36**: p. 2025-2030.
59. Pang, J., et al., *Catalytic conversion of cellulose to hexitols with mesoporous carbon supported Ni-based bimetallic catalysts*. Green Chemistry, 2012. **14**(3): p. 614-617.

A Impregnation of Zn precursor and calculation of ZnO-loading

All of the CNT-supported catalysts prepared at DICP were loaded with 26% ZnO. In addition, four 20Ni-ZnO/CNT catalysts with different ZnO-loading were prepared at NTNU the fall of 2012. The calculation method for the ZnO-loading is identical for all the Ni-ZnO/CNT catalysts, and have therefore been done in excel, as presented in Table 24. An example of the calculation of the ZnO-loading is demonstrated for the 15Ni-26ZnO/CNT catalyst.

The ZnO-loading on the CNTs can be calculated from the following equation:

$$\frac{m_{ZnO}}{m_{CNT} + m_{ZnO}}$$

The mass of ZnO is given by

$$m_{ZnO} = n_{ZnO} * MW_{ZnO} = \frac{m_{ZnX}}{MW_{ZnX}} * MW_{ZnO}$$

Example: The 15Ni-26ZnO/CNT catalyst:

The complex solution was prepared by using the following amounts of chemicals:

Table 23 - Chemicals used in the complex solution for the impregnation of zinc precursor on the 15Ni-26ZnO/CNT catalyst

PEG	CA	Distilled water	CNT	Zn(NO ₃) ₂ * 6H ₂ O
[g]	[g]	[ml]	[g]	[g]
1,0052	3,1448	10	3,0476	7,2261

5,5 ml complex solution was impregnated on the CNT #1D support.

$$Mw (Zn(NO_3)_2 * 6H_2O) = 297,49 g/mol$$

$$Mw (ZnO) = 81,39 g/mol$$

$$m_{ZnO} = \frac{7,2261g}{297,49g/mol} * \frac{81,39g}{mol} = 1,9770 g$$

$$The\ ZnO\ -\ loading = \frac{1,9770g * \frac{5,5ml}{10ml}}{3,0476g + 1,9770g * \frac{5,5ml}{10ml}} = 26,30\%$$

Table 24 – The complex solution used for the impregnation of zinc-precursor on the pretreated CNTs

Catalyst	CA [g]	PEG [g]	Zn(NO ₃) ₂ * 6H ₂ O [g]	CNT [g]	CNT #	Deionized Water [ml]	Complex solution impregnated on CNT[ml]	Calculated ZnO-loading [%]
20Ni-26ZnO/CNT	3,1235	1,0349	7,2183	3,0021	0N ^a	10	5,5	26,1395
20Ni-28ZnO/CNT	3,1093	1,0793	7,2009	3,0691	0N ^a	10	6	28,2507
20Ni-40ZnO/CNT	4,6316	1,5047	10,835	2,6467	0N ^a	10	6	40,1914
20Ni-46ZnO/CNT	6,2130	2,0804	14,201	3,1453	0N ^a	10	7	46,3714
5Ni-26ZnO/CNT	3,1052	1,0076	7,2073	3,0217	1D	10	5,5	26,4115
10Ni-26ZnO/CNT	3,1482	1,0139	7,2129	3,0070	1D	10	5,5	26,5215
15Ni-26ZnO/CNT	3,1448	1,0052	7,2261	3,0476	1D	10	5,5	26,2964
25Ni-26ZnO/CNT ^b	3,1448	1,0052	7,2261	3,0476	1D	10	5,5	26,2964
30Ni-26ZnO/CNT-red400 ^c	3,1052	1,0076	7,2073	3,0217	2N	10	5,5	26,4115
30Ni-26ZnO/CNT-red300	3,1334	1,0116	7,2155	3,0460	2N	10	5,5	26,2781
30Ni-26ZnO/CNT-red350	3,114	1,0084	7,2126	3,0506	2N	10	5,5	26,2411
30Ni-26ZnO/CNT-red450 ^d	3,1334	1,0116	7,2155	3,0460	2N	10	5,5	26,2781
26ZnO/CNT	3,1605	1,0299	7,2121	3,0729	1N	10	5,5	26,0991
20Ni-26ZnO/AC (pechini)	3,1257	1,0006	7,2330	3,0475 ^e	AC ^a	10	5,5	26,3155

a: CNT #0N was prepared as part of the author's specialization project the fall of 2012 (NTNU), and further details can be found in [51]. b: The 26ZnO/CNT used for the 25Ni-26ZnO/CNT catalyst was from the same batch as the 26ZnO/CNT used for the 15Ni-26ZnO/CNT catalyst. c: The 26ZnO/CNT used for the 30Ni-26ZnO/CNT catalyst was from the same batch as the 26ZnO/CNT used for the 5Ni-26ZnO/CNT catalyst. d: The 26ZnO/CNT used for the 30Ni-26ZnO/CNT-red450 catalyst was from the same batch as the 26ZnO/CNT used for the 30Ni-26ZnO/CNT-red300 catalyst. e: AC was used as support, not CNT.

In addition to the catalysts prepared by the pechini method (Table 24), a 20-26ZnO/AC catalyst was prepared by incipient wetness impregnation. The calculation of the ZnO-loading is given below:

The amounts of chemical used for the incipient wetness impregnation of Zn-precursor onto AC is given in Table 25.

Table 25 - Chemicals used for the incipient wetness impregnation of zinc precursor on AC

Catalyst name	Zn(NO ₃) ₂ * 6H ₂ O [g]	Deionized water [mL]	AC [g]
20Ni-26ZnO/AC (incipient)	3,8423	4	2,9559

$$m_{ZnO} = n_{ZnO} * Mw_{ZnO} = \frac{m_{ZnX}}{Mw_{ZnX}} * Mw_{ZnO}$$

$$m_{ZnO} = \frac{3,8423 \text{ g}}{297,40 \text{ g/mol}} * 81,39 \frac{\text{g}}{\text{mol}} = 1,0515 \text{ g}$$

$$ZnO - loading = \frac{m_{ZnO}}{m_{AC} + m_{ZnO}}$$

$$ZnO - loading = \frac{1,0515}{2,9559 + 1,0515} * 100\% = \mathbf{26,24\%}$$

B Impregnation of Ni precursor and calculation of Ni-loading

Nickel was added to the catalysts by incipient wetness impregnation according to the following calculations, in which the 15Ni-26ZnO/CNT catalyst is used as an example:

$$Mm_{\text{Nickel}} = 58,693 \text{ g/mol}$$

$$Mm_{\text{Nickel Nitrate}} = 290,79 \text{ g/mol}$$

A 15Ni-26ZnO/CNT catalyst was prepared according to the chemicals in Table 26:

Table 26 - Chemicals used for the impregnation of nickel for the 15Ni-26ZnO/CNT catalyst

Loading [%]	ZnO/CNT Cat [g]	m_{Nickel Nitrate} [g]	Deionized Water [ml]
15	2,5524	2,2204	3

$$m_{Ni} = \frac{m_{\text{Nickel Nitrate}}}{MW_{\text{Nickel Nitrate}}} * MW_{Ni} = \frac{2,2204g}{290,79 \text{ g/mol}} * 58,693 \frac{g}{mol} = 0,4482 \text{ g}$$

$$Ni - loading = \frac{m_{Ni}}{m_{ZnO/CNT} + m_{Ni}} * 100\% = \frac{0,4482 \text{ g}}{2,5524 \text{ g} + 0,4482g} * 100\% = 14,9\%$$

The calculation of Ni-loading is similar for all the Ni-ZnO/CNT catalysts, the 20Ni-ZnO/AC catalysts and the Ni/CNT or AC catalysts. The calculations were done in excel, and the detailed information is presented in Table 27.

Table 27 - Chemicals used for the nickel impregnation on the carbon supported catalysts

Catalyst	ZnO/CNT [g]	Nickel Nitrate [g]	Deionized water [mL]	Calculated Ni-loading [%]
20Ni-26ZnO/CNT	2,424	2,9772	4,8	19,8656
20Ni-28ZnO/CNT	2,4504	3,0048	4,8	19,8401
20Ni-40ZnO/CNT	2,253	2,9545	4,8	20,9289
20Ni-46ZnO/CNT	2,4046	2,9903	4,8	20,0641
5Ni-26ZnO/CNT	0,7472	2,8501	3	5,0256
10Ni-26ZnO/CNT	1,4846	2,7024	3	9,9816
15Ni-26ZnO/CNT	2,2204	2,5524	3	14,9360
25Ni-26ZnO/CNT	3,2602	1,9557	2	25,1761
30Ni-26ZnO/CNT-red300	7,4822	3,5021	4	30,1210
30Ni-26ZnO/CNT-red350	7,4413	3,5044	4	30,0009
30Ni-26ZnO/CNT-red400	2,9319	1,4126	1	29,5241
30Ni-26ZnO/CNT-red450	7,4561	3,5032	4	30,0498
20Ni/CNT	2,4106 ^a	2,9690	4,8	19,9010
Catalyst	AC [g]	Nickel Nitrate [g]	Deionized water [mL]	Calculated Ni-loading [%]
20Ni/AC	2,4002	2,9929	4	20,1075
20Ni-26ZnO/AC (incipient)	2,4141	2,9986	3	20,0454
20Ni-26ZnO/AC (pechini)	2,4064	2,9655	3	19,9190

a: CNT were used not ZnO/CNT

C Nickel and zinc oxide loading in the Ni/ZnO catalysts

Two batches of 20Ni/26ZnO catalysts were prepared by incipient wetness impregnation according to the following calculation:

$$m_{Ni}: m_{ZnO} = 20:26$$

For 1g of catalyst:

$$m_{ZnO} = \frac{1 * 26}{(26 + 20)} = 0,5652 \text{ g}$$

$$m_{Ni} = \frac{1 * 20}{(20 + 26)} = 0,4348 \text{ g}$$

$$n_{Ni} = n_{Nickel Nitrate} = \frac{m_{Ni}}{Mw_{Ni}} = \frac{0,4348 \text{ g}}{58,693 \text{ g/mol}} = 0,0074 \text{ mol}$$

$$m_{Nickel Nitrate} = n_{Ni} * Mw_{Nickel Nitrate} = 0,0074 \text{ mol} * 298,81 \frac{\text{g}}{\text{mol}} = 2,2112 \text{ g}$$

Herein, 3 g of catalyst was prepared for each batch:

$$m_{ZnO} = \frac{3 * 26}{(26 + 20)} = 1,6957 \text{ g}$$

$$m_{Nickel Nitrate} = 3 * m_{Nickel Nitrate,1g \text{ cat}} = 3 * 2,2112 \text{ g} = 6,6336 \text{ g}$$

Thus, approximately 6,6336 g *Nickel Nitrate* was mixed with deionized water and impregnated on the ZnO support (approximately 1,6957 g). The exact values used for batch A and B are given in the following Table.

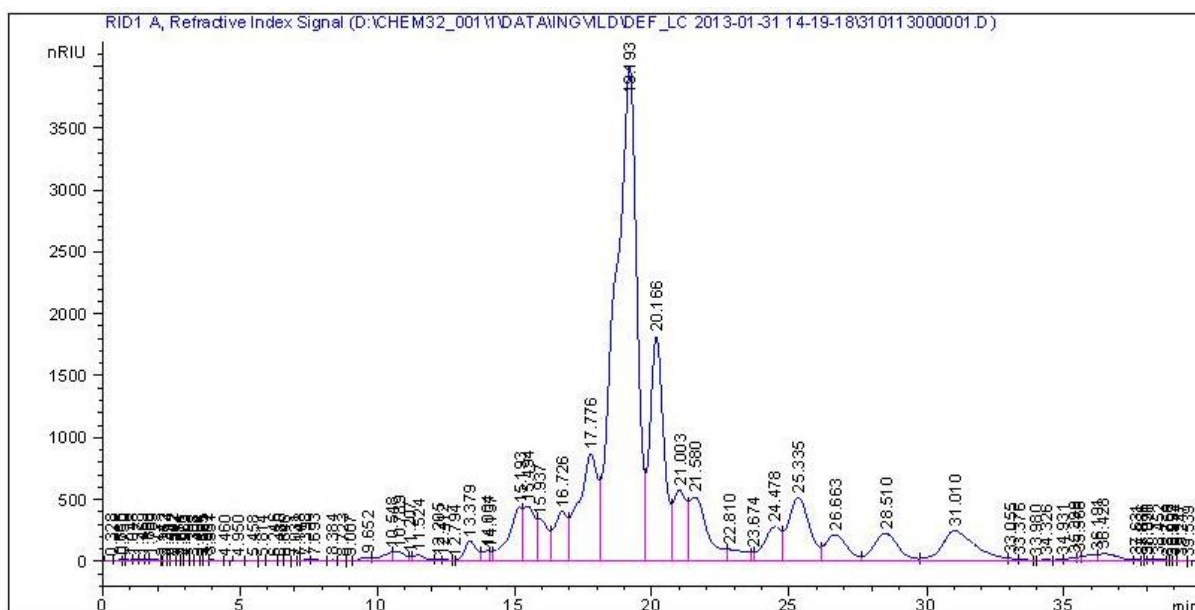
Table 28 - Chemicals used for the nickel impregnation on commercial zinc oxide support

Catalyst name	Nickel nitrate [g]	Deionized water [mL]	ZnO support [g]
20Ni/26ZnO A	6,6384	4	1,6988
20Ni/26ZnO B	6,6416	4	1,7011

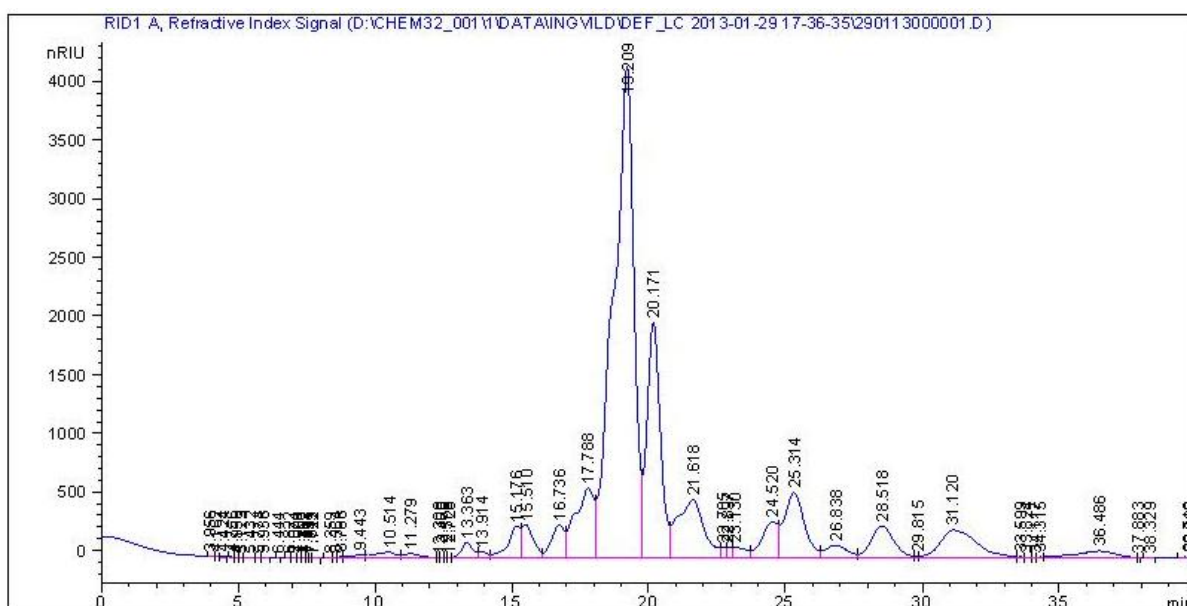
D HPLC plots

The HPLC plots from the liquid samples are presented in the following Figures. Unless stated otherwise, reaction conditions: P= 60 bar (RT), T= 245°C, Rx. time= 2,5 h, and stirring rate: 800rpm was used. A 75 mL reactor was loaded with 0,025 g cellulose, 0,075 g catalyst and 25 mL water.

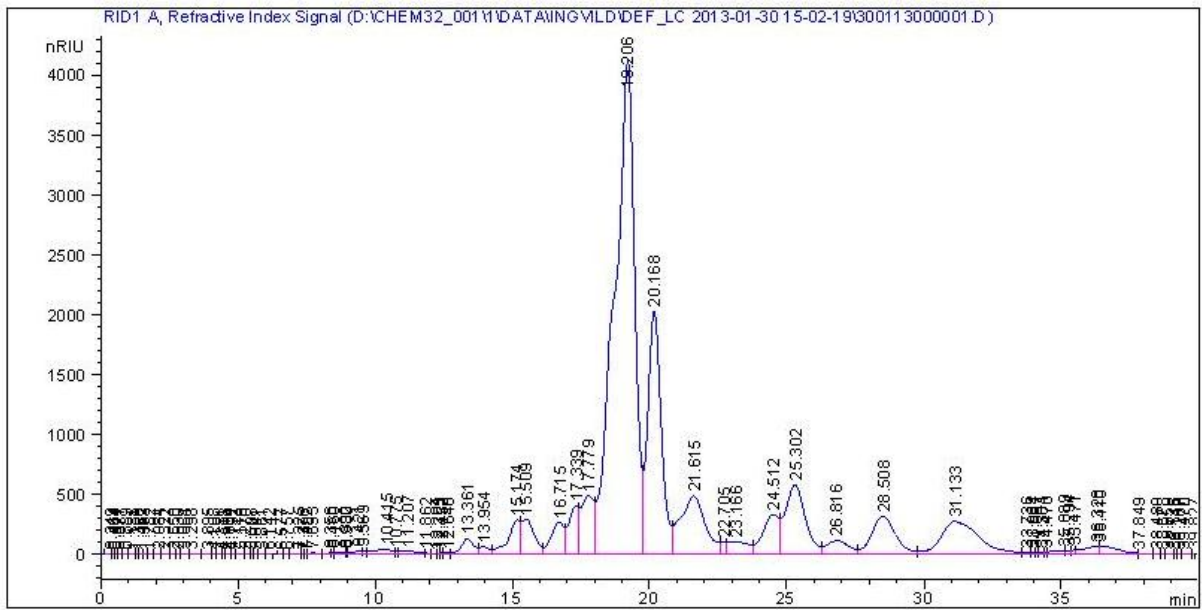
- Catalyst: 20Ni-40ZnO/CNT, Rx. Time: 2h, T: 245°C



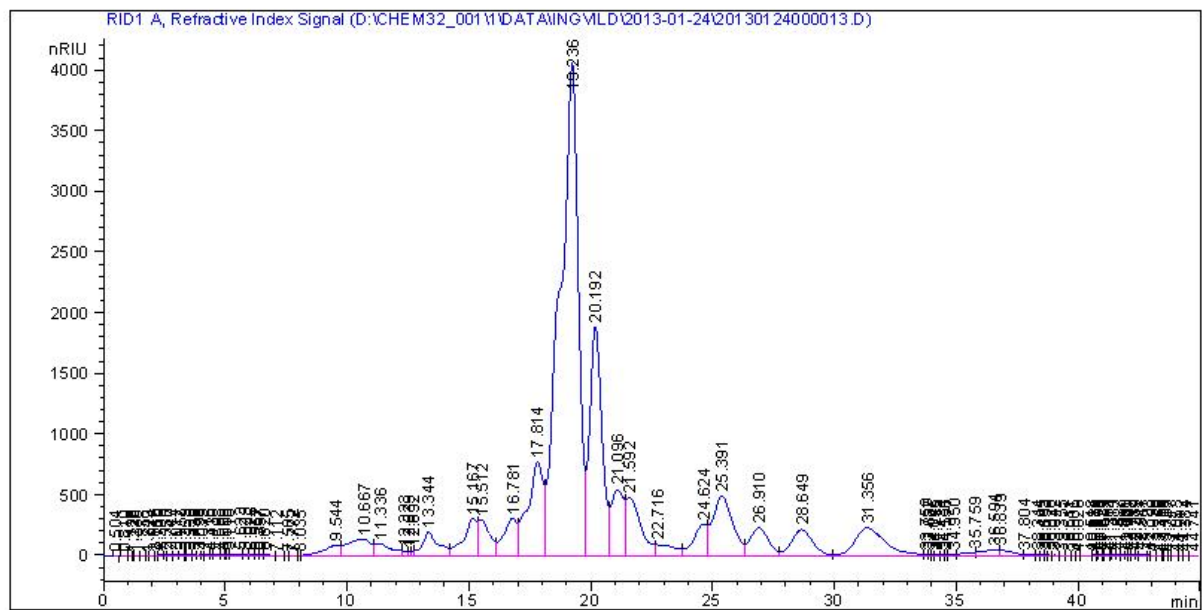
- Catalyst: 20Ni-40ZnO/CNT, Rx. Time: 2,5h, T: 245°C



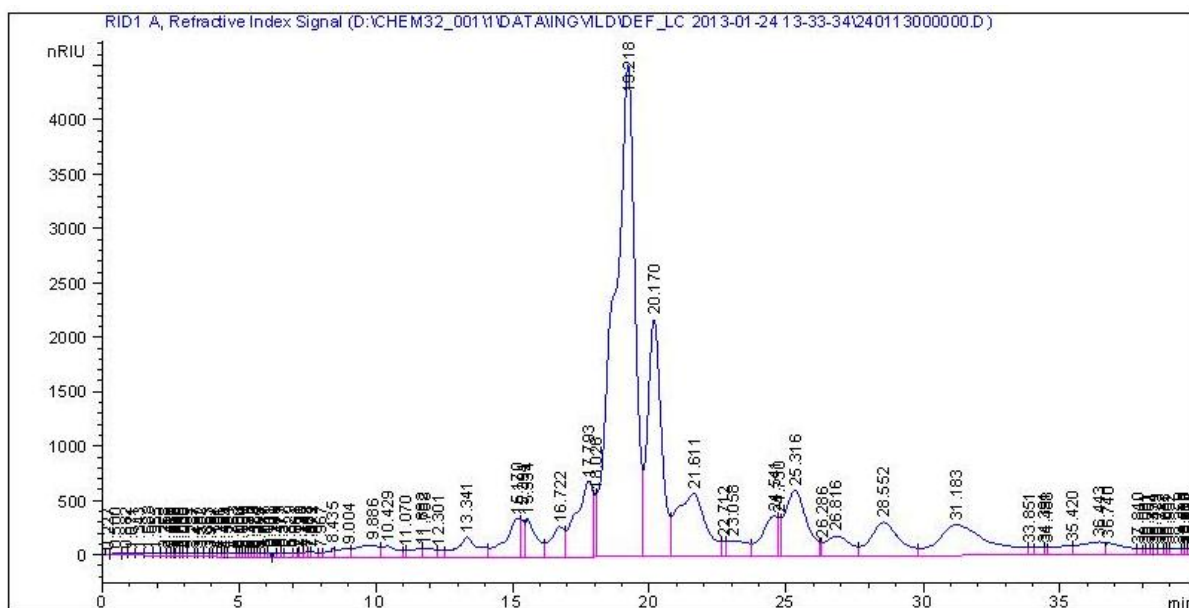
- Catalyst: 20Ni-40ZnO/CNT, Rx. Time: 3h, T: 245°C



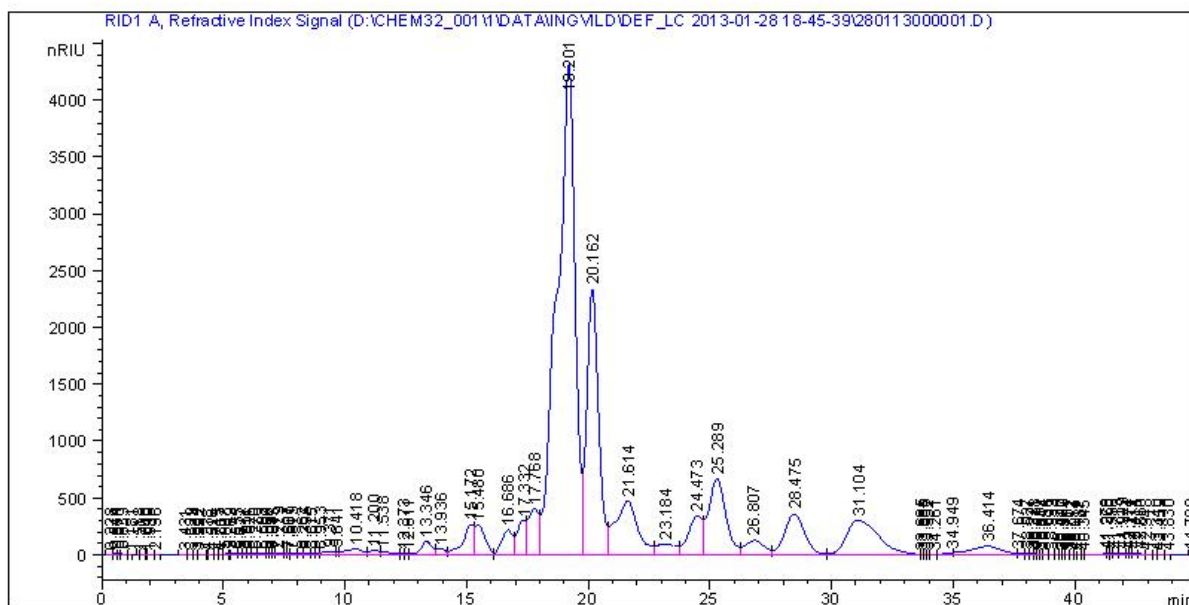
- Catalyst: 20Ni-26ZnO/CNT, Rx. Time: 2h, T: 245°C



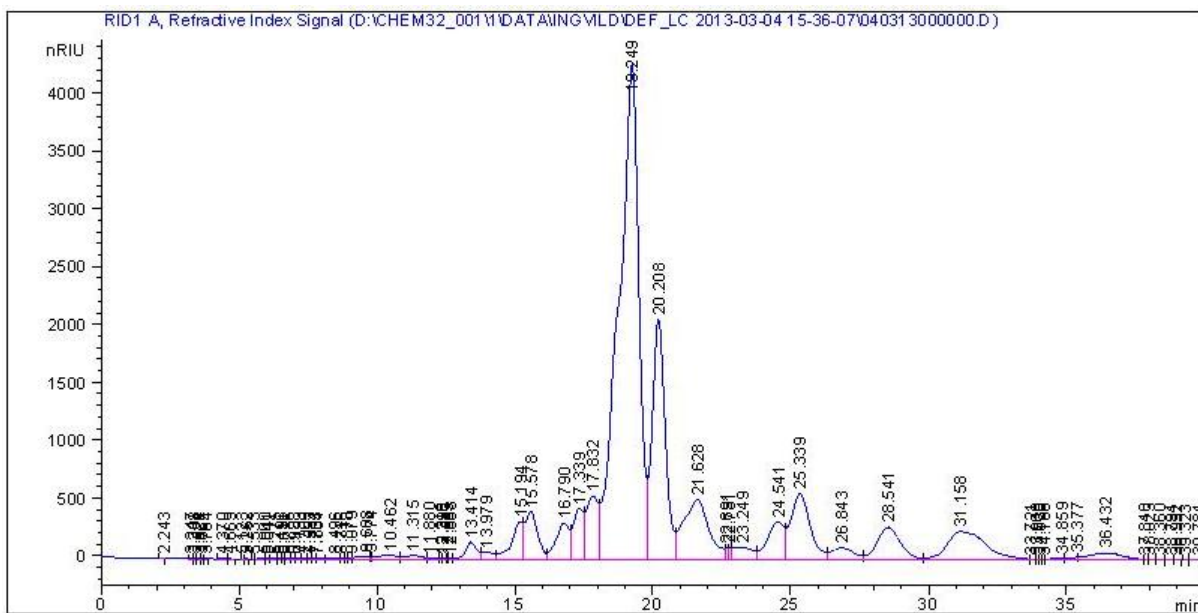
- Catalyst: 20Ni-26ZnO/CNT, Rx. Time: 2,5h, T: 245°C



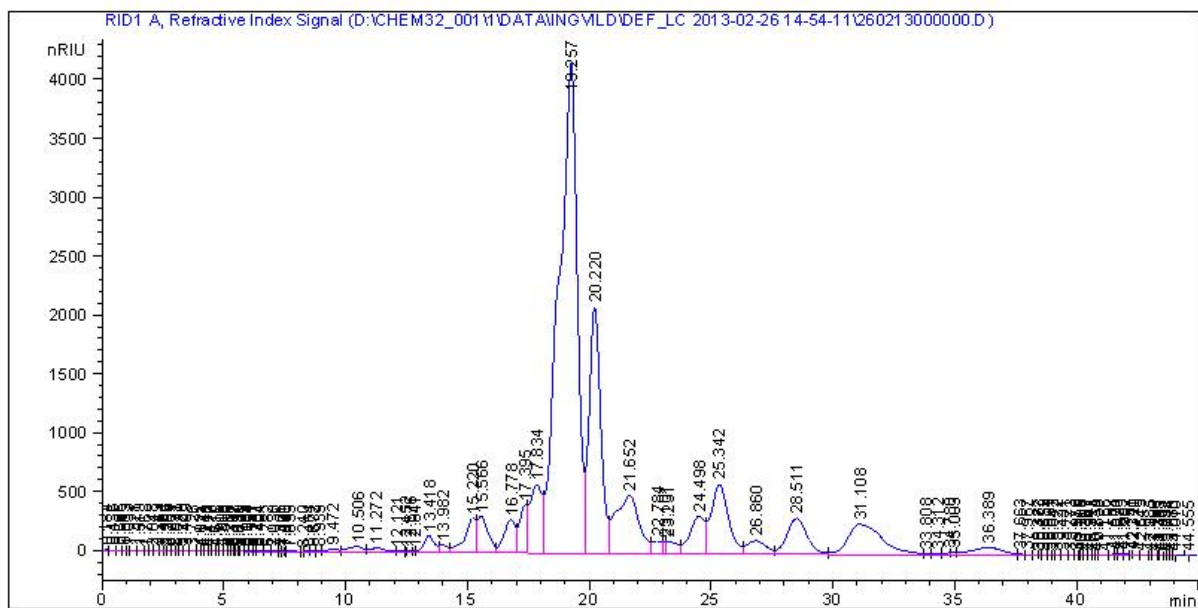
Catalyst: 20Ni-26ZnO/CNT, Rx. Time: 3h, T: 245°C



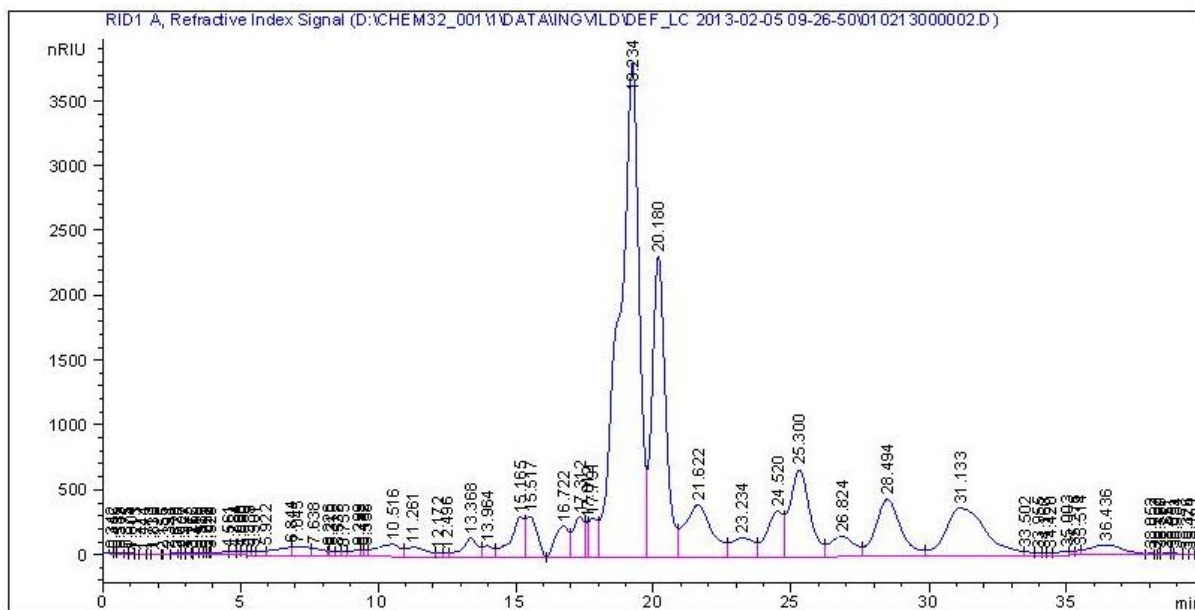
- Catalyst: 20Ni-28ZnO/CNT, Rx. Time: 2,5h, T: 245°C



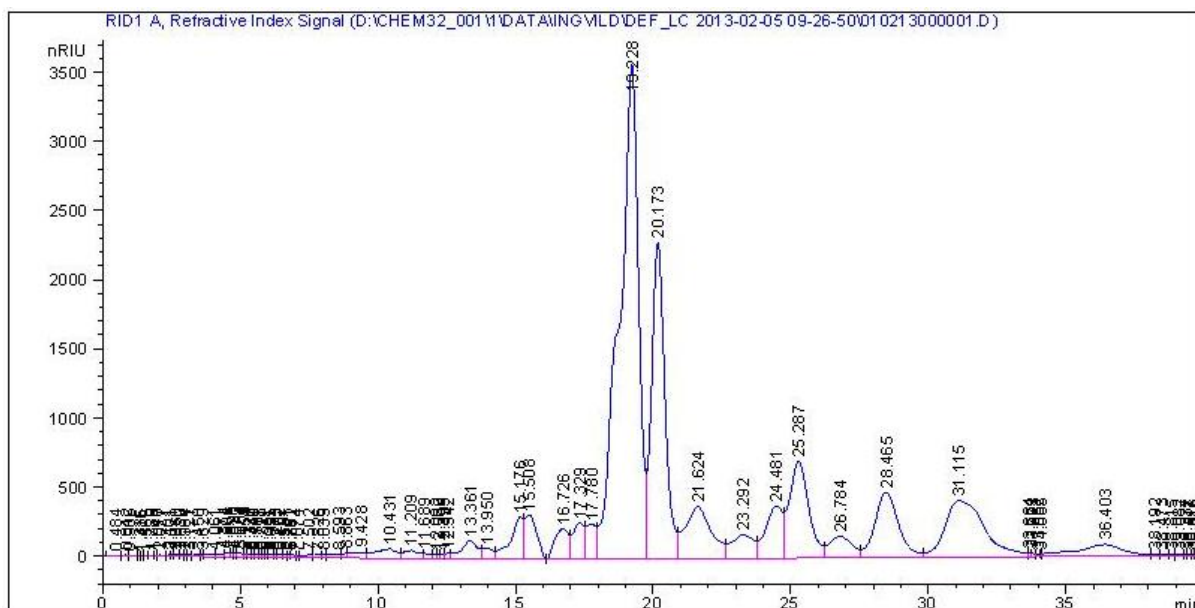
- Catalyst: 20Ni-46ZnO/CNT, Rx. Time: 2,5h, T: 245°C



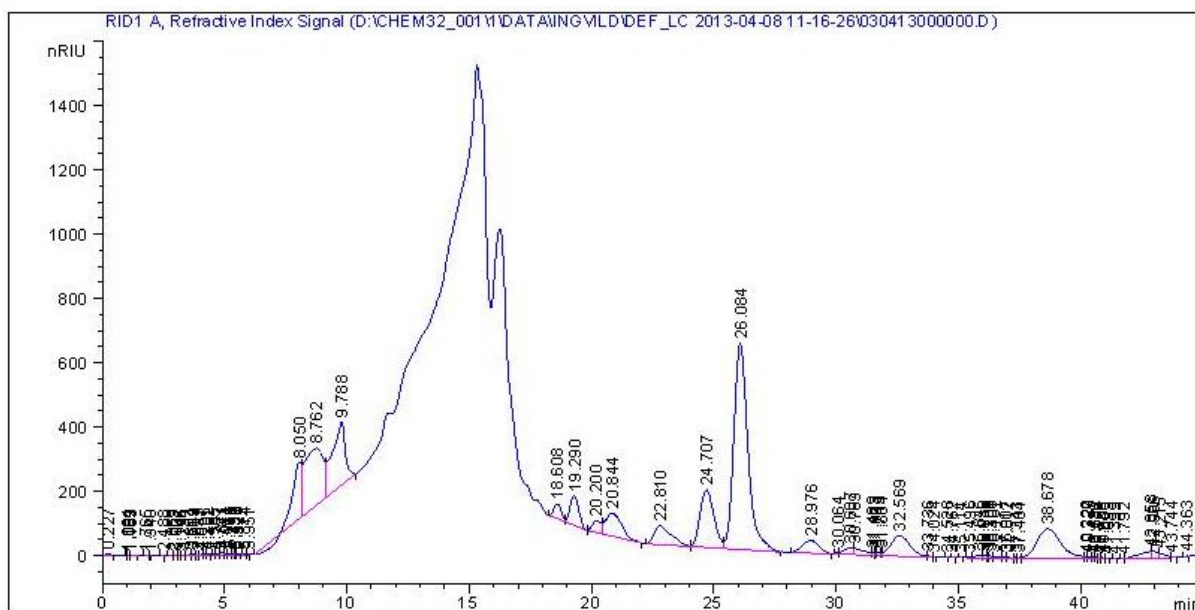
- Catalyst: 20Ni-26ZnO/CNT, T: 255°C, P= 60 bar (RT) Rx. time= 2h



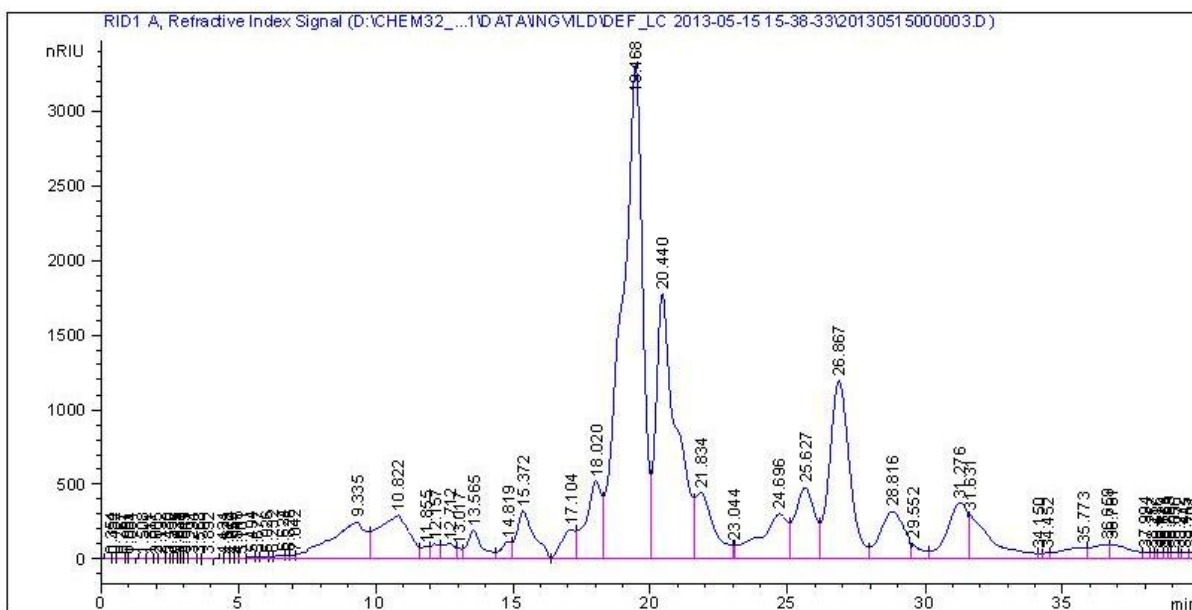
- Catalyst: 20Ni-26ZnO/CNT, T: 255°C, P= 60 bar (RT) Rx. time= 2,5h



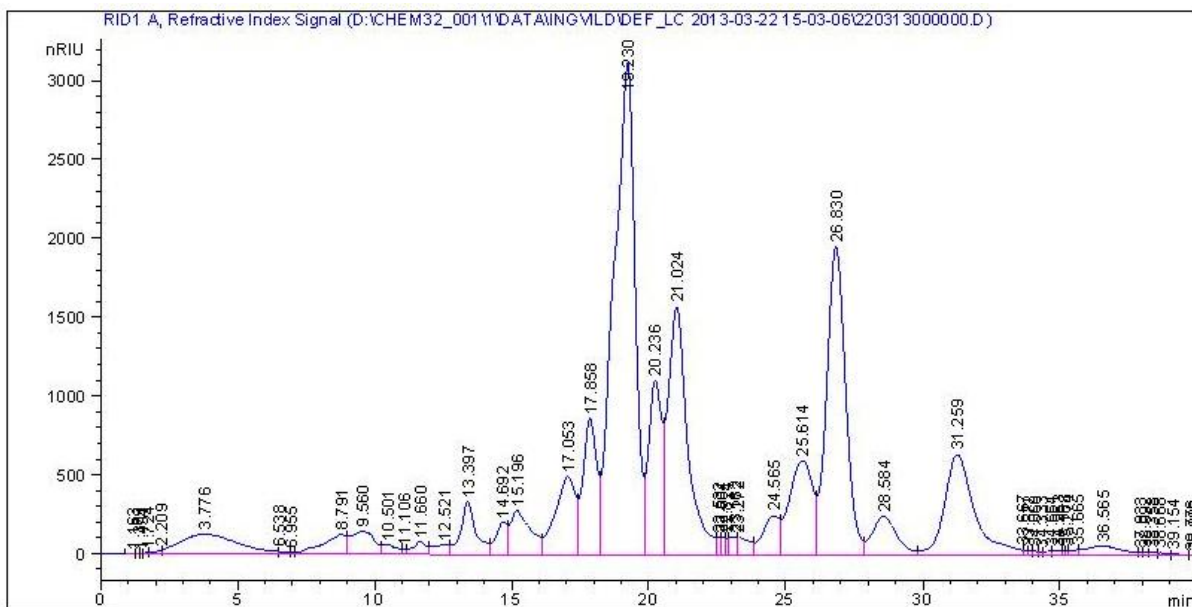
- Catalyst: 26ZnO/CNT, Rx. Time: 2,5 h, T= 245°C, P= 60 bar (RT)



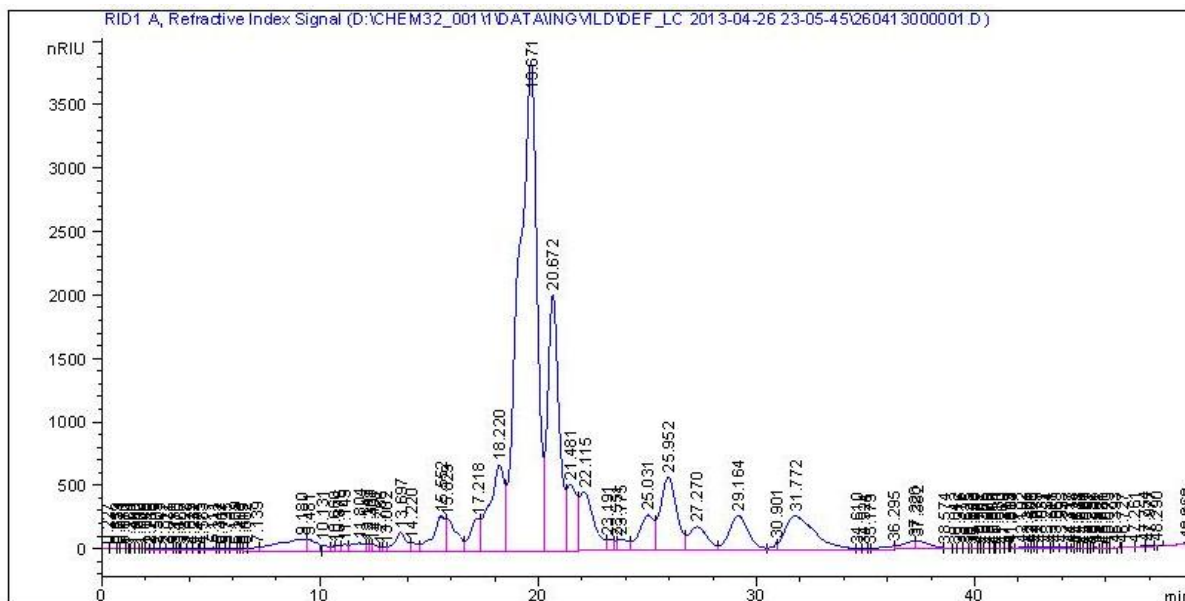
- Catalyst: 20Ni/26ZnO B, Rx. Time: 2,5 h, T= 245°C, P= 60 bar (RT)



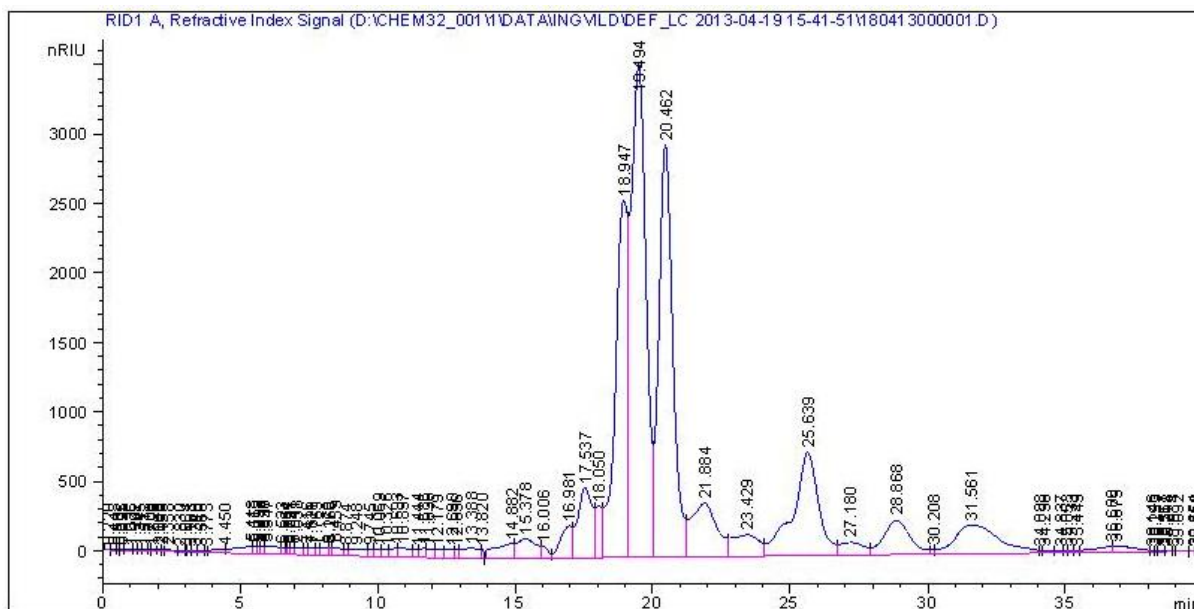
- Catalyst: 20Ni/CNT, Rx. Time: 2,5 h, T= 245°C, P= 60 bar (RT)



- Catalyst: 20Ni-26ZnO/AC (pechini), Rx. Time: 2,5 h, T= 245°C, P= 60 bar (RT)

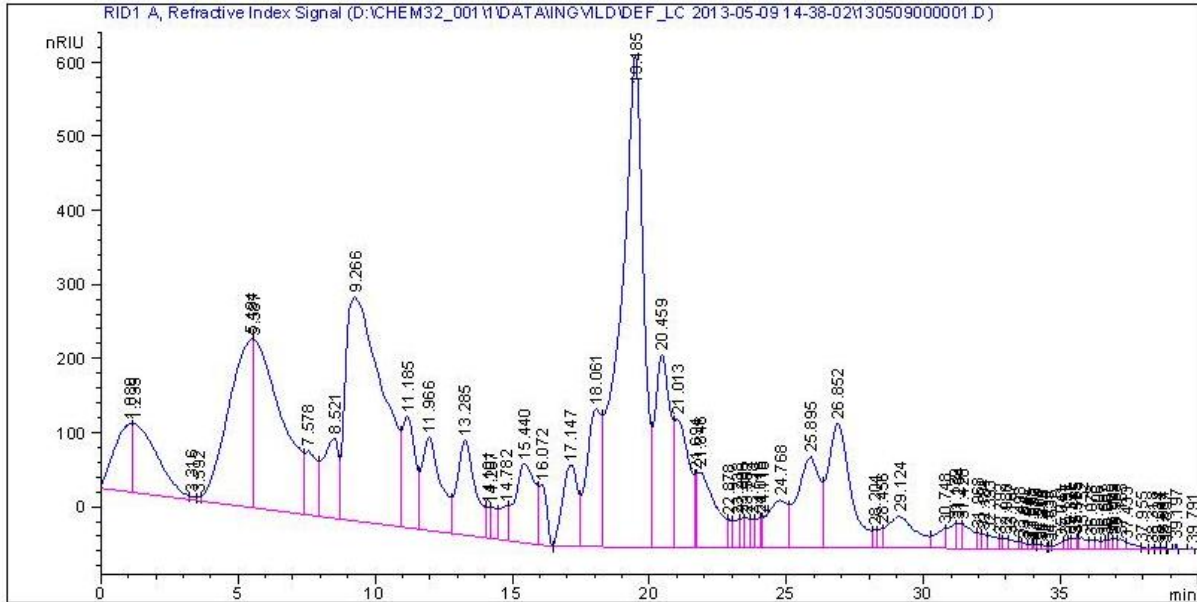


- Catalyst: 20Ni-26ZnO/CNT, Rx. Time: 2,5 h, T= 245°C, P= 60 bar (RT), Feedstock: Sorbitol

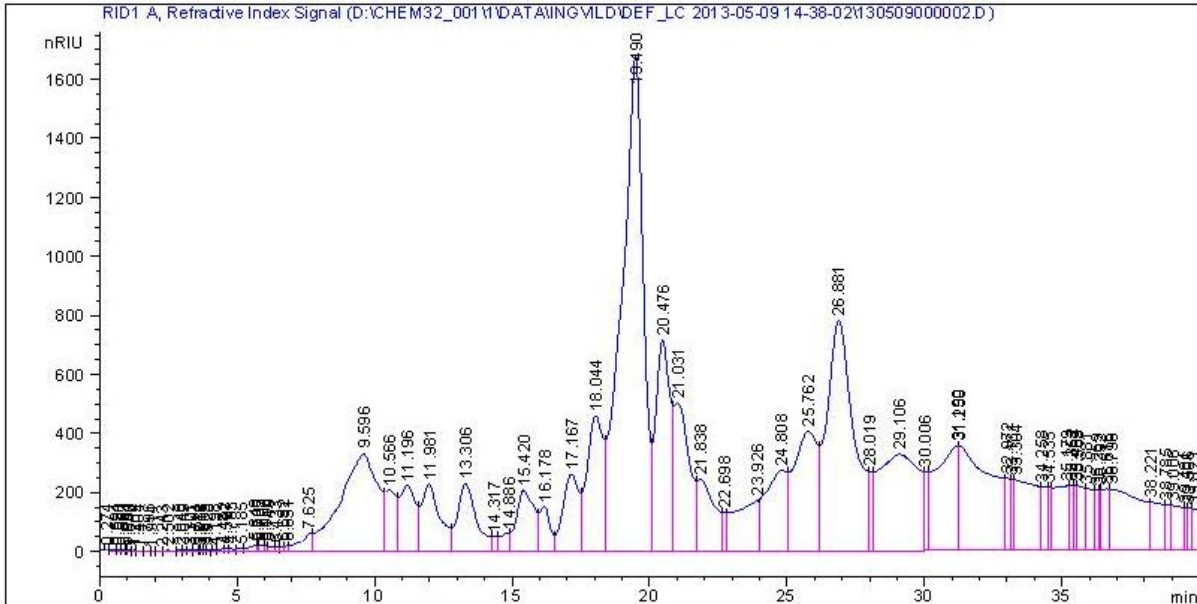


- Catalyst: 20Ni-26ZnO/CNT, Rx. Time: 2,5 h, T= 245°C, P= 60 bar (RT), Reactor: 300 mL, Cellulose: 0,8015 g , Water: 80 mL , Catalyst: 0,2427 g

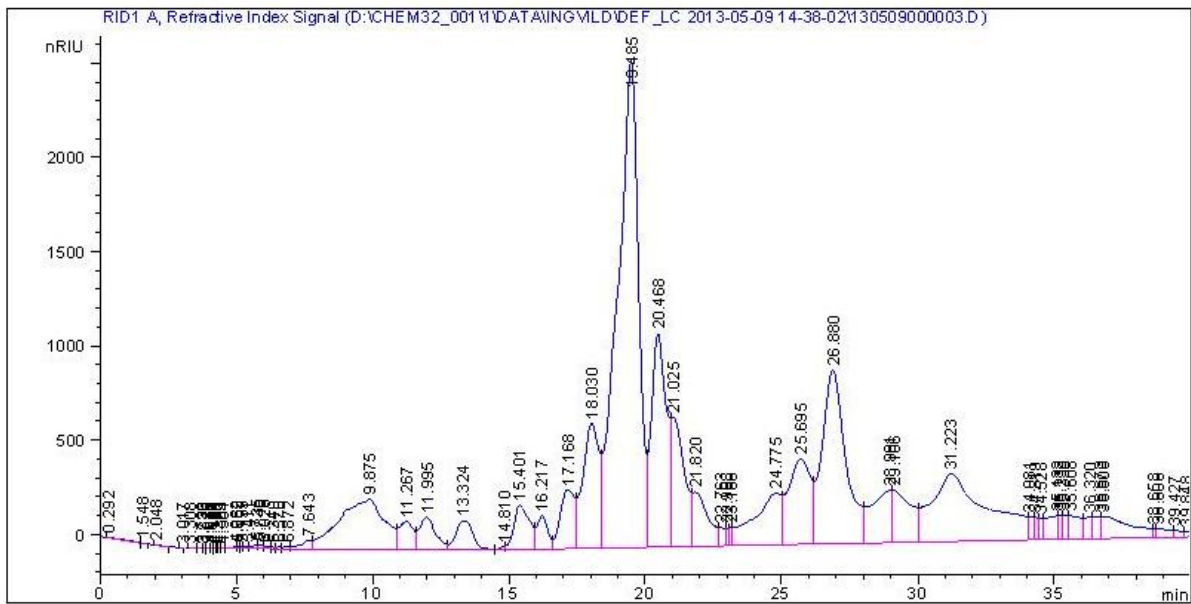
1) Liquid sample taken after after 20 min:



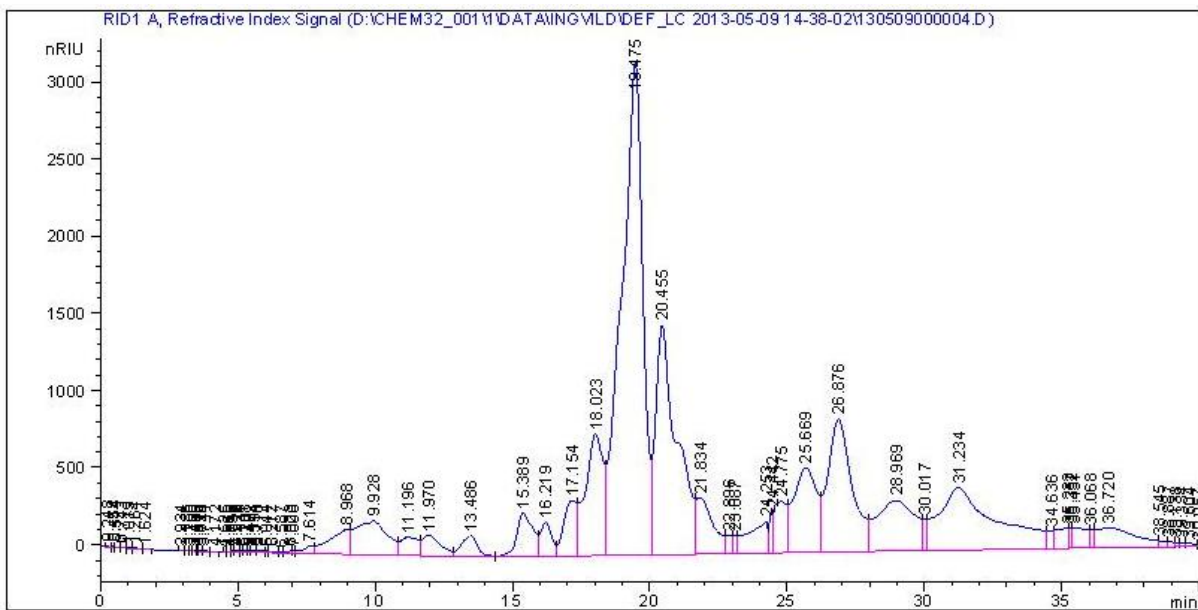
2) Liquid samples taken after 40 min:



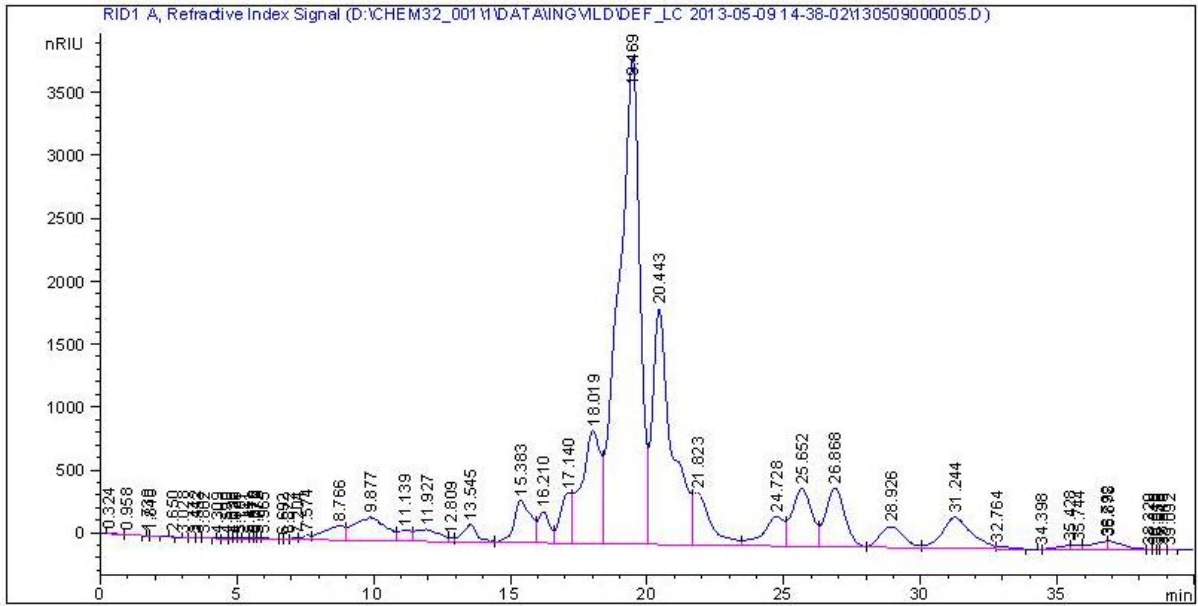
3) Liquid sample taken after 60 min:



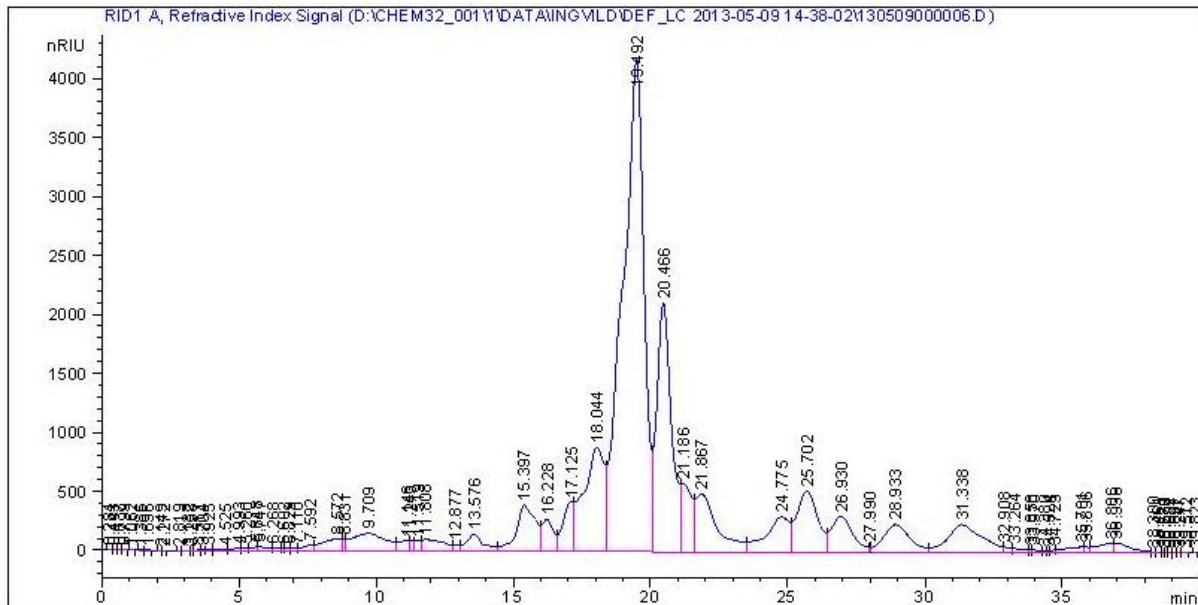
4) Liquid sample taken after 80 min:



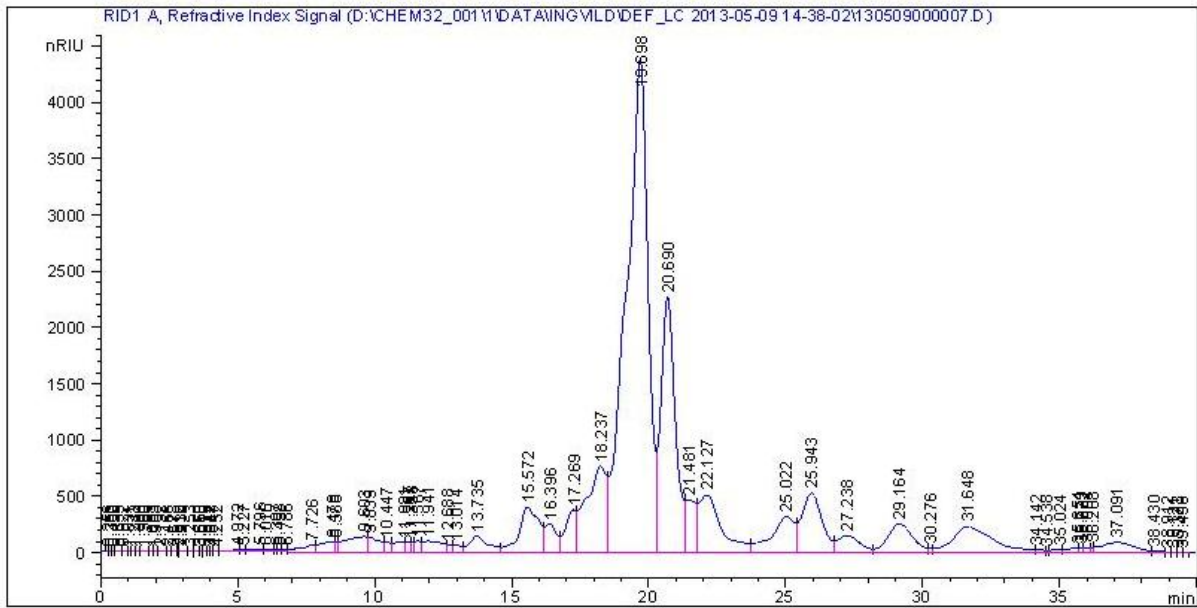
5) Liquid sample taken after 100 min:



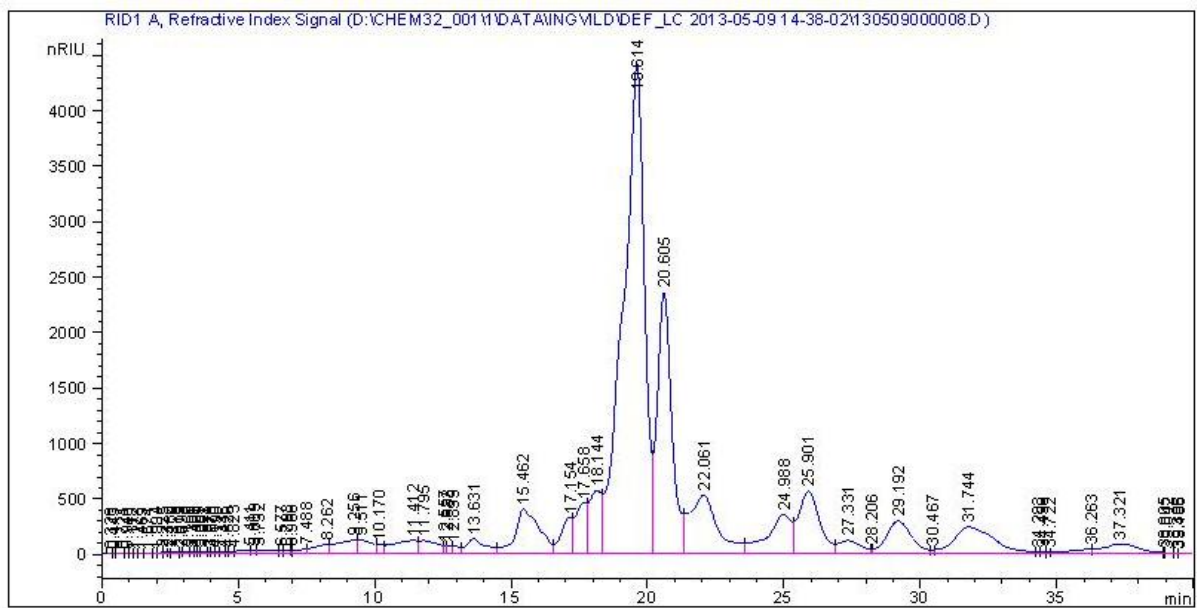
6) Liquid sample taken after 120 min:



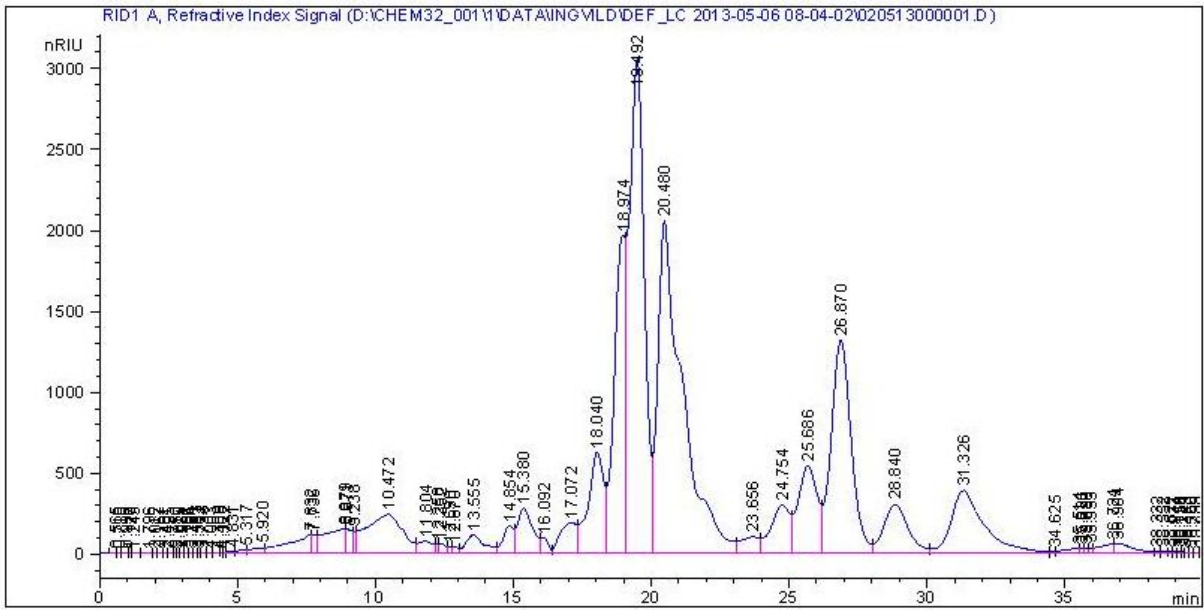
7) Liquid sample taken after 150 min:



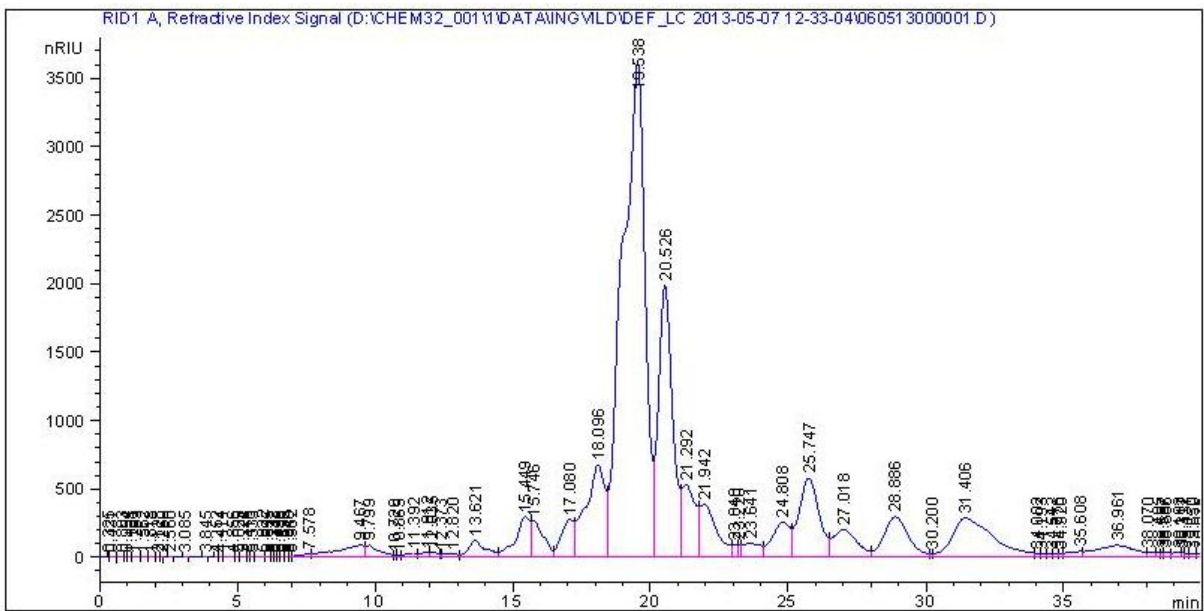
8) Liquid sample taken after 150 min:



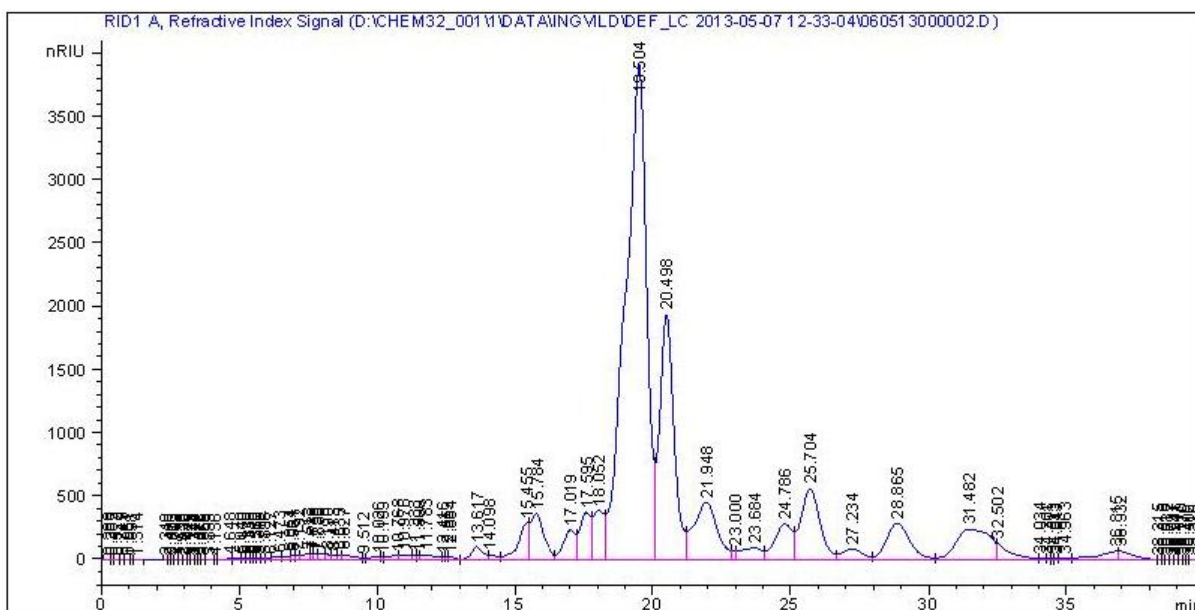
- Catalyst: 5Ni-26ZnO/CNT, Rx. Time: 2,5 h, T= 245°C, P= 60 bar (RT)



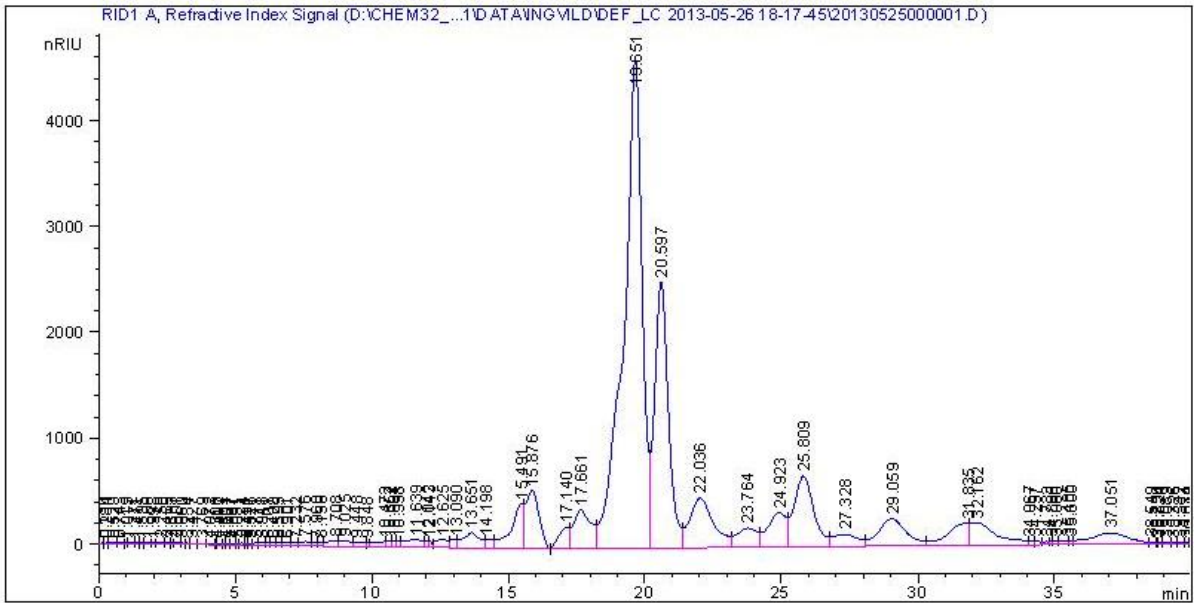
- Catalyst: 10Ni-26ZnO/CNT, Rx. Time: 2,5 h, T= 245°C, P= 60 bar (RT)



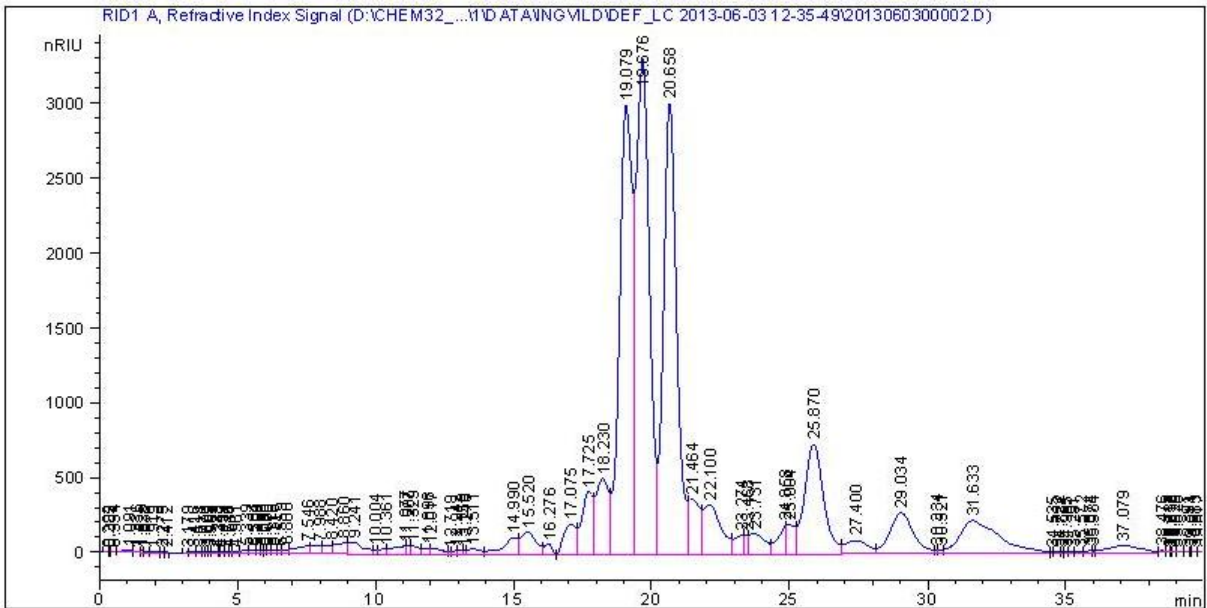
- Catalyst: 15Ni-26ZnO/CNT, Rx. Time: 2,5 h, T= 245°C, P= 60 bar (RT)



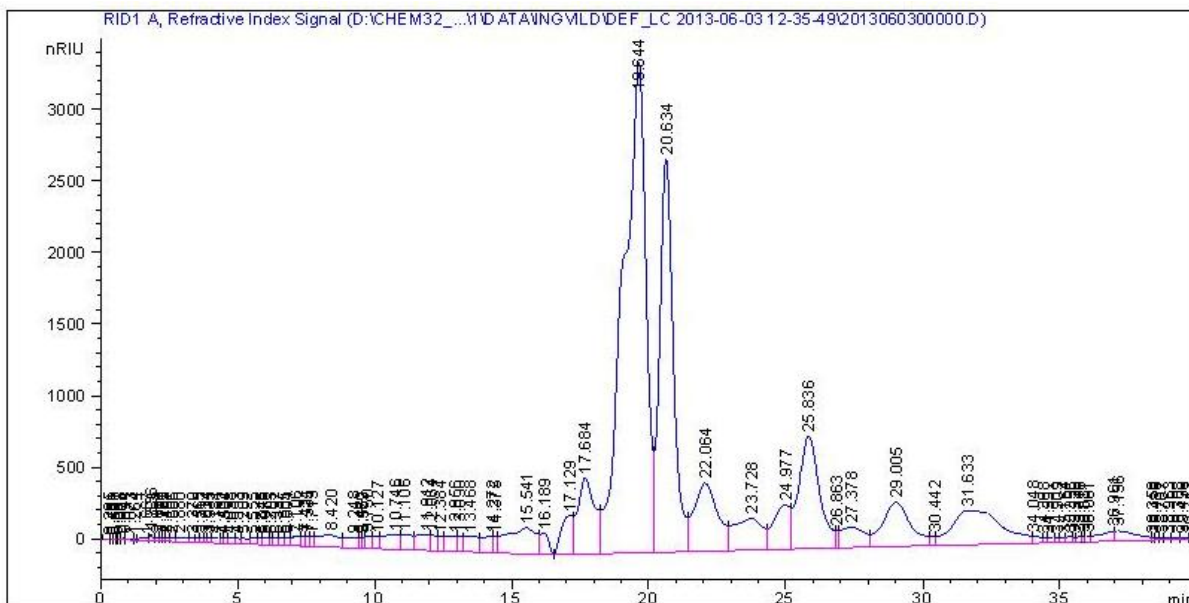
- Catalyst: 30Ni-26ZnO/CNT-red400, Rx. Time: 2,5 h, T= 245°C, P= 60 bar (RT)



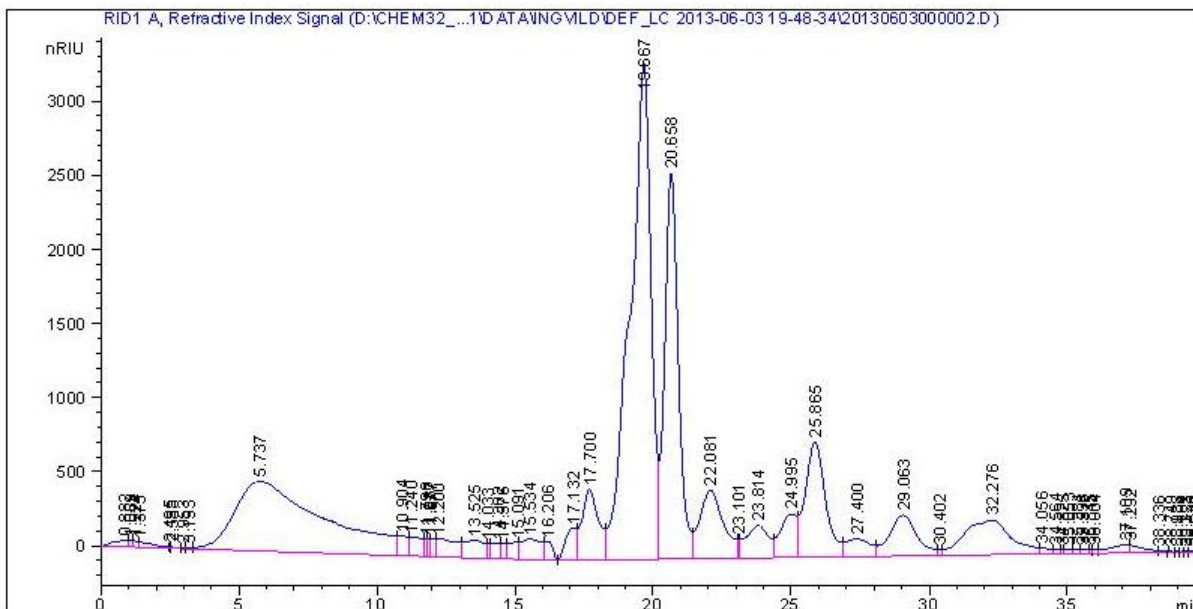
- Catalyst: 30Ni-26ZnO/CNT-red300, Rx. Time: 2,5 h, T= 245°C, P= 60 bar (RT),
Feedstock: Sorbitol



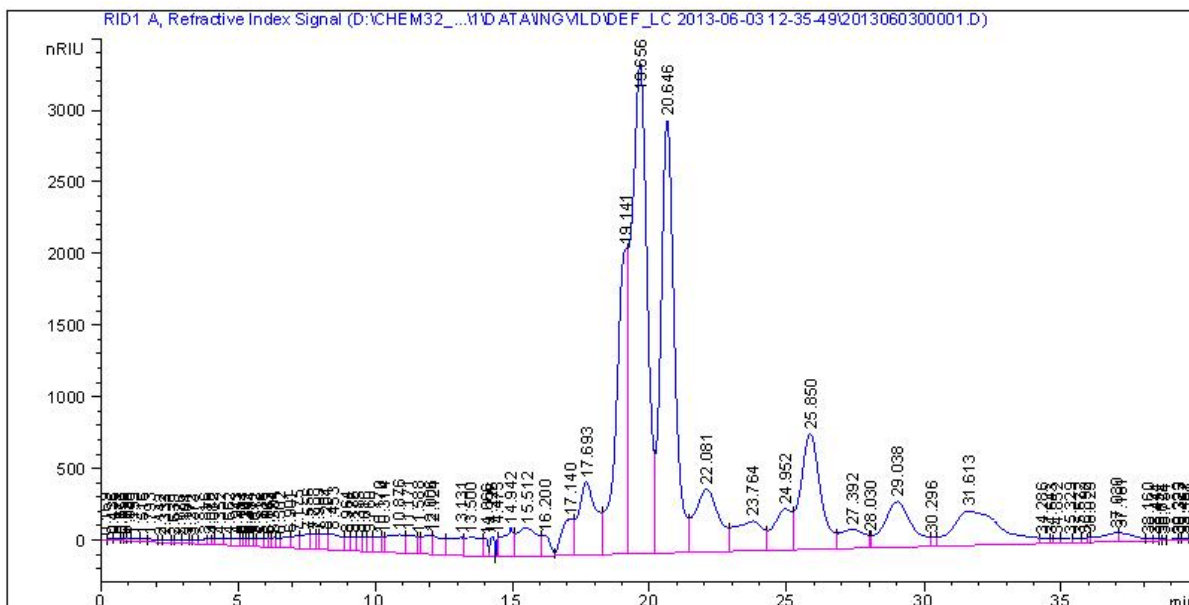
- Catalyst: 30Ni-26ZnO/CNT-red350, Rx. Time: 2,5 h, T= 245°C, P= 60 bar (RT), Feedstock: Sorbitol



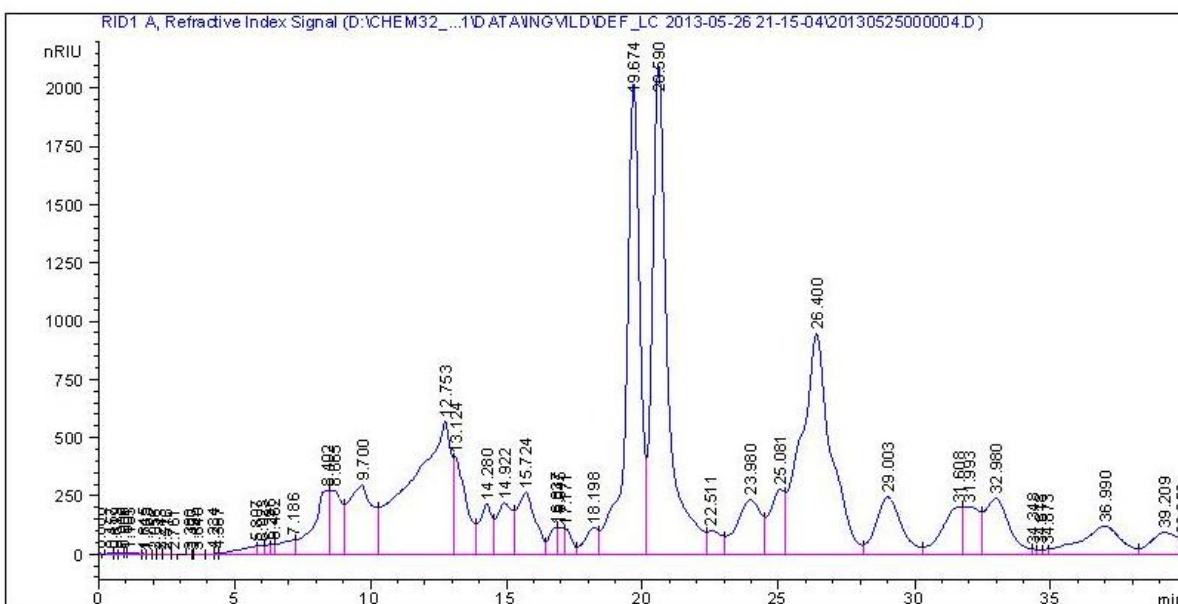
- Catalyst: 30Ni-26ZnO/CNT-red400, Rx. Time: 2,5 h, T= 245°C, P= 60 bar (RT), Feedstock: Sorbitol



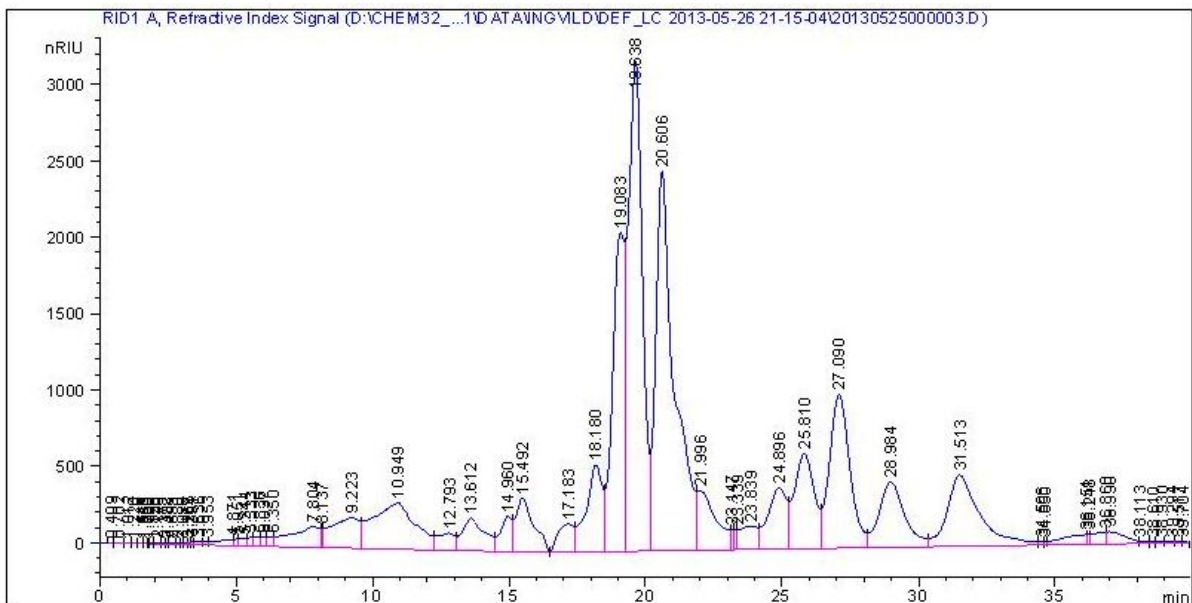
- Catalyst: 30Ni-26ZnO/CNT-red450, Rx. Time: 2,5 h, T= 245°C, P= 60 bar (RT), Feedstock: Sorbitol



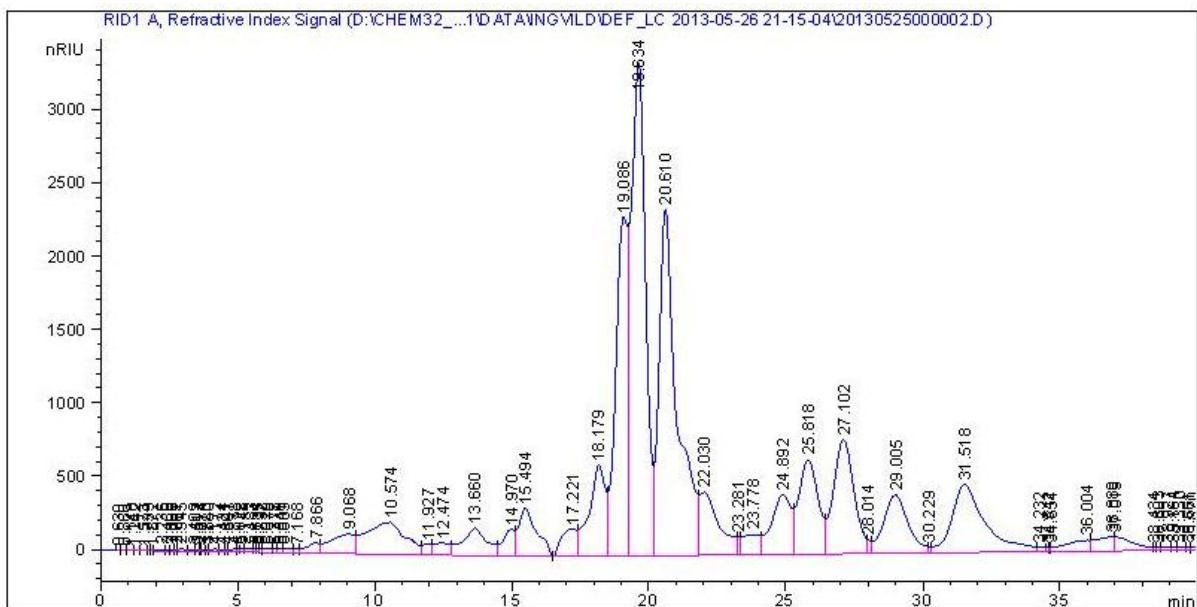
- Catalyst: 5Ni-26ZnO/CNT, Rx. Time: 2,5 h, T= 245°C, P= 60 bar (RT), 2nd run (reusability)



- Catalyst: 20Ni-28ZnO/CNT, Rx. Time: 2,5 h, T= 245°C, P= 60 bar(RT),2nd run (reusability)



- Catalyst: 20Ni-46ZnO/CNT, Rx. Time: 2,5 h, T= 245°C, P= 60 bar(RT),2nd run (reusability)

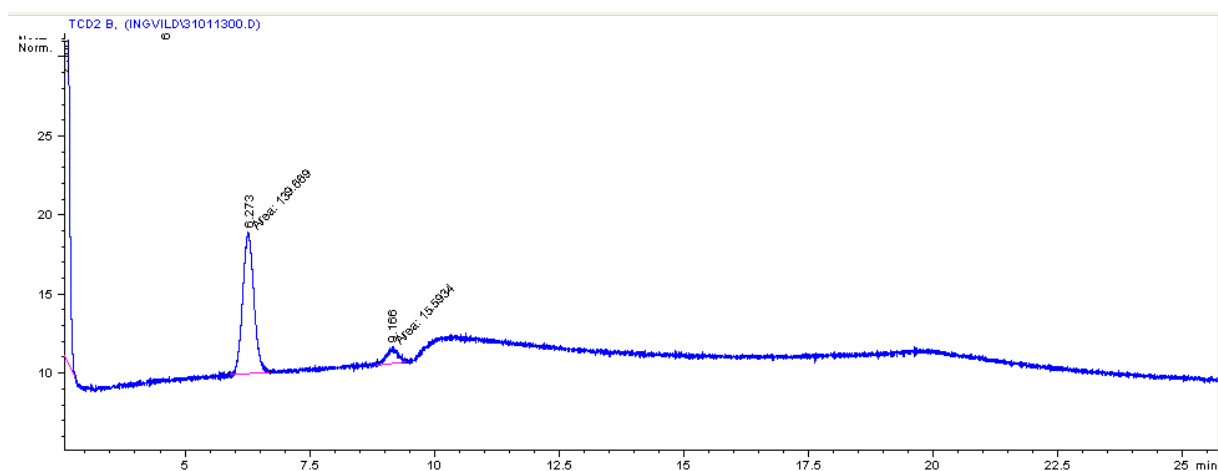


E GC results

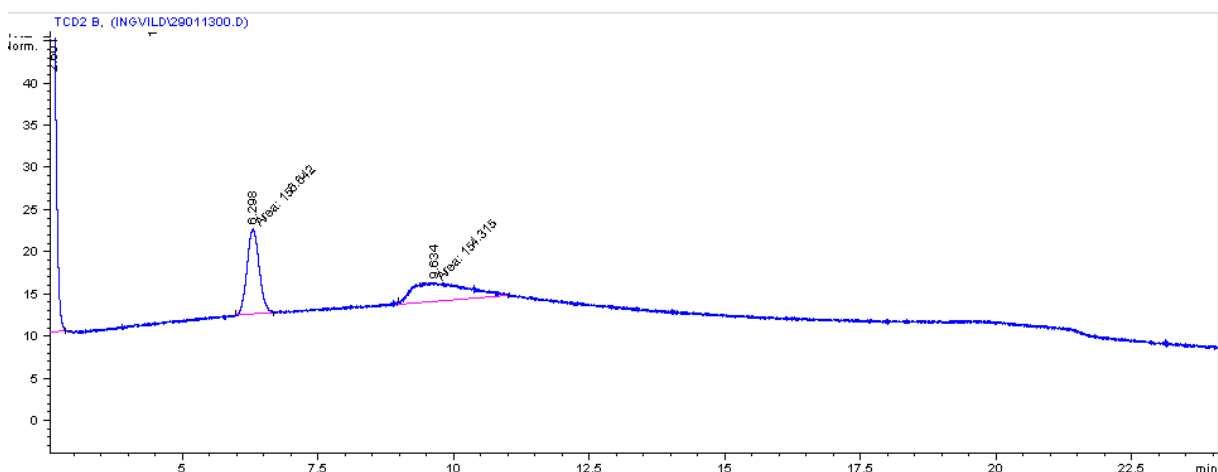
E. 1 GC plots

The GC plots from the gas samples are presented in the following Figures. Unless stated otherwise, reaction conditions: P= 60 bar (RT), T= 245°C, Rx. time= 2,5 h, and stirring rate: 800rpm was used. A 75 mL reactor was loaded with 0,025 g cellulose, 0,075 g catalyst and 25 mL water. Gas samples were taken for most of the reactions, but there are a few missing due to lack of gas bags in the lab.

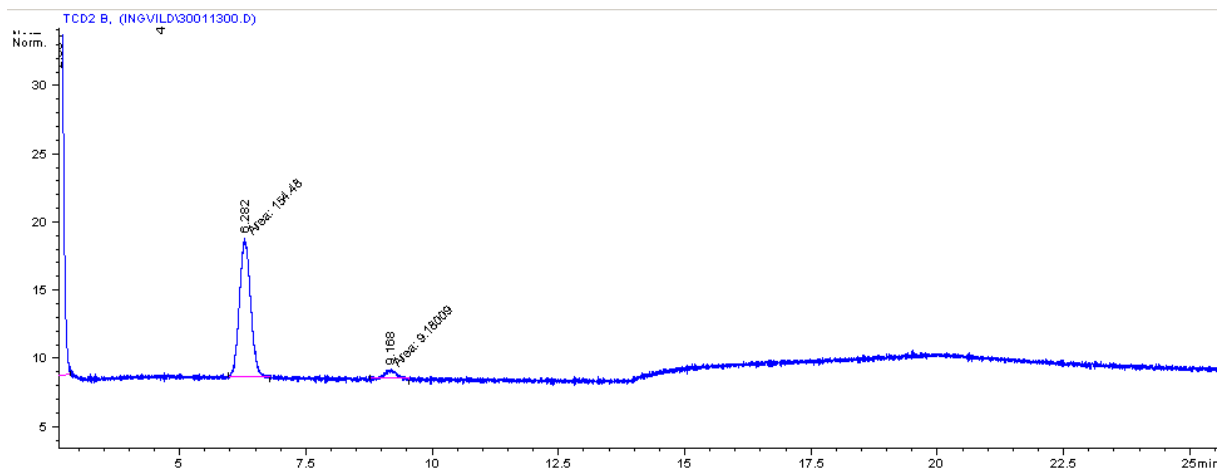
1) Catalyst: 20Ni-40ZnO/CNT, Rx. Time: 2h, T: 245°C



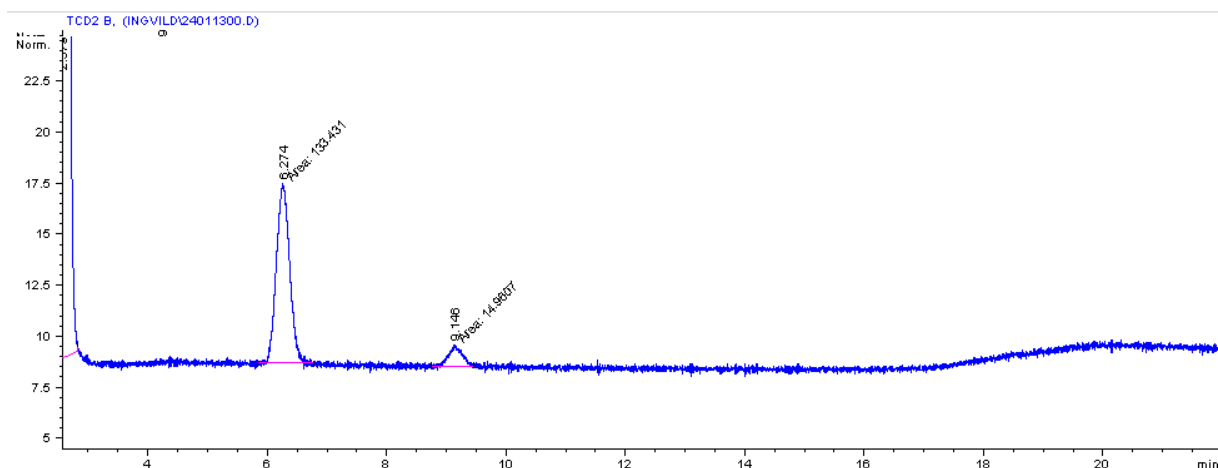
2) Catalyst: 20Ni-40ZnO/CNT, Rx. Time: 2,5, T: 245°C



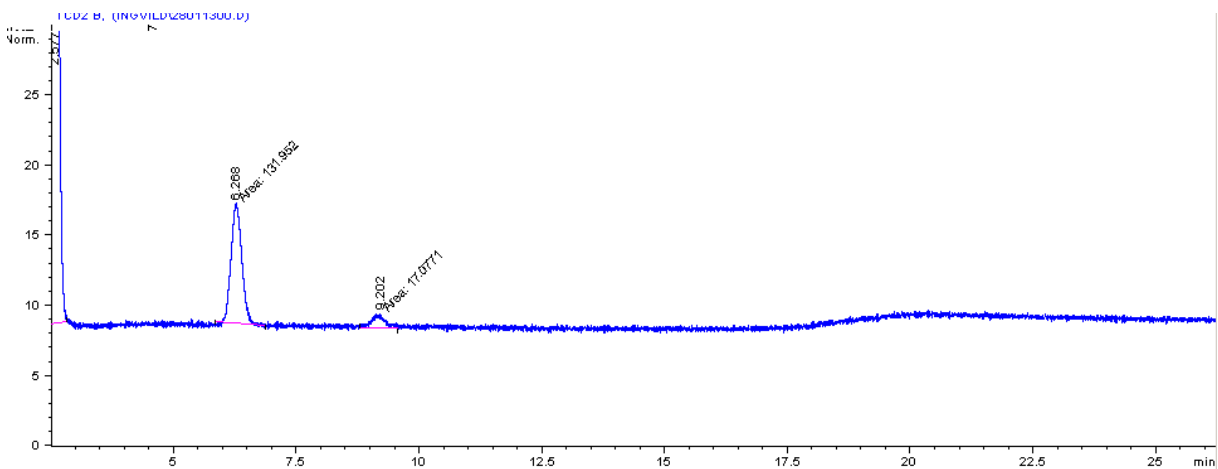
3) Catalyst: 20Ni-40ZnO/CNT, Rx. Time: 3h, T: 245°C



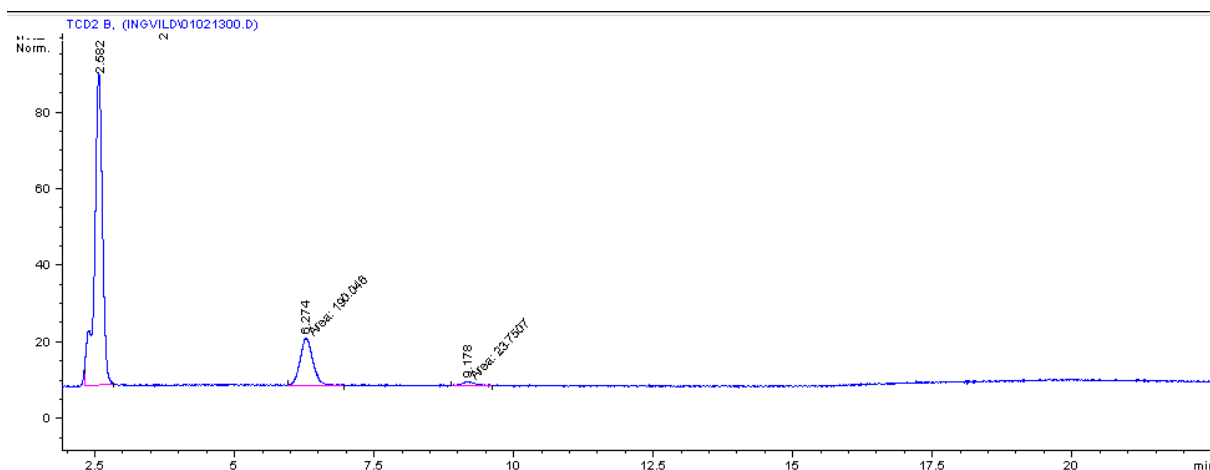
4) Catalyst: 20Ni-26ZnO/CNT, Rx. Time: 2,5h, T: 245°C



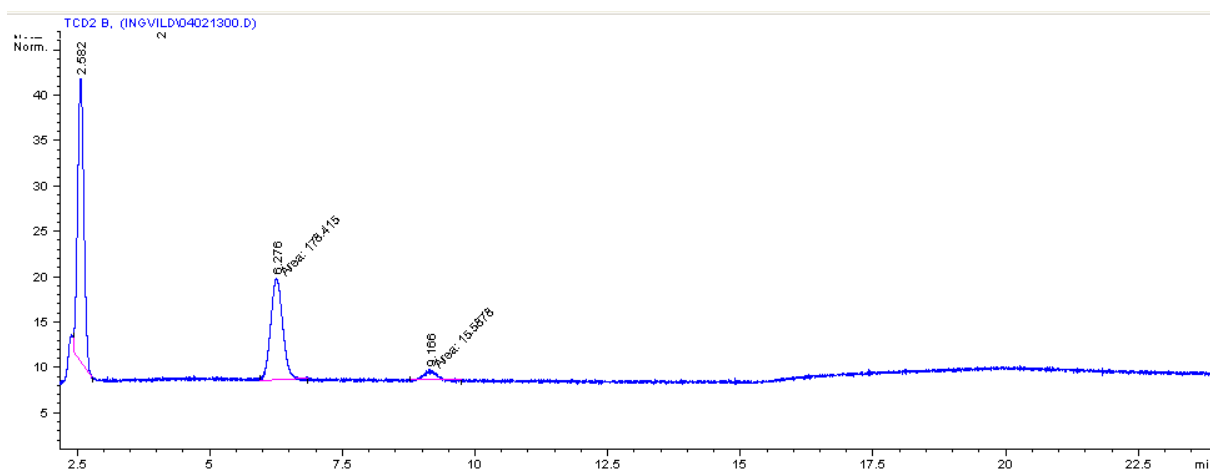
5) Catalyst: 20Ni-26ZnO/CNT, Rx. Time: 3h, T: 245°C



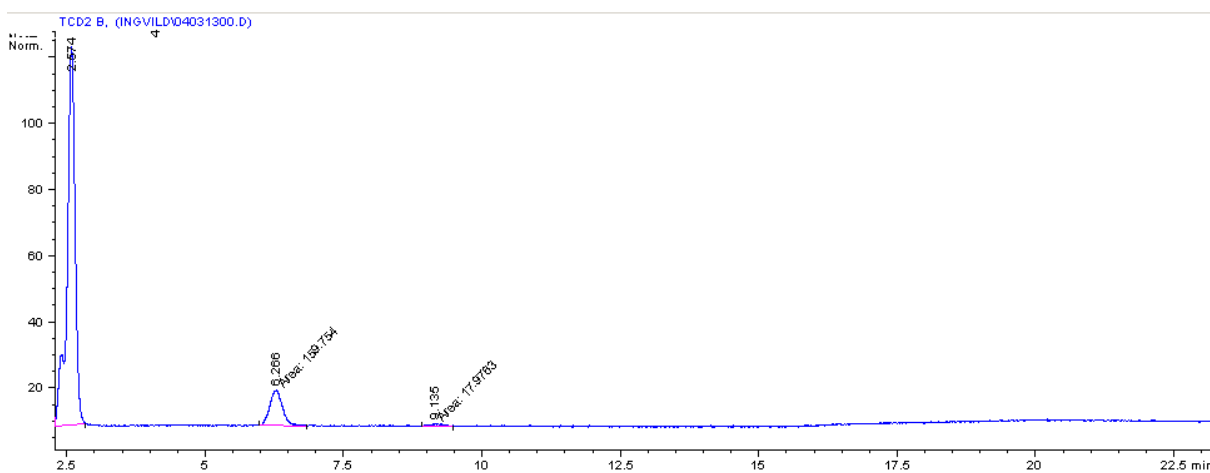
6) Catalyst: 20Ni-26ZnO/CNT, Rx. Time: 2,5h, T: 255°C



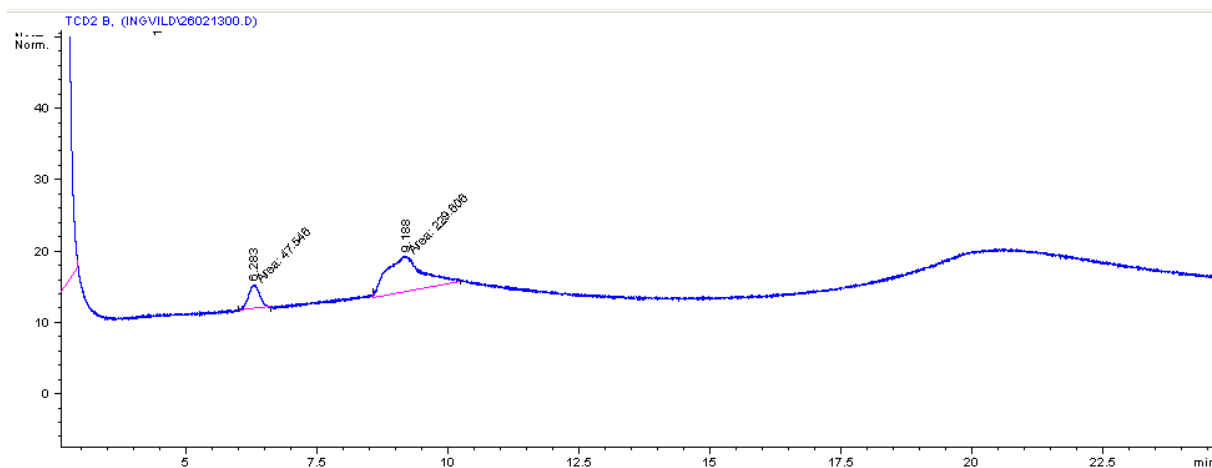
7) Catalyst: 20Ni-26ZnO/CNT, Rx. Time: 2h, T: 255°C



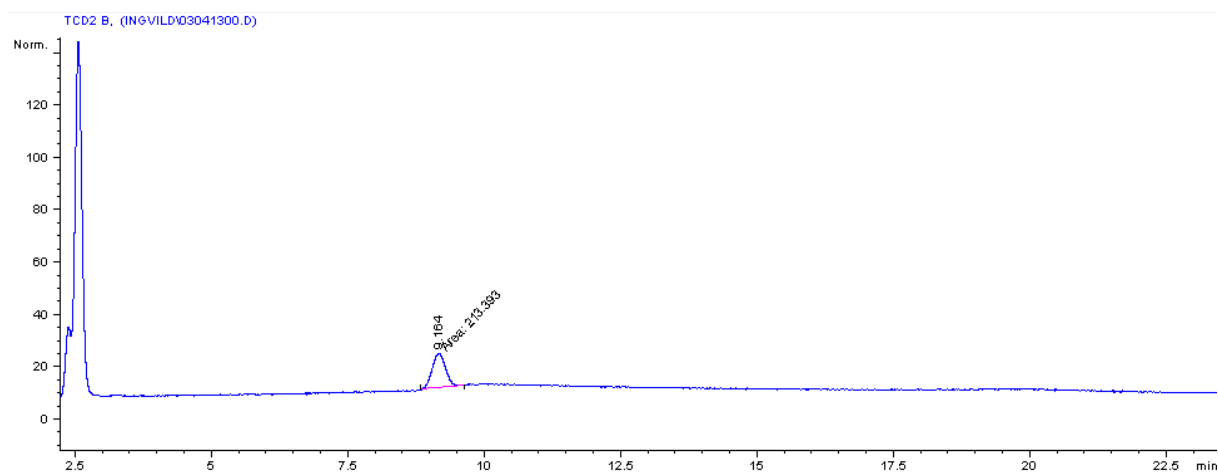
8) Catalyst: 20Ni-28ZnO/CNT, Rx. Time: 2h,5, T: 245°C



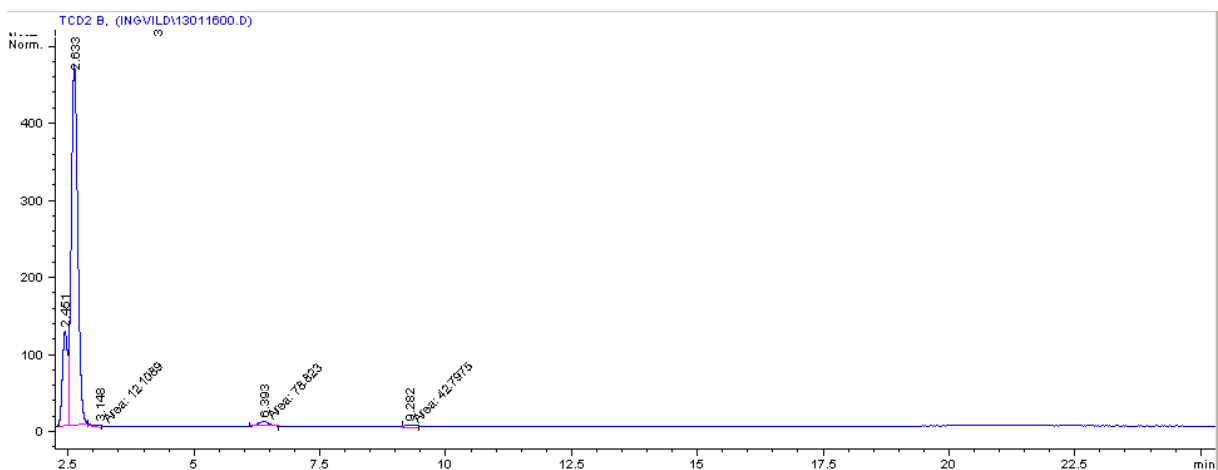
9) Catalyst: 20Ni-46ZnO/CNT, Rx. Time: 2h,5, T: 245°C



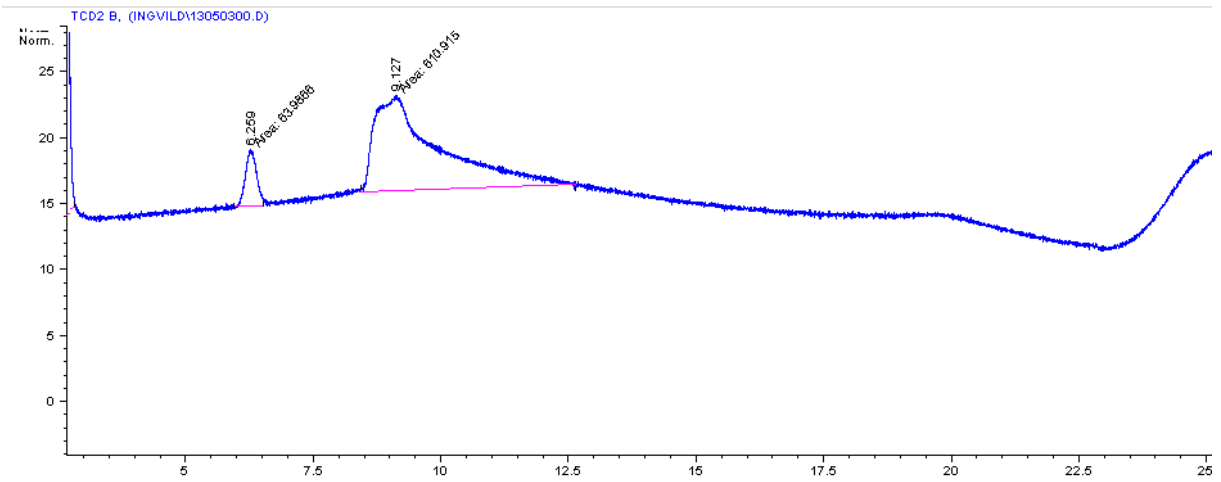
10) Catalyst: 26ZnO/CNT, Rx. Time: 2h,5, T: 245°C



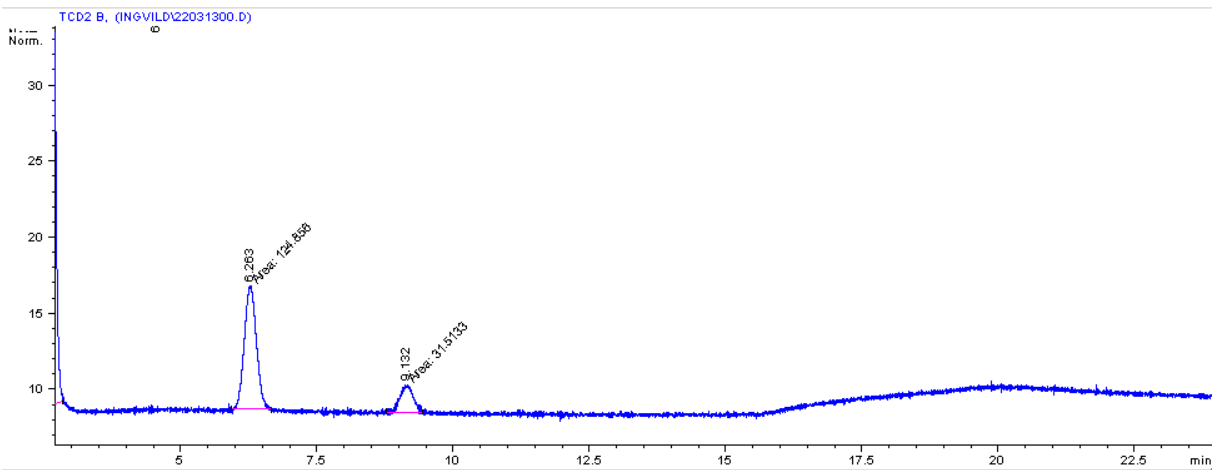
11) Catalyst: 20Ni/26ZnO A, Rx. Time: 2h,5, T: 245°C



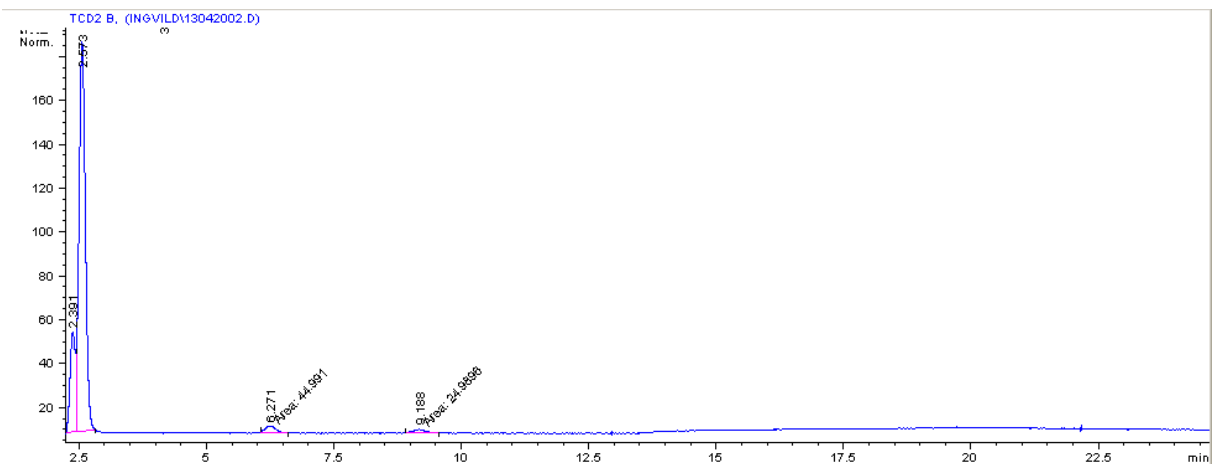
12) Catalyst: 20Ni/26ZnO B, Rx. Time: 2h,5, T: 245°C



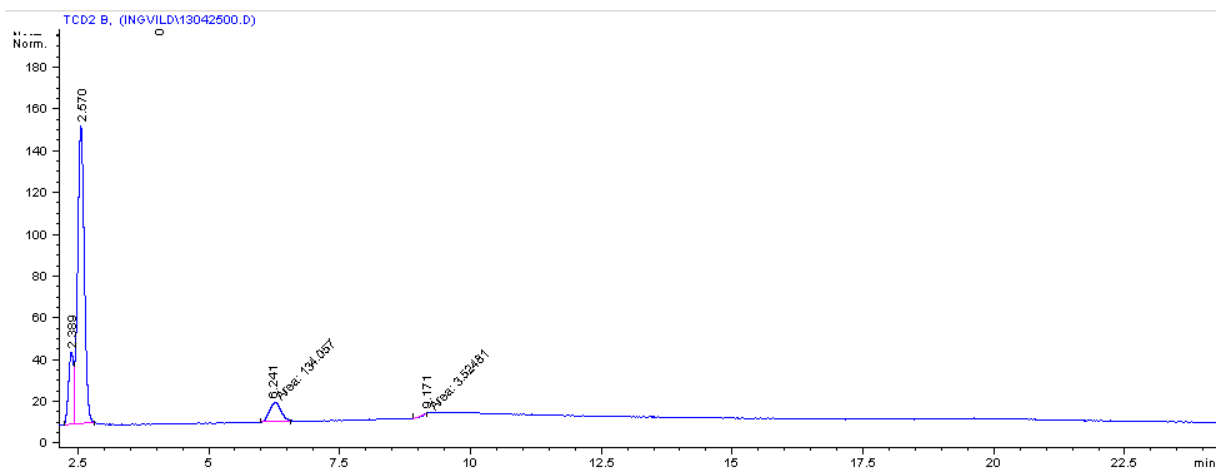
13) Catalyst: 20Ni/CNT, Rx. Time: 2h,5, T: 245°C



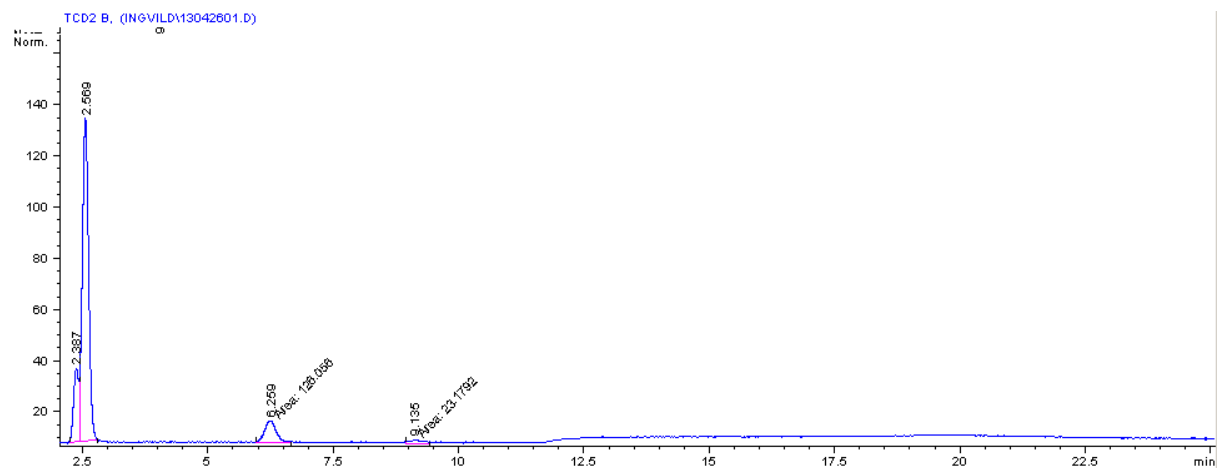
14) Catalyst: 20Ni/AC, Rx. Time: 2h,5, T: 245°C



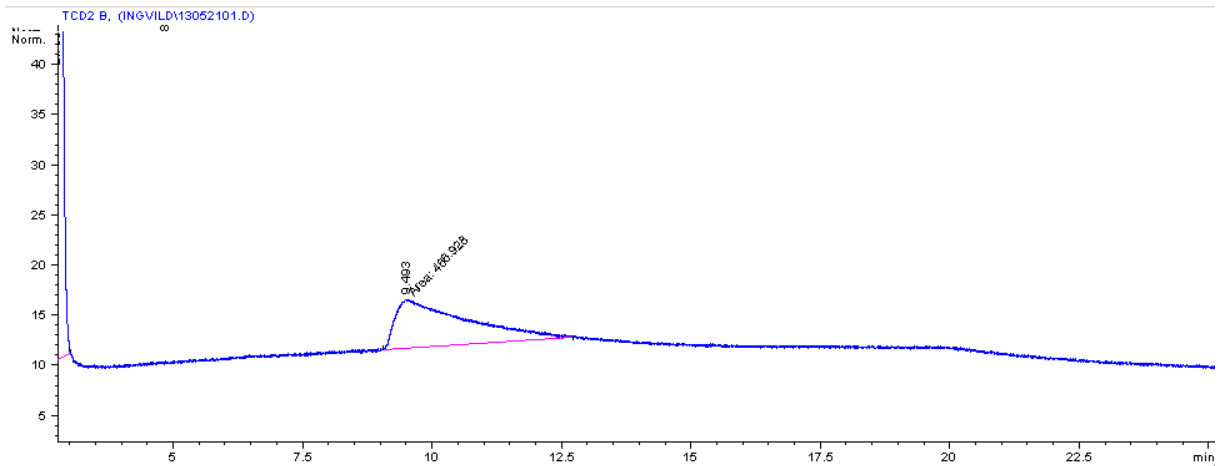
15) Catalyst: 20Ni-26ZnO/AC (incipient), Rx. Time: 2h,5, T: 245°C



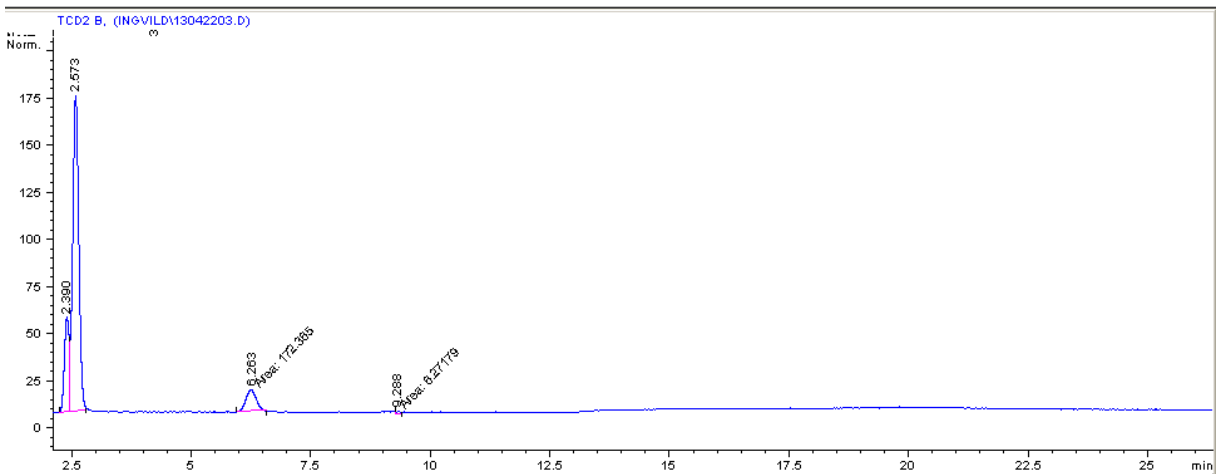
16) Catalyst: 20Ni-26ZnO/AC (pechini), Rx. Time: 2h,5, T: 245°C



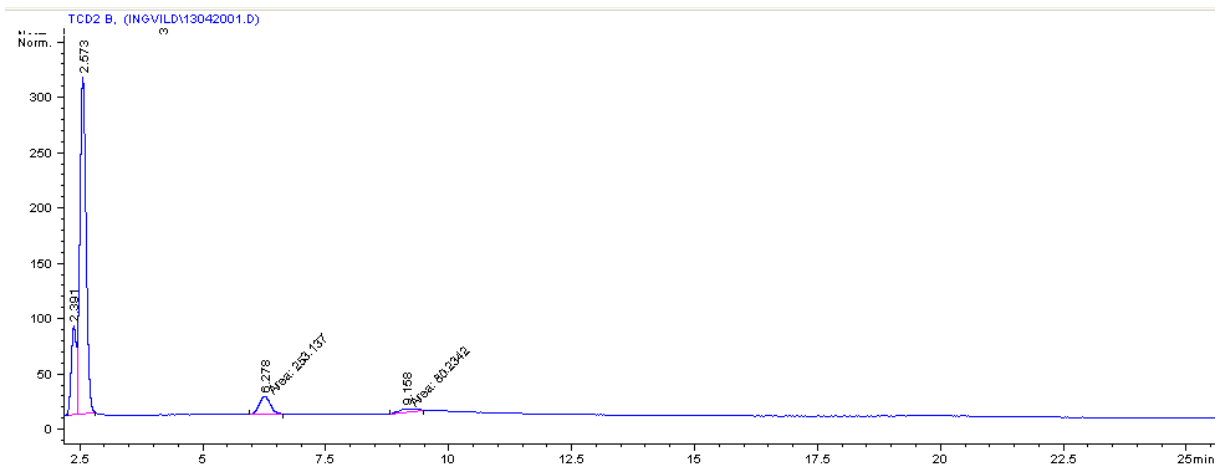
17) Catalyst: Ni-WO₃/CNT, Rx. Time: 2h,5, T: 245°C, Feedstock: Sorbitol



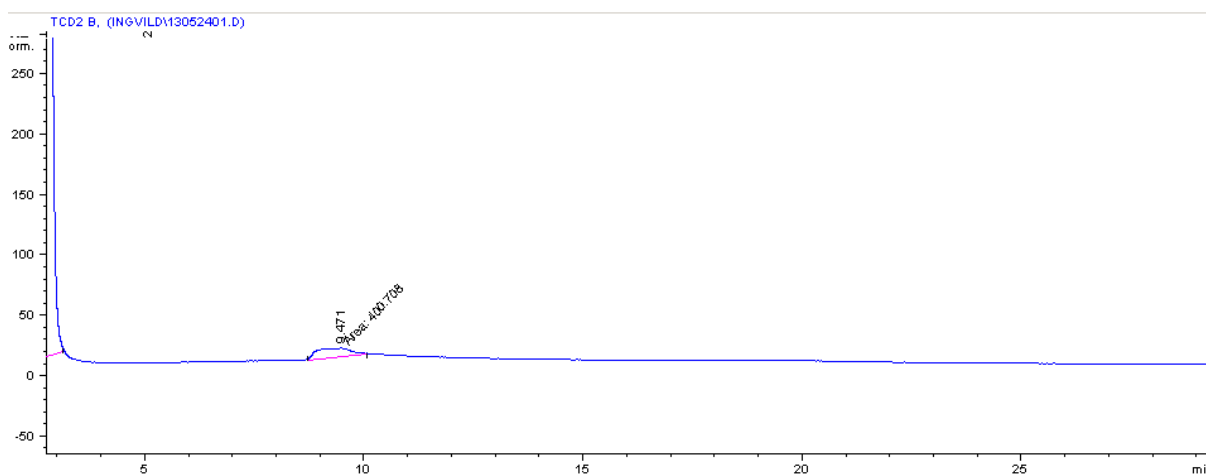
18) Catalyst: 20Ni-26ZnO/CNT, Rx. Time: 2h,5, T: 245°C, Feedstock: Sorbitol



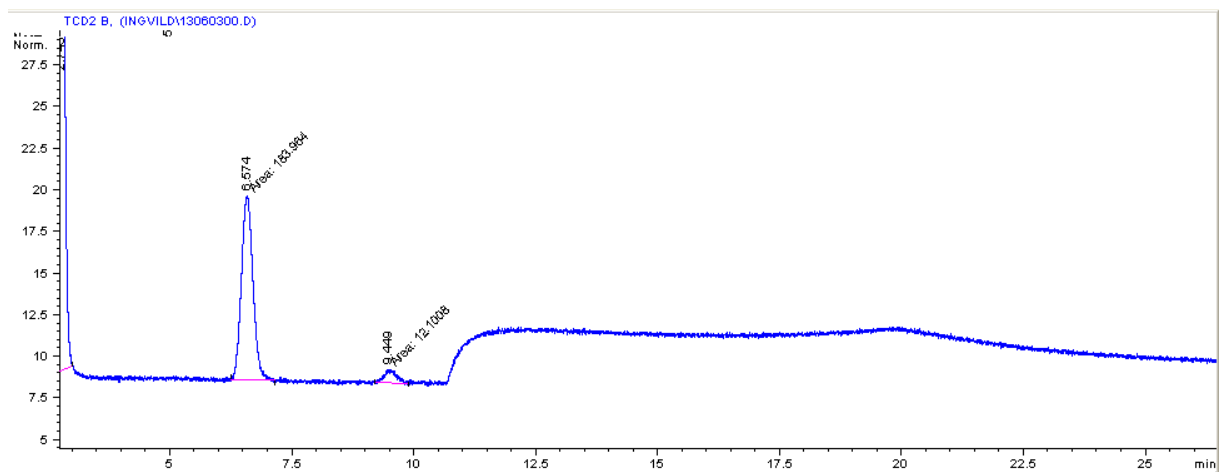
19) Catalyst: 20Ni-26ZnO/CNT, Rx. Time: 2h,5, T: 245°C, Feedstock: Mannitol



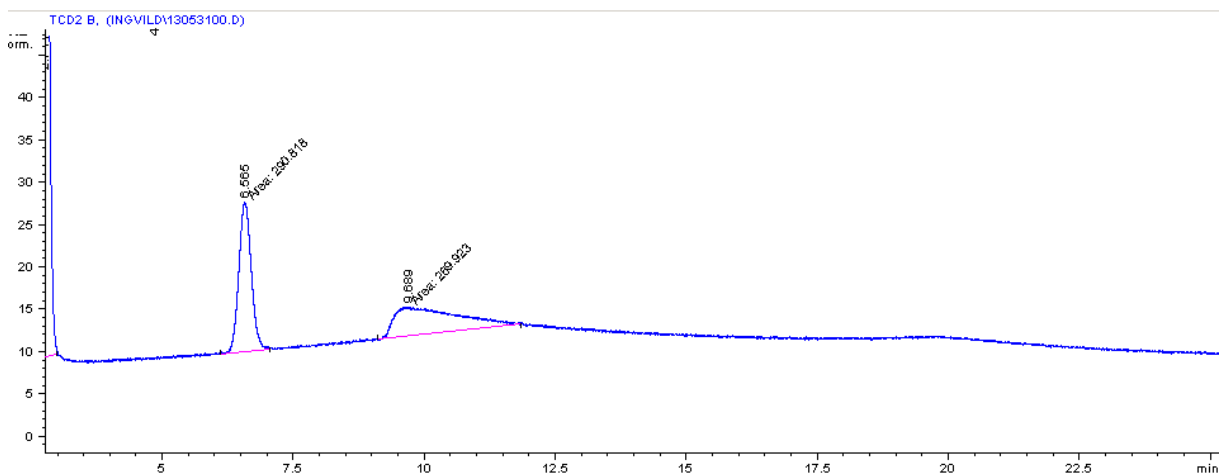
20) Catalyst: 25Ni-26ZnO/CNT, Rx. Time: 2h,5, T: 245°C



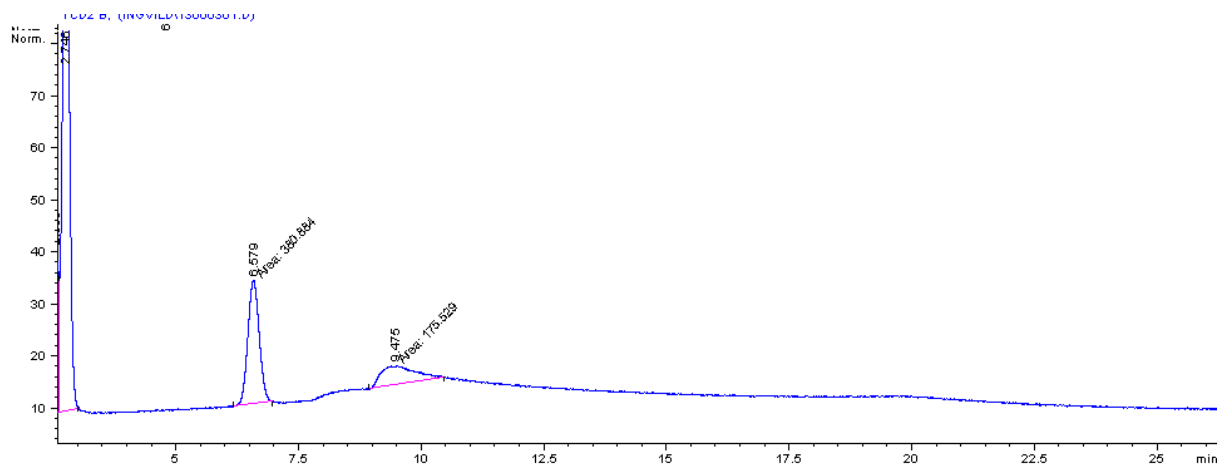
21) Catalyst: 30Ni-26ZnO/CNT-red300, Rx. Time: 2,5 h, T= 245°C, P= 60 bar (RT),
Feedstock: Sorbitol



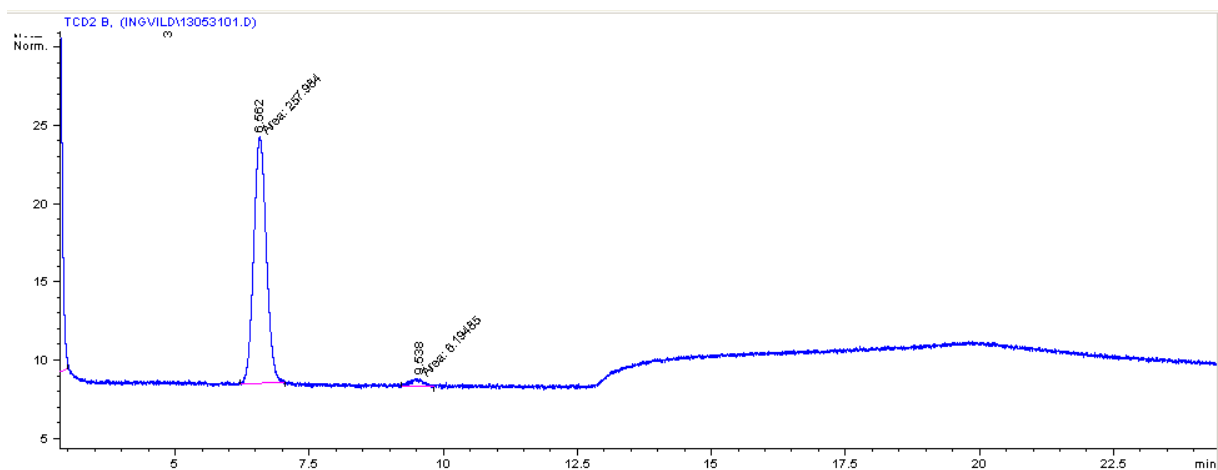
22) Catalyst: 30Ni-26ZnO/CNT-red350, Rx. Time: 2,5 h, T= 245°C, P= 60 bar (RT),
Feedstock: Sorbitol



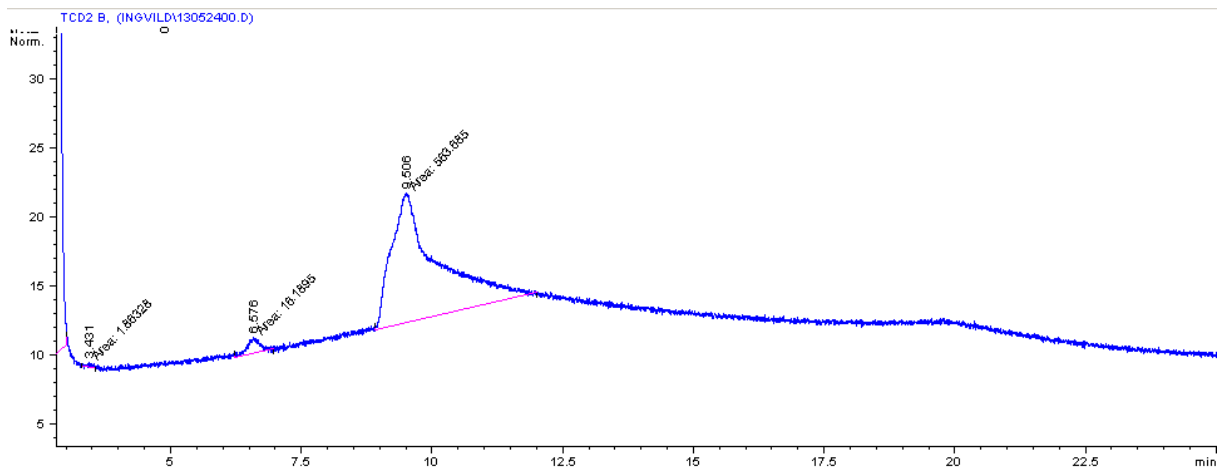
23) Catalyst: 30Ni-26ZnO/CNT-red400, Rx. Time: 2,5 h, T= 245°C, P= 60 bar (RT),
Feedstock: Sorbitol



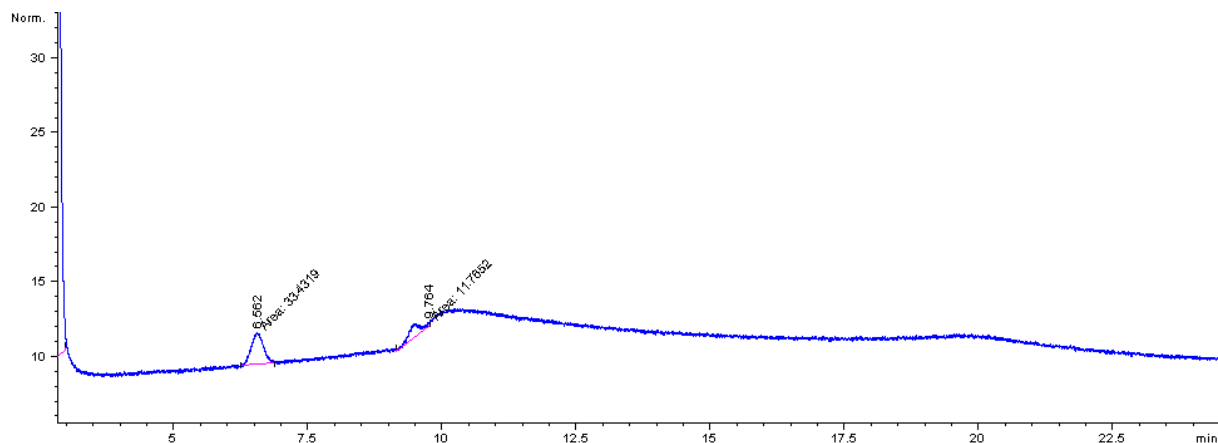
24) Catalyst: 30Ni-26ZnO/CNT-red450, Rx. Time: 2,5 h, T= 245°C, P= 60 bar (RT),
Feedstock: Sorbitol



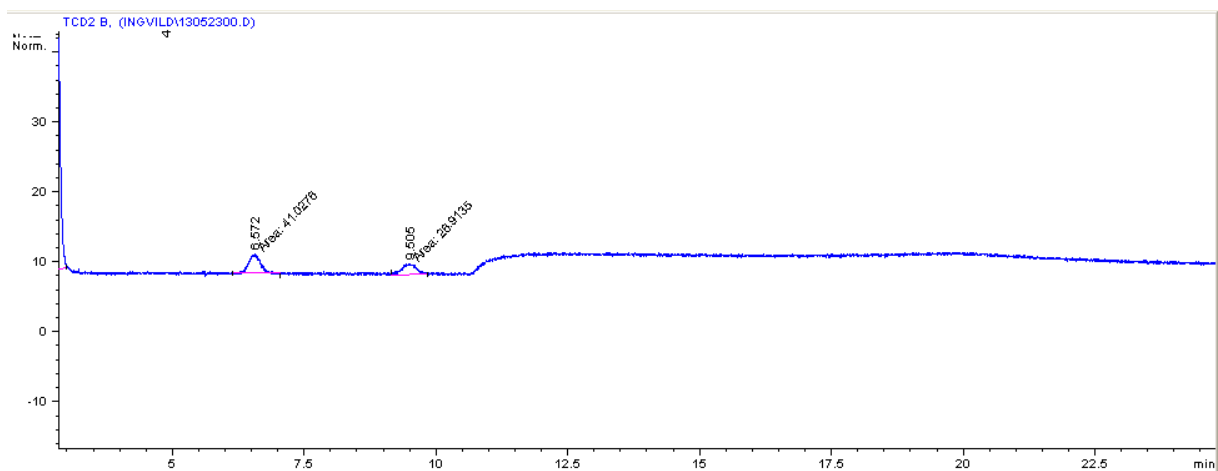
25) Catalyst: 5Ni-26ZnO/CNT, Rx. Time: 2,5 h, T= 245°C, P= 60 bar(RT), 2nd run
(reusability)



26) Catalyst: 20Ni-28ZnO/CNT, Rx. Time: 2,5 h, T= 245°C, P= 60 bar(RT), 2nd run (reusability)



27) Catalyst: 20Ni-46ZnO/CNT, Rx. Time: 2,5 h, T= 245°C, P= 60 bar(RT), 2nd run (reusability)



E.2 Calculation of gas products

The standard gas used to find the correlations for the calculation of the GC yields was composed of 1% CO, 1% CH₄, 1% CO₂ and 1% C₂H₆. Peak area 600, 470, 637,3 and 660,9 corresponds to CO, CH₄, CO₂ and C₂H₆ respectively. The autoclave reactor used for the reactions was 75 mL and the amount of water used was 25 mL, thus 50 mL volume was occupied by gas. Reaction conditions: 60 bar and 245°C. 0,25 g of cellulose was used as feedstock. The calculations for the yields of CO, CH₄, CO₂ and C₂H₆ are presented below.

Ideal gas law:

$$PV = nRT \rightarrow n = \frac{PV}{RT}$$

Unit conversion:

$$mL = cm^3 = 10^{-6}m^3$$

$$1 atm = 101000 Pa$$

$$1 atm \sim 1 bar$$

Yield of products

$$\frac{\%_{prod}}{Area_{prod}} = \frac{\%_{standard\ gas}}{Area_{standard\ gas}} \rightarrow \%_{prod} = \frac{\%_{standard\ gas}}{Area_{standard\ gas}} * Area_{prod}$$

1) The CO yield

$$n_{CO} = \frac{PV}{RT} = \frac{60 * 101000 * 50 * 10^{-6}}{298,15 * 8,314} * \frac{Peak\ area_{CO}}{600} * 1\%$$

$$Yield_{CO} = \frac{n_{CO}}{n_{cellulose}} = \frac{n_{CO}}{\frac{0,25 * 6}{162,14}}$$

2) The CH₄ yield

$$n_{CH_4} = \frac{PV}{RT} = \frac{60 * 101000 * 50 * 10^{-6}}{298,15 * 8,314} * \frac{Peak\ area_{CH_4}}{470} * 1\%$$

$$Yield_{C_2H_6} = \frac{n_{C_2H_6}}{n_{cellulose}} = \frac{n_{C_2H_6}}{\frac{0,25 * 6}{162,14}}$$

3) The CO₂ yield

$$n_{CO_2} = \frac{PV}{RT} = \frac{60 * 101000 * 50 * 10^{-6}}{298,15 * 8,314} * \frac{Peak\ area_{CO_2}}{637,3} * 1\%$$

$$Yield_{CO_2} = \frac{n_{CO_2}}{n_{cellulose}} = \frac{n_{CO_2}}{\frac{0,25 * 6}{162,14}}$$

4) The C₂H₆ yield

$$n_{C_2H_6} = \frac{PV}{RT} = \frac{60 * 101000 * 50 * 10^{-6}}{298,15 * 8,314} * \frac{Peak\ area_{C_2H_6}}{660,9} * 1\%$$

$$Yield_{CO_2} = \frac{n_{CO_2}}{n_{cellulose}} = \frac{n_{CO_2}}{\frac{0,25 * 6}{162,14}}$$

The calculations for the gas products were done in excel according to the calculation method described above, and the results are summarized in Table 29 and Table 30.

Table 29 – Gas products from the conversion of cellulose over Ni-ZnO catalysts with carbon support and Ni catalysts with carbon support

Catalyst	# of plot in Appendix E.1	CO	CH4	CO2	C2H6	Tot.
20Ni-40ZnO/CNT	1	0,00	4,00	0,32	0,00	4,32
20Ni-40ZnO/CNT	2	0,00	4,40	3,20	0,00	7,60
20Ni-40ZnO/CNT	3	0,00	4,34	0,19	0,00	4,53
20Ni-26ZnO/CNT	4	0,00	3,75	0,31	0,00	4,06
20Ni-26ZnO/CNT	5	0,00	3,71	0,35	0,00	4,07
20Ni-26ZnO/CNT	6	0,00	5,34	0,49	0,00	5,38
20Ni-26ZnO/CNT	7	0,00	5,02	0,32	0,00	5,34
20Ni-28ZnO/CNT	8	0,00	4,49	0,37	0,00	4,87
20Ni-46ZnO/CNT	9	0,00	1,34	4,76	0,00	6,10
26ZnO/CNT	10	0,00	0,00	4,42	0,00	4,42
20Ni/26ZnO A	11	0,07	1,46	0,06	0,00	1,59
20Ni/26ZnO B	12	0,00	1,80	12,67	0,00	14,46
20Ni/CNT	13	0,00	3,51	0,65	0,00	4,16
20Ni/AC	14	0,00	1,27	0,52	0,00	1,78
20Ni-26ZnO/AC (incipient)	15	0,00	3,77	0,07	0,00	3,84
20Ni-26ZnO/AC (pechini)	16	0,00	3,54	0,48	0,00	4,03
Ni-WO ₃ /CNT	17	0,00	0,00	9,68	0,00	9,68
20Ni-26ZnO/CNT	18	0,00	4,84	0,13	0,00	4,97
20Ni-26ZnO/CNT	19	0,00	7,12	1,66	0,00	8,78
25Ni-26ZnO/CNT	20	0,00	0,00	8,31	0,00	8,31
30Ni-26ZnO/CNT-red300	21	0,00	5,14	0,25	0,00	5,42
30Ni-26ZnO/CNT-red350	22	0,00	6,77	5,60	0,00	12,37

Table 30 – Gas products for the conversion of cellulose over Ni-ZnO/CNT catalysts

Catalyst	# in Appendix X	CO	CH4	CO2	C2H6	Tot.
30Ni-26ZnO/CNT-red400	23	0,00	10,71	3,64	0,00	14,35
30Ni-26ZnO/CNT-red450	24	0,00	7,20	0,13	0,00	7,33
5Ni-26ZnO/CNT (2nd run)	25	0,04	0,46	11,69	0,00	12,18
20Ni-28ZnO/CNT (2nd run)	27	0,00	0,94	0,24	0,00	1,18
20Ni-46ZnO/CNT (2nd run)	28	0,00	1,15	0,56	0,00	1,71

F Calculation of conversion of cellulose

Rough estimates for the conversion of cellulose were done according to mass measurements before and after the reactions. The calculations were done in excel, and the equations are given below.

Before reaction:

$m_{\text{cellulose}}$

m_{catalyst}

After reaction:

$m_{\text{filter paper}}$

$m_{\text{filter paper} + \text{remaining mass}}$

- 1) The remaining mass after reaction was calculated according to:

$$m_{\text{remaining}} = m_{\text{filter paper} + \text{remaining mass}} - m_{\text{filter paper}}$$

- 2) Assuming that no catalyst was lost during the reaction the conversion, x , was calculated according to:

$$m_{\text{remaining}} - m_{\text{catalyst}} = m_c$$

$$x = \frac{m_{\text{cellulose}} - m_c}{m_{\text{cellulose}}} * 100\%$$

G The conversion of cellulose over 20Ni-26,1ZnO/CNT - Yield vs. time

In section 4.6.2 yield as a function of time was discussed for the cellulose conversion over the 20Ni-26ZnO/CNT in order to reveal the reaction mechanism. Additional data is given in Table 31, describing the product distribution from the experiment was started, time=0, to the end after 2,5h. The corresponding plots can be found in Figure 47-50.

Table 31 - Product distribution as a function of time for the cellulose conversion over a 20Ni-26ZnO/CNT catalyst

#	Time	EG	1,2-PD	1,2-BUT	Sor	Man	Gly	Ery	HA	Sum
1	0	5,9	2,1	0,6	1,0	0,6	1,9	0,6	1,9	14,6
2	20	14,0	5,3	2,9	5,3	2,0	4,4	1,7	6,8	42,4
3	40	20,3	8,7	2,7	5,6	2,4	7,3	2,5	7,2	56,7
4	60	24,8	11,5	2,0	5,3	2,3	9,4	3,1	8,8	67,3
5	80	29,1	13,4	2,1	2,3	2,5	12,7	3,2	6,5	71,7
6	100	31,6	15,8	2,7	1,7	1,6	13,9	4,1	7,6	78,9
7	120	32,4	16,9	3,0	0,9	1,2	15,9	2,5	7,6	80,2
8	150	29,5	17,4	2,9	0,7	0,6	18,5	1,7	8,5	82,6

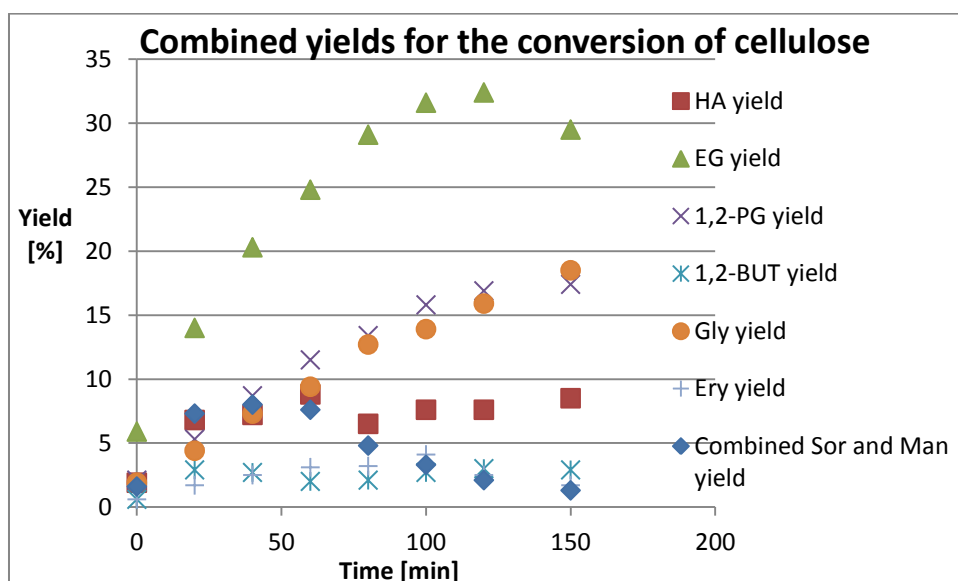


Figure 47 - Plots of the product distribution as a function of time for the cellulose conversion over a 20Ni-26ZnO/CNT catalyst

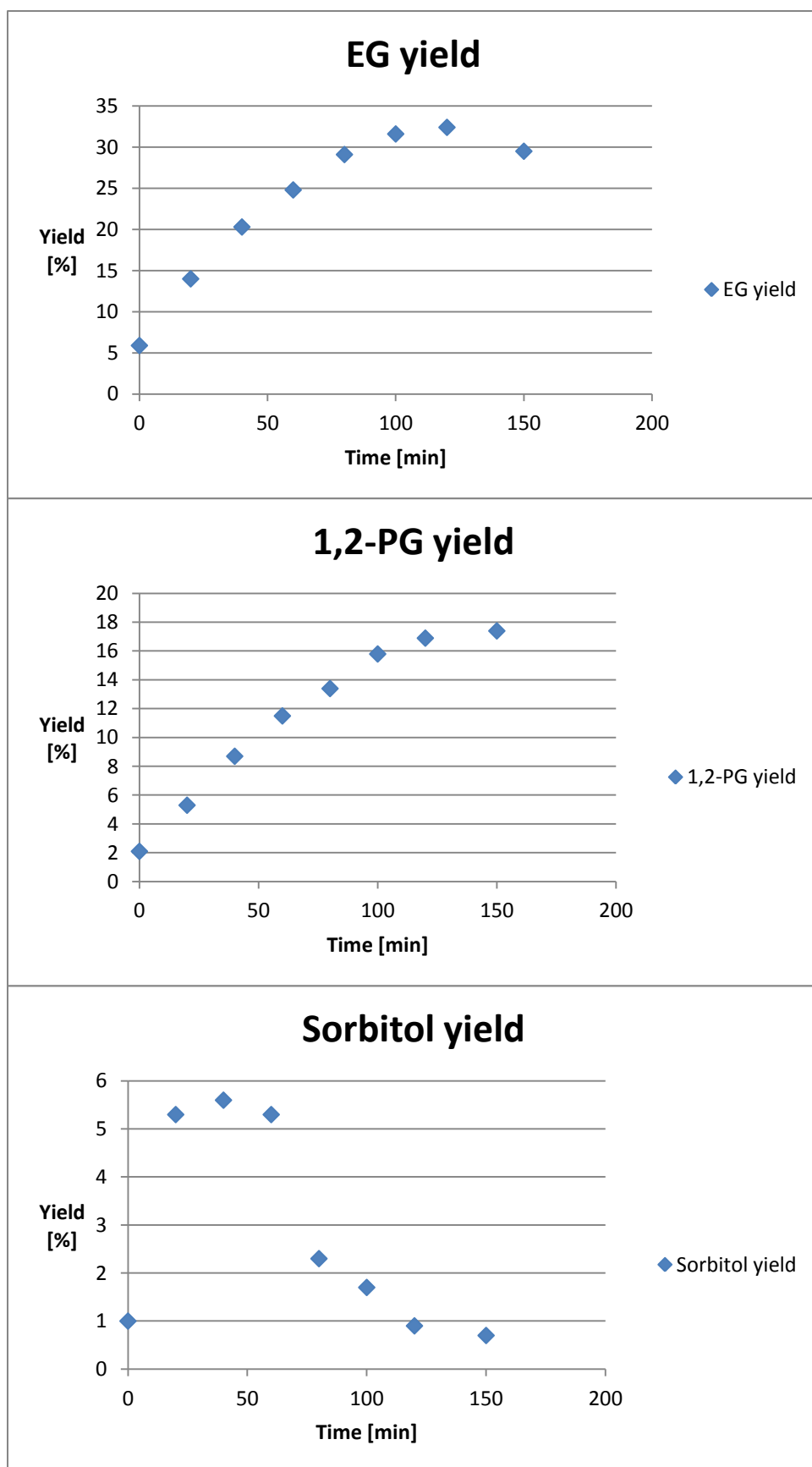


Figure 48 - Plots of the EG, 1,2-PG and Sor yields as a function of time for the cellulose conversion over a 20Ni-26ZnO/CNT catalyst

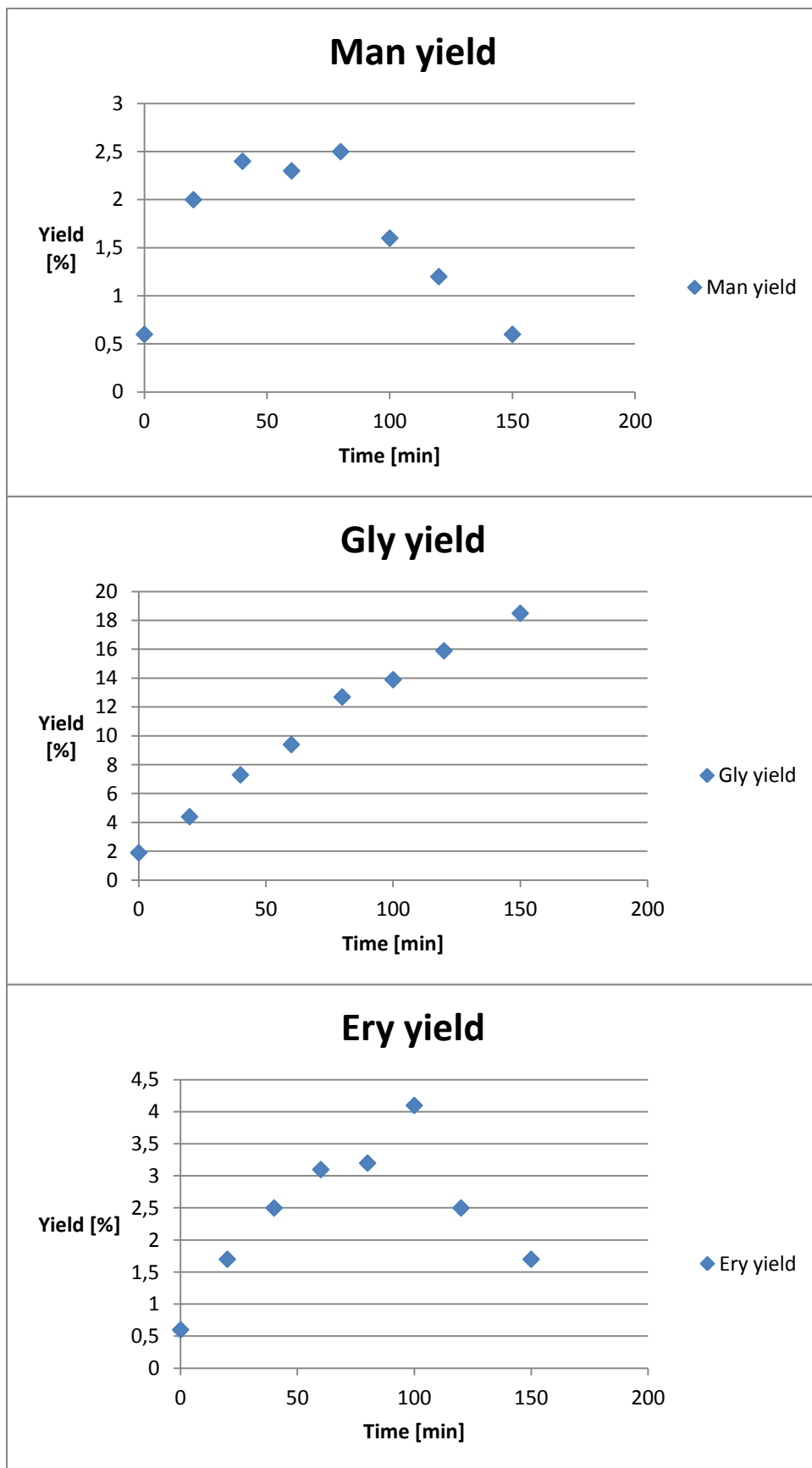


Figure 49 - Plots of the Man, Gly and Ery yields as a function of time for the cellulose conversion over a 20Ni-26ZnO/CNT catalyst

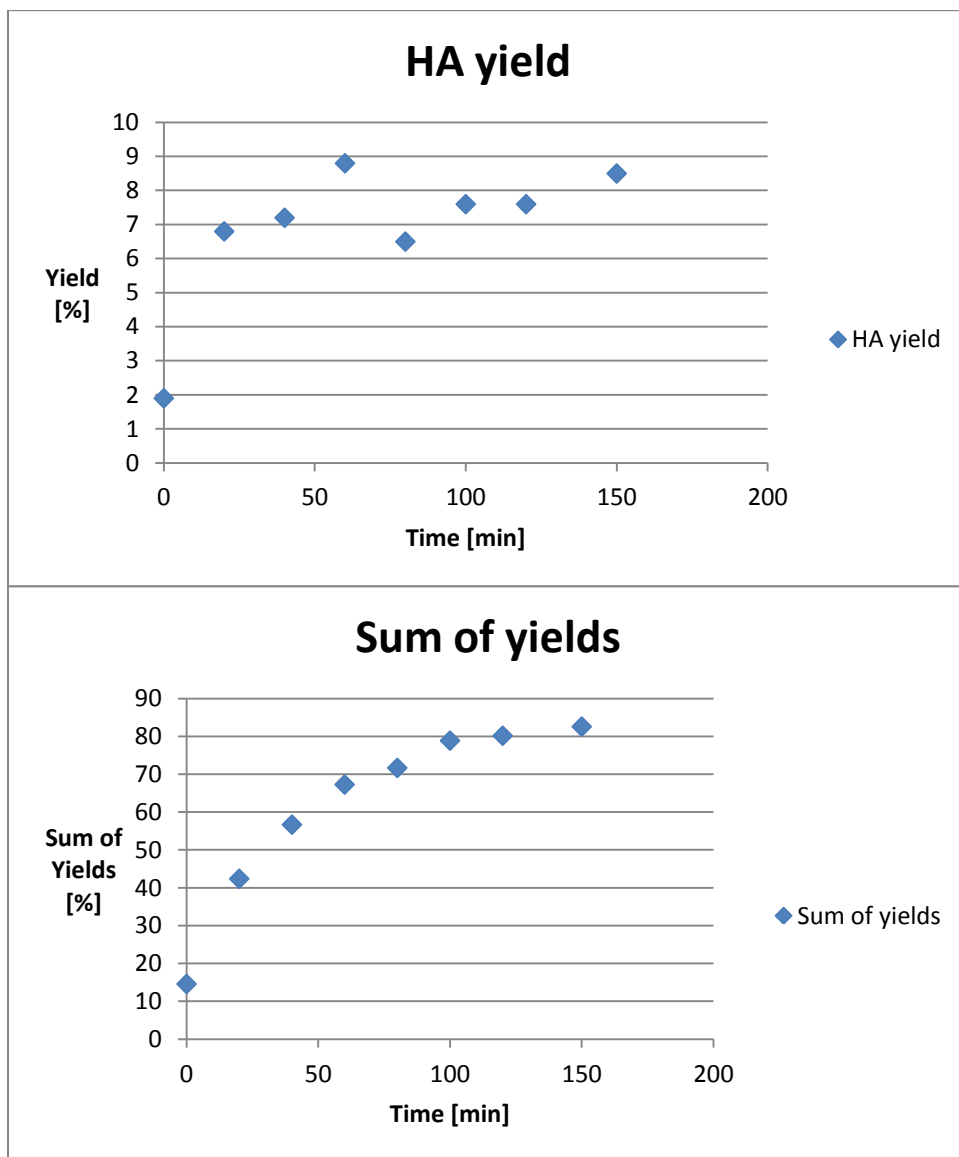


Figure 50 - Plots of the HA yield and the sum of yields as a function of time for the cellulose conversion over a 20Ni-26ZnO/CNT catalyst

H SEM/TEM pictures of the Ni-ZnO/AC catalysts

In section 4.7.1 SEM/TEM pictures of the 20Ni-26ZnO/AC catalysts were presented. Additional pictures of the 20Ni-26ZnO/AC (incipient) catalyst can be found in Figure 51-52, and several pictures of the 20Ni-26ZnO/AC (pechini) catalyst are given in Figure 53-56.

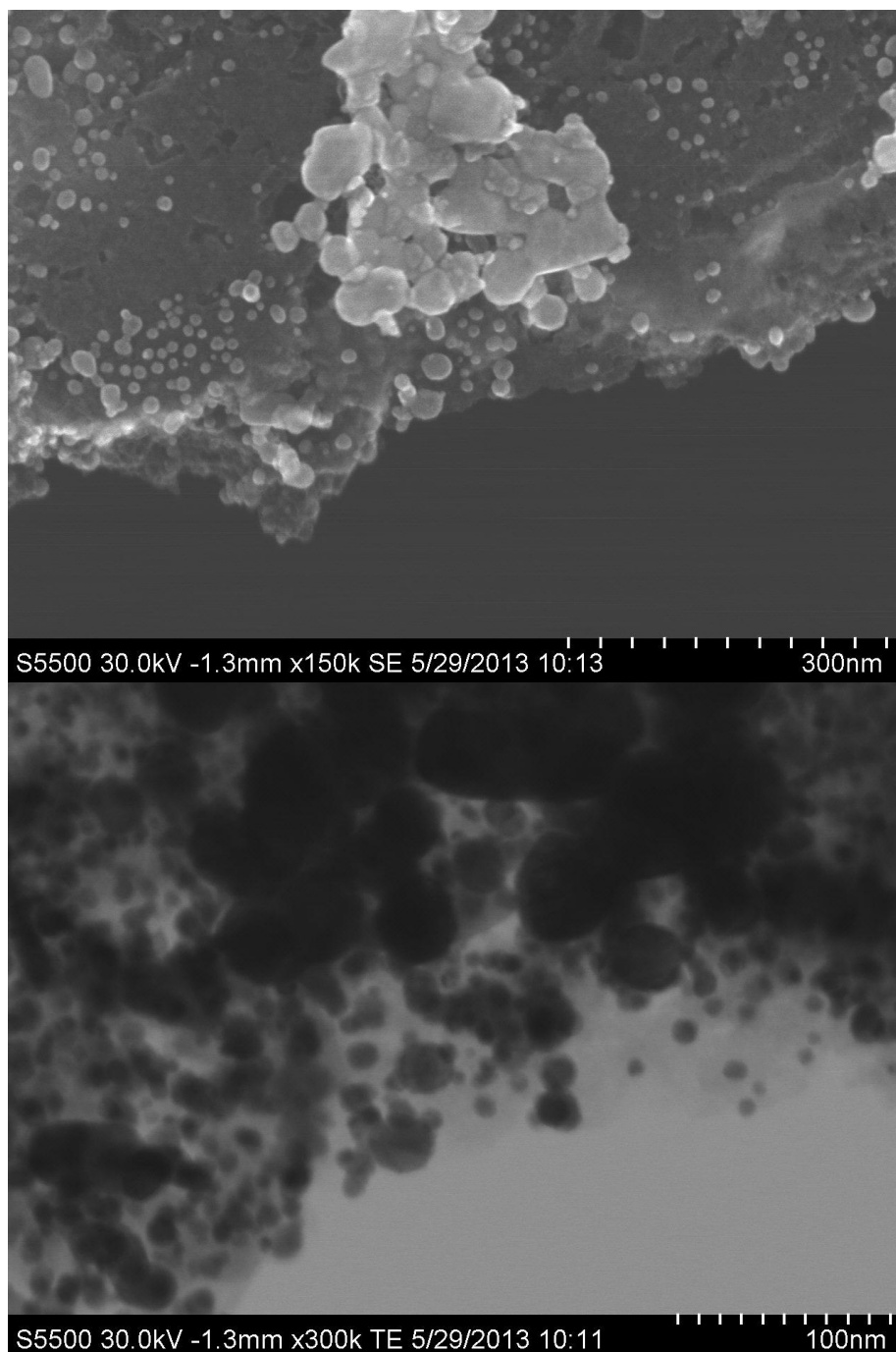


Figure 51 – SEM and TEM pictures of the 20Ni-26ZnO/AC (incipient) catalyst

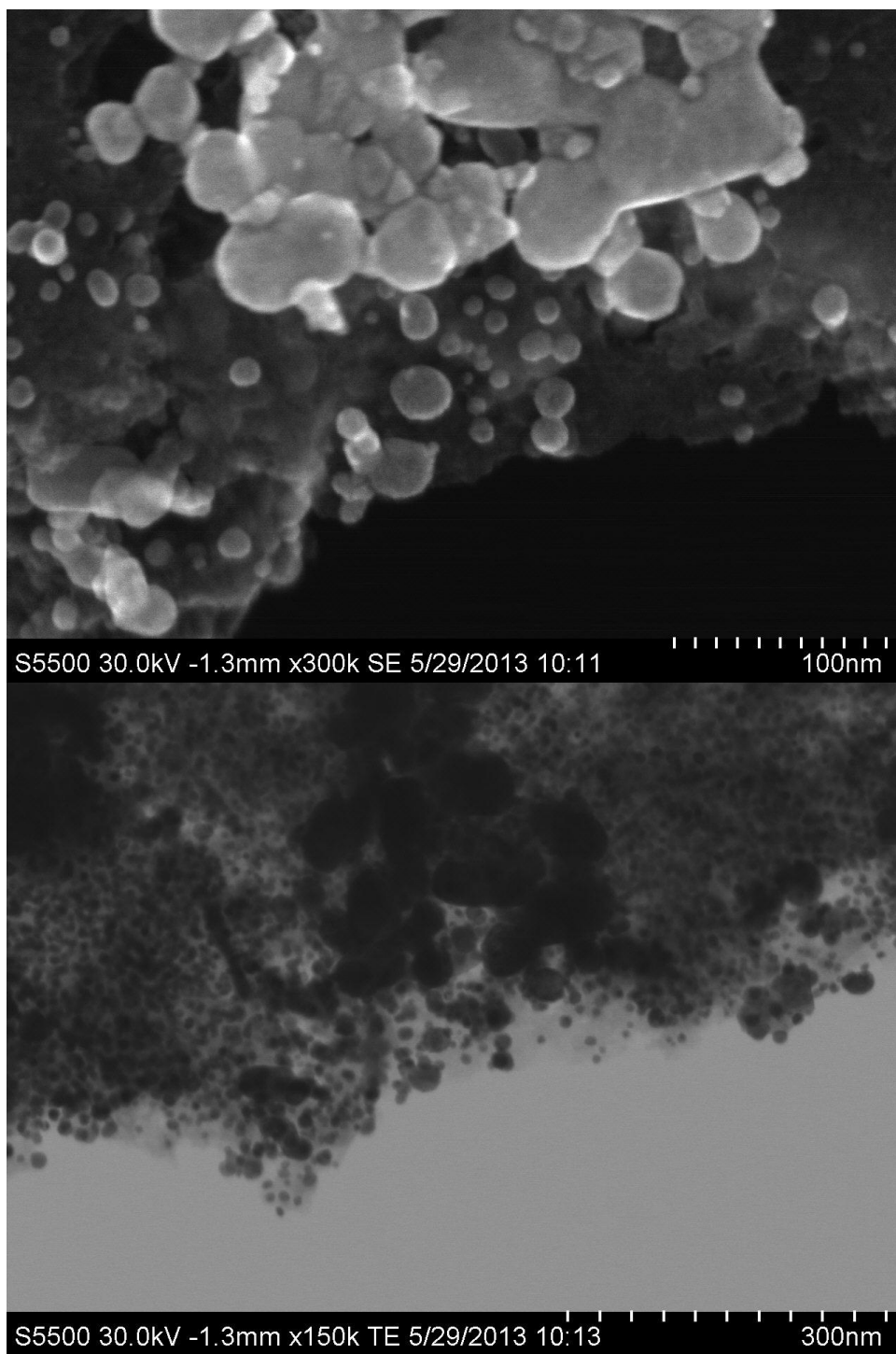


Figure 52 - SEM and TEM pictures of the 20Ni-26ZnO/AC (incipient) catalyst

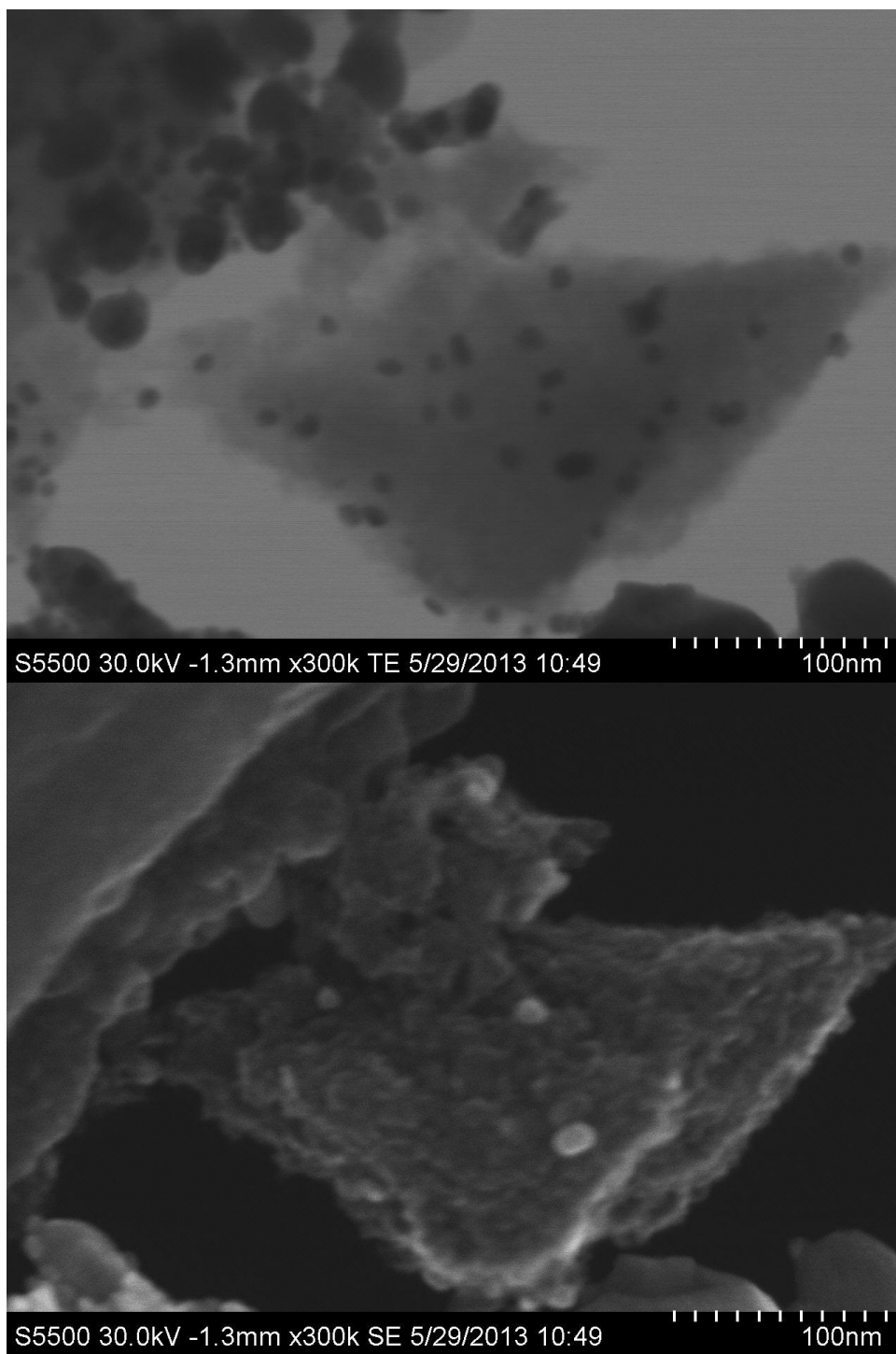


Figure 53 - SEM and TEM pictures of the 20Ni-26ZnO/AC (pechini) catalyst

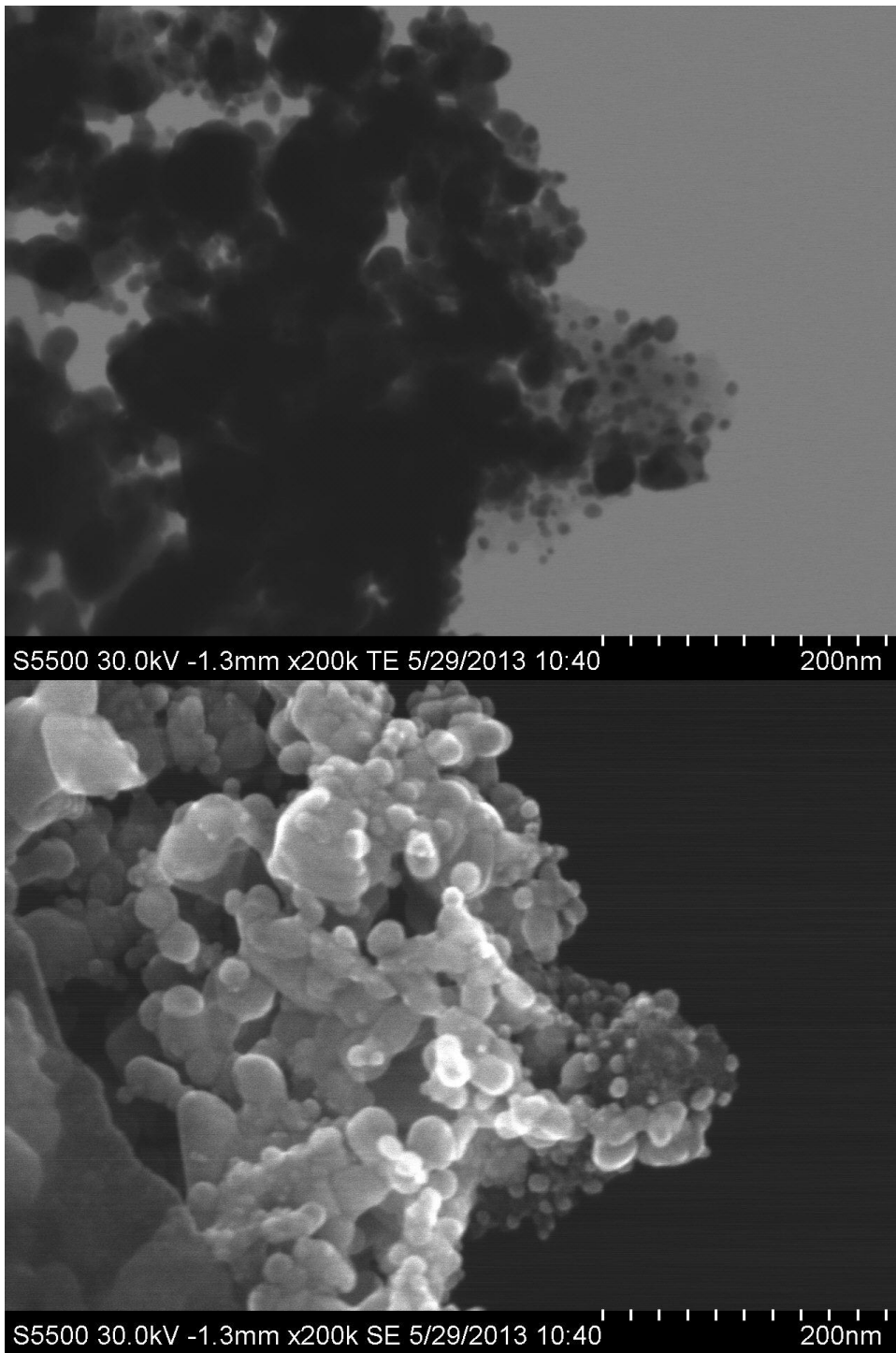


Figure 54 - SEM and TEM pictures of the 20Ni-26ZnO/AC (pechini) catalyst

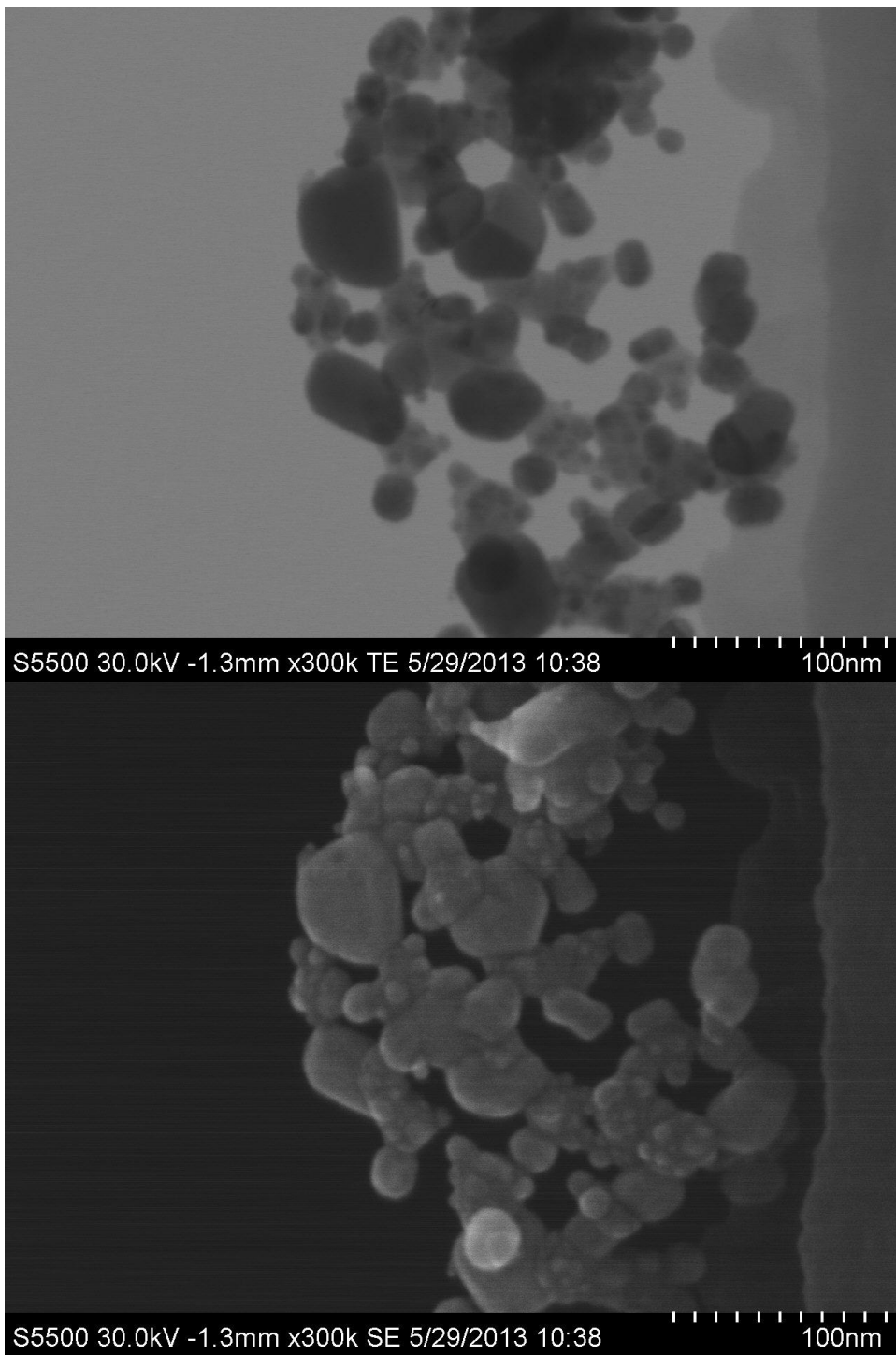


Figure 55 - SEM and TEM pictures of the 20Ni-26ZnO/AC (pechini) catalyst

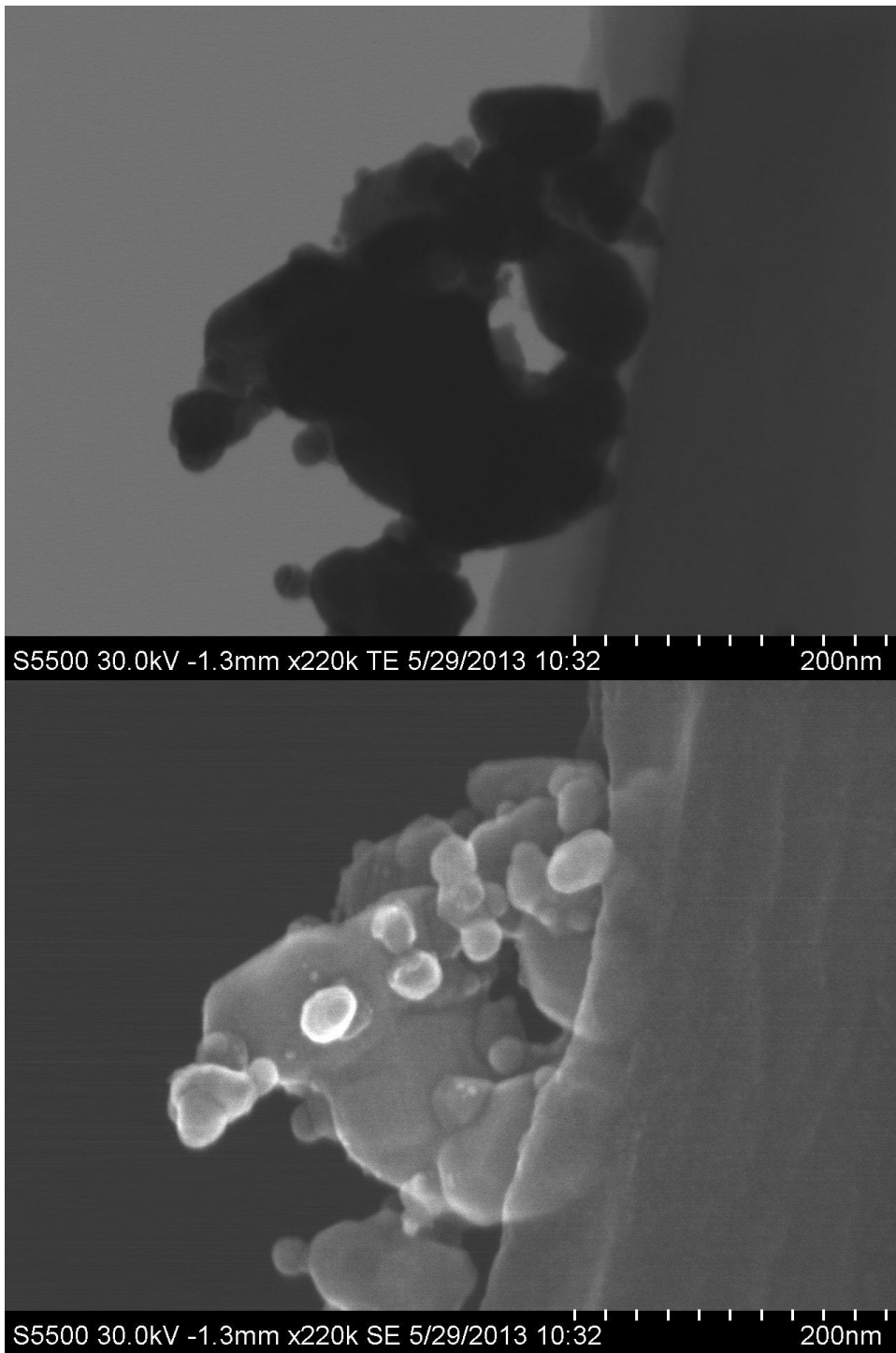


Figure 56 - SEM and TEM pictures of the 20Ni-26ZnO/AC (pechini) catalyst

I Calculation of the theoretical loading of the catalysts for TGA analysis

1) Calculation of the NiO-loading

During the TGA analysis there will be NiO present in the catalyst, therefore calculations of the NiO-loading is necessary in order to determine the overall theoretical loading of the catalysts. An example of the calculation of NiO-loading is given for the 15Ni-26ZnO/CNT catalyst. The similar calculations for the rest of the catalysts were done in excel, and the results are presented in Table 33.

$$MW_{Ni} = 58,693 \frac{g}{mol}$$

$$MW_{Nickel\ Nitrate} = 290,79 \frac{g}{mol}$$

$$MW_{NiO} = 74,69 \frac{g}{mol}$$

$$NiO - loading = \frac{m_{NiO}}{m_{ZnO/CNT} + m_{NiO}}$$

$$m_{NiO} = n_{Ni} * MW_{NiO} = \frac{m_{Ni}}{MW_{Ni}} * MW_{NiO}$$

An example: The 15Ni-26ZnO/CNT catalyst:

Table 32 - Amounts of chemicals used for the impregnation of nickel in the 15Ni-26ZnO/CNT catalyst

Catalyst	Mass of nickel nitrate [g]	Mass of ZnO/CNT [g]	Deionized water [ml]
15Ni-26ZnO/CNT	2,2204	2,5524	3

$$m_{Ni} = \frac{m_{Nickel\ Nitrate}}{MW_{Nickel\ Nitrate}} * MW_{Nickel} = \frac{2,2204\ g}{290,79\ g/mol} * 58,693 \frac{g}{mol} = 0,4482\ g$$

$$m_{NiO} = \frac{0,4482\ g}{58,693\ g/mol} * 74,69 \frac{g}{mol} = 0,5704\ g$$

$$NiO - loading = \frac{0,5704\ g}{2,5524\ g + 0,5704\ g} * 100\% = 18,26\ \%$$

Table 33 - The theoretical NiO loading in the Ni-ZnO/CNT catalysts

Catalyst	Mass of nickel nitrate [g]	Mass of ZnO/CNT [g]	Deionized water [ml]	NiO-Loading [%]
5Ni-26ZnO/CNT	0,7472	2,8501	3	6,31
10Ni-26ZnO/CNT	1,4846	2,7024	3	12,37
15Ni-26ZnO/CNT	2,2204	2,5524	3	18,26
25Ni-26ZnO/CNT	3,2602	1,9557	2	29,98
30Ni-26ZnO/CNT-red300	7,4822	3,5021	4	35,43
30Ni-26ZnO/CNT-red350	7,4413	3,5044	4	35,29
30Ni-26ZnO/CNT-red400	2,9319	1,4126	1	34,77
30Ni-26ZnO/CNT-red450	7,4561	3,5032	4	35,35
20Ni-26ZnO/AC (pechini)	2,9655	2,4064	3	24,04
20Ni-26ZnO/AC (incipient)	2,9986	2,4141	3	24,19

2) Calculation of ZnO-loading and total theoretical loading for TGA analysis

The calculation for the ZnO-loading is identical to the calculations done in Appendix A, and the total theoretical loading for the catalysts tested with TGA analysis is presented in Table 34

Table 34 - The total theoretical loading for the Ni-ZnO catalysts with carbon support that were tested with TGA

Catalyst	Calculated ZnO-loading [%]	Calculated NiO-loading [%]	Total theoretical loading
5Ni-26ZnO/CNT	26,41	6,31	32,72
10Ni-26ZnO/CNT	26,52	12,37	38,89
15Ni-26ZnO/CNT	26,30	18,26	44,56
25Ni-26ZnO/CNT	26,30	29,98	56,28
30Ni-26ZnO/CNT-red400	26,41	34,77	61,18
30Ni-26ZnO/CNT-red300	26,28	35,43	61,71
30Ni-26ZnO/CNT-red350	26,24	35,29	61,53
30Ni-26ZnO/CNT-red450	26,28	35,35	61,62
20Ni-26ZnO/AC (incipient)	26,24	24,19	50,43
20Ni-26ZnO/ AC (pechini)	26,32	24,04	50,14

J TGA of the CNT support

TGA was carried out for the different batches of CNT support (CNT #1N, CNT #2N and CNT #1D). The DTG and TG cor. plots as a function of temperature are given in Figure 57-59. For the CNT #1N support, the total mass loss according to the TGA was -97,8 %, thus the loading on the CNTs was 2,2%.

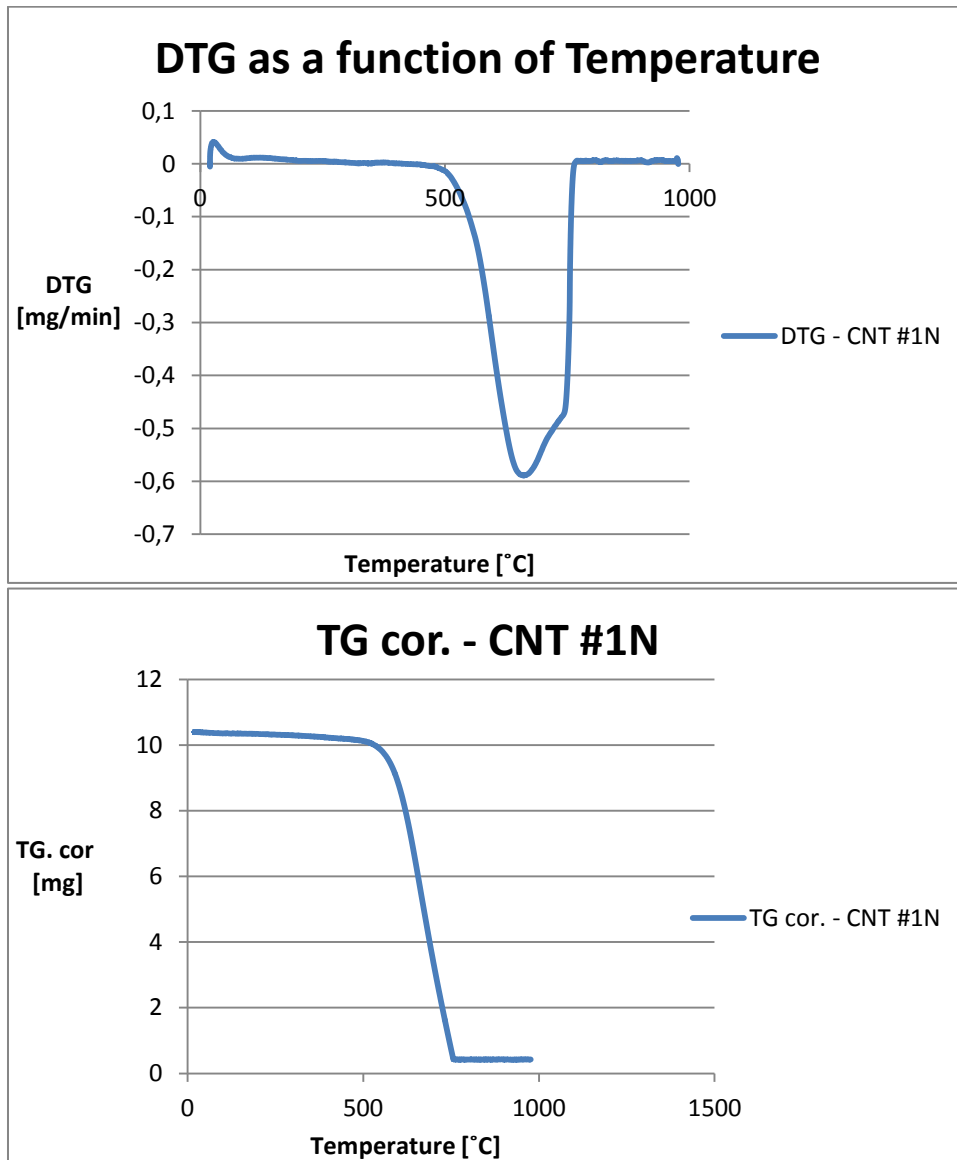


Figure 57 - DTG and TG cor. (from TGA) as a function of temperature for the CNT #1N support

The total mass loss for the CNT #2N support was according to the TGA results -94,0 %, thus the remaining mass from production was 6,0 %.

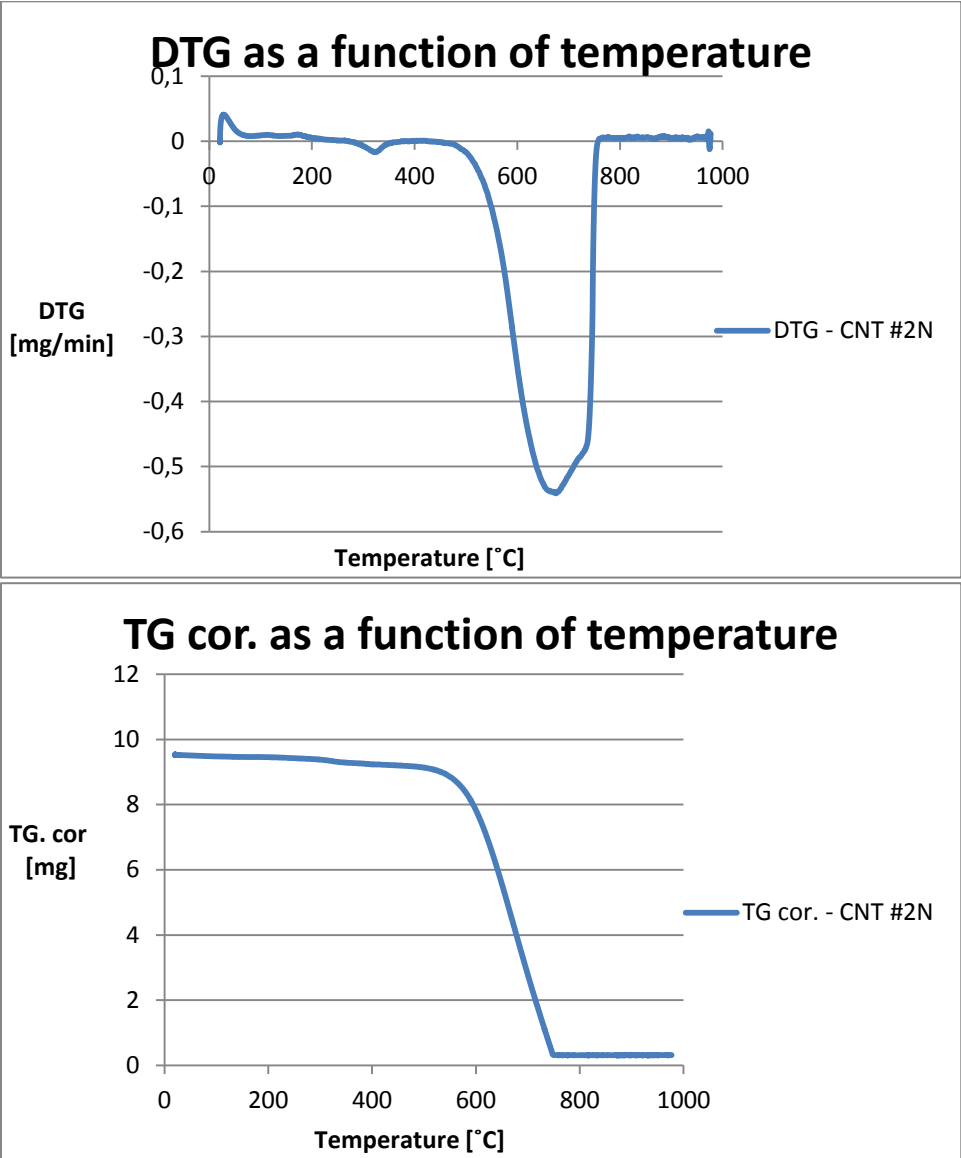


Figure 58 - DTG and TG cor. (from TGA) as a function of temperature for the CNT #2N support

The total mass loss for the CNT #1D support was according to the TGA results 100%, thus these results indicate that all the impurities from production are removed, which seem unlikely.

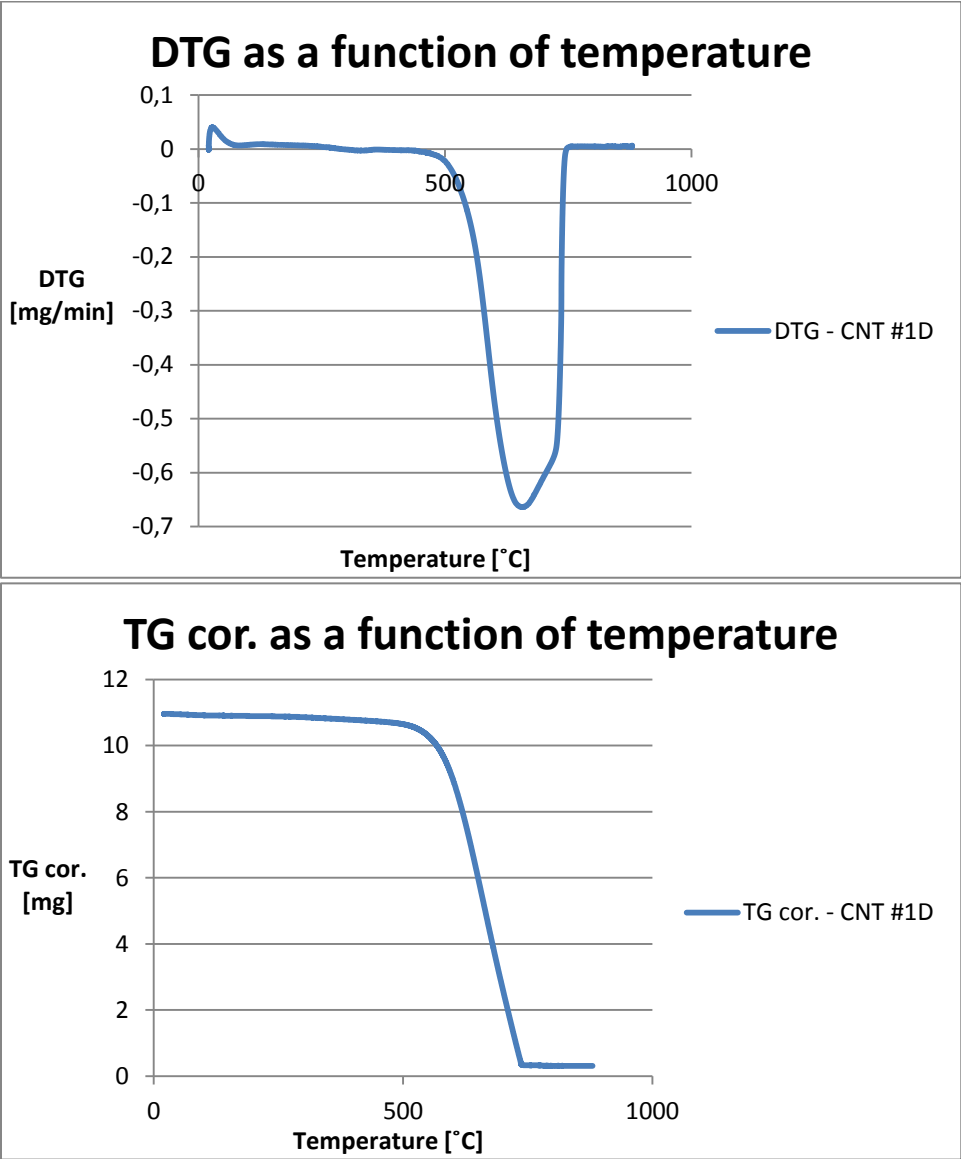


Figure 59 – DTG and TG cor. (from TGA) as a function of temperature for the CNT #1D support

K CO₂-TPD for the 30Ni-26ZnO/CNT catalysts

In section 4.9.1 a combined plot for the CO₂-TPD analysis was presented. The individual plots can be found in Figure 60-63

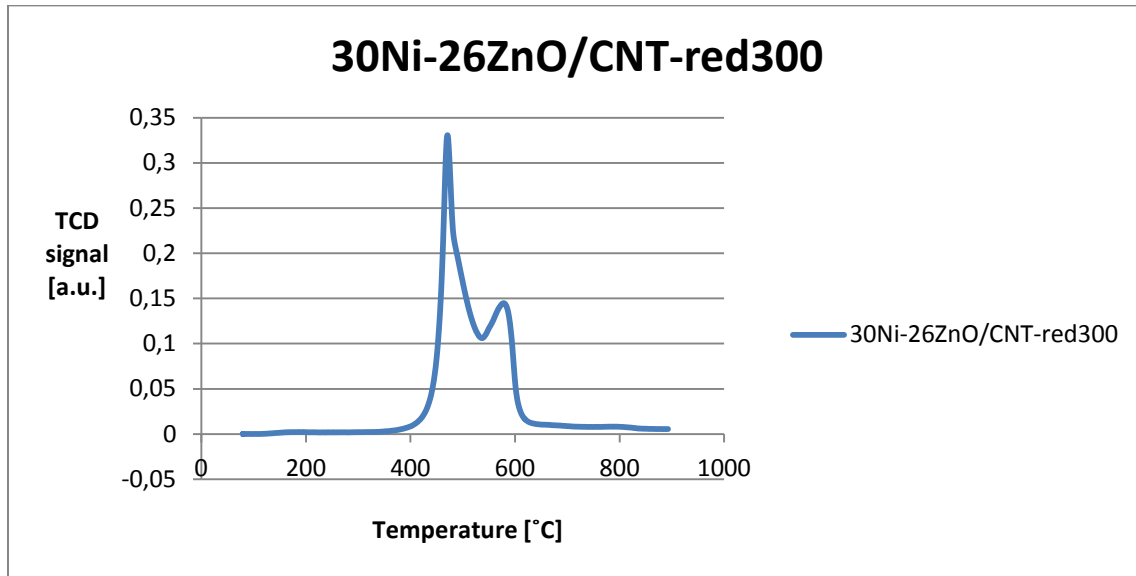


Figure 60 - CO₂-TPD: TCD signal as a function of temperature for the 30Ni-26ZnO/CNT-red300 catalyst

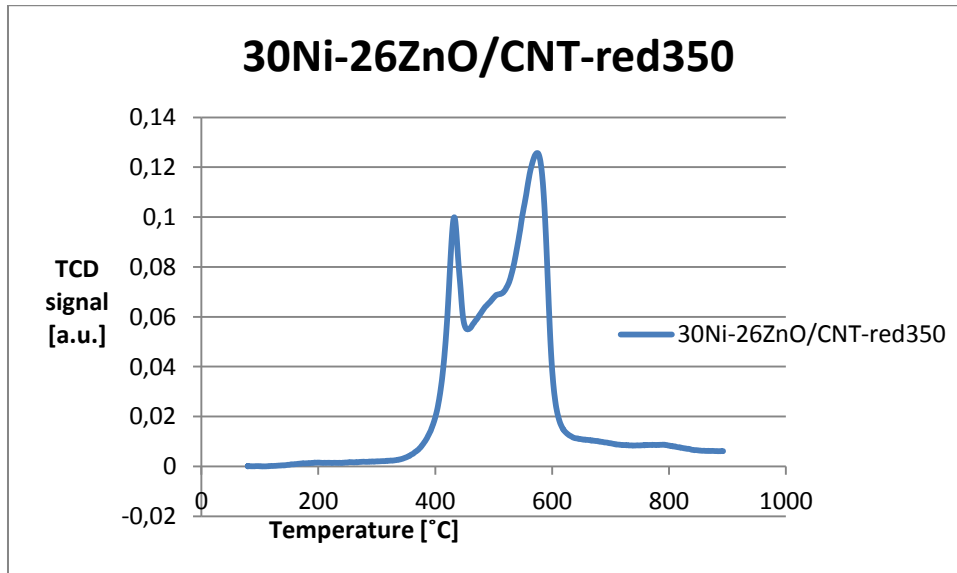


Figure 61 - CO₂-TPD: TCD signal as a function of temperature for the 30Ni-26ZnO/CNT-red350 catalyst

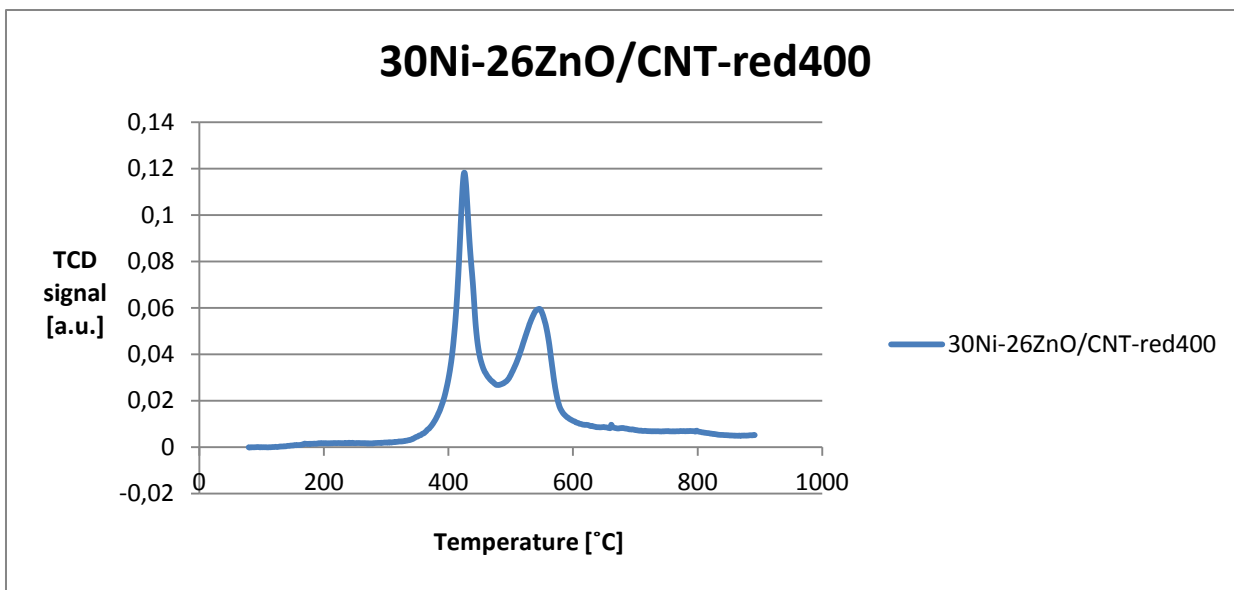


Figure 62 - CO₂-TPD: TCD signal as a function of temperature for the 30Ni-26ZnO/CNT-red400 catalyst

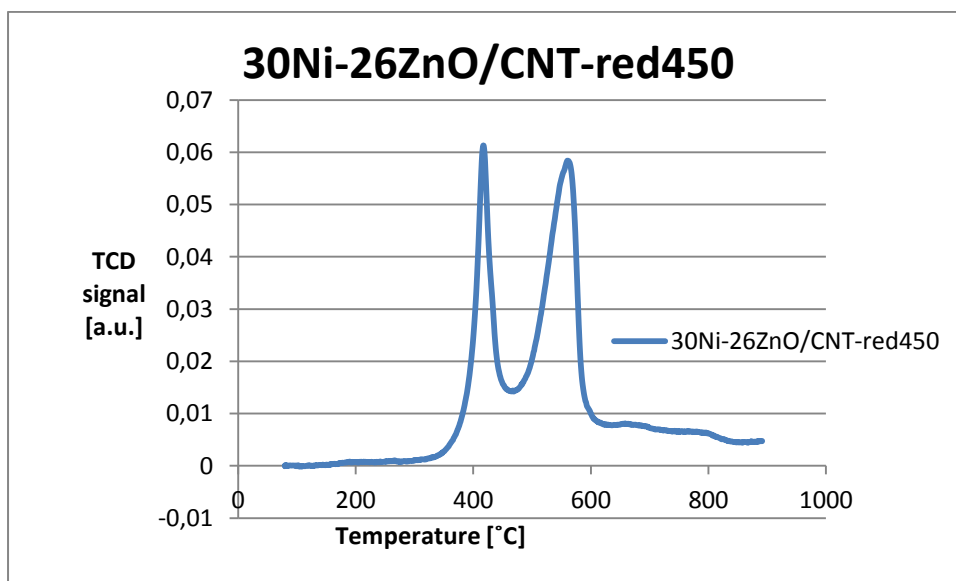


Figure 63 - CO₂-TPD: TCD signal as a function of temperature for the 30Ni-26ZnO/CNT-red450 catalyst

L ICP analysis

ICP analysis was carried out in order to investigate the leaching of zinc and nickel. Two samples were prepared by diluting 0,2 mL of the filtrate from the conversion of cellulose (over the 20Ni-26ZnO/CNT catalyst) in a 10 mL measuring bottle. The following results were detected for nickel and zinc:

Ni: 0,0179 ppm

Zn: 0,465 ppm

L.1 Nickel leaching - Conversion from ppm to %

ppm=mg/L

Ni amount in the sample: 0,0179 ppm

$$0,0179 \text{ ppm} = 0,0179 * 10^{-6} \text{ g/mL}$$

$$0,0179 * 10^{-6} \text{ g/mL} * \frac{10}{0,2} = 8,95 * 10^{-7} \text{ g/mL}$$

Thus, there was $8,95 * 10^{-7}$ g/mL of nickel in the sample used for the ICP analysis. In the cellulose conversion, 25 mL of water was used:

$$8,95 * 10^{-7} \text{ g/mL} * 25 \text{ mL} = 2,24 * 10^{-5} \text{ g}$$

In the conversion of cellulose 0,075g of 20Ni-26ZnO/CNT catalyst was used:

$$m_{Ni} = 0,075 \text{ g} * 20\% = 0,015 \text{ g}$$

The leaching of nickel (%) in the reaction:

$$\frac{2,24 * 10^{-5} \text{ g}}{0,015 \text{ g}} = 0,0015 = 0,15\%$$

L.2 Zinc leaching – Conversion from ppm to %

→ Result from ICP of Zn-sample: 0,465 ppm

$$0,465 \text{ ppm} = 0,465 * 10^{-6} \text{ g/mL}$$

$$0,465 * 10^{-6} \text{ g/mL} * 50 = 2,33 * 10^{-5} \text{ g/mL}$$

There was $2,33 * 10^{-5}$ g/mL of Zn in the sample flask used for the ICP analysis.

In the conversion for cellulose 25 mL of water was used:



$$2,33 * 10^{-5} \text{ g/mL} * 25 \text{ mL} = 5,81 * 10^{-4} \text{ g}$$

In the conversion of cellulose 0,075g of 20Ni-26,1ZnO/CNT catalyst was used:

$$\text{Zn: } 0,075\text{g} * 26,1\% = 0,0196 \text{ g}$$

$$5,81 * 10^{-4} \text{ g} / 0,0196 \text{ g} = 0,0297 = 2,97$$

M Risk Assessment

NTNU	Risk assessment	Prepared by	Number	Date	
		HSE section	HMSRV2603E	04.02.2011	
HSE/KS		Approved by	Page	Replaces	
		The Rector	2 out of 2	01.12.2006	

Criteria for the assessment of likelihood and consequence in relation to fieldwork

Each activity is assessed according to a worst-case scenario. Likelihood and consequence are to be assessed separately for each potential undesirable incident. Before starting on the quantification, the participants should agree what they understand by the assessment criteria:

Likelihood

Minimal 1	Low 2	Medium 3	High 4	Very high 5
Once every 50 years or less	Once every 10 years or less	Once a year or less	Once a month or less	Once a week

Consequence

Grading	Human	Environment	Financial/material
E Very critical	May produce fatality/ies	Very prolonged, non-reversible damage	Shutdown of work >1 year.
D Critical	Permanent injury, may produce serious serious health damage/sickness	Prolonged damage. Long recovery time.	Shutdown of work 0.5-1 year.
C Dangerous	Serious personal injury	Minor damage. Long recovery time	Shutdown of work < 1 month
B Relatively safe	Injury that requires medical treatment	Minor damage. Short recovery time	Shutdown of work < 1week
A Safe	Injury that requires first aid	Insignificant damage. Short recovery time	Shutdown of work < 1day



The unit makes its own decision as to whether opting to fill in or not consequences for economy/materiel, for example if the unit is going to use particularly valuable equipment. It is up to the individual unit to choose the assessment criteria for this column.

Risk = Likelihood x Consequence

Please calculate the risk value for "Human", "Environment" and, if chosen, "Economy/materiel", separately.

About the column "Comments/status, suggested preventative and corrective measures":

Measures can impact on both likelihood and consequences. Prioritise measures that can prevent the incident from occurring; in other words, likelihood-reducing measures are to be prioritised above greater emergency preparedness, i.e. consequence-reducing measures.

NTNU	Hazardous activity identification process	Prepared by,	Number	Date	
		HSE section	HMSRV-26/01	01.12.2006	
HSE		Approved by	Page	Replaces	
		The Rector	1 out of 1	15.12.2003	

Unit: Kjemisk prosessteknologi

Date: 28.01.2013

Participants in the identification process (including their function): Ingvild Skeie Liland (master student), Professor A. Wang (supervisor).



Ingvild S. Liland

A. Wang

Short description of the main activity/main process: Catalyst preparation and the conversion of cellulose under high pressure hydrogen conditions.

Activity/process	Responsible person	Laws, regulations etc.	Existing documentation	Existing safety measures	Comment
Use of toxic and flammable gases (H ₂)	A. Wang and C. Li		Safety data sheet*	Room detector, local detector, leak testing, gloves, goggles, lab coat.	No open flames in lab
Assembling/use of non toxic and inert gases: CO ₂ /N ₂ /Ar/He	A. Wang and C. Li		Safety data sheet*	Leak testing, gloves, goggles, lab coat.	
Use of acetone for cleaning procedures	A. Wang and C. Li		Safety data sheet*	Gloves, lab coat, goggles.	
Use of CNT	A. Wang and C. Li		Safety data sheet*	Gloves, lab coat, goggles, dust mask.	Unknown long term health effects
Use of liquid nitrogen for BET	A. Wang and C. Li		Safety data sheet*	Lab coat, goggles, special gloves	

* Printed safety data sheets are not available in the lab area at DICP. The relevant data sheets are available on Ecoonline.

NTNU	Risk assessment	Prepared by	Number	Date	
		HSE section	HMSRV2603E	04.02.2011	
HSE/KS		Approved by	Page	Replaces	
		The Rector	1 out of 2	01.12.2006	

Unit: Kjemisk prosessteknologi

Date: 28.01.2013

Line manager: Øyvind Gregersen

Participants in the risk assessment (including their function): Ingvild Skeie Liland (master student), Professor A. Wang (supervisor).

Ingvild S. Liland

A. Wang

Activity from the identification process form	Potential undesirable incident/strain	Likelihood:	Consequence:			Risk value	Comments/status Suggested measures
		Likelihood (1-5)	Human (A-E)	Environment (A-E)	Economy/material (A-E)		
Use of toxic and flammable gases (H2)	Leaks, fire, explosion	2	B			2B	Leak testing with noble gases and room and local detectors
Assembling/use of non toxic and inert gases: CO2/N2/Ar/He	Leaks	2	B			2B	Use of gloves, lab coat, goggles.
Use of acetone for cleaning procedures	spill, fire	3	A			2B	Use of gloves, lab coat, goggles.
Use of CNT	Spill	3	A			2B	Use of gloves, lab coat, goggles, dust mask.
Use of liquid nitrogen for BET	spill	3	B			2B	Lab coat, goggles, special gloves.

Likelihood, e.g.:

1. Minimal
2. Low
3. Medium
4. High
5. Very high

Consequence, e.g.:

- A. Safe
- B. Relatively safe
- C. Dangerous
- D. Critical
- E. Very critical

Risk value (each one to be estimated separately):

Human = Likelihood x Human Consequence

Environmental = Likelihood x Environmental consequence

Financial/material = Likelihood x Consequence for Economy/material

Potential undesirable incident/strain

Identify possible incidents and conditions that may lead to situations that pose a hazard to people, the environment and any materiel/equipment involved.